A. P. KARPINSKY RUSSIAN GEOLOGICAL RESEARCH INSTITUTE

Manuscript

Brusnitsyna Ekaterina Alekseevna

Reconstruction of provenance for the Riphean clastic succession in Middle Timan: constraints from integrated analytical studies

Scientific specialty 1.6.1. General and regional geology. Geotectonics and geodynamics

Dissertation for the degree of Candidate of Geological and Mineralogical Sciences

Translation from Russian

Scientific supervisor:

Doctor of Geological and Mineralogical Sciences

A.K. Khudoley

Saint-Petersburg 2023

Contents

Introduction

Research relevance. Geology of the Timan Ridge has been extensively studied by many geologists since the end of the 19th century. However, genesis, age, and the clastic material provenance, especially for the Precambrian rocks, remain the subject of intense debate. The reasons for this are the lack of fossil fauna in the Precambrian sedimentary strata and the limited amount of geochronological data available.

Within the Timan Ridge, isolated blocks of variably deformed Precambrian rocks are observed. This study focuses on the Riphean rock outcrops within two blocks that are the Chetlassky Kamen and the Volsko-Vymskaya Ridge. The most complete section of Precambrian rocks is exposed within the Chetlassky Kamen. Integrated isotope-geochronological, petrographic and mineralogical studies were carried out for several Riphean stratigraphic units. The new data obtained make it possible to better constrain the rocks ages and to reconstruct the provenances and transport pathways of clastic material in the Riphean.

Research goal. Reconstruction of detrital material provenances and clarification of ages of the Chetlasskaya, Bystrinskaya and Vymskaya Groups rocks in Middle Timan, traditionally attributed to the Middle and Late Riphean.

Research objectives:

1. Mineralogical and petrographic studies of the Riphean clastic rocks in Middle Timan.

2. Microprobe analysis of detrital tourmalines from the Upper Precambrian clastic sediments of Middle Timan to determine their chemical composition and origin.

3. U-Th-Pb dating of detrital zircons from the Upper Precambrian clastic rocks of Middle Timan to constrain their age and the main sources of detrital material.

4. Lu-Hf isotopic-geochemical analysis of detrital zircons to determine the melt source.

5. U-Th-Pb dating of detrital rutiles to constrain the age of metamorphic events in the provenance area of clastic material.

Factual material. Samples for this study were collected by the author during field work within the framework of the project “Geological Mapping within Quadrangles Q-39-XXXIII, XXXIV (Vymskaya Area)” (“Polyargeo”, “VSEGEI”). A total of 40 samples were collected. Detrital zircons from 8 samples were selected for age dating, and detrital tourmalines from 8 samples were subjected to chemical composition analysis. Detrital rutiles were extracted from 2 samples of the Precambrian clastic rocks of Middle Timan. For 6 samples, the Lu-Hf isotopic study of zircons was performed, with

prior determination of their U-Th-Pb ages. Petrographic description was done for 40 thin sections covering all studied Riphean stratigraphic units.

Author's contribution. When preparing the dissertation, the author was directly involved in field work in Middle Timan (2015, 2016), including participation in geological traverses, rock sampling, and data recording. Also, the author carried out petrographic studies, determined the degree of roundness of detrital zircons and tourmalines, selected detrital tourmaline and rutile grains for analyses, and took part (together with analysts) in all analytical studies including U-Th-Pb dating of zircons and rutiles, Lu-Hf isotope analysis of zircons, and determination of the chemical composition of detrital tourmalines.

Scientific novelty. The results of the integrated isotope-geochemical study of the Riphean clastic sediments of Middle Timan enabled refinement of the existing views on the detrital material sources. The U-Th-Pb ages of detrital zircons from 8 samples taken from different stratigraphic units of the Riphean section in the Chetlassky Kamen and the Volsko-Vymskaya Ridge were determined and compared with the ages obtained for zircons from neighboring regions of Timan, the Urals, the Leningrad Region, and the Kola Peninsula.

For 5 samples, the Lu-Hf isotope characteristics of zircons were first obtained, which allowed establishing the origin of their source rocks. For the first time, U-Th-Pb detrital rutile dates were gained, which in combination with the results of detrital zircon dating enabled determining the timing of the last thermal event that affected the rocks in the provenance area.

The chemical composition of detrital tourmalines extracted from the Riphean sedimentary rocks of Middle Timan was first determined. The results obtained provided information on the composition of the source rocks for the sedimentary strata of Middle Timan.

Practical significance. The results of U-Th-Pb dating of detrital zircons and rutiles provide constraints on the age of the Precambrian clastic sediments in Middle Timan. A paleogeographic sketch map is prepared that complements the existing reconstructions of the Timan Range and adjacent areas for Precambrian time. The results obtained can be used both in working out stratigraphic charts to provide a base for compiling the State Geological Map at various scales and in carrying out tectonic and metallogenic studies.

Structure and scope of work. The dissertation consists of an introduction, 4 chapters, conclusions, and a list of references. It contains 168 pages, 42 figures, 3 tables and 7 appendices. References include 154 sources.

Approbation. The research results were presented in 11 publications, among them 3 papers in peer-reviewed journals included in the HCC (Highest Certifying Commission) List, and at Russian and International conferences and meetings.

Relevant papers by E.A. Brusnitsyna:

1. Brusnitsyna, E.A., Ershova, V.B., Khudoley, A.K., Andersen, T., Maslov, A.V. Age and provenance of the Riphean rocks of the Chetlas Group of the Middle Timan: U–Th–Pb (LA-ICP-MS) dating of detrital zircons // Stratigraphy and Geological Correlation. 2021. v. 29, p. 607–626. DOI: 10.1134/S0869593821060022
2. Brusnitsyna, E.A., Vereshchagin, O.S., Ershova, V.B. Detrital tourmaline from Riphean clastic deposits of Middle Timan: Chemical Composition and Genesis // Geology of Ore Deposits. 2022. № 64. P. 646–656.
3. Brustnitsyna E., Ershova V., Khudoley A., Maslov A., Andersen T., Stockli D., Kristoffersen M. Age and provenance of the Precambrian Middle Timan clastic succession: Constraints from detrital zircon and rutile studies // *Precambrian Research*, 2022, v. 371, 106580, DOI: 10.1016/j.precamres.2022.106580.

Abstracts of presentations:

1) Brusnitsyna E.A., Ershova V.B., Khudoley A.K., Andersen T. Results of the U-Pb isotope study of detrital zircons from the Middle-Upper Riphean deposits of the Chetlassky Kamen (Timan Range) // L tectonic meeting "Problems of tectonics and geodynamics of the Earth's crust and mantle", Moscow, 2018, V.2, p. 384-388.
2) Brusnitsyna E.A., Ershova V.B., Khudoley A.K., Andersen T. Age and provenance of the Mesoproterozoic-Lower Neoproterozoic strata of the Chetlass Stone (Timan Range): Constraints from U-Pb detrital zircon study // The International Conference on Arctic Margins (ICAM) (Stockholm, 2018),
3) Brusnitsyna E.A., Ershova V.B., Khudoley A.K., Andersen T. Results of U-Pb and Hf isotope dating of detrital zircons from Middle-Upper Riphean clastic rocks of Middle Timan // LI tectonic meeting "Problems of tectonics of continents and oceans", Moscow, 2019, p. 90-94.
4) Brusnitsyna E.A., Ershova V.B., Khudoley A.K., Andersen T. New U-Pb and Hf isotopic data for detrital zircons from the Middle and Upper Riphean clastic rocks of Middle Timan // XVII Geological Congress of the Komi Republic "Geology and mineral resources of the northeastern portion of the European part of Russia", Syktyvkar, 2019, V.1, p. 16-18

5) Brusnitsyna E.A., Ershova V.B., Khudoley A.K., Andersen T. Age and provenance of the Mesoproterozoic strata of the Timan Range: Constraints from U-Pb-Hf detrital zircon study // European Geosciences Union (EGU) General Assembly, Vienna, 2019
6) Brusnitsyna E.A., Ershova V.B., Khudoley A.K., Andersen T. Results of studying the U-Pb isotope age of detrital zircons from the Middle-Upper Riphean deposits of the Chetlassky Kamen (Timan Range) // 28th Scientific Conference “Structure, substance, and history of the lithosphere of the Timan-North Urals segment”, Syktyvkar, 2019, p. 7-11.
7) Brusnitsyna E.A., Ershova V.B., Khudoley A.K. Reconstruction of provenances for Riphean clastic deposits of Middle Timan // VII Youth Conference "New in Geology and Geophysics of the Arctic, Antarctic and the World Ocean" St. Petersburg, 2021, p. 20-22.
8) Brusnitsyna E.A., Ershova V.B., Khudoley A.K. Reconstruction of provenances for the Riphean clastic deposits of Middle Timan based on the results of integrated analytical studies // VI International Scientific Conference "Geodynamics and Minerageny of Northern Eurasia", Ulan-Ude, 2023, p. 87-90

Acknowledgments. The author is most grateful to her scientific supervisor A.K. Khudoley for great assistance in writing the dissertation. V.B. Ershova is thanked very much for support, assistance, numerous consultations, and organization of analytical research.

Thanks are due to T. Anderson, M. Kristofferson (University of Oslo, Department of Geosciences), D. Stockli and L. Stockli (UTChron Laboratory of the Department of Geosciences (Jackson School of Geoscience) of the University of Texas, Austin, Texas, USA), V.V. Shilovskikh and N.S. Vlasenko (“Geomodel” Resource Center, St. Petersburg State University), and A.V. Antonov (FGBU "VSEGEI") for preparatory procedures and analytical studies.

The author is indebted to A.V. Maslov (Institute of Geology and Geochemistry, Ural Branch of the Russian Academy of Sciences, GIN RAS), and O.S. Vereshchagin (St. Petersburg State University) for advice and assistance in conducting analytical studies and interpreting the data obtained.

The author expresses her gratitude to V.G. Kotelnikov, A.A. Parkhachev, A.T. Terentyev, and D.V. Zarkhidze, representatives of "POLYARGEO" (currently the Department of Regional Geology of the Polar and Subpolar Territories) and the Syktyvkar Sector of the Federal State Budgetary Institution "VSEGEI", for providing the opportunity to participate in the field work.

Analytical work and participation in Russian and international conferences were supported by RFBR grant 17-05-00858 and RSF grants 20-17-00169 and 18-35-00407.

Thesis statements to be defended:

1. The age of the youngest detrital rutile populations formed by at least three to five grains (~ 900-1050 Ma) defines the age of the last phase of metamorphism in the provenance area for clastic rocks.

2. A significant number of rounded detrital zircon grains, the composition of sandstones, and the chemical composition of detrital tourmalines indicate a widespread occurrence of sedimentary (metasedimentary) rocks in the source area.

3. The integrated study of the Riphean clastic successions of Middle Timan indicates that the main provenance of clastic material was the Sveconorwegian-Grenvillian Orogen (including associated older terranes).

Main scientific results:

1. The obtained detrital zircon ages indicate a younger age of sedimentary rocks than was determined earlier (RF_{1-2}). The age of the Middle Timan clastic rocks is estimated as late Middle Riphean-early Late Riphean (Brusnitsyna et. al., 2022, pp. 13).
2. The study of the chemical composition of detrital tourmalines from the clastic rocks of Middle Timan showed they were sourced from metamorphosed sedimentary rocks Brusnitsyna et. al., 2022, pp. 6).
3. The youngest detrital rutile ages obtained define the ages of metamorphic events in the source area of detrital material (Brusnitsyna et. al., 2022, pp. 13).

Chapter 1: Geology of the Timan-Pechora region

1.1 Geological setting of the study area

The Timan Range is located on the territory of the Komi Republic and the Arkhangelsk Region and stretches for about 1000 km northwestward from the Kolva-Vishera region in the Northern Urals to the Chesha Bay of the Barents Sea. In this study, the term East European Platform (EEP) is used when referring to modern boundaries of this tectonic structure; however, when discussing tectonic reconstructions for Precambrian time, the EEP is traditionally called as Baltica.

The Timan Range is expressed topographically as a series of strongly eroded topographic highs (Figure 1.1). The most significant of them, referred to as "Kamen'' (Mount) in the Timan region, display outcrops of variably metamorphosed Precambrian complexes crosscut by different-aged intrusions (Olovyanishnikov, 1998). From southeast to northwest, the following uplifts, composed of Riphean rocks, are exposed: Dzhedzhim-Parma, Ochparma, Volsko-Vymskaya Ridge, Chetlassky Kamen, Tsilemsky Kamen, Northern Timan, and Kanin Kamen (Figure 1.1).

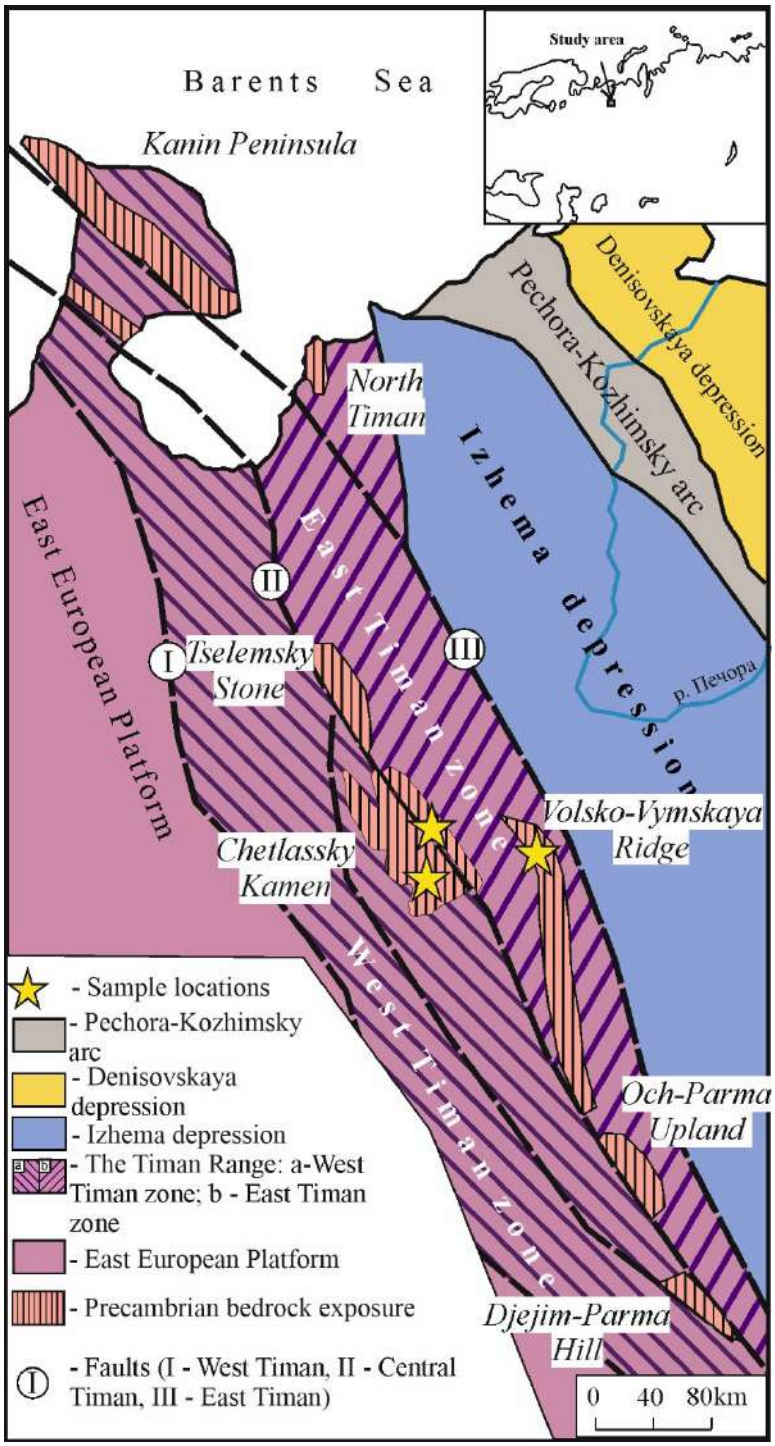

Figure1.1. Schematic tectonic map of the Pechora Plate and its framing, simplified from Olovyanishnikov (1998).

From north to south, the Timan Range is divided into two large zones - East Timan and West Timan. The West Timan zone is bounded on the southwest by the West Timan thrust, and on the northeast by the Central Timan thrust. The main structure of the West Timan zone is the Chetlassky Kamen, an uplifted block (Olovyanishnikov, 1998) composed of Riphean clastic rocks metamorphosed to the sericite-chlorite subfacies, which are gently folded and cut by numerous NE-trending faults (Parmuzin et al., 2015).

The East Timan zone is separated from the West Timan zone by the Central Timan thrust, and is bounded on the northeast by the East Timan thrust. Within the East Timan zone, several uplifts composed of Precambrian deposits are exposed, among them the Volsko-Vymskaya Ridge consisting of Middle- to Late-Riphean sandstones and shales metamorphosed to the greenschist, locally to the epidote-amphibolite facies. The rocks are folded with predominant dipping to the east at angles up to 80° [Parmuzin et al., 2015].

1.2. Brief overview of previous studies of the Timan region

Geological study of the Timan Range has been going on for more than 200 years (Olovyanishnikov, 1998).

The Timan Range was first described by A.I. Fomin in his Book "Description of the White Sea with its shores and islands ..." (1797), who called it Kamen (Mount). The first systematic descriptions of the Timan geology (1843-1855) with characterization of the orography and hydrography of the region are given in the works of A.A. Keyserling, K.I. Griving, A.N. Shrenk and A.F. Shtukenberg. In 1847, A.A. Keyserling and P.I. Kruzenshtern compiled the first map of the Timan Range, one of the first geological maps of Russia.

In 1915, F.N. Chernyshev compiled a geological map of the European part of Russia (Figure 1.2), which included the Timan Range area. On this map the Kanin-Timan deformation zone is shown as a continuation of the deformed rocks of the Varanger Peninsula, Rybachiy Peninsula, and Kildin Island. This was fully confirmed by further studies. The researcher explained deformations by ruptures in the earth's crust considering that folding became stronger toward the edges of horsts and grabens. According to F.N. Chernyshev, deformations in Timan and Kanin Peninsula were associated with two NW and NE fault zones bounding the Baltic Shield. The composition and structure of meta-sedimentary rocks were first studied by the Finnish scientist William Ramsey in the Kanin Kamen in 1911. He compiled a geological map of the Kanin Peninsula and for the first time established a different nature of deformations between the Paleozoic metasedimentary and sedimentary rocks.

The "reconnaissance" stage in the geological study of the Timan Range, associated with research by N.N. Yakovlev, A.P. Pavlova, A.A. Chernov and V.A. Varsanofieva, ended in 1902-1918.

The second stage in the Timan study was marked by a growing interest in this region, where F.N. Chernyshev, A.I. Zamyatin, V.K. Likharev, N.N. Tikhonovich, A.A. Malakhov and other researchers worked for many years. The results of their investigations published in the literature were used by many other geologists involved in the studies of Timan. The most important are works by A.P.

Karpinsky, A.D. Arkhangelsky, N.S. Shatsky, I.M. Gubkin, and A.N. Mazarovich, who considered Timan as a branch of the Uralian fold belt. It should be noted that at the time of Kaiserling and Chernyshev, geotectonics had not yet accumulated a sufficiently large body of descriptive data, so in many cases researchers could only make assumptions.

A.D. Arkhangelsky (1922) was the first to establish a platform nature of Timan representing, in his opinion, a subsided massif that once adjoined the Baltic Shield on the east. Subsequently, when describing the East European Platform, he identified its megaswell with Timan forming its part. He connected the formation of that structure to orogenesis in the Uralian geosyncline (Arkhangelsky 1933).

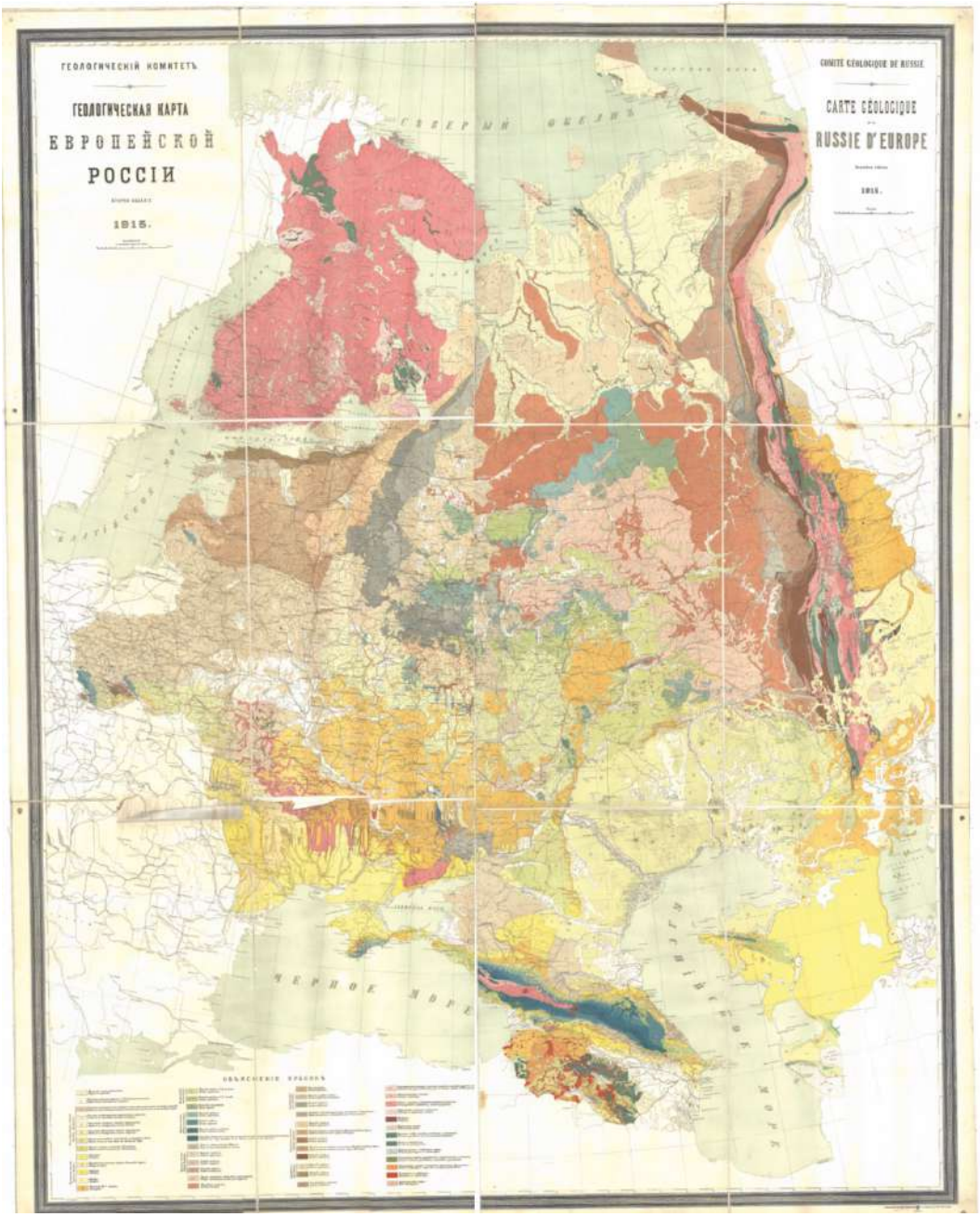

Figure1.2. Geological map of the European part of Russia, compiled by F.N. Chernyshev (1915)

The third stage (1921-1946) was aimed at geological mapping of the territory and prospecting for oil and gas. In 1929, the Ukhta Exploration Expedition was set up in Timan (Olovyanishnikov, 1998). This stage is associated with of researches by A.N. Rozanov, T.E. Khudyaev and B.K. Likharev, N.N. Tikhonovich, N.I. Strizhkov, K.K. Vollosovich, A.A. Malakhov, and P.E. Offman. In the 1930s, mapping and prospecting works in Northern Timan and Kanin Peninsula were carried out by M.M. Ermolaev, M.B. Edemsky, V.P. Barkhatova, A.A. Chernov, K.K. Vollosovich, and V.I. Shmygalev. Investigations were suspended during the Great Patriotic War (1941-1945), and only after its completion systematic studies and geological mapping were resumed. As a result, by the end of the

1950s, a standard geological map of the northeastern portion of the European part of the USSR was compiled (Olovyanishnikov, 1998). Important tectonic studies of Timan also were made at this time, including, first of all, papers and monographs by A.A. Malakhov, P.E. Offman, N.N. Tikhonovich, and A.A. Chernov. Most geologists divide the geological section in Timan into a sedimentary cover and a metasedimentary basement and consider that Timan was at a geosynclinal stage of its development in the Precambrian.

From the mid-50s to the early 90s, the fourth stage took place, which is distinguished by increased geophysical research and prospecting for placers, bauxites, and oil and gas, with extensive drilling. Synchronously, a large-scale geological mapping, thematic studies, and airborne geological surveys were carried out. This period is characterized by a growing body of geological and geophysical information and the appearance of new interpretations of the geological and tectonic evolution of the region. The most important summarizing works on the regional geology were written by Yu.P. Ivensen, V.A. Raznitsyn, G.A. Chernov, V.S. Zhuravlev, R.A. Gafarov, V.N. Puchkov, V.G. Getsen, V.A. Dedeev, I.V. Zaporozhtseva and others.

Since 1991, the scope of geological and geophysical studies and thematic works was drastically reduced. At that time, a number of summarizing papers on regional geology were published and some models were proposed for the geodynamic development of the region (Getsen, 1991; Belyakova, Stepanenko, 1991; Zaporozhtseva, Pystin, 1994; Kostyuchenko, 1994; Berlyand, 1993; Olovyanishnikov, 1996; Pachukovsky, Traat, Mishchenko, Dovzhikov (1996).

Starting in the 1940s, a systematic geological mapping at a scale of 1:200,000 was carried out throughout Russia, including the Timan region. In 1965, V.I. Gorsky-Kruchinin on the stuff of the Ukhta Territorial Geological Department compiled the first 1:1,000,000 map for the Middle Timan territory. A map for South Timan at a scale of 1:1,000,000 was compiled in 1960 by K.K. Vollosovich. The 1:1,000,000 map for North Timan, including the Kanin Peninsula, was constructed earlier (1939) by Ya.D. Zekkel. The "Polyarnouralgeologiya"and "Arkhangelskgeologia" Companies and the Ukhta Geological Department carried out the first geological mapping of the territories of Middle Timan (T.N. Zorenko; M.I. Osadchuk, V.P. Ponomarev; H.O. Traat, R. Ya Mishchenko, G.F. Proskurin, V.I. Lipanov), North Timan (L.S. Kolosova) and South Timan (V.N. Oparenkov).

Beginning in the 2000s, VSEGEI, VNIIOkeangeologiya and UGRE Companies have been engaged in updating geological information for the Timan Range territory including compilation of new maps on a scale of 1:1,000,000 (S.I. Shkarubo, V.V. Orgo, B.G. Lopatin, G.M. Cheremkhina, A.A. Cherepanov; S.I. Shkarubo, V.A. Zhuravlev, N.M. Parmuzin, K.E. Yakobson, A.Yu. Vovshina,

N.M. Parmuzin) and on a scale of 1:200,000 (A.A. Cherepanov, N.A. Erokhina; S.I. Kirillin). The study of the Timan region geology is still ongoing.

In the mid-90s, with the discovery of oil fields in the Arctic shelf, the era of active exploration of this region began. Major Russian and foreign companies are involved in evaluation of oil resources within the shelf zone of the Arctic Ocean. Since 2013, oil has been produced from the Prirazlomnoye field within the Timan-Pechora oil-and-gas province (the southeastern part of the Pechora Sea). This is the first oil-producing field on the Russian Arctic Ocean shelf.

Over the past 20 years, many leading Russian and international scientists have been studying the geology of Timan. Much research has been done on igneous rocks in the northeastern part of the East European Platform, including the Northern Urals, Novaya Zemlya Islands, and Timan Range (e.g., Backholmen et al, 2004; Bogolepova and Gee, 2004; Pease, 2004; Korago et al., 2004; Larionov et al., 2004). With the development of new analytical methods, it became possible to study the isotopic composition and age of zircons not only from igneous and metamorphic rocks, but from sedimentary strata too.

Historically, the study of clastic rocks included two stages: a search for index flora and fauna fossils and determination of mineralogical composition of rocks. Precambrian rocks are poorly fossiliferous, which makes it impossible to determine their age. In recent years, modern analytical approaches based on U-Th-Pb dating of detrital zircons have found wide application in the provenance studies and reconstruction of tectonic settings. Beginning in 2006, the number of publications on the dating of detrital zircons from the rocks of the Timan Range and adjacent areas has been increasing from year to year (Andreichev et al. 2017, 2018; Kuznetsov et al., 2010; Orlov et al., 2011; Soboleva et al. 2019; Udoratina et al. 2017). The detrital zircon ages in combination with the available geophysical and paleomagnetic data enabled compilation of large-scale regional tectonic reconstructions for the Russian Platform (EEP) and the Timan-Urals region (Kuznetsov et al. 2006, 2007; Pystin et al. 2018; Bogdanova et al. 2008, 2016; Kostyuchenko et al. 2006; Kuznetsov et al. 2010 and others).

The above methods allowed determination, for the first time, of the ages of granitic intrusions whose emplacement marked the final stage of the Timanian Orogeny (Andreichev et al., 2017). In addition, it became possible to significantly constrain the stratigraphic setting of the Riphean clastic rocks of the Timan Range.

1.3 Geology of the Chetlassky Kamen and the Volsko-Vymskaya Ridge

Two rock complexes with different structural styles are traditionally identified within the Chetlassky Kamen and the Volsko-Vymskaya Ridge: the basement and the platform cover of the Timan-Pechora Plate. Within these uplifts Precambrian rocks are exposed (Figure 1.3). It should be noted that the Riphean rocks of Timan were formed on the passive margin of Baltica (Getsen, 1987; Olovyanishnikov, 1998).

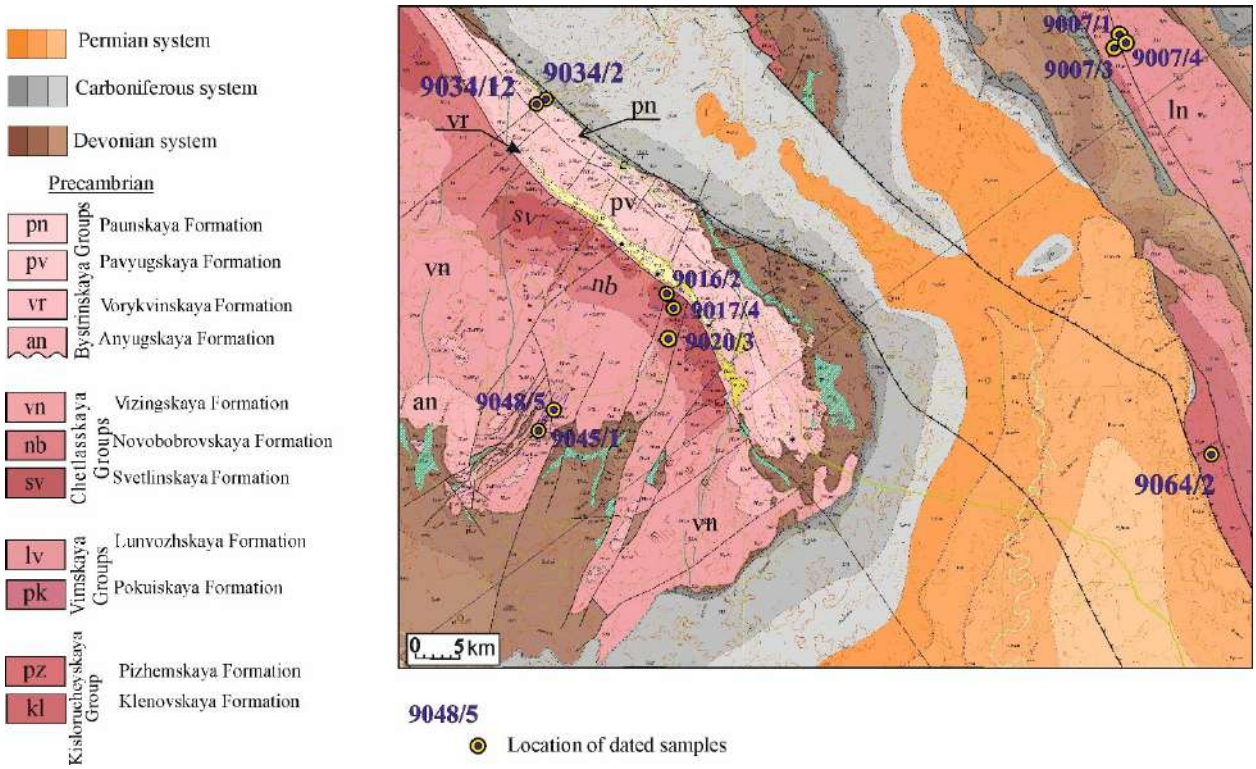

Figure 1.3. Geological map of the Chetlassky Kamen and the Volsko-Vymskaya Ridge with sample locations (simplified after Kirillin et al., 2020).

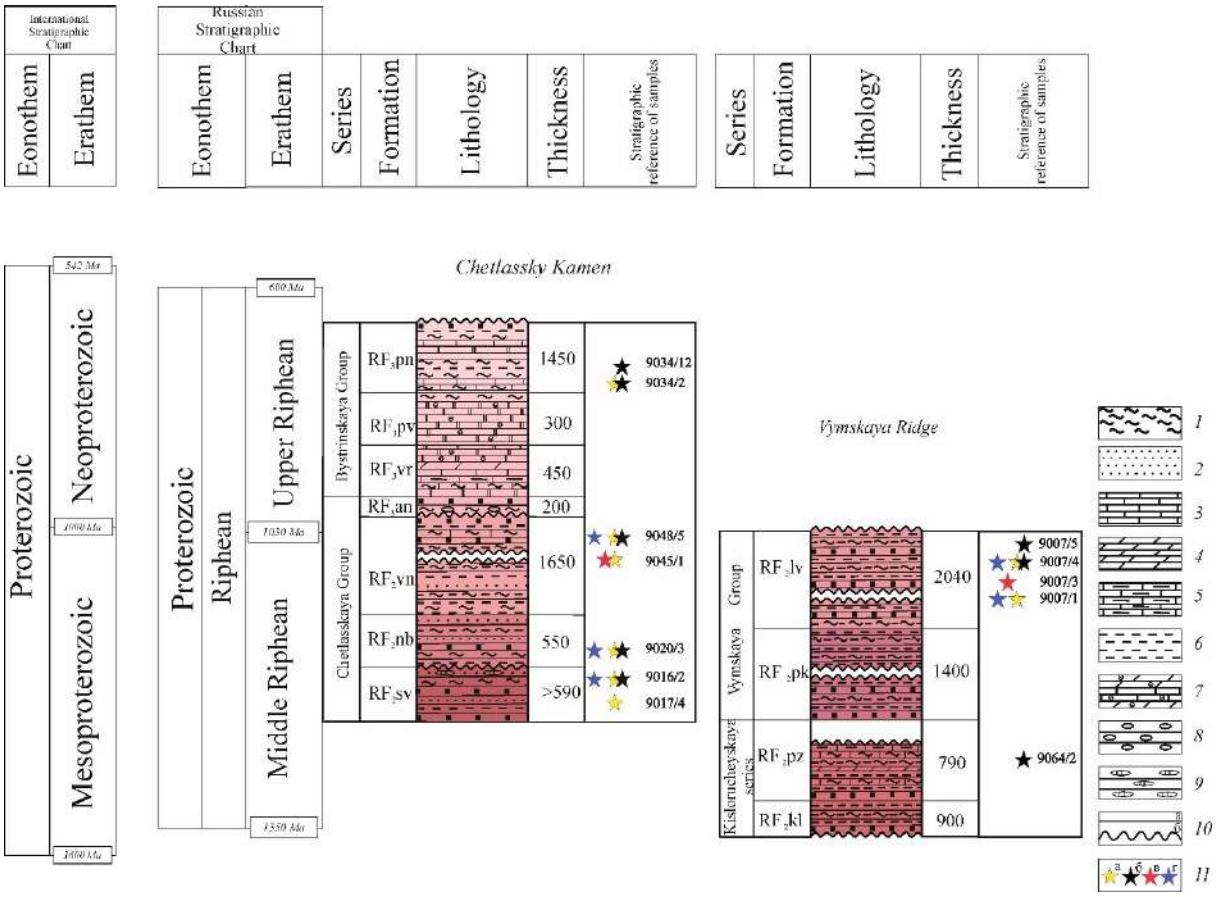

Fig 1.4. Composite stratigraphic section of the Riphean sediments of the Chetlassky Kamen and the Volsko-Vymskaya Ridge, with positions of samples.

1 – slate; 2 – metasandstone; 3 - limestone; 4 - marl; 5 - dolomite; 6 – metasiltstone; 7 – limestone and dolomite with stromatolites; 8 - conglomerate; 9 – chert interbed; 10 – stratigraphic contacts (a – conformable, b – unconformable); 11 – stratigraphic setting of the studied samples (a – samples for U-Th-Pb detrital zircon dating; b – samples for microprobe study of detrital tourmalines; c – samples for U-Th-Pb detrital rutile dating; d – samples for Lu-Hf isotopic-geochemical studies of detrital zircons).

Formations: RF_2sv – Svetlinskaya; RF_2nb - Novobobrovskaya; RF_2vn - Vizingskaya; RF_3an - Anyugskaya; RF_3vr - Vorykvinskaya; RF3pv - Pavyugskaya; RF_3pn - Paunskaya; RF2kl - Kleonovskaya; RF_2pz - Pizhemskaya; RF_2pk - Pokyuskaya; RF_2lv - Lunvozhskaya.

In this study, we divide the Upper Precambrian into Riphean and Vendian as is generally accepted in Russia.

Chetlassky Kamen

The Chetlassky Kamen displays outcrops of Riphean clastic rocks that are divided into two groups: Chetlasskaya and Bystrinskaya. The Chetlasskaya Group comprises the Svetlinskaya,

Novobobrovskaya, and Vizingskaya Formations (Getsen, 1987; Olovyanishnikov, 1998). The Chetlasskaya Group rocks are overlain by Devonian clastic sediments on the southwest, and are in tectonic contact with the Bystrinskaya Group rocks on the northeast. The Chetlasskaya Group represents an intercalation of quartzites, metasandstones, siltstones, and chlorite-mica slates (Figure1.4).

Svetlinskaya Formation (RF_2sv) is the oldest exposed unit; it lies at the base of the Chetlasskaya Group (Kirillin et al., 2020). It has been mapped as several isolated fragments within an area of up to 30 km^2, in the northeastern part of the Chetlassky Kamen along the Central Timan fault (Figure 1.3). The rocks of the formation are exposed in the river basins of Bobrovaya and Vizinga and in the upper reaches of the Mezen River. The lower contact of the formation is not exposed. According to previous studies (Olovyanishnikov, 1998; Kirillin et al., 2020) and our field observations, the Svetlinskaya Formation consists of two subformations. The lower subformation (recovered by boreholes) consists largely of slates, mica-quartz and feldspar-quartz-mica metasiltstones (60%) and subordinate metasandstones (40%). The exposed thickness of the section is 270 m. The upper subformation is composed mainly of metasandstones (70%) with units of mica slates interbedded with metasiltstones. It rests conformably on the lower subformation, the boundary between them is conventionally located at the first thick quartzite member (up to 50 m) (Kirillin et al., 2020). In the upper part of the section, there are present lenticular bodies of coarse-grained sandstones, with characteristic small pebbles of bluish and smoky quartz (Olovyanishnikov, 1998; Kirillin et al., 2020. Thickness of the upper subformation is estimated at 320 m, and that of the entire Svetlinskaya Formation is over 590 m.

Novobobrovskaya Formation (RF_2nb) is identified in the central, axial part of the Chetlassky Kamen, and can be traced from the upper reaches of the Mezen River to the headwaters of the Svetlaya and Lower Paun Rivers. It is exposed as a band 50 km long and 5 to 10 km wide. The sediments of the Novobobrovskaya Formation rest, with erosion, on the deposits of the Svetlinskaya Formation (Olovyanishnikov, 1998). The complete section of the Novobobrovskaya Formation, as that of the Svetlinskaya Formation, was recovered by boreholes. The Novobobrovskaya Formation consists of slates, quartz-chlorite-sericite metasiltstones with metasandstone interbeds. The lower part of the formation is represented by an alternation of metasiltstones and quartz-mica, quartz, and mica slates (with carbonaceous matter). Quartz metasandstones with an admixture of gravelly quartz grains are noted in the upper part of the section. The uppermost part of the section (ca. 100 m thick) consists of alternating metasandstones, metasiltstones, and slates. The thickness of the formation is up to 550 m (Kirillin et al., 2020).

Vizingskaya Formation (RF_2vn) composes the bulk of the Chetlassky Kamen. It overlies conformably the subjacent deposits of the Novobobrovskaya Formation. Some authors (Kirillin et al., 20) distinguish three subformations within the Vizingskaya Formation. In the lower part of the section there are alternating members of metasandstones, metasiltstones, and chlorite-sericite slates. Higher up quartz metasandstones predominate (Olovyanishnikov, 1998; Kirillin et al., 2020). Variegated members of alternating metasiltstones and slates with rare interbeds of metasandstones are described from the middle part of the section. The upper part of the section is composed of a thick sequence of quartz metasandstones, with rare lenses and interbeds of slates. In the lower part of the upper subformation, the section consists of alternating quartz metasandstones, metasiltstones, and slates. The thickness of the Vizingskaya Formation is estimated at 1650-1750 m.

It is generally accepted that the Chetlasskaya Group rocks deposited in a shallow marine environment (Olovyanishnikov, 1998).

The Bystrinskaya Group, exposed along the northeastern boundary of the Chetlassky Kamen (Figure 1.3), is composed predominantly of carbonates. It includes the Anyugskaya, Vorykvinskaya, Pavyugskaya, and Paunskaya Formations (Figure 1.4), which consists of interbedded dolomites, marls, calcareous slates, and stromatolitic limestones. The upper part of the section (Paunskaya Formation) consists of quartz-sericite-chlorite metasiltstones, metasandstones, and quartz metasandstones.

Anyugskaya Formation (RF_3an) is located at the base of the Bystrinskaya Group; it rests with erosion and angular unconformity on the Novobobrovskaya and Vizingskaya Formations of the Chetlasskaya Group. The most complete section was penetrated by boreholes; however, there are several outcrops observed in the areas of the Kosyu, Vizinga and Mezen Rivers (Olovyanishnikov, 1998; Kieillin et al., 2020). In the lower part of the section, large-pebbled conglomerates and quartz metasandstones with thin (up to 2.5 m) metasiltstone and slate interbeds are described. Up section occurs a sequence of interbedded metasiltstones, slates, and metasandstones. The section ends with rhythmically interbedded mica-quartz siltstones, slates, and quartz metasandstones. Interlayers of calcareous rocks are observed throughout the section. The thickness of the formation is 200 m.

Vorykvinskaya Formation (RF_3vr) crops out as a narrow (400–600 m) band along the northeastern slope of the Chetlassky Kamen (along the Central Timan Fault). In natural outcrops, the formation is in tectonic contact with the rocks of the Chetlasskaya Group. The drilling data, however, show that it overlies, with gradual transition, deposits of the Anyugskaya Formation (Kirillin et al., 2020). The Vorykvinskaya Formation is divided into two subformations. The lower subformation is composed of interbedded limestones, dolomites, slates, metasiltstones, and quartz metasandstones. Above them lies a sequence of carbonate rocks represented by silty dolomites, limestones, and

dolomitic limestones with rare thin interbeds of slates. The upper subformation consists of massive, banded, brecciated, and stromatolitic dolomites. In the upper part of the section, there is a unit of banded limestones with marl interbeds. The thickness of the Vorykvinskaya Formation reaches 350-450 m (Kirillin et al., 2020).

Pavyugskaya Formation (RF_3pv) outcrops as a thin strip along the northeastern slope of the Chetlassky Kamen and is exposed in the valleys of the Vorykva, Pavyuga, Pravaya Bobrovaya, Bobrovaya and Paun Rivers. It conformably rests on the rocks of the Vorykvinskaya Formation. The constituent rocks are bedded and thin-bedded, brecciated, and stromatolitic dolomites. Black carbonaceous limestones and pyritized silicified dolomites are documented in the upper part of the section. The thickness of the Pavyugskaya Formation is up to 300 m (Kirillin et al., 2020).

Paunskaya Formation (RF_3pn) completes the section of the Bystrinskaya Group. It crops out as a thin (ca. 2.5 km) band framing the northeastern part of the Chetlassky Kamen. The contact with the underlying Pavyugskaya Formation is tectonic, and only in the southeastern part is a small fragment with conformable bedding observed. In the north and northeast, the Paunskaya Formation is overlain, with erosion, by Devonian and Carboniferous rocks (Kirillin et al., 2020). The lower part of the section is represented by a sequence of interbedded slates and limestones. Above them lie quartz-sericite-chlorite metasiltstones with interbeds and units of dolomites, limestones, metasandstones, quartz metasandstones as well as limy and carbonaceous slates. The middle part of the formation consists of carbonaceous slates with interlayers of metasandstones, quartz metasandstones, and sericite-chlorite slates, which are overlain by a sequence of alternated slates and metasiltstones with rare interbeds of quartz metasandstones and limy and carbonaceous slates. The uppermost part of the Paunskaya Formation section consists of metasandstones with thin slate interbeds. The thickness of the formation reaches 1350-1450 m (Kirillin et al., 2020).

It is believed (Getsen, 1987) that deposits of the Chetlasskaya Group accumulated in a shallow marine environment, and the rocks of the overlying Bystrinskaya Group formed a large reef-like belt.

Volsko-Vymskaya Ridge

The Riphean rocks of the Volsko-Vymskaya Ridge are divided into two groups: Vymskaya and Kislorucheiskaya (Figure 1.3). The Kislorucheiskaya Group comprises the Kleonovskaya and Pizhemskaya Formations (Figure 1.4).

Kleonovskaya Formation (RF_2kl). The rocks of the formation are found in the northern part of the Volsko-Vymskaya Ridge, where they are exposed in the form of a strip up to 1.2 km wide and 9 km long. On the west, the formation is in tectonic contact with Carboniferous deposits, and on the east

is overlain, with erosion, by Devonian sediments (Kirillin et al., 2020). The lower part of the formation consists of quartz metasandstones, metasiltstones and slates, with predominance of metasiltstones and slates. Metasiltstones and slates are sericite-chlorite, sericite-chlorite-quartz, and biotite-quartz in composition (Getsen et al., 1987). Up section lies a sequence of alternating mica slates and metasiltstones. The thickness of the Kleonovskaya Formation is 900 m.

Pizhemskaya Formation ($RF_2pž$) conformably rests on the deposits of the Kleonovskaya Formation. The Pizhemskaya Formation rocks are described from the southwestern part of the Volsko-Vymskaya Ridge, where they form a slice with thrust contacts. On the southwest, the rocks of the formation are thrust over Paleozoic deposits, and on the northeast, they plunge beneath a thrust slice composed of the Vymskaya Group deposits (Kirillin et al., 2020). The Pizhemskaya Formation is predominantly composed of originally silty and clay-silty shales metamorphosed to the biotite-chlorite subfacies of the greenschist facies (Getsen et al., 1987). Dolomite and siderite interbeds and lenses are documented as well. A characteristic feature of the Pizhemskaya Formation is the presence of a marker bed composed of magnetite-bearing slates with large biotite laths. The lower part of the formation is dominated by limy sericite-chlorite-quartz and chlorite-sericite metasiltstones and slates. In its upper part, a sequence of carbonaceous chlorite-quartz, carbonaceous quartz-chlorite, and carbonaceous chlorite-sericite metasiltstones and slates, with thin interbeds of sericite-quartz-chlorite metasiltstones and metasandstones, is described. The thickness of the Pizhemskaya Formation is 790 m (Kirillin et al., 2020).

In the study area, the rocks of the Kleonovskaya and Pizhemskaya Formations are separated in space and make a tectonic contact with the overlying Riphean and Devonian strata. When describing the type section on the Pizhma River it was established that the Pizhemskaya Formation conformably overlies the Kleonovskaya Formation. According to (Olovyanishnikov, 1998), deposits of the Kislorureiskaya Group occur locally within the Volsko-Vymskaya Ridge and were formed simultaneously with the deposits of the Chetlasskaya and Vymskaya Groups, and their close location is a result of displacement along thrusts (Kirillin et al., 2020; Olovyanishnikov, 1998).

The Vymskaya Group includes the Pokyuskaya and Lunvozhskaya formations (Figure 1.4). The rocks of the Vymskaya Group make up the bulk of the Volsko-Vymskaya Ridge (Figure 1.1).

Pokyuskaya Formation (RF_2pk) outcrops in the southeastern part of the Volsko-Vymskaya Ridge. The formation composes the western part of the Vymskaya fault slice overthrusting the rocks of the Pizhemskaya Formation (Kirillin et al., 2020). Traditionally, three sequences are distinguished in the Pokyuskaya Formation section (Olovyanishnikov, 1998; Kirillin et al., 2020). The lower sequence is dominated by quartz metasandstones, with subordinate beds of slates intercalated with

metasiltstones. The middle sequence consists of alternating carbonaceous chlorite-sericite and sericite-chlorite slates, with interbeds of metasiltstones and calcareous metasiltstones. The upper sequence is composed of rhythmically interbedded slates, metasiltstones, and quartz metasandstones; rare lenses of calcareous metasiltstones, metasandstones, and limestones are observed too. The thickness of the Pokyuskaya Formation ranges up to 1400 m (Olovyanishnikov, 1998; Kirillin et al., 2020).

Lunvozhskaya Formation (RF_2lv) occurs in the central and northeastern parts of the Volsko-Vymskaya Ridge and conformably overlies deposits of the Pokyuskaya Formation. Two large sedimentary megacycles are distinguished in the section of the Lunvozskaya Formation (Kirillin et al., 2020). The first megacycle begins with a sequence of quartz metasandstones and metasandstones with slate interbeds. Up section lies a sequence of chlorite-sericite slates with thin interlayers of light gray sericite-chlorite-quartz metasiltstones, sometimes calcareous (Kirillin et al., 2020). The megacycle ends with a sequence of rhythmically interbedded black slates and silty slates, with rare metasandstones. The second sedimentary megacycle begins with quartz metasandstones, metasiltstones, and silty slates. Above lies a sequence of alternating black and dark gray carbonaceous sericite-chlorite and sericite-chlorite slates. Dark gray metasiltstones and silty slates are subordinate in quantity, and metasandstones and light gray quartz metasandstones are rare (Kirillin et al., 2020). The total thickness of the Lunvozhskaya Formation is ca. 2040 m.

The Kyvvozhskaya Formation was excluded from the stratigraphic chart since its section is identical to that of the Lunvozhskaya Formation. The rocks previously attributed to the Kyvvozhskaya Formation now form part of the upper sequence of the Lunvozhskaya Formation (Kirillin et al., 2020).

According to V.G. Olovyanishnikov (1998), deposition of Precambrian rocks of the Volsko-Vymskaya Ridge occurred in a deep-water basin or continental slope environment.

1.4. Substantiation of the Riphean age of clastic successions of Middle Timan

The age of Precambrian rocks of Middle Timan is normally identified on the basis of geological position of the rock units, fossil evidence (acritarchs and stromatolites), and rare K-Ar age determinations. The results obtained by these methods are ambiguous, and this has led to occurrence of numerous local stratigraphic charts shown in Figs. 1.5 and 1.6. The age of the Chetlasskaya Group was established from its geological position in the section and the presence of acritarchs (found in slates of the Vizingskaya Formation). A poor complex of microfossils was reported from the Novobobrovskaya Formation (Kirillin et al., 2020) indicating, in the authors' opinion, its Middle-Late Riphean age. Using the K-Ar method, V.G. Getsen (1987) determined the age of sericite from the Vizingskaya Formation slates as 725 ± 25 Ma, which he believes to be the upper age limit for the rock

accumulation. The Late Riphean age of the Anyugskaya Formation was determined from microfossils (acritarchs), as well as from the presence, at its base, of conglomerates with fragments of the underlying rocks of the Chetlasskaya Group (Kirillin et al., 2020). Almost all of Timan researchers assigned the Bystrinskaya Group to the Late Riphean (Getsen, 1987; Oparenkova et al., 1999; Yakobson et al., 2002; Olovyanishnikov, 2004; Parmuzin et al., 2015; Kirillin et al., 2020). The presumably Late Riphean age of the Pavyugskaya and Paunskaya Formations is based on their position in the section and ambiguous stromatolite and acritarch determinations.

The age of the Vymskaya Group is the most debatable among geologists, ranging from Middle Riphean to Vendian (Figure 1.6). The Pokyuskaya Formation, which lies at the base of the Vymskaya Group, contains a Middle Riphean acritarch complex (Kirillin et al., 2020). When compiling the 1:1 000 000 map, the age of the Lunvozhskaya Formation was accepted as Middle Riphean (Parmuzin et al., 2015; Kirillin et al., 2020), though some authors (Getsen, 1987; Oparenkova et al. 1999) estimate it at the Late Riphean-to-Vendian.

The stratigraphic significance of stromatolites is currently questioned. Stromatolitic buildups may indicate a depositional environment in a basin (desalted or saline zones, or zones with periodically changing fresh and salt water), but by no means the age of sediments (e.g., Dolnik, 2000). However, they may serve as a marker bed in correlations with carbonate successions in neighboring areas (Mikhailenko, 2017).

When using the K-Ar isotope method, one should bear in mind that there are some limitations to it. In the case of the rocks not affected by secondary alteration processes, the K-Ar method is likely to show the age of early diagenesis close to depositional age and, thus, may be considered geologically meaningful. The post-diagenetic processes in the course of geological evolution of a region can cause changes in the chemical composition of rocks and minerals and their transformations resulting in the loss of accumulated radiogenic ^{40}Ar and, therefore, can lead to “rejuvenation” of rock ages (Faure, 1989). It is well known that Precambrian strata of Middle Timan underwent metamorphism of the greenschist facies. From this it follows that K-Ar isotope ages cannot be considered reliable, because metamorphism undoubtedly led to their “rejuvenation”.

Over the past decade, new age determinations were obtained based on U-Th-Pb dating of detrital zircons from Riphean clastic deposits of Middle Timan. Detrital zircons from the Svetlinskaya and Vizingskaya Formations (Udoratina et al., 2017), as well as from the Lunvozhskaya Formation (Soboleva et al., 2019) were dated. Distribution of detrital zircon ages is similar for all three formations likely pointing to their common sedimentary basin and the same source region of clastic

material. The age of the youngest zircon population is within 1022-1122 Ma, which makes it possible to constrain the lower age limit of the rocks as the late Middle Riphean-early Late Riphean.

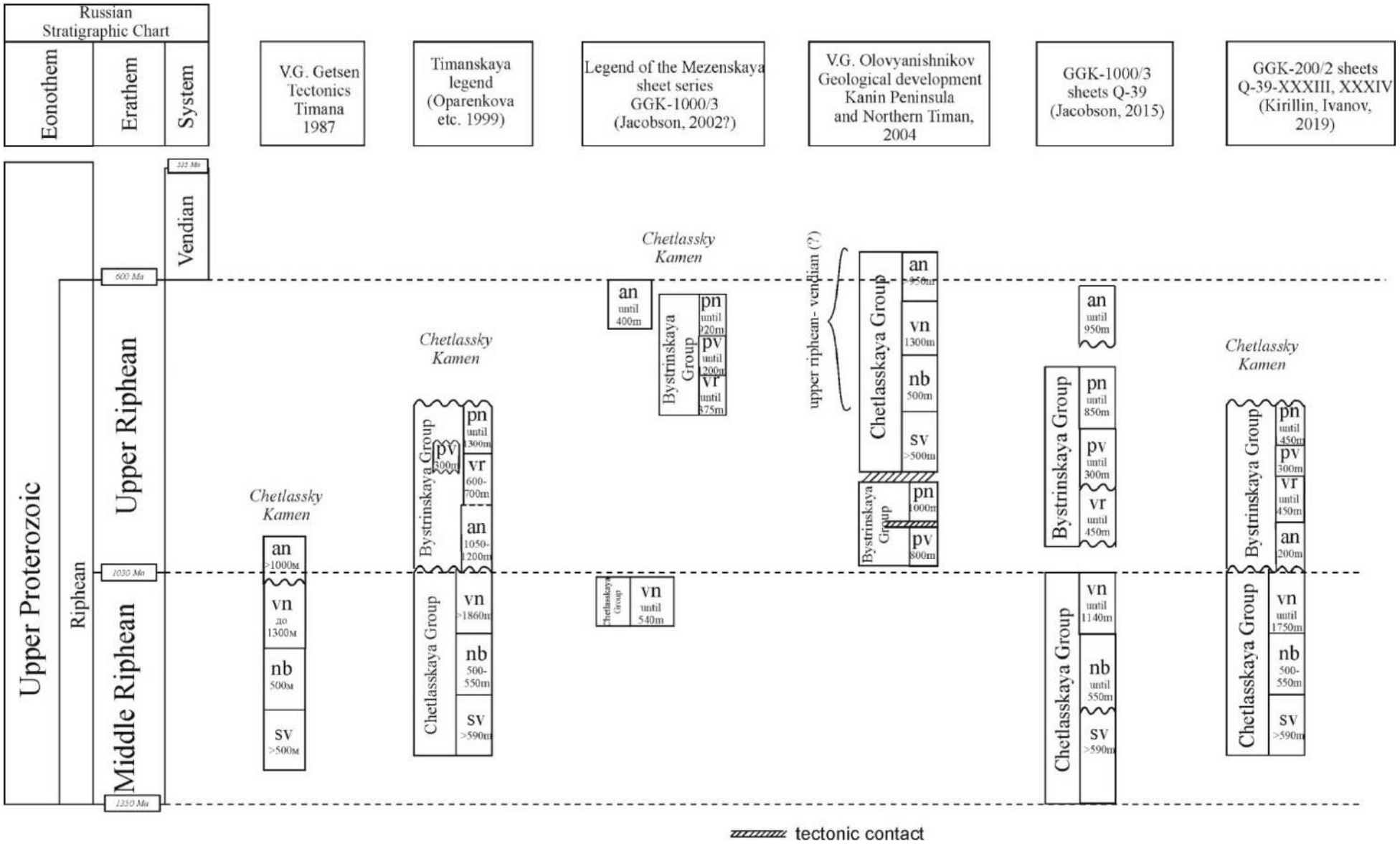

Figure 1.5. Comparison of stratigraphic charts for Riphean deposits in Middle Timan (Chetlassky Kamen) after different authors

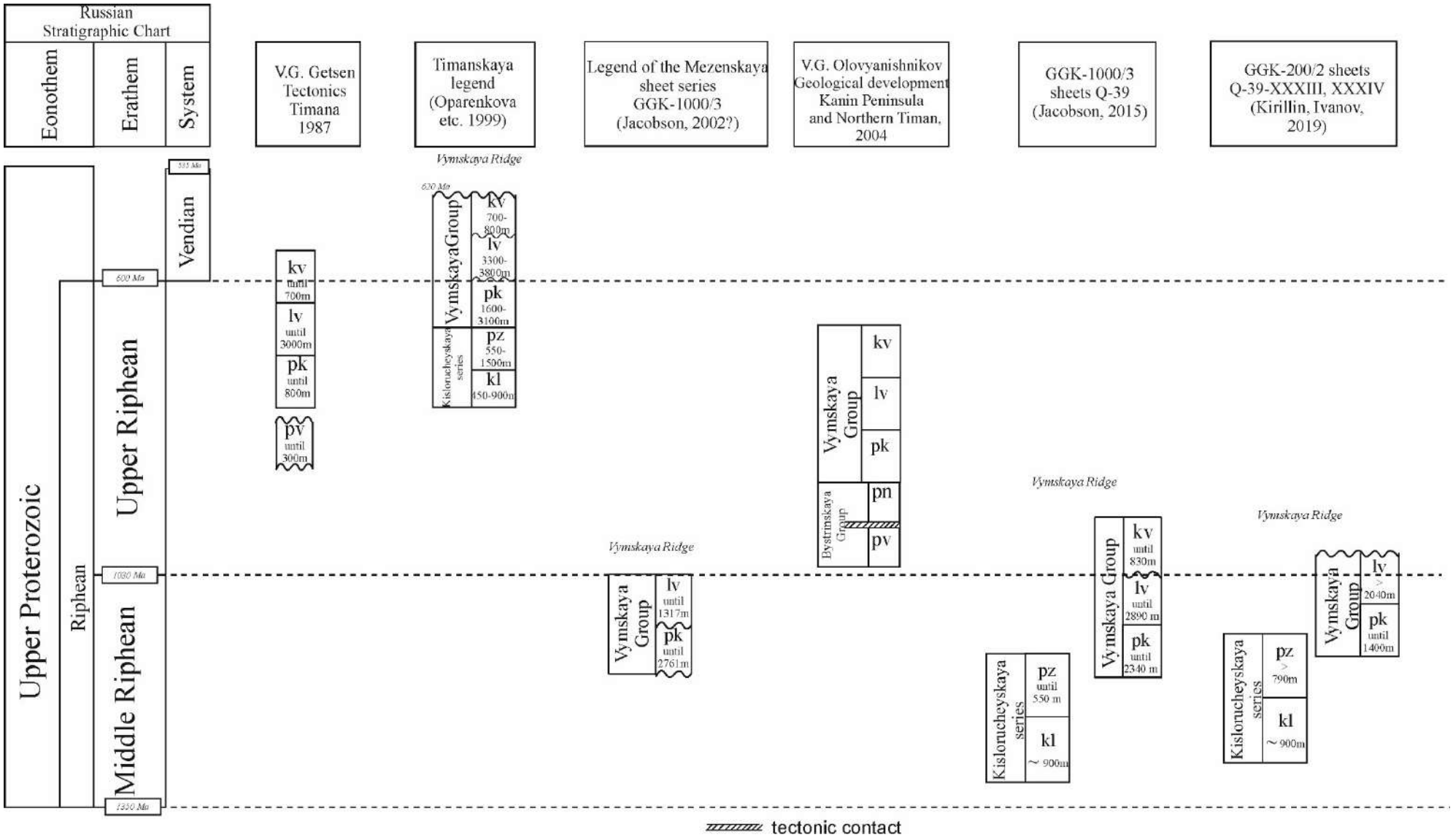

Figure 1.6. Comparison of stratigraphic charts for Riphean deposits in Middle Timan (Volsko-Vymskaya Ridge) after different authors

1.5. Overview of current interpretations of regional tectonics

The problems of the Timan origin and the geological history of the northeastern EEP are still debatable (Olovyanishnikov, 1998). The EEP basement is composed of Archean-Early Proterozoic metamorphic rocks, and the platform cover consists of Late Proterozoic-Cenozoic deposits.

Precambrian rocks of the Timan Range crop out as separated blocks within structural highs (horsts) such as Ochparma, Dzhedzhim-Parma, Chetlassky Kamen, Volsko-Vymskaya Ridge, Tsilemsky Kamen, Northern Timan, and Kanin Peninsula. The accumulation of clastic material during deposition of the Precambrian sedimentary strata in Timan took place on the passive margin of the Baltica paleocontinent. This is evidenced by the facies change from shallow-water sediments (Chetlasskaya Group) to barrier reef sediments (Bystrinskaya Group) in the direction from southwest to northeast. Furthermore, within the Volsko-Vymskaya Ridge, there are observed outcrops of dark sandy slates and flysch-like rocks of the continental slope or a deep-water basin (Vymskaya Group) (Figures 1.7, 1.8) (Olovyanishikov 1998, 2004; Puchkov, 2010; Roberts and Olovyanishnikov, 2004). All studied Riphean strata are metamorphosed to the greenschist facies, except for the Kanin Peninsula where the rocks are in the amphibolite facies (Zonenshain, 1990). The Riphean rocks of Timan are often correlated with coeval deposits of the Bashkirian anticlinorium (Kirillin et al., 2020).

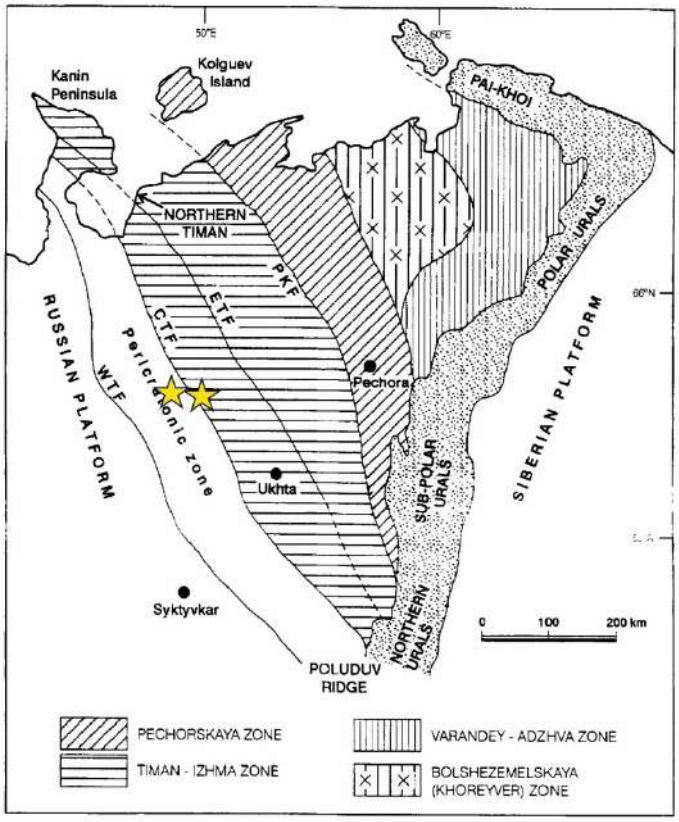

Figure 1.7. Main structural zones of the pre-Paleozoic basement of the Timan-Pechora region (after Roberts and Olovyanishnikov, 2004). Main faults: WTF - West Timan fault; CTF - Central Timan Fault; ETF - East Timan Fault; PKF - Pechora-Kozhva fault. Yellow stars indicate sampling sites for this study.

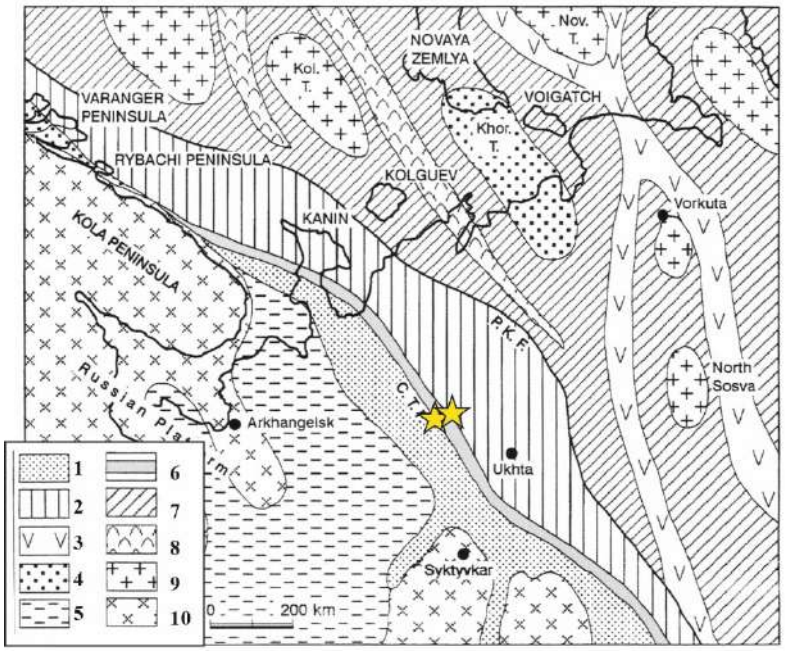

Figure 1.8. Paleogeographic/paleotectonic sketch map showing the inferred position of sedimentary and volcanogenic belts, and basement blocks along the northeastern margin of the East European Craton in the Late Riphean (after Roberts and Olovyanishnikov, 2004). CTF - Central Timan Fault; PKF - Pechora-Kozhva fault; Kol. T. - Kolguev terrane; Khor. T. - Khoreyver terrane; Nov. T. - Novaya Zemlya terrane.

Symbols: 1 - shelf sediments; 2 - continental slope sediments; 3 – island-arc volcanic rocks and carbonate reef rocks; 4 – shallow-marine sediments on microcontinental block; 5 – fluvial and lagoonal sediments; 6 – stromatolite buildups; 7 – marine volcanic-sedimentary rocks; 8 - zones of intense submarine volcanism; 9 – pre-Riphean blocks or terranes in the TPP basement; 10 - Archean and Lower Proterozoic rocks of the EEP basement. Yellow stars indicate sampling sites for this study.

It is believed that formation of the EEP passive margin began in the early Middle Riphean, when spatially separated small grabens were formed under weak extension conditions. The timing of initiation of the EEP passive margin is determined from Rb-Sr isotope ages (1050±26 Ma) and Sm-Nd isochron ages (1040±80 Ma) of mafic dikes and sills in North Timan. The dikes and sills cut through clastic rocks of the Barminskaya Group, thus indicating their Middle Riphean age (Andreichev, 2010). V.G. Getsen (1991) suggested that at the beginning of the Middle Riphean, rift-related troughs had already existed at the site of the present-day Kanin-Timan Ridge, wherein continental and shallow-marine rocks accumulated.

According to N.A. Malyshev (2002), by the late Early Riphean–early Middle Riphean, continental-marginal rifts have transformed into a pericratonal depression passing laterally, toward the present-day eastern slope of Timan and the Izhemskaya depression, into a passive continental margin.

The formed rift zones overlapped and reworked the relatively small earlier grabens, and reached as far as the edge of the pericratonal depression. By the end of the Riphean, the rift zones assumed a similar shape to that of major structural units observed in the present-day basement of the Mezen basin. Overall, the Middle to Late Riphean basins formed within rift troughs and along the northeastern part of the present-day Mezen basin, in a pericratonal depression that was part of the passive margin of the East European Craton (Malyshev, 2002). Deposition of sediments occurred in shallow-marine and lagoonal environments.

Major NW-SE faults in the Timan-Kanin-Pechora region (Figure 1.7) likely represent Early Proterozoic and older tectonic structures reactivated as a result of Middle-to-Late Riphean extension on the Proto-Baltican margin (Roberts and Olovyanishnikov, 2004). In Timan, the main fault zone is the Central Timan fault (CTF) on which the Riphean section is divided into the shelf and slope types (Figure 1.7). Further northwest, along the northern coast of the Kola Peninsula, that very zone is known as the Sredne-Rybachiy fault zone. It extends as far as the Varanger Peninsula in Norway, where it is called as the Trollfjord-Komagelva fault zone (Roberts and Olovyanishnikov, 2004). The deformations here are mainly represented by thrusts, among them low-angle ones, along which the carbonate and clastic sequences of the Riphean section were tectonically juxtaposed and thrust, together, onto the EEP margin.

The folded basement, composed of Riphean strata, extends under the entire Pechora lowland; it was penetrated by drilling to a depth of 4-5 km over a distance as far as Bolshaya Zemlya tundra (Zonenshin, 1990; Kuznetsov, 2006, 2007). In the area up to the boundary of the Izhemskaya depression and the Pechora-Kolva swell, slates similar to those in Timan were recovered, and further northeast, calc-alkaline volcanic rocks of felsic and intermediate composition were penetrated. The basement within the Timan-Pechora Plate is of Baikalian age (~650-550 Ma) and likely includes a number of pre-Baikalian consolidated blocks (Malyshev, 2002 and references therein; Kuznetsov et al., 2010]. The metamorphosed Riphean sequences cut through granites, pegmatites, gabbro, syenites, and nepheline syenites whose isotopic ages range within 614-550 Ma, with rare 500 Ma dates (Andreichev 1998; Andreichev et al. 2018; Makeev et al. 2009; Andreichev et al. 2020; Kuznetsov et al. 2010 and others). Those igneous rocks provide evidence for the Timanian Orogeny that defined the structural style of the region.

According to Roberts and Olovyanishnikov (Roberts et al., 2004), the Middle to early Late Riphean passive margin turned into the active one in the late Riphean. That change in the tectonic regime from extension to compression marked the onset of the Timanian orogenic cycle that peaked during the middle to the end of Vendian (Roberts et al., 2004). It is believed that an accretionary-collision event occurred in the study area in the late Vendian–early Cambrian, which caused the

formation of the Timan Orogen (Orlov et al., 2011; Kuznetsov et al., 2006, 2007; Puchkov, 2010; and others).

In North Timan, igneous rocks are exposed, while in other parts of the Timan Range they are buried under the thick sedimentary cover of the TPP. The syenites, gabbro, and granites of North Timan are dated at 613–600 Ma (Andreichev et al., 2021; Larionov et al., 2004). The ages of granitoids from wells drilled within the Bolshaya Zemlya zone are 558±6 and 607±6 Ma (Andreichev et al. 2022). These data confirm the occurrence of a tectonic event in the Late Riphean-Vendian which led to the formation of the Timan Orogen. Erosion products of igneous rocks of "Timanian" age are widespread in the Vendian-Cambrian rocks of the EEP, TPP, Pay-Khoy, and even Taimyr (Ivleva et al. 2018; Kuznetsov et al., 2010; Kaneva et al., 2015; and others).

Currently, there are two main hypotheses for the formation of the Timan Range structures. Traditionally, the researchers of Timan and the Western Urals considered the formation of the Timan folded zone as related to the accretion of various blocks (terranes?), now located in the TPP basement, to the northeastern part of Baltica (Olovyanishnikov, 1998, 2004; Getsen, 1987; Puchkov, 2010, and others). An important role of the Central Timan Fault in this process has been noted, which at that time functioned as a large thrust along which weakly metamorphosed deep-water deposits of the eastern zone were thrust onto the shallow-water sediments of the western zone (Olovyanishnikov, 2004). “In the northeastern part of the TPP, in the basement of the Pechora-Kolva Megaswell, there are widespread sedimentary and volcanic-sedimentary rocks metamorphosed and deformed to high grades, including collisional igneous rocks. The inner region of the “Timanides” is a system of microcontinents (Khorvey, Kolguev, Novaya Zemlya, etc.) and island arcs separated by rift (spreading?) zones that built up northeastern Baltica in the late Vendian–early Cambrian in the process of lateral accretion” (Olovyanishnikov, 2004) (Figure 1.9).

The second hypothesis assumes that the southwestern part of the "Timanides" (pre-Ordovician rocks of Timan and the Timanian block of the TPP basement) and the pre-Ordovician deposits of the southern Urals (Kvarkushinsky and Bashkirsky uplifts) were deposited on the passive margin of Baltica (Kuznetsov et al., 2006, 2007). The basement rocks of the northeastern part of the TPP (Bolshaya Zemlya block) and the ancient rock complexes of the northern Urals (Lyapinsk anticlinorium) were formed on the active margin of Arctida (paleocontinent with continental crust blocks in the basement such as Svalbard, Kara, Barents Sea, Lomonosov Ridge, Novosibirsk, and Chukotka) and in the collision zone between Arctida and Baltica (Kuznetsov et al., 2006, 2007). The main tectonic event, in the opinion of authors of the second hypothesis, was the collision of the northeastern part of the Baltica paleocontinent (Timanian passive margin) and the Arctida

paleocontinent (Bolshezemel active margin) that occurred at the Vendian–Cambrian boundary (Kuznetsov et al., 2006, 2007) (Figure .1.10).

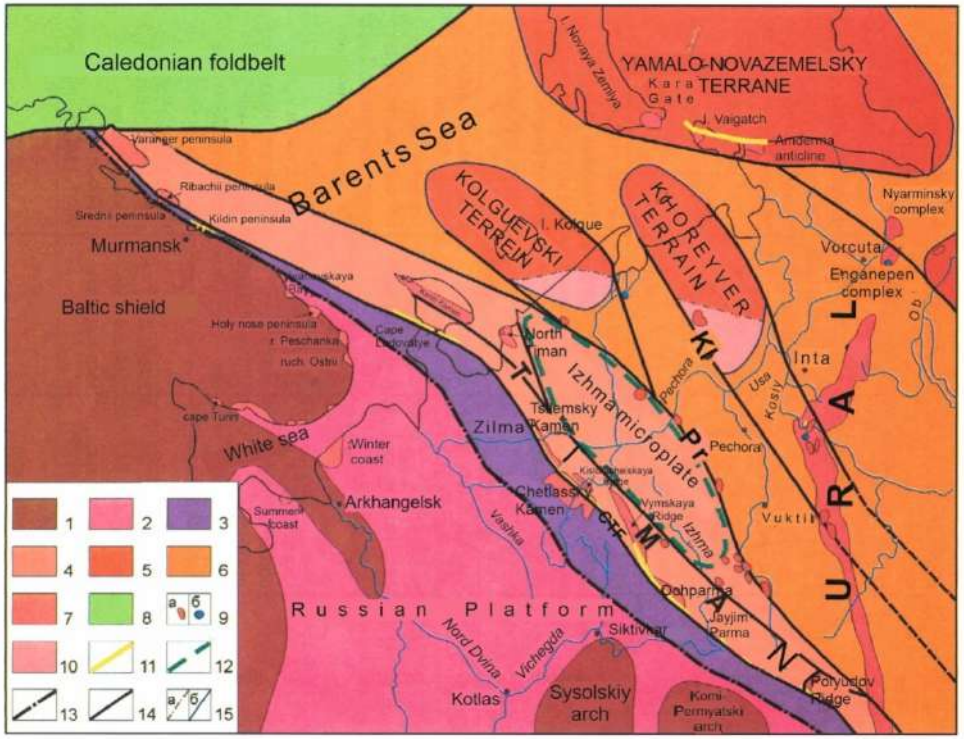

Figure 1.9. Geodynamic map of the northeastern EEP basement (after Olovyanishnikov, 2004)

1 - Lower Precambrian rocks; 2 – Lower Precambrian basement with Upper Precambrian platform cover; 3 – Pre-Timan craton margin (shallow shelf zone in the Late Riphean); 4 - zone of deep shelf and continental slope in the Late Riphean; 5 - pre-Late Riphean terranes; 6 – inner part of Timanides; 7 – outcrops of Upper Precambrian rocks; 8 - Caledonides; 9a – pre-Ordovician granites; 9b – ophiolites and deep-sea complexes; 10 – Vendian-Cambrian (?) volcaniclastic complex; 11 - stromatolitic reefs; 12 - 13 – boundaries of: 12 - Izhma microplate,13 – inner boundary of the Pre-Timan craton margin; 14 - faults: CTF - Central Timan, Pr - Pripechora, Kl - Kolva; 15 – boundaries of: a) volcaniclastic complexes; b) terranes.

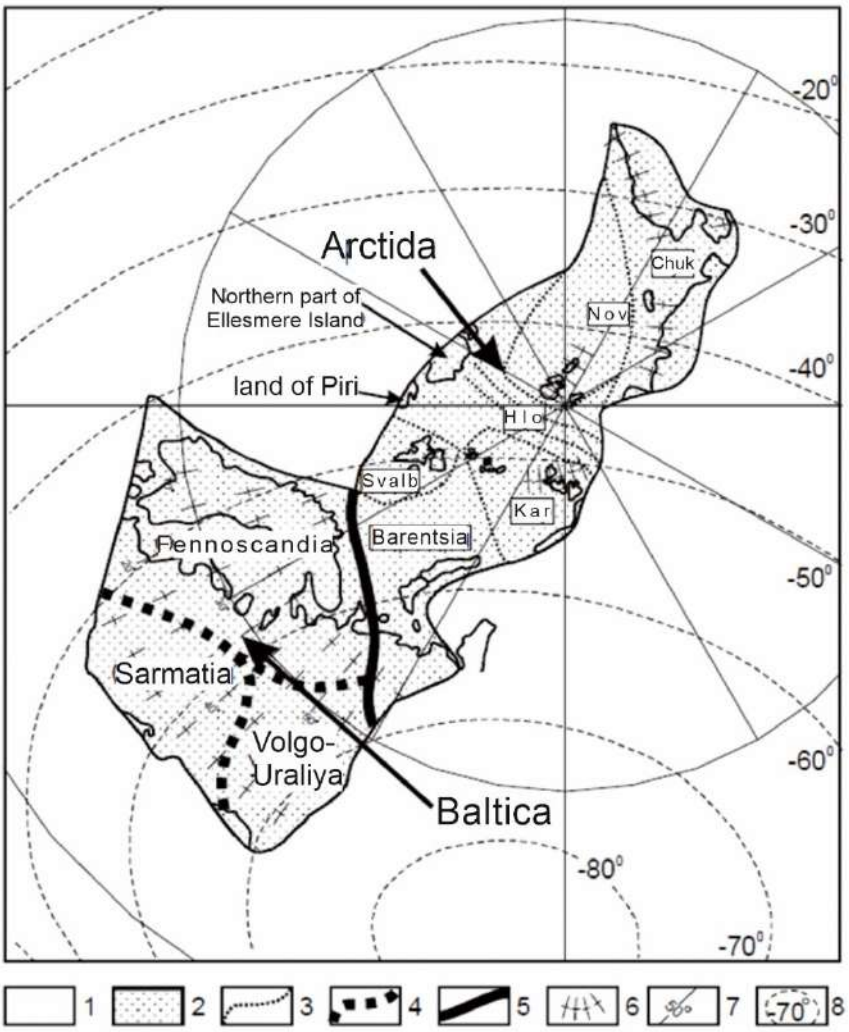

Figure 1.10. Paleotectonic reconstruction for the early Cambrian (after Kuznetsov et al., 2007 and reference therein). 1 – ocean basin; 2 - paleocontinent; 3 – boundaries of continental crust blocks of the Arctida paleocontinent; (4) boundaries of continental crust blocks of the East European paleocontinent (Baltica); (5) collision zone (Pripechora suture) of the East European paleocontinent (Baltica) and Arctida; 6 - nodes of modern coordinate grid (intersections of modern latitudes and longitudes); 7 - modern coordinate grid; 8 – ancient coordinate grid.

Chapter 2. Analytical methods

This work is based on the study of accessory minerals (zircon, rutile and tourmaline) extracted from Precambrian sedimentary rock samples collected by the author in Middle Timan (Chetlassky Kamen and Volsko-Vymskaya Ridge) during field work in 2015 and 2016.

A total of 40 samples have been studied. U-Pb detrital zircon dating was performed on 8 samples, composition of detrital tourmaline was determined in 8 samples, rutile was dated from 2 samples, and Lu-Hf isotopic data were obtained for detrital zircon grains from 5 samples. Petrographic description was done for 40 thin sections covering all studied Riphean stratigraphic units. Positions of the rock sequences in the stratigraphic section are presented above (Figure 1.4).

2.1. Petrography

At the first stage of this study, thin sections of the sampled Riphean rocks of Middle Timan were prepared and examined under a Leica DM EP optical microscope. A detailed petrographic description is given in the next chapter.

In addition to thin section descriptions, Q–F– L[1] diagrams were plotted using the Gazzi–Dickinson method (Dickinson, 1970; Ingersoll et al., 1984), based on counting of at least 300 detrital grains exclusive of matrix and/or cement (the thin section is moved at equal distances and grains located at the intersection of crosshairs are counted). The calculation of lithic grains by this method has a specific drawback: for instance, if the clastic fraction of sandstones contains granite fragments composed of quartz and feldspar, the dimensions of which are larger than silty in size, they are registered as quartz and feldspar rather than a rock (granite) lithoclast (Dickinson, 1970; Ingersoll et al., 1984). However, the number of such grains is insignificant in the studied samples, and we used both the classical Q-F-L diagram after Pettijohn (1975) and the Q–F–L diagram after Dickinson et al. (1983) for the interpretation of metasandstone compositions.

2.2. Mineralogy

Preliminary preparation of samples for analyses was carried out at the Institute of Precambrian Geology and Geochronology, Russian Academy of Sciences (St. Petersburg) in compliance with the routine procedure. Samples with a weight of 1.5–2.0 kg were crushed to fragments of ca. 0.25 mm in

[1] Here Q is quartz, F is feldspars, L is rock fragments.

size, washed, and dried. This was followed by magnetic separation to remove highly magnetic minerals. The heavy mineral portion was then subjected to heavy liquid (bromoform) separation, and the obtained heavy mineral concentrate was rinsed with distilled water and dried. Next, the heavy fraction was treated with dilute methylene iodide; washed with alcohol and dried. Finally, separation into electromagnetic and non-magnetic fractions was made in accordance with the paramagnetic properties of minerals.

Rutile and tourmaline grains were separated out of the heavy mineral fractions after extraction of zircons. Tourmaline grains were arranged in rows and mounted in epoxy and polished. Rutile grains handpicked under binocular were mounted on standard epoxy disks and polished for further (LA-ICP-MS) U-Th-Pb dating.

Zircons from six samples (9016/2, 9020/3, 9048/5, 9034/2, 9007/1, 9007/4) were mounted on standard epoxy disks.

Two samples (9045/1 and 9017/4) were dated at the Laboratory of the University of Austin (Texas, USA). Zircon grains were mounted (no polishing) on standard round disks (2.5 cm in diameter) with double-sided tape.

To determine the degree of roundness of the dated tourmaline and zircon grains the author (Brusnitsyna et al., 2021) used the scale after (Pettijohn, 1975), which enables their classification to one of the following groups: rounded, subrounded, subangular and angular (Figure 2.1).

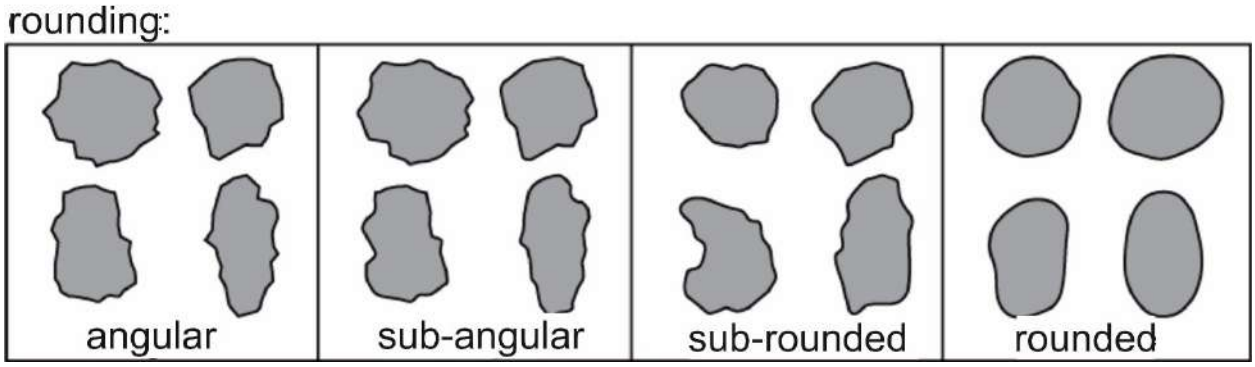

Figure 2.1. Roundness classes of minerals after (Pettijohn 1975)

2.3. Chemical composition of tourmaline

For chemical composition analysis, tourmaline grains were extracted from 8 samples collected from six Riphean formations in Middle Timan such as Paunskaya (9034/12; 9034/2), Vizingskaya (9048/5),

Novobobrovskaya (9020/3), Svetlinskaya (9016/2), Lunvozhskaya (9007/5; 9007/ 4) and Pizhemskaya (9064/2). Positions of samples in the section are shown in Figure 1.4.

The chemical composition of tourmaline was analyzed on a Hitachi S-3400N scanning electron microscope equipped with an AzTec Energy X-Max 20 energy dispersive spectrometer (analytical conditions: accelerating voltage 20 kV, beam current 1 nA, data acquisition time 30 s (excluding dead time)). Natural and synthetic compounds were used as standards. The measurement accuracy for major elements is within ~3% of the actual amount; for trace elements, within ~ 10%. The chemical formulas of tourmalines were calculated on the basis of 15 (Y + Z + T) atoms per formula unit, with the assumption that: (1) boron content is taken to be 3, and O and OH contents are calculated from the charge balance, (2) X position may be vacant; and (3) all iron is taken to be divalent.

2.4. U-Th-Pb dating of detrital zircons and rutiles and Lu-Hf isotopic-geochemistry of detrital zircons

The U–Th–Pb (LA-ICP-M) dating of zircons from six samples (9016/2, 9020/3, 9048/5, 9034/2, 9007/1, 9007/4) and Lu-Hf isotopic analyses were performed at the University of Oslo on a Nu Plasma HR mass spectrometer with a CETAC Nd-YAG 213 laser. Isotope ratios and ages are given within 1σ error. Crater diameter did not exceed 40 μm. Calibration was carried out using GJ1 ($^{206}Pb/^{238}U$ = 601.7 ± 1.3 Ma, $^{207}Pb/^{206}Pb$ = 607 ± 4 Ma; Jackson et al., 2004), 91500 (1065 ± 1 Ma; Wiedenbeck et al., 1995) and A382 (1877 ± 2 Ma; Huhma et al., 2012) standards. The analytical procedure is described in detail in (Andersen et al., 2009, 2019; Rosa et al., 2009). The Lu-Hf-isotopic study was conducted at the University of Oslo on the same Nu Plasma HR mass spectrometer as was used for zircon dating. Zircons with less than ±10% discordance were only analyzed. Crater diameter was 55–60 μm. Prior to each analysis a 30 s background measurement was made. The counting time of 120-150 seconds was used in order to obtain accuracy within 1σ error. The isotope ratios were calculated using Nu Plasma software. Calibration was made according to LV-11 standard, which is a euhedral nepheline syenite crystal from Laven Island in Oslo Rift (290 Ma, from mineralogical collection of the Museum of Natural History, University of Oslo). The $^{178}Hf/^{177}Hf$ ratios higher than 1,46741 or lower than 1,4671 (2-12%) were excluded from the following interpretation. The procedure of the Lu-Hf isotopic-geochronological study is described in detail in (Elburg et al., 2013). The results of the Lu-Hf isotopic study of detrital zircons are given in Appendix 4.

Zircons from samples 9017/4 and 9045/1 were analyzed at the UTChron geochronology facility in the Department of Earth Sciences (Jackson school of geoscience) at the University of Texas, Austin,

TX, USA. All grains were depth-profiled using a ThermoElement2 mass spectrometer equipped with 193 nm Excimer laser. For U-Th-Pb geochronological analyses of detrital zircons, the masses ^{202}Hg, ^{204}Pb/Hg, ^{206}Pb, ^{207}Pb, ^{208}Pb, ^{232}Th, ^{235}U, and ^{238}U were measured. Data reduction was performed using the Igor Pro-based (Paton et al., 2011) Iolite software with the VizualAge data reduction scheme (Petrus and Kamber 2012). GJ1 (^{206}Pb / ^{238}U 601.7 ± 1.3 Ma, ^{207}Pb / ^{206}Pb 607 ± 4 Ma; Jackson et al. 2004) was used as a primary standard, and Plesovice (internal standard - PL-1, 337.1 ± 0.4 Ma; Sláma et al., 2008) was used as a secondary standard. No common Pb correction was applied. All zircon ages are given with 2σ error, except for standard samples. Obviously erroneous results and data obtained for minerals other than zircon were excluded from age calculation. Concordia plots constructed with the use of VizualAge™ live concordia diagramm (Petrus and Kamber, 2012) were corrected in the course of analyses.

All detrital zircons analyzed are older than 1 Ga, so the zircon ages mentioned hereafter are ^{207}Pb/^{206}Pb ages. The KDE (kernel density estimation) plotting of the U-Th-Pb age distributions was performed using the DensityPlotter software (Vermeesch, 2012). In plotting and further interpretation of data, ages with discordance within ±10% were only taken into account. Discordance was calculated from the formula: 100*(1-(^{207}Pb/^{206}Pb)/(^{206}Pb/^{238}U). The results of zircon dating are presented in Appendices 1and 2.

A statistical comparison of the detrital zircon age distributions from the studied deposits was made based on the Likeness Test (Satkoski et al. 2013). The test involves comparison of similarities or differences between a pair of samples from which detrital zircons were dated. After constructing the cumulative curves, a confidence interval was calculated for each of them. Next, the degree of overlap of confidence intervals was calculated (Andersen et al., 2015, 2018). In the case when the confidence intervals of two cumulative curves overlap throughout the probability area, the samples are coincident within error stemming from random selection of zircon grains for dating. If the overlap is partial, the portion of the probability area wherein the confidence intervals overlap is a measure of similarity (0) and difference (1-0) between the two curves (Appendix 5).

U-Th-Pb (LA-ICPMS) detrital rutile dating

Detrital rutiles were handpicked from the heavy fractions of two samples 9045/1 and 9007/3.

The prepared epoxy disks were loaded into a large volume Helix cuvette and analyzed using a Photon Machines Analyte G2 Excimer Laser combined with a ThermoElement2 single collector, magnetic sector ICP-MS (Isotope Laboratory of the University of Texas in Austin). The U-Th-Pb analysis of rutile was performed under the same ablation and ICP-MS data acquisition conditions as used for U-Th-Pb zircon analysis. Crater diameter did not exceed 40 μm. Rutile R10 (1090 ± 0.9 Ma;

Luvizotto et al., 2009) was used as primary standard, and rutile R19 (489.5 ± 0.9 Ma; Zack et al., 2011) as secondary standard. The primary standard rutile $^{238}U/^{206}Pb$ R10 (Luvizotto et al., 2009) was used for age calculation and fractionation control, while the secondary standard rutile R19 (Zack et al., 2011) was used to monitor data quality. Data reduction was performed using Iolite software with the VizualAgeDRS (Ludwig, 2003; Paton et al., 2011; Petrus and Kamber, 2012). Pb correction was applied based on the modeling of lead composition (after Stacey and Kramers, 1975). Analytical results are presented in Appendix 3 in the form of KDE plots, as in the case with detrital zircons. In KDE plotting, we used ages obtained from $^{206}Pb/^{238}U$ isotope ratios; discordance was not calculated (Zack et al., 2011).

Chapter 3. Petrographic, geochemical and isotopic-geochronological studies of the Middle Timan clastic rocks

3.1. Petrography of Riphean rocks of the Chetlassky Kamen and the Volsko-Vymskaya Ridge

Location coordinates of all studied samples are given in Appendices 1 and 2, and their position in the composite stratigraphic section is shown in Chapter 1 (Figure 1.4).

A petrographic study of the Chetlassky Group metasedimentary rocks (Figure 3.1.) showed that sandstones of the Svetlinskaya Formation compositionally correspond to subarkoses, sublitharenites and litharenites, while sandstones of the Novobobrovskaya and Vizingskaya Formations, in which feldspar clasts prevail over rock fragments, have compositions varying from arkoses to quartz arenites. Two samples from the Lunvozhskaya Formation are subarkose and quartz arenite.

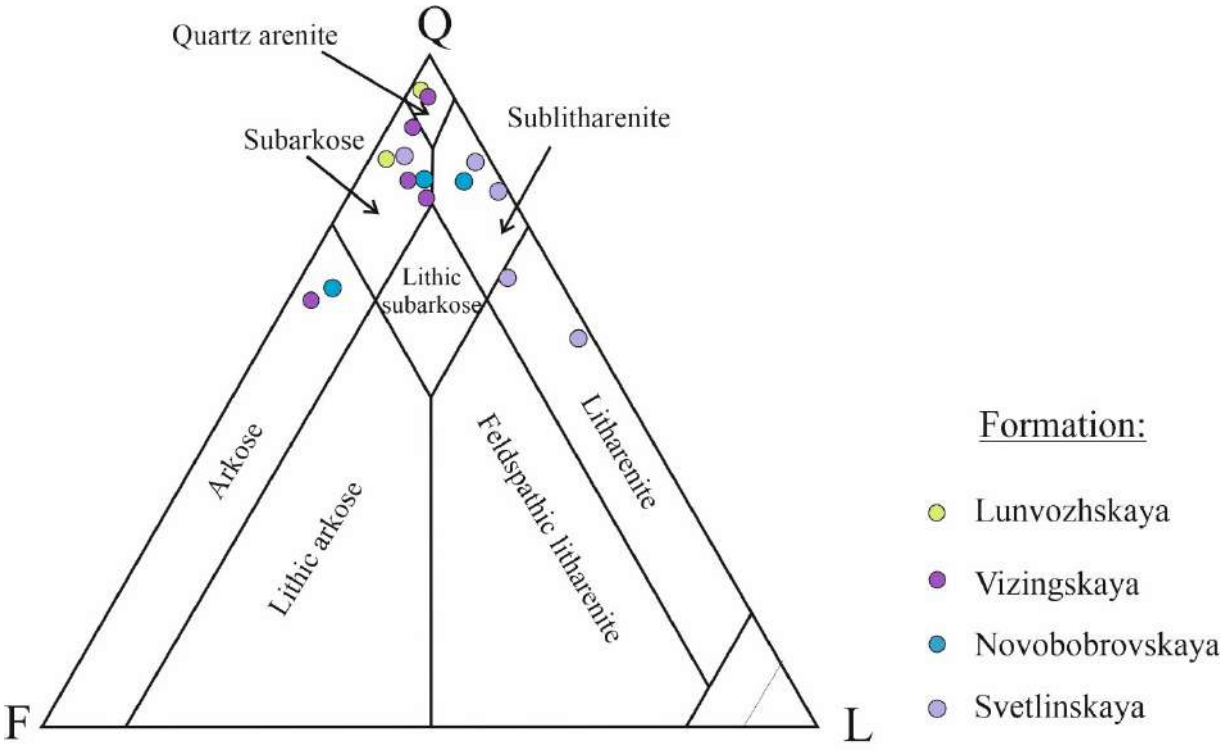

Figure 3.1. Classification diagram (after Pettijohn, 1975)

Chetlasskaya Group

Svetlinskaya Formation (Fig.3.2)

Petrographic description of thin sections was made for six samples from the Svetlinskaya Formation collected from a section in the central part of the Chetlassky Kamen, in the upper reaches of

the Mezen River. All six samples were classified as litharenites, sublitharenites, and subarkoses. They have a psammitic texture, with an interstitial and basal cement of chlorite-sericite composition. The clastic fraction of the rocks is represented by variably rounded quartz and feldspar clasts. Quartz grains are subrounded and rounded in shape. The grain size varies over a wide range from 0.1 mm to 0.5 mm. One sample (9016/1) contains rounded quartz grains of gravel size (4-5 mm). The quartz content varies within 73-85% of the total rock volume. Feldspar occurs in subordinate amount (not more than 10%). All samples show a fine-grained saussurite (?) aggregate developed after feldspar grains, which looks like a thin gray film in a thin section. Metasandstones of the Svetlinskaya Formation contain fragments of various rocks (sandstones and siltstones?). Their content varies from 4 to 19%. Secondary minerals are represented by fine-grained aggregates of chlorite and sericite (fine-grained muscovite) in interstices between quartz and feldspar grains. In sample 9016/2, the amount of secondary chlorite reaches 7-10% of the total rock volume. The sericite and chlorite grains are oriented parallel to each other. In sample 9017/1, biotite occurs interstitially between quartz grains, with characteristic pleochroism in brown shades. Sample 9017/2 contains, in addition to sericite and chlorite, secondary feldspar filling fractures in the rock. Accessory minerals in the studied metasandstones include zircon, tourmaline, muscovite, and ore mineral (hematite, pyrite?).

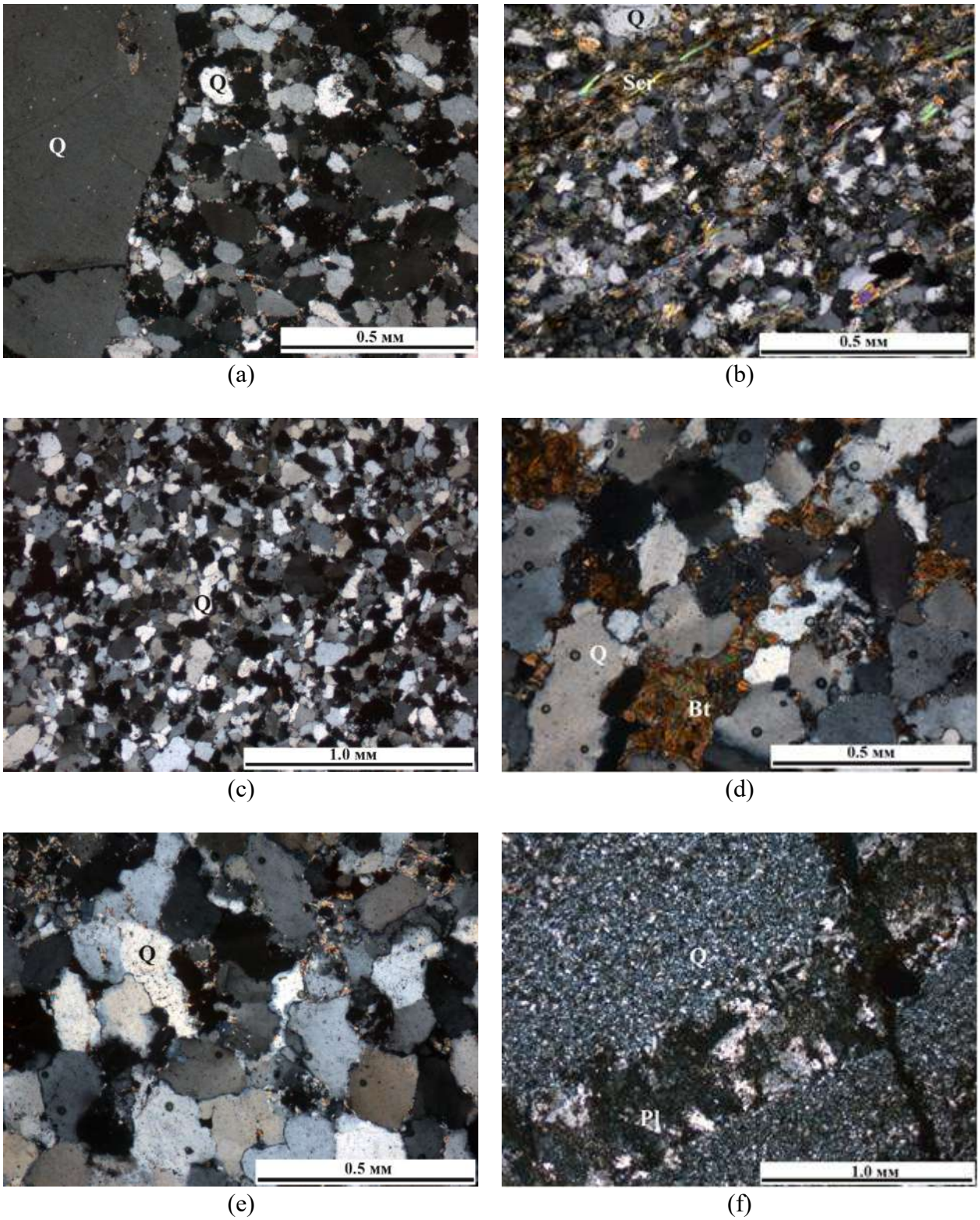

Figure 3.2. Photos of thin sections of the Svetlinskaya Formation metasandstones. Crossed nicols. (a - 9016/1; b - 9016/2; c - 9019/1; d - 9017/1; e - 9020/2; f - 9017/2)

Bt – biotite; Q - quartz; Ser – sericite; Pl - plagioclase

Novobobrovskaya Formation (Figure 3.3)

Petrography of four samples of the metasedimentary rocks was described. All of them were collected from the Chetlassky Kamen, two from a section in the upper reaches of the Mezen River and the other two from a section in the riverhead of Bobrovaya (a tributary of the Svetlaya River, which in itself is a tributary of the Pechorskaya Pizhma River). The Novobobrovskaya Formation is composed of arkoses, subarkoses, and sublitharenites. The rocks have a psammitic, inequigranular texture, silty grains are less often, with basal and interstitial chlorite-sericite cement. The clastic fraction is dominated by subrounded quartz grains (34 - 81%). One sample (9062/3) contains rounded quartz grains and single gravelly grains (2-3 mm). In two samples (9062/1 and 9020/3), the size of quartz grains varies from 0.1 to 0.3 mm. In sample 9028/1, the quartz grain size is within 0.02- 0.05 mm, while sericite and hematite grains are smaller, up to silt size. Feldspar is found in all the rocks studied; its amount rarely exceeds 9-16%. A fine-grained (virtually cryptocrystalline) aggregate of grayish saussurite (?) is often developed after feldspar grains. Partial replacement of feldspar by chlorite is observed. Secondary sericite is also found in all rocks of the Novobobrovskaya Formation. It forms thin flakes, tabular and acicular grains with a size rarely exceeding 0.05 mm. In sample 9028/1, the amount of sericite makes up 15–20% of the total rock volume. It occurs mostly in interstices between quartz grains. That sample (9028/1) also displays a high-Fe zone in the form of thin curved partings enriched in hematite (?). Present are columnar crystals of tourmaline replaced by hematite. The crystal size is much larger (up to 0.25 mm) than in the groundmass. In sample 9062/1, carbonate (calcite?) was found among secondary minerals. It forms irregular aggregates filling interstices between quartz grains and voids. Accessory minerals in the studied rocks include zircon, tourmaline, and ore mineral (pyrite?).

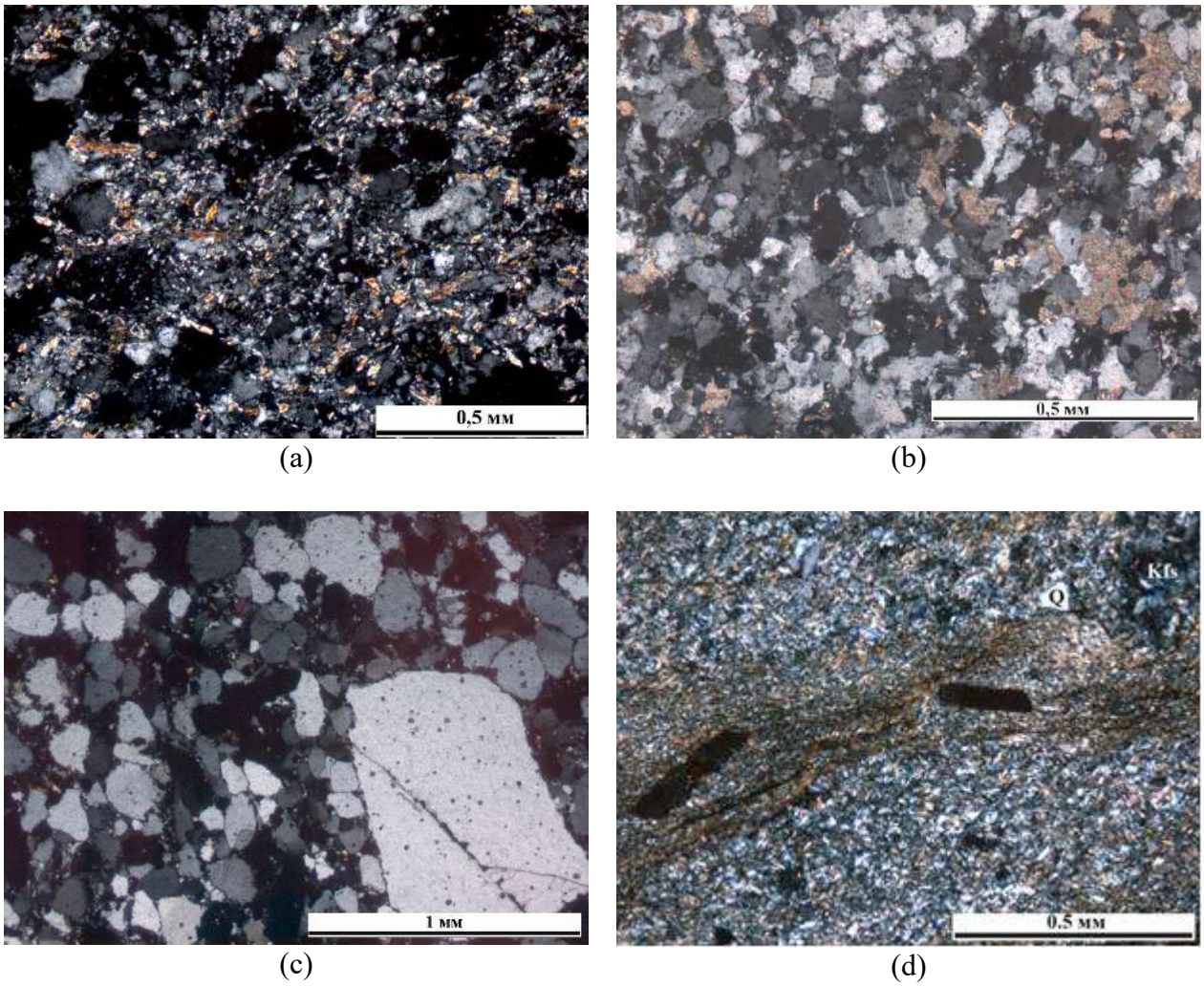

(a) (b)

(c) (d)

Figure 3.3. Photos of thin sections of the Novobobrovskaya Formation sedimentary rocks. Crossed nicols. (a - 9020/3; b - 9062/1; c - 9062/3; d - 9028/1)

Bt - biotite; Q - quartz; Ser - sericite; Kfs - potassium feldspar

Vizingskaya Formation (Figure 3.4)

The petrographic description of thin sections of the Vizingskaya Formation rocks was made for seven samples collected from two sections on the Kosyu River (right tributary of the Mezen River) in the central part of the Chetlassky Kamen. Composition of the rocks corresponds to arkoses, subarkoses, and quartz arenites consisting mainly of quartz (60-90%), feldspar (up to 30%), and secondary sericite (3-10%). The texture of the rocks is psammitic, with interstitial chlorite-sericite cement. Quartz grains are subrounded. The grain size does not exceed 0.25 mm, normally 0.1 mm. Feldspar forms tabular grains 0.1-0.05 mm in size. Sericite occurs as fine flakes filling interstices between quartz and feldspar grains. Sericite-quartz metasiltstones have a fine-granular silty texture with less often grains of sand size. A slaty structure defined by parallel orientation of micaceous minerals in the interstitial and basal cement is typical. The clastic fraction consists of quartz (1-3%),

feldspar (up to 3%) and rare grains of muscovite. The metasiltstones also contain fine-grained aggregates of secondary chlorite that appear to have replaced feldspar (?). The groundmass consists of chlorite in association with sericite. In the middle reaches of the Kosyu River, a few meters thick zone of metasomatically altered sandstones composed of quartz and feldspar was sampled. Metasomatic alteration is expressed in the formation of acicular and radiating-columnar chlorite and amphibole crystals filling fractures and cavities in the rock. The size of amphibole crystals attains 1.5-2 mm. Amphibole is greenish-blue, with pronounced pleochroism and high interference colors. Chlorite is greenish-brown and shows low interference colors, sometimes an anomalous indigo-blue color.

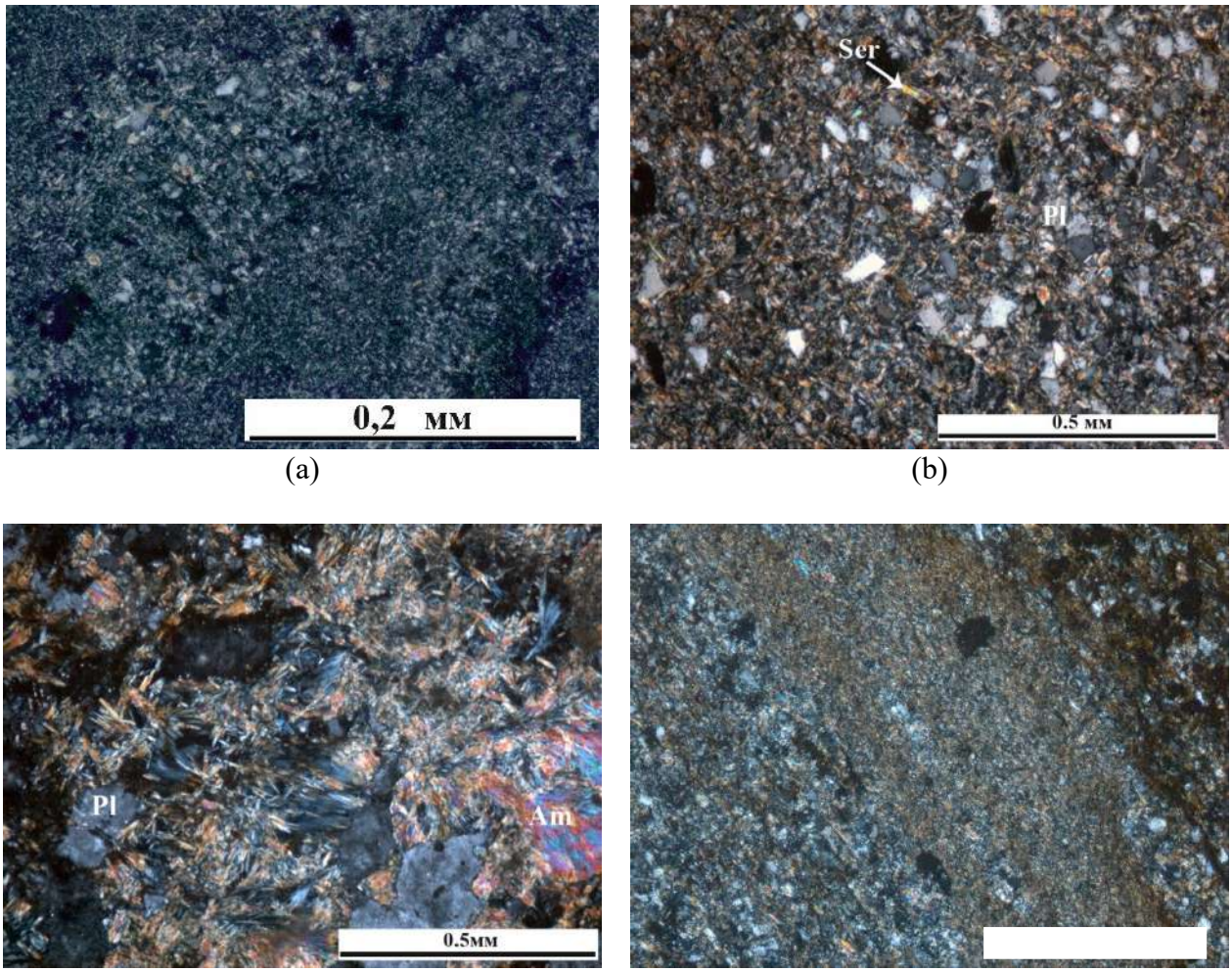

(a) (b)

(c) (d)

Figure 3.4. Photos of thin sections of the Vizingskaya Formation metasedimentary rocks. Crossed nicols. (a - 9048/5; b - 9030/1; c - 9044/4; d - 9048/4)

Pl - plagioclase; Q - quartz; Ser - sericite; Am – amphibole

Bystrinskaya Group

The Bystrinskaya Group, consisting of the Vorykvinskaya, Pavyugskaya, and Paunskaya Formations, outcrops along the northeastern edge of the Chetlassky Kamen. The Vorykvinskaya Formation was not sampled; therefore, the petrographic description of the Bystrinskaya Group begins with the Pavyugskaya Formation.

Pavyugskaya Formation (Figure 3.5)

The Pavyugskaya Formation consists of dolomites of varying texture and color, with stromatolites present at some levels of the section. Samples were collected from a pit bottom on the right bank of the Vorykva River. Dolomites are predominantly fine-grained, locally slaty. They consist of dolomite (90-95%), quartz (3-5%), sericite (1%), and calcite (<1%). Sample 907/2 consists of rhombohedral dolomite grains with smooth edges up to 0.2–0.05 mm in size. Also found are rare rounded grains of quartz with up to 0.1 mm size. The texture is medium-crystalline, mosaic. Sample 905/2 has a bedded microstructure defined by alternation of partings composed of different-sized dolomite grains. The rock is crosscut by curved thin (0.5-1 mm) quartz and sericite beds saturated with fine-grained aggregates of iron hydroxides.

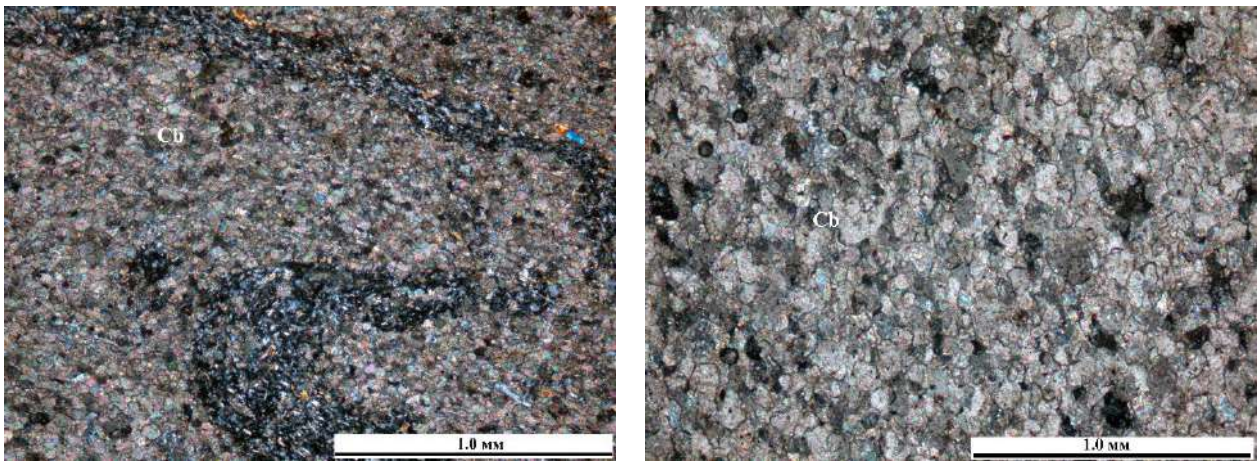

(a) (b)

Figure 3.5. Photos of thin sections of the Pavyugskaya Formation carbonate rocks. Crossed nicols. (a- 905/2; b - 907/2)

Paunskaya Formation (Figure 3.6)

The Paunskaya Formation includes carbonate and clastic rocks. Clayey limestones, dolomites, and limestones are described from the lower part of the section, while metasandstones, sericite-quartz metasiltstones and carbonaceous slates dominate in the upper part. The petrographic description was made for ten samples, of which seven were taken from a section on the right bank of the Lower Paun River (a tributary of the Svetlaya River) and two from a pit bottom on the right bank of the Vorykva

River. Sericite-quartz metasiltstones (metasubarkose in composition?) have a silty texture, with interstitial chlorite-sericite cement. The clastic fraction is composed of quartz (1-5%) and secondary minerals such as sericite (85-90%), chlorite (1-3%), and hematite (1-3%). Rare quartz grains have subangular and subrounded shape, and are up to 0.1 mm in size. The rock structure is slaty, which is due to parallel orientation of sericite and chlorite flakes in the rock cement. Secondary chlorite occurs in the rock matrix and also replaces clasts (probably of primary feldspar). Hematite was found in two samples (904/1 and 902/2); it occurs as fine-grained aggregates unevenly distributed in partings with a thickness varying from 0.1 to 1 mm.

The carbonate rocks of the Paunskaya Formation vary widely in composition and texture. Common to all samples is well-pronounced bedding or banding. All studied samples contain 65-80% of carbonates (dolomite and calcite?), 1-5% quartz, and 1-3% sericite. Secondary minerals are represented by fine-grained aggregates of iron hydroxides and biotite (sample P9034/5). The rock banding is defined by alternation of thin carbonate and sericite-quartz beds. Samples K901/2, 901/5, K901/3 and P9034/4 contain zones, partings or lenses enriched with iron hydroxide minerals. Sample P9034/5 includes thin (up to 0.5 mm) beds consisting of thin-columnar, brown biotite crystals. In samples K901/2 and K901/3, the carbonate grains have a similar to oolite shape; they are dark brown (possibly ankerite?) in the core and lighter in the rims.

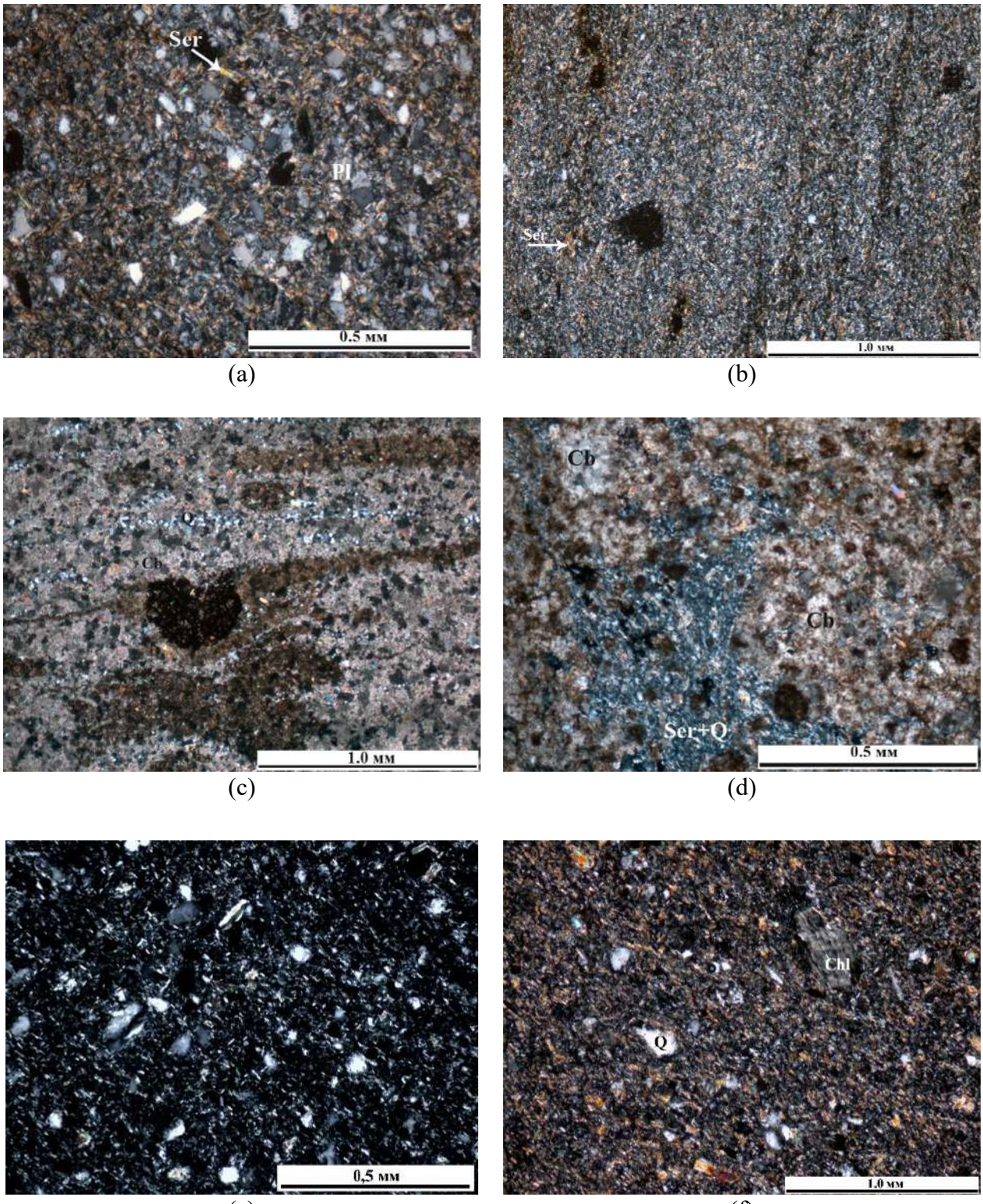

Figure 3.6. Photos of thin sections of clastic (a, b, e, f) and carbonate (c, d) rocks of the Paunskaya Formation. Crossed nicols. (a - 9034/1; b - 904/1; c - K901/2; d - K901/3; e - 9034/2; f - P9034/8)

Q - quartz; Pl - plagioclase; Ser - sericite; Chl - chlorite; Cb - carbonate (dolomite)

The Volsko-Vymskaya Ridge includes the Vymskaya and Kislorucheiskaya Groups.

Kislorucheiskaya Group

The Kislorucheiskaya Group includes the Kleonovskaya and Pizhemskaya Formations. A petrographic description was done for the rocks of the Pizhemskaya Formation.

Pizhemskaya Formation (Figure 3.7)

Petrographic description of thin sections was done for two samples taken from a section in the upper reaches of the Lower Vidzyu River. In terms of lithology, both samples have a similar composition corresponding to metasublitarenites and meta-arkoses. The clastic fracture of the rocks is dominated by rounded quartz grains set in interstitial sericitic cement. A characteristic feature of the rocks is the presence of biotite in the clastic portion, which occurs as tabular crystals and irregularly shaped aggregates. Biotite is brown-green, with distinct pleochroism and high interference colors. Accessory minerals are magnetite (up to 3%) and tourmaline (up to 1%). Tourmaline is only found in sample 9064/1, where it forms columnar crystals with distinct pleochroism from pale pink to dark blue. Sample 9062/2 is characterized by the presence of secondary carbonate.

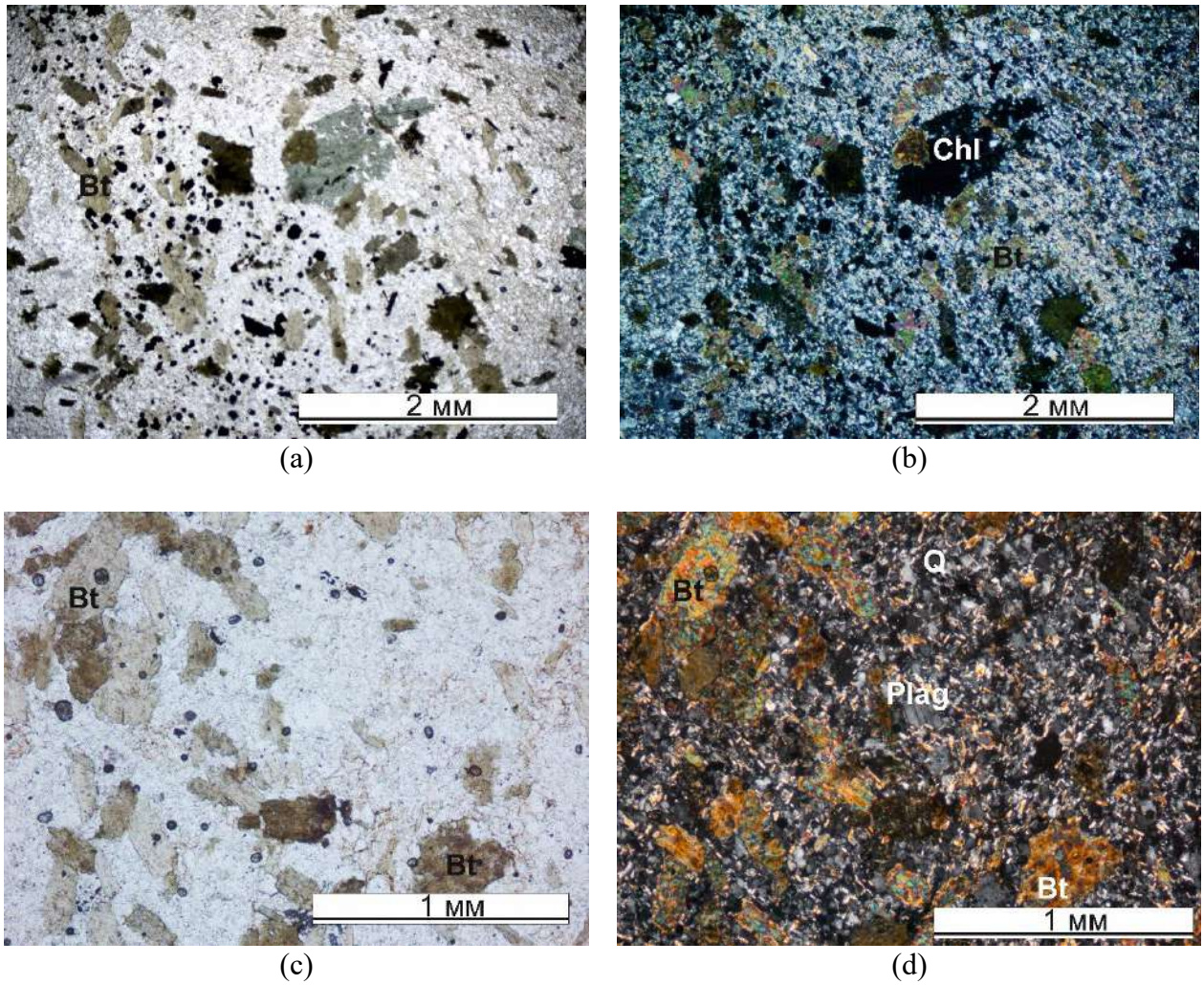

Figure 3.7. Photos of thin sections of the Pizhemskaya Formation clastic rocks. Crossed nicols. (a, b - 9064/2; c, d - 9064/1)

Vymskaya Group

The Vymskaya Group is composed of the Pokyuskaya, Lunvozhskaya, and Kyvvozhskaya Formations. A petrographic description of thin sections was done for the rocks of the Lunvozhskaya Formation.

Lunvozhskaya Formation (Figure 3.8)

The petrographic composition of clastic rocks of the Lunvozhskaya Formation was studied in 8 samples collected in the northern part of the Volsko-Vymskaya Ridge, on its western slope. One sample (9000/1) was taken from fine-grained sedimentary rocks enclosing kimberlite pipes in the northern part of the Volsko-Vymskaya Ridge. Five samples were obtained from a section in the upper reaches of the second right tributary of the Srednyaya River. Two more samples were taken in the headwaters of the Srednyaya River (a tributary of the Umba River). The rocks are classified as metasublitarenites, litharenites, subarkoses, and quartz arenites. Chlorite-sericite metasiltstones

(sample 9000/1) have a silty texture with rare grains of sand size. Parallel orientation of fine chlorite and sericite blades is typical. Slates are greenish in color due to the large amount of chlorite. Quartz occurs in phenocrysts oriented along the rock foliation. The undulatory extinction of quartz grains is indicative of the rock cataclasis, probably associated with the intrusion of kimberlite pipes. There are found single clasts of feldspar almost completely replaced by secondary chlorite. Lenses are also present in which the volume of quartz clasts, subangular and subrounded in shape, is much greater than that of the groundmass. Accessory minerals include biotite and ore mineral. Sericite-chlorite siltstones (metasubarkoses in composition) are characterized by silty texture, with interstitial and, more often, basal sericite-chlorite cement. The clastic fraction consists of fine quartz grains (up to 15% of the rock volume). The slaty structure of the rock is defined by parallel orientation of sericite and chlorite grains. Grains of quartz and feldspar (up to 1%) are subangular and subrounded in shape. Secondary chlorite often forms fine-grained aggregates filling (replacing?) voids elongated parallel to the general slaty structure of the rock. Thin fractures filled with iron hydroxide minerals, oriented parallel to slaty stricture, are observed. Metasandstones (subarkoses and quartz arenites) have a psammitic texture, with interstitial sericite-chlorite cement. The clastic portion consists mainly of quartz (75-80%) and feldspar (1-3%). The grain size varies from 0.01 mm to 0.3 mm; the shape of the grains is subrounded. In the interstices between quartz and feldspar clasts, fine-grained (0.1 mm) acicular sericite is found. In the groundmass of the rock, secondary chlorite that replaced feldspar is often observed. Chlorite forms fine-grained aggregates of green color, with low birefringence. Accessory minerals in metasandstones include ore mineral, tourmaline, and zircon.

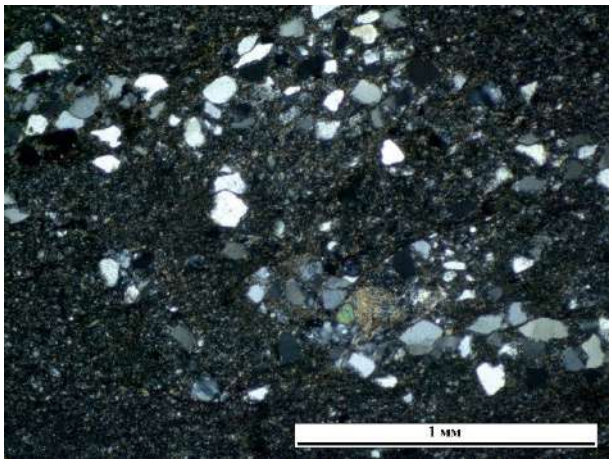

(a)

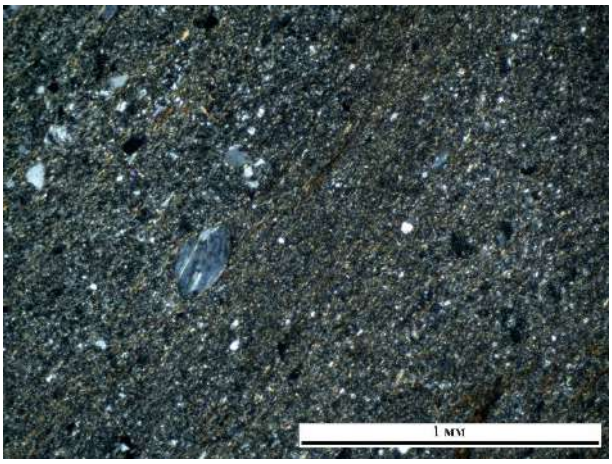

(b)

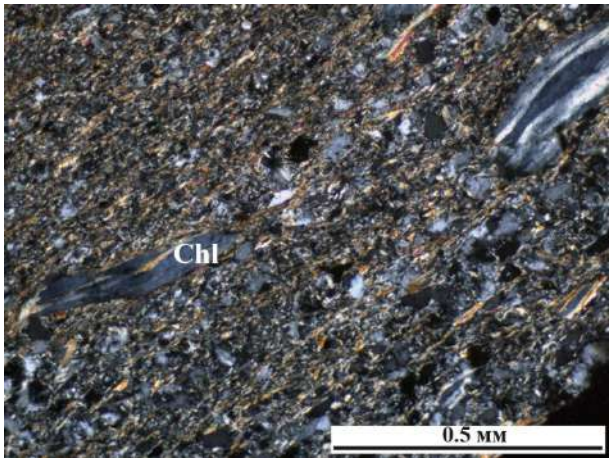

(c)

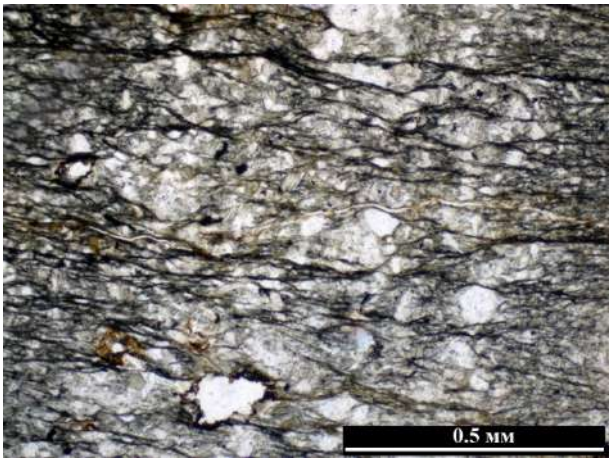

(d)

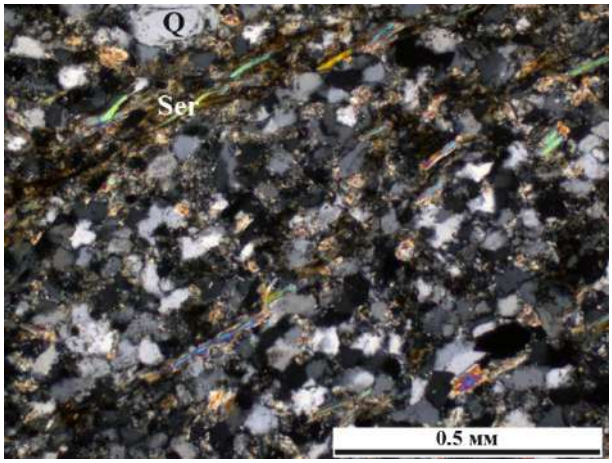

(e)

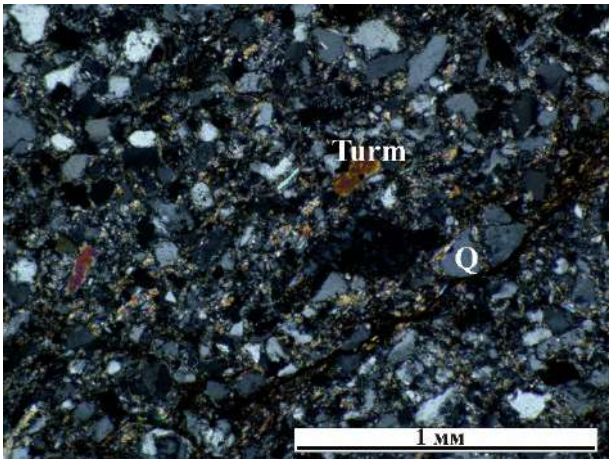

(f)

Figure 3.8. Photos of thin sections of the Lunvozhskaya Formation clastic rocks. Crossed nicols. (a, b - 9000/1; c - 9007/4; d - 9007/2; e - 9007/1; f - 9011/1)

Q – quartz; Ser – sericite; Chl – chlorite; Turm - tourmaline

3.2. Roundness of detrital zircons and tourmalines

Most detrital zircon grains from the metasandstones of Middle Timan are elongate in shape and vary from 70 to 200 μm in size. Some grains retain the fragments of primary faces, but most of them are subangular or subrounded. Cathodoluminescence images suggest that a greater part of the grains are characterized by the presence of distinct oscillatory zoning and some grains display cores and overgrown rims (Figure 3.9).

The degree of roundness of the dated zircon grains was determined using the scale after (Pettijohn, 1975). The scale enables their classification to one of the following groups: rounded, sub-rounded, subangular and angular. Examples of grains of these morphology classes are shown in Figure 3.9.

The studies of the roundness classes of the analyzed zircon grains revealed that the Svetlinskaya metasandstones and Novobobrovskaya metamorphosed silty sandstones consist chiefly of subrounded and subangular grains (Figure 3.10). The metasandstones of the Vizingskaya Formation are characterized by the prevalence of subrounded and rounded zircon grains. As regards the Novobobrovskaya Formation, ~15% of the entire population of zircons has angular grains with close to subhedral shape. The proportion of angular zircon grains in the Svetlinskaya and Vizingskaya Formations is lower, approximately 4–6% of the total zircon population. The vast majority of zircons from the Paunskaya Formation rocks (~60%) are subrounded. Two samples from the Lunvozhskaya Formation showed the predominance of subrounded zircons (45-50%), with rounded grains amounting to ca. 15-30%.

Figure 3.9. Morphology and internal structure of detrital zircon crystals from metasedimentary rocks of the Svetlinskaya, Novobobrovskaya, Vizingskaya, Paunskaya, and Lunvozhskaya Formations, with indication of the roundness class and ages (Ma).

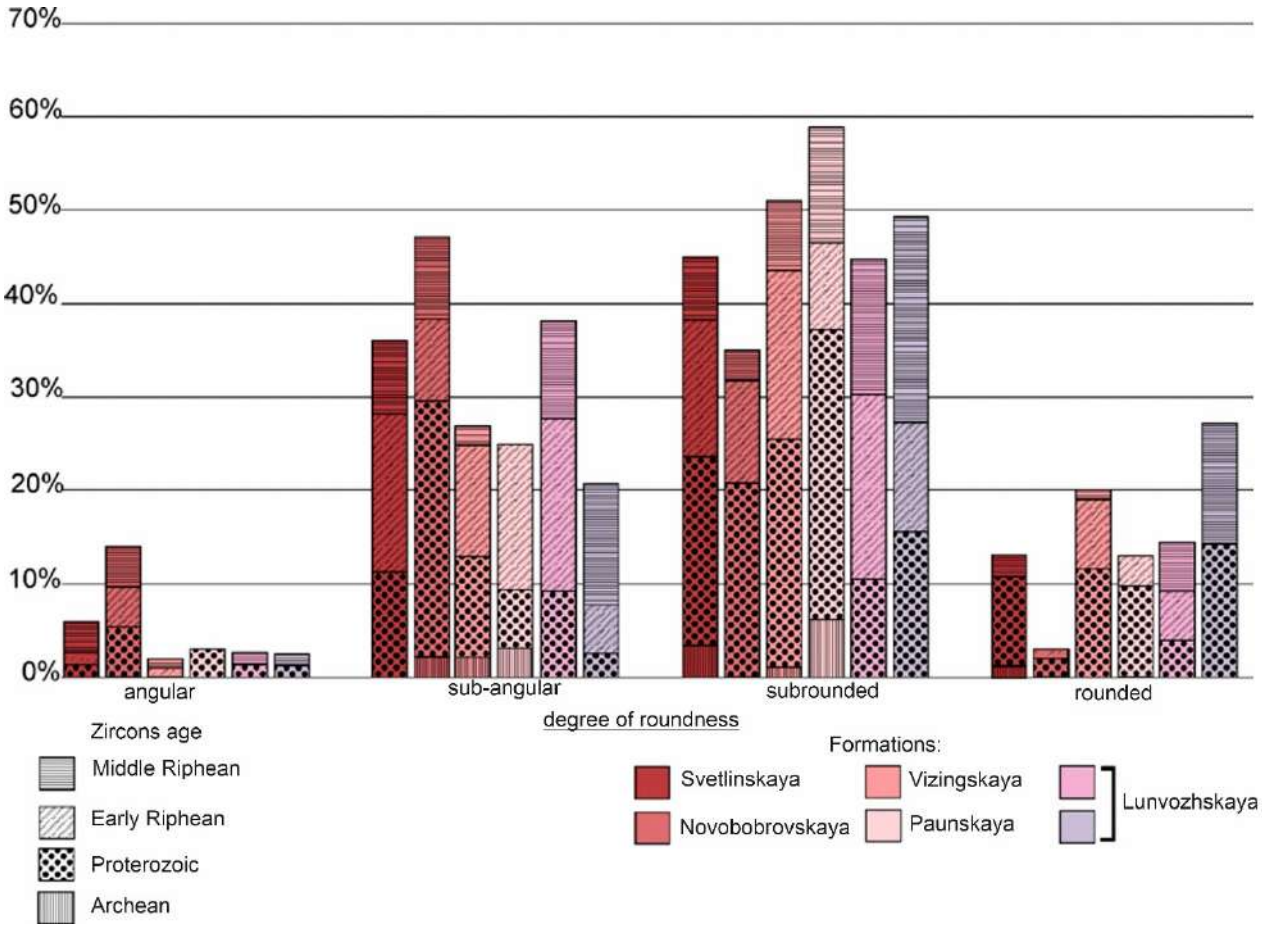

Figure 3.10. Histogram of the roundness (%) of zircon grains for the studied metasedimentary rocks of Middle Timan.

Degrees of roundness of detrital tourmaline grains were also determined (Figure 3.11). The results obtained show the predominance of angular (46%) and subangular (49%) grains (Figure 3.12). The amount of subrounded grains does not exceed 5%. No rounded tourmaline grains have been found.

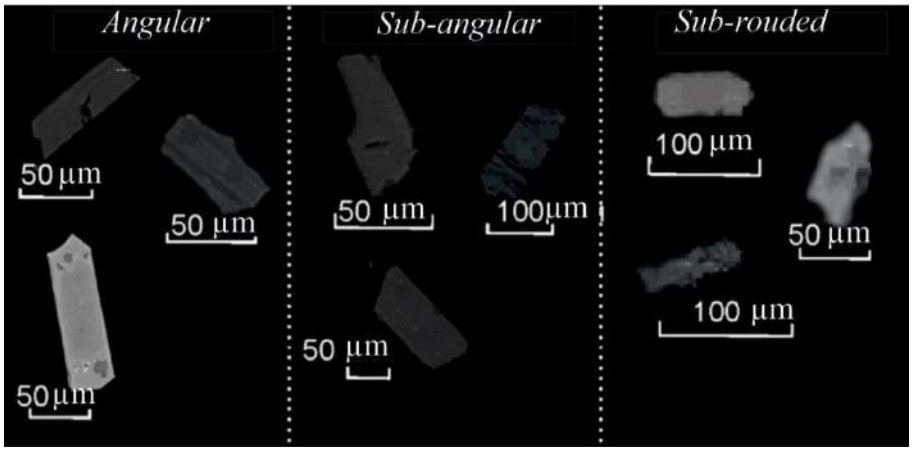

Figure 3.11. Morphology of detrital tourmaline crystals from the Riphean metasedimentary rocks of Middle Timan.

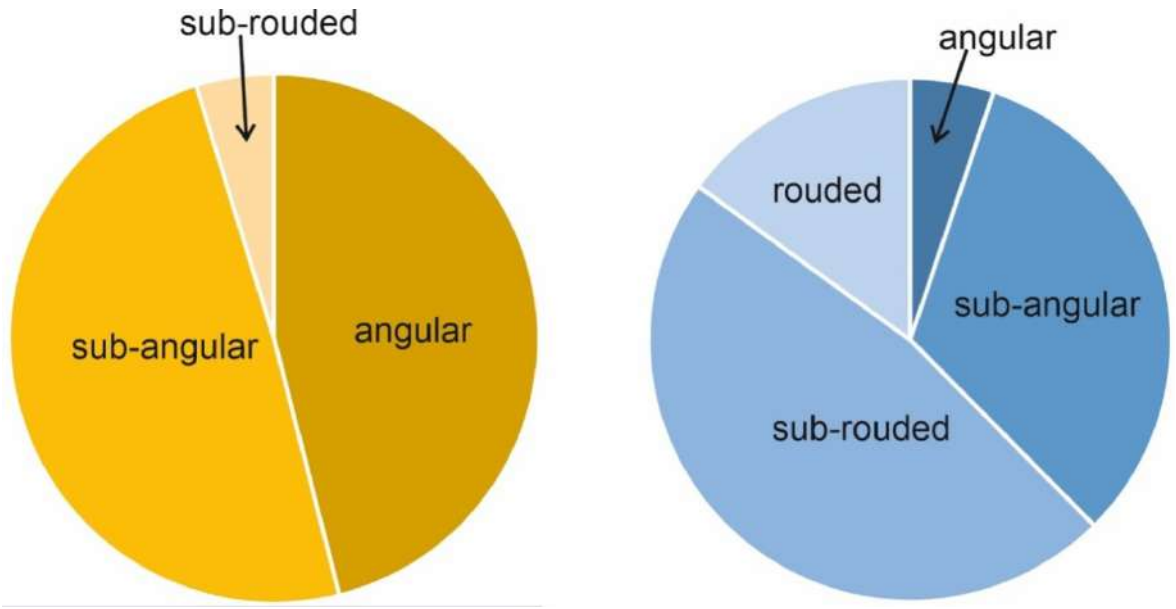

(a) (b)

Figure 3.12. Circular diagram of the roundness of detrital tourmalines (a) and detrital zircons (b) from the studied samples of metasedimentary rocks of Middle Timan

Roundness classes (1–4) are given according to (Pettijohn 1975).

3.3. Chemical composition of detrital tourmalines

Crystallization of minerals of the tourmaline supergroup occurs under widely ranging thermobarochemical conditions (Ertl et al. 2010; Berryman et al. 2019; Biernacka, 2019). The most common minerals of the tourmaline supergroup are schorl, elbaite, and dravite (Ertl et al. 2010; Biernacka, 2019, etc.). Schorl and Li-bearing tourmaline normally form during crystallization of granite massifs and granitic pegmatites, while dravite often forms in metamorphic rocks under P-T conditions of 3-5 GPa and > 950 °C, respectively (Baksheev and Kudryavtseva, 2004; Trumbull et al 2008; Arif et al. 2010; Ertl et al. 2010; Biernacka, 2019). The chemical composition of tourmaline is indicative of the physico-chemical conditions of its formation (van Hinsberg et al., 2011) and depends on the composition of the host rocks (Henry and Gudotti, 1985). The highly variable compositions of the tourmaline supergroup minerals make it possible to use them for reconstruction of provenances and transport pathways of clastic material (Biernacka, 2012; Kowal-Linka and Stawikowski, 2013; Vereshchagin et al., 2018).

The tourmaline supergroup minerals are complex borosilicates with a general formula X $Y_3Z_6(T_6O_{18})$ $(BO_3)_3V_3W$ (Henry et al., 2011), where X position may be occupied by Na^+or Ca^{2+}, or it may be vacant (□). Y position represents an octahedron that may be occupied by a wide range of

multivalent cations: Fe^{2+}, Mg^{2+}, Mn^{2+}, Al^{3+}, Li^{+}, Fe^{3+}, and Cr^{3+}. Z position is taken up by trivalent cations such as Al^{3+}, Fe^{3+}, V^{3+} and Cr^{3+}, and may also contain a small amount of Mg^{2+}. The tetrahedral T position is normally occupied by Si^{4+} and excess Al^{3+}. The BO_3 triangle enters only B position. V position mainly contains OH^{-} group, and may also comprise a significant amount of O^{2-}. W position contains only F^{1-} and excess OH^{1-} and O^{2-}. Tourmalines are divided into groups on the basis of elements placed in X position: alkaline (Na^{+}, K^{+}), calcic (Ca^{2+}), and a group with vacant X position ($^{\square}$). Depending on which anions occupied W position, tourmalines are divided into three subgroups: oxy- (O^{2-}), fluoro- (F^{1-}) and hydroxy- (OH^{1-}).

The chemical composition of 63 tourmalines of various shapes was analyzed (Appendix 6). None of the grains contains inclusions, the color is brownish-green.

Within the Chetlassky Kamen, chemical composition was determined for detrital tourmaline grains extracted from five samples. Sample 9016/2 from the Svetlinskaya Formation is a subarkosic metasandstone taken from deposits in the upper reaches of the Mezen River.

Sample 9020/3 from the Novobobrovskaya Formation is a metamorphosed silty arkosic sandstone taken from a section in the upper reaches of the Mezen River. Sample 9048/5 from the Vizingskaya Formation is a quartz arenite collected from a section in the headwaters of the Kosyu River (right tributary of the Mezen River). Two samples (9034/2 and 9034/12) from the Paunskaya Formation are muscovite-quartz matasiltstones obtained from a section in the middle reaches of the Lower Paun River (a tributary of the Svetlaya River which in itself is a tributary of the Pizhma River).

Three samples were analyzed from the Volsko-Vymskaya Ridge. Sample 9064/2 from the Pizhemskaya Formation is a biotite-muscovite slates with magnetite, which was taken from a section in the upper reaches of the Lower Vidzyu River (a tributary of the Vym River). Two samples (9007/4 and 9007/5) from the Lunvozhskaya Formation are quartz arenite and arkose, respectively. They were collected from a section in the middle reaches of the Srednyaya River.

As revealed by the microprobe analysis, the studied tourmaline grains are chemically unzoned. According to the data obtained (Appendix 6), all the grains analyzed are alkaline tourmalines (Figure 3.13a), with Na (0.52-0.95 apfu) prevailing over K (<0.03 apfu) and Ca (<0.26 apfu) and a vacancy in X position ($^{X\square}$ from 0.05 to 0.50 apfu). Tourmalines from the Paunskaya Formation contain more Na (0.68-0.97 apfu) as compared to those from other formations in which Na content averages 0.60 apfu.

In the sample from the Paunskaya Formation no tourmalines with Mg/(Mg+Fe) <0.5 and a vacancy in X position > 0.3 apfu were found, while in samples from other formations Mg/(Mg+Fe) reaches 1.0, and vacancies in X position are up to 0.5 apfu.

With regard to W position, all studied tourmalines are divided into two subgroups. Most grains (56) belong to the hydroxy-subgroup of alkaline tourmalines (dravite and schorl, Figure 3.13b). Seven grains are assigned to the oxy-subgroup (oxydravite) of the alkaline tourmaline group.

All tourmalines analyzed contain more than 6 apfu Al^{3+} (Appendix 6) testifying that Al is placed in both Y and Z positions. The main octahedral cations (besides aluminum) are magnesium and iron. The Mg/(Mg + Fe) ratio varies from 0.45 to 1.00 (Figure 3.13c). There is no significant variation in Ti content in the studied samples. The distribution of Mg, Fe, Mn, and Ti ions in two nonequivalent octahedral sites (YO_6 and ZO_6) cannot be reliably established without conducting single-crystal X-ray diffraction analysis (Vereshchagin et al., 2018). However, based on the chemical composition data available, we can assume that most of the studied tourmalines (53 grains) compositionally correspond to dravite, and only five grains correspond to schorl (Figure 3.13c). Five tourmaline grains have an oxydravite composition (Brusnitsyna et al., 2022).

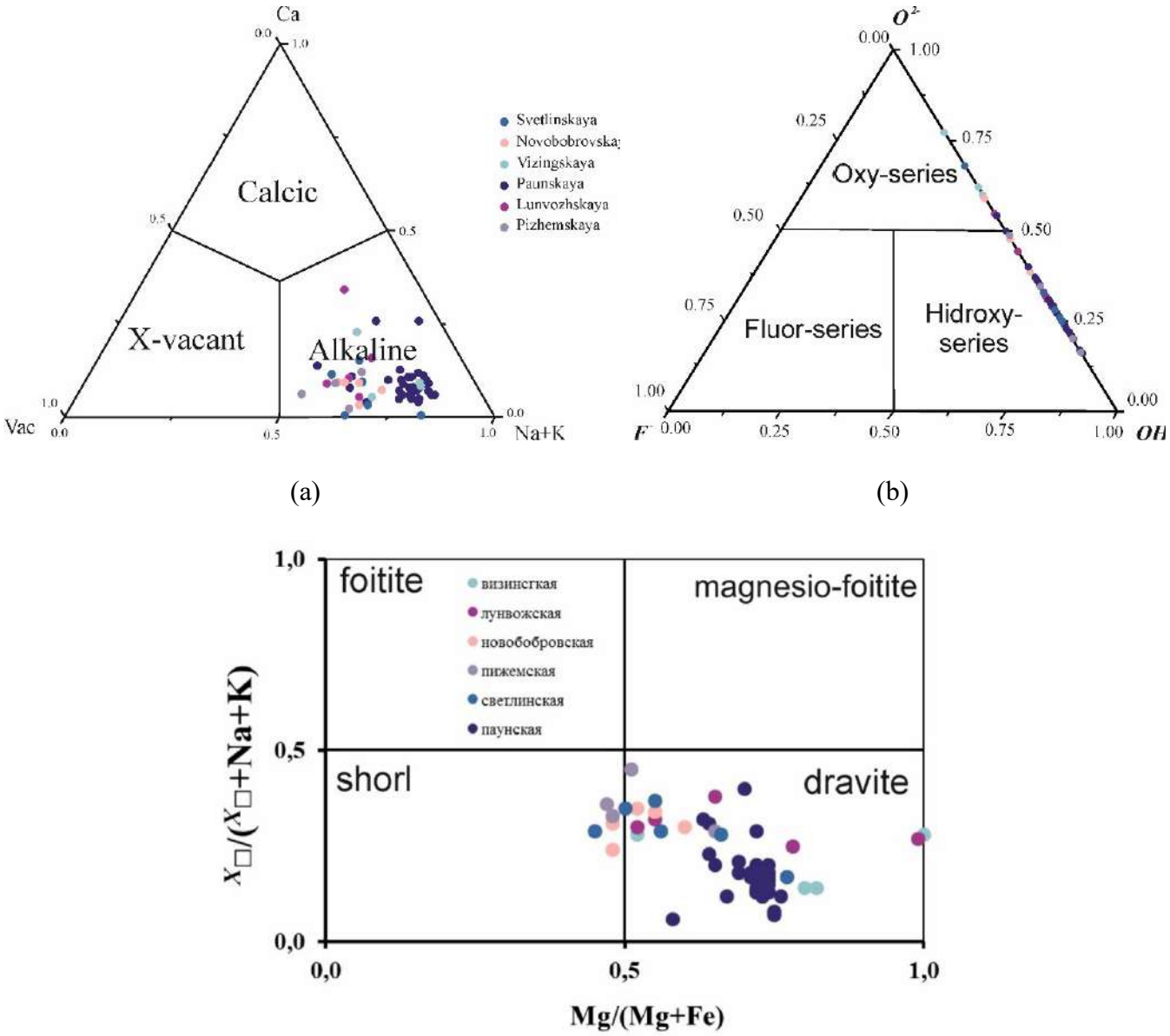

Figure 3.13. Chemical composition of detrital tourmalines on: (a) ternary Ca-Na+K-vacancy diagram (Henry et al. 2011), (b) O-OH-F ternary diagram (Henry et al. 2011), and (c) $^{X\square}$ / ($^{X\square}$ + Na + K) and Mg/(Mg + Fe) diagrams (Henry and Dutrow, 1996)

3.4. U-Th-Pb detrital zircon dating

In order to elucidate the age and origin of Precambrian clastic rocks of Middle Timan, U-Th-Pb detrital zircon dating was carried out on six samples collected from the rocks of the Chetlassky Kamen and two samples taken from the Volsko-Vymskaya Ridge deposits.

Chetlassky Kamen

The Riphean section within the Chetlassky Kamen consists of deposits of the Chetlasskaya and Bystrinskaya Groups. The Chetlasskaya Group includes the Svetlinskaya, Bystrinskaya, and Vizingskaya Formations. The Bystrinskaya Group consists of the Vorykvinskaya, Pavyugskaya, and Paunskaya Formations.

The U-Th-Pb ages of detrital zircons from the Svetlinskaya Formation were determined in two samples (9016/2 and 9017/4). For a subarkosic sample (9016/2), dates with a lower than 10% discordance were obtained for 88 of 110 grains (Appendix 1); among them, ca. 42% of zircons have Early Proterozoic age, 34% have Early Riphean age, and 20% have Middle Riphean age. The KDE plot displays two distinct peaks in the interval of Early Proterozoic ages (1791 and 1727 Ma) and four peaks with Riphean ages (1221, 1338, 1478 and 1552 Ma) (Figure 3.14). The age of the youngest zircon is 1150 ± 16 Ma (Brusnitsyna et al., 2021).

The 9017/4 sample is a light gray metasandstone. Seventy-five of the 130 grains analyzed yielded ages with discordance lower than 10% (Appendix 2). The age of zircons ranges within 1084 - 2635 Ma. Approximately 43% of the grains are Archean-Early Proterozoic, 41% are Early Riphean, and 16% are Middle Riphean in age. On the KDE plots (Figure 3.14), Archean-Early Proterozoic zircons form peaks at 1755, 1841, 2493 and 2631 Ma, Early Riphean zircons, at 1363, 1495, and 1547 Ma, and Middle Riphean zircons, at 1153 and 1197 Ma. The age of the youngest zircon grain is 1084±27 Ma (Brusnitsyna et al., 2022).

The U–Th–Pb ages of detrital zircons from the Novobobrovskaya Formation were determined in a metamorphosed arkosic silty sandstone sample (9020/3). Dates with lower than 10% discordance were obtained for 91 of 118 grains (Appendix 1); among them, ca. 60% of zircons have Archean-Early Proterozoic age, 27% have Early Riphean age, and 14% have Middle Riphean age. The KDE plot shows three peaks of Early Proterozoic ages (1787, 1860, and 2073 Ma) and four peaks with Riphean ages (1219, 1343, 1467, and 1602 Ma) (Figure 3.14). The Archean zircons form peaks at 2753 and 2929 Ma. The youngest zircon age is 1140±6 Ma (Brusnitsyna et al., 2021).

The U-Th-Pb ages of detrital zircons from the Vizingskaya Formation were determined in two samples (9048/5 and 9045/1). Composition of sample 9048/5 corresponds to quartz arenites. Ages with lower than 10% discordance were obtained for 94 of 111 grains (Appendix 1). Approximately 57% of detrital zircons have Archean-Early Proterozoic ages, 30% have Early Riphean ages, and not more than 10% of grains have Middle Riphean ages. Only 3% of the dated zircons are Archean in age. The KDE plot displays peaks with Archean-Early Proterozoic ages (1677, 1721, 1837, 1962, 2094, 2802,

and 2952 Ma) and four peaks with Riphean ages (1212, 1382, 1434, and 1511 Ma) (Fig. 3.14) (Brusnitsyna et al., 2021).

For the 9045/1 sample from the Vizingskaya Formation, ages with discordance lower than 10% were obtained for 113 of 141 grains (Appendix 2). Approximately 33% of detrital zircons have Archean-Early Proterozoic ages, 51% have Early Riphean ages, and 16% have Middle Riphean ages. The probability density distribution plots display four peaks with Early Proterozoic and Archean ages (1705, 1754, 1812, and 2830 Ma) and four peaks with Riphean ages (1125, 1474, 1507, and 1561 Ma). The youngest zircon age is 1111±31 Ma (Brusnitsyna et al., 2022).

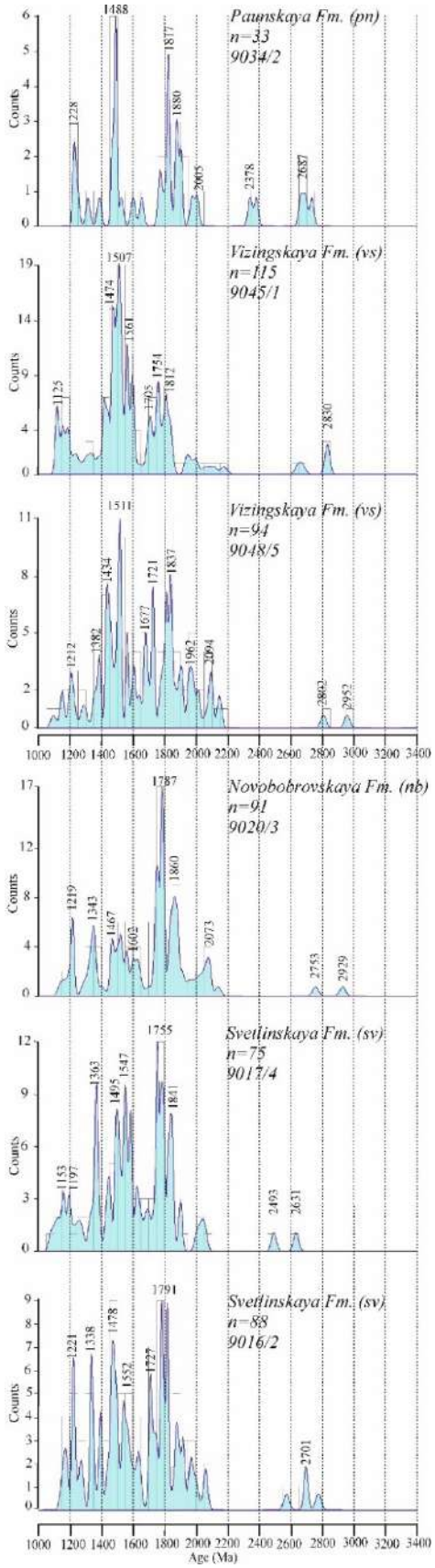

Figure 3.14. KDE plots of the U-Th-Pb age distribution of detrital zircons from metasedimentary rocks of the Chetlasskaya and Bystrinskaya Groups of Middle Timan ($^{207}Pb/^{206}Pb$ dating, n - number of measurements).

Within the Bystrinskaya Group, 132 zircons from the Paunskaya Formation (sample 9034/2) were dated. Only 33 grains showed ages with less than 10% discordance (Appendix 1). The age of zircons varies from 1225 to 2734 Ma. Sixty percent of grains are Archean-Early Proterozoic, 28% are Early Riphean, and 12% are Middle Riphean in age. On the KDE plot, Archean-Early Proterozoic zircons form peaks at 1817, 1880, 2005, 2378, and 2687 Ma, while those of Riphean age display peaks at 1228 and 1488 Ma. The youngest zircon is 1225±11 Ma old (Brusnitsyna et al., 2022).

However, the distribution of grains in the concordia plot (Appendix 7) indicates that many of them locate along one or more discordia. This suggests that a significant number of zircon grains with high discordance may be considered in age calculation. Calculation by the method proposed in (Reimink et al., 2016) shows that zircon population from the 9034/2 sample defines two discordia (Figure 3.15) of which one has an upper intercept age with concordia at ca. 2900 Ma, and the lower intercept age at ca. 1150 Ma. The second discordia has an upper intercept age at ca. 1900 Ma, and the lower intercept age at ca. 300 Ma. The upper intercept age defines the time of zircon crystallization. Zircons with close to 1900 Ma ages form a peak at 1880 Ma on the KDE plot. Zircons with ages close to 2900 Ma are absent from the KDE plot for this sample, but they are present in samples from the Vizingskaya and Novobobrovskaya Formations. The lower intercept age of discordia defines the time of the U-Th-Pb system disruption, and its interpretation is ambiguous.

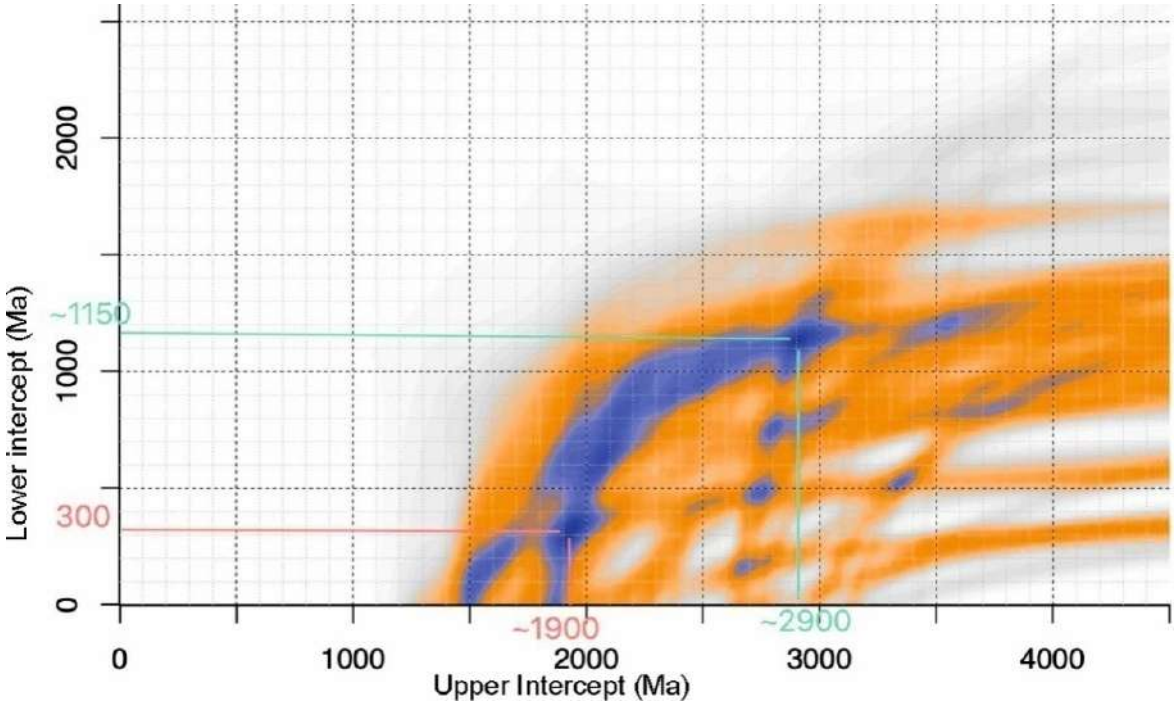

Figure 3.15. Calculation of discordia parameters for zircon grains from sample 9034/2 by the method of Reimink et al. (2016).

Volsko-Vymskaya Ridge

The Precambrian section within the Volsko-Vymskaya Ridge is represented by the rocks of the Vymskaya and Kislorucheiskaya Groups. The Vymskaya Group includes the Pokyuskaya and Lunvozhskaya Formations. The Kislorucheiskaya Group comprises the Pizhemskaya and Kleonovskaya Formations. In this study, detrital zircons from two samples (9007/1 and 9007/4) collected from clastic deposits of the Lunvozhskaya Formation were only dated.

In sample 9007/1, ages with a lower than 10% discordance were obtained for 76 of 110 zircon grains dated. The age of zircons ranges within 1042- 2493 Ma. Approximately 26% of the dated grains are Early Proterozoic, 42% are Early Riphean, and 32% are Middle Riphean in age. In the KDE plot (Figure 3.16), Early Proterozoic zircons form peaks at 1885, 1974, and 2490 Ma, while Riphean grains show peaks at 1172, 1226, 1356, 1531, 1564, and 1611 Ma. The youngest zircon age is 1042±29 Ma (Brusnitsyna et al., 2022).

In sample 9007/4, ages with a lower than 10% discordance were gained for 77 of 114 detrital zircons. The age of zircons varies from 1012 to 2142 Ma. Thirty-three percent of dated zircon grains are Early Proterozoic, 17% are Early Riphean, and 49% are Middle Riphean in age. In the KDE plot (Figure 3.16), Early Riphean detrital zircons display peaks at 1676, 1772, and 1948 Ma, while Riphean zircons form peaks at 1167, 1216, and 1505 Ma. The age of the youngest zircon from sample 9007/4 is 1012±11 Ma (Brusnitsyna et al., 2022).

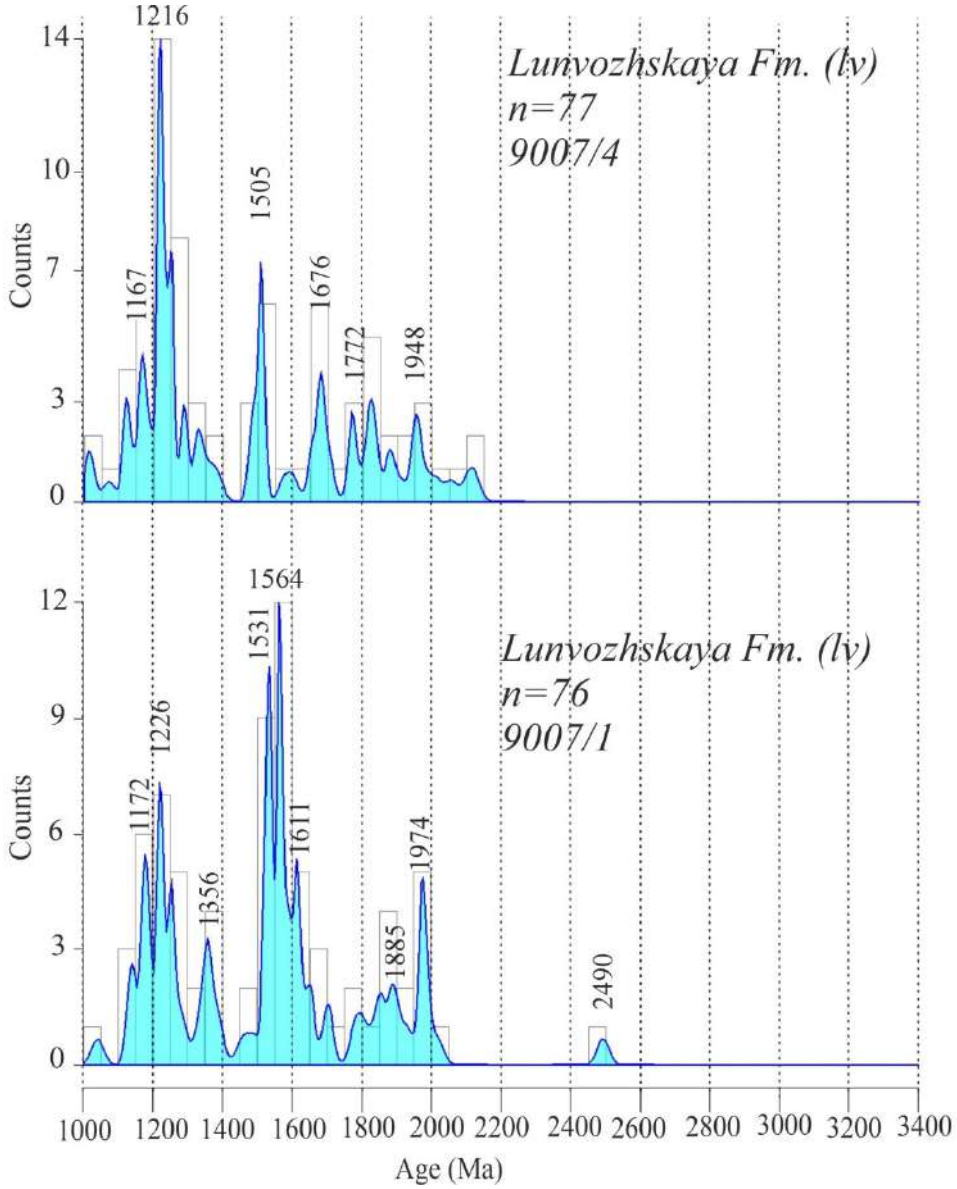

Figure 3.16. KDE plots of U-Th-Pb isotope age distribution of detrital zircons from metasedimentary rocks of the Vymskaya Group in Middle Timan ($^{207}Pb/^{206}Pb$ dating, n - number of measurements).

3.5. Lu-Hf isotopic-geochemistry of detrital zircons

The Lu-Hf isotope geochemical analysis of zircons was made on five samples (9016/2, 9020/3, 9048/5, 9007/1 and 9007/4) (Appendix 4). Prior to analysis, U-Th-Pb dating of zircons from each sample was carried out. Zircons with a lower than 10% discordance and a crystal size of more than 40 μm were only selected for the analysis.

The Lu-Hf isotopic composition was determined for 50 zircon grains from sample 9016/2 collected from the Svetlinskaya Formation. Thirty-nine analyses were taken into consideration in

diagram plotting (Figure 3.17) and in further interpretation of data. Most of εHf (t) values (85%) obtained for zircons from the Svetlinskaya Formation lie above the line of the chondritic uniform reservoir (CHUR), ranging from 0 to +15. Fifteen percent of zircons have negative εHf (t) values from -1 to -4.9.

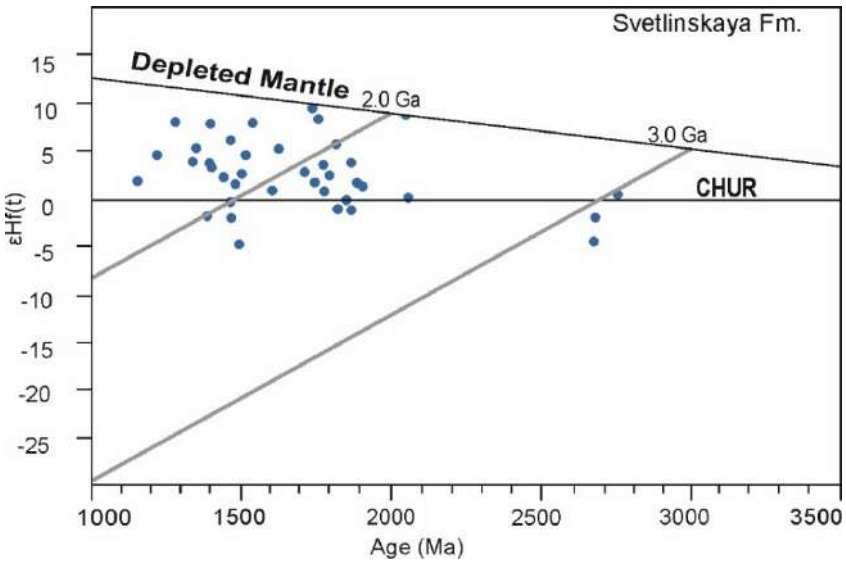

Figure 3.17. Lu-Hf isotopic-geochemical characteristics of the Svetlinskaya Formation (sample 9016/2).

The Lu-Hf isotopic composition was determined for 50 detrital zircons from the Novobobrovskaya Formation (sample 9020/3). Forty-six analyses were considered in diagram plotting (Figure 3.18) and in further interpretation of data. Eighty percent of the total zircon population is located between the CHUR and depleted mantle lines. Their εHf (t) values vary from +1 to +15. About 20% of detrital zircons have negative εHf (t) values from +1 to -5.2.

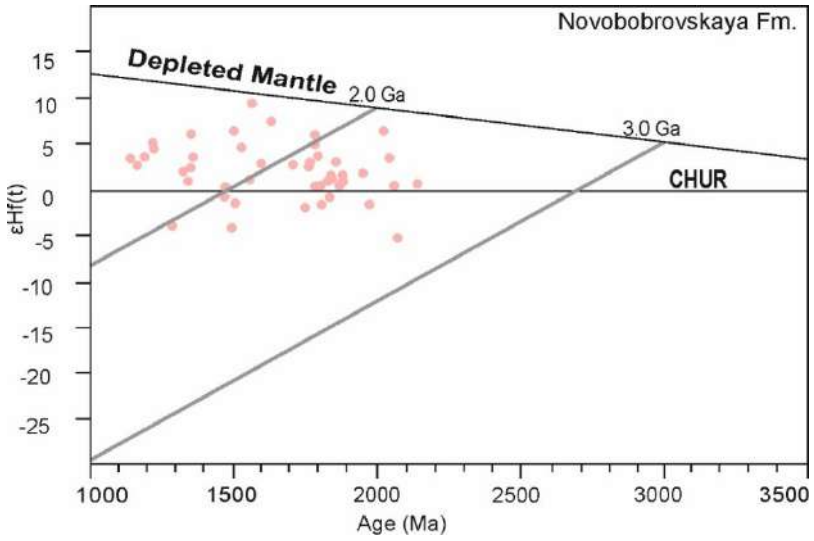

Figure 3.18. Lu-Hf isotopic-geochemical characteristics of the Novobobrovskaya Formation (sample 9020/3)

For the Vizingskaya Formation, the Lu-Hf isotopic composition of 50 zircons from sample 9048/5 was determined. The results obtained for 30 grains were considered in diagram plotting (Figure 3.19) and in further interpretation of data. About 87% of the zircon population has positive εHf (t) values from +1 to +16.2. Only 4 grains (13%) lying below the CHUR line have negative εHf (t) values from - 1.7 to -6 (Brusnitsyna et al., 2022).

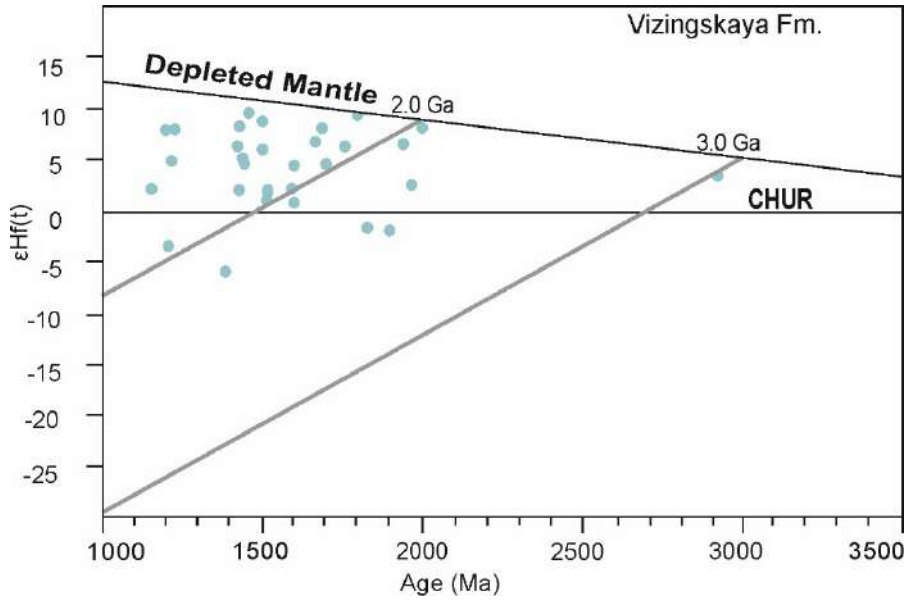

Figure 3.19. Lu-Hf isotopic-geochemical characteristics of the Vizingskaya Formation (sample 9048/5)

For the Lunvozhskaya Formation, the Lu-Hf isotopic composition was determined for detrital zircons extracted from two samples. In diagram plotting for sample 9007/1 (Figure 3.20) data obtained for 46 of 52 grains were considered. Five zircons (11%) have negative εHf (t) values (from -0.1 to -12) and, accordingly, lie below the CHUR line. Most of grains (89%) are located between the CHUR and depleted mantle lines, and have positive εHf (t) values from 1.5 to 15.5 (Brusnitsyna et al., 2022).

Forty-eight detrital zircons were analyzed from sample 9007/4. Forty-five analyses were considered in diagram plotting (Figure 3.20) and in further interpretation of data. Twenty-four percent of grains have negative εHf (t) values varying from -1.1 to -16.2. Seventy-five percent of the studied detrital zircon grains locate between the CHUR and depleted mantle lines and have positive εHf(t) values (from 0.2 to 9.1) (Brusnitsyna et al., 2022).

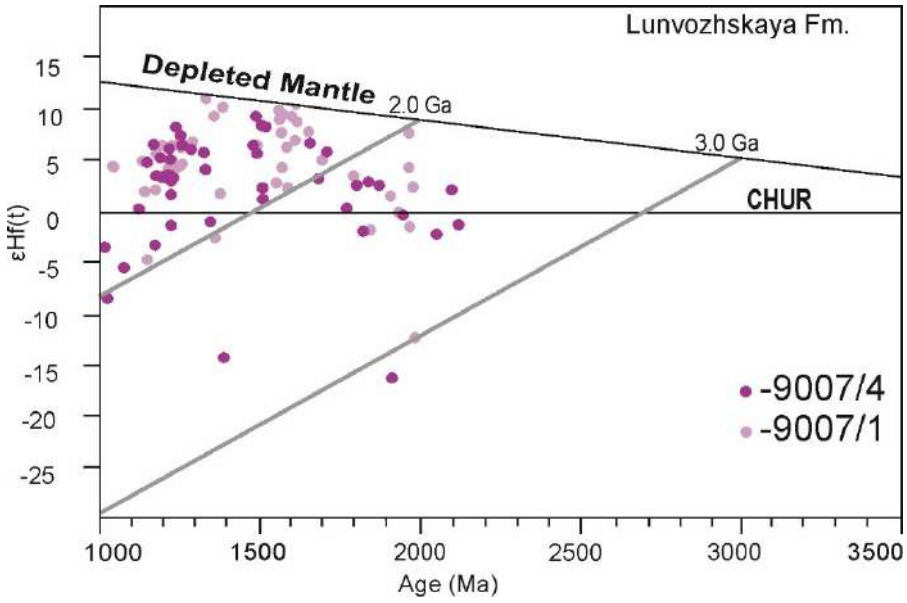

Figure 3.20. Lu-Hf isotopic-geochemical characteristics of the Lunvozhskaya Formation (samples 9007/1 and 9007/4)

3.6. U-Th-Pb detrital rutile dating

For the U-Th-Pb analysis, rutile grains were separated from two metasandstone samples collected from the Lunvozhskaya Formation (sample 9007/3) and the Vizingskaya Formation (sample 9045/1). The grains are characterized by a diversity of shapes, sizes, and colors. Rutile mostly occurs in euhedral crystals (more often crystal fragments) with hatching due to crystal growth, while rounded grains are subordinate. Such a wide variety of rutile grains is likely indicative of their different sources of detrital material or their relation to different metamorphic events. The sedimentary rocks in the study area are metamorphosed to the greenschist facies. The temperature conditions for the occurrence of greenschist facies metamorphism are estimated at 350-550°C (e.g., Dobretsov, 1972). The closing temperature of the U-Th-Pb system in rutile is about 500–600°C (Cherniak, 2000; Vry and Baker, 2006). Therefore, rutile could not have formed with such a low metamorphic grade of the studied sedimentary rocks. The data obtained define the age of crystallization and/or transformation of rutile grains in the clastic material provenance area.

The U-Th-Pb ages of detrital rutiles from the Lunvozhskaya Formation were determined in a metasandstone sample 9007/3. Concordant ages were obtained for 5 of 52 grains analyzed (Appendix 3). The age of rutiles is from 747 to 3612 Ma. Only 4% of grains of the total rutile population have Archean age, 11% have Early Proterozoic age, and 13% have Early Riphean age. Almost half of the dated rutiles (49%) are Middle Riphean and 22% are Late Riphean in age. On the KDE plots (Figure 3.21), the youngest group of rutiles form peaks at 864, 925, and 1004 Ma. Archean grains do not form

statistically significant peaks, while Early Proterozoic rutiles display a peak at 1986 Ma. The Early Riphean rutiles show peaks at 1341 and 1521 Ma. The Middle Riphean group of rutiles form peaks at 1211, 1164, 1112, and 1054 Ma. The age of the youngest rutile is 747±12 Ma, and the youngest peak on the KDE plots is at 864 Ma (Brusnitsyna et al., 2022).

Forty-nine rutile grains were analyzed from sample 9045/1 collected from metasandstones of the Vizingskaya Formation, 46 of them have concordant ages (Appendix 3). The age of rutiles ranges widely from 858 to 2164 Ma. About 48% of the grains are Early Proterozoic, 15% are Early Riphean, 22% are Middle Riphean, and 15% are Late Riphean in age. Archean rutiles were not found in sample 9045/1. On KDE plots, rutiles with Early Proterozoic ages form peaks at 2115, 2064, 1888, 1800, and 1685 Ma. The Riphean group of rutiles display peaks at 1590, 1519, 1395, and 1215 Ma. Rutiles of the youngest Late Riphean group form peaks at 1001 and 867 Ma. The youngest rutile age is 858±12 Ma (Brusnitsyna et al., 2022).

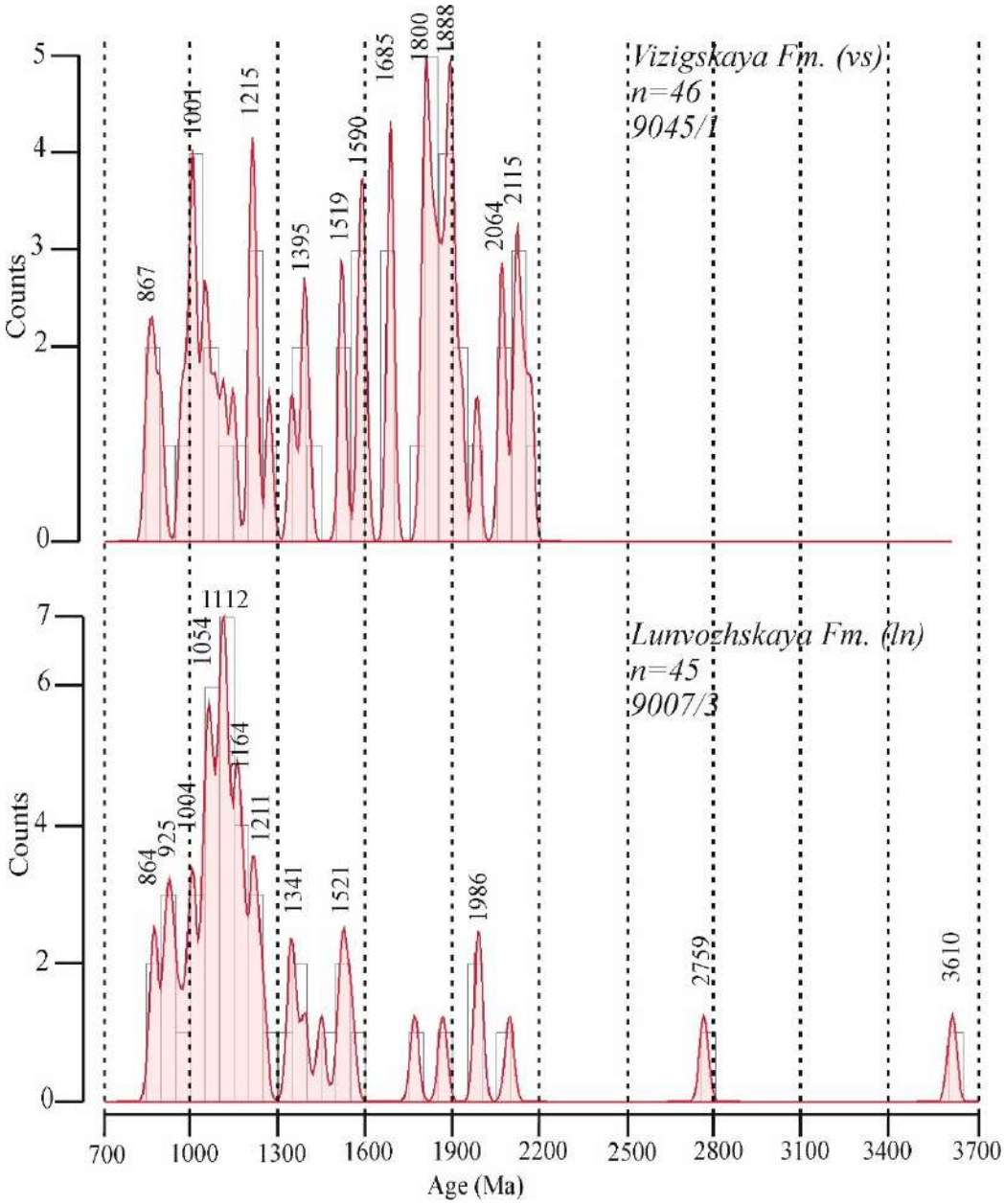

Figure 3.21. KDE plots showing U-Th-Pb isotopic age distributions of detrital rutiles from metasedimentary rocks of the Lunvozhskaya and Vizingskaya Formations in Middle Timan ($^{207}Pb/^{206}Pb$ dating, n - number of measurements).

Chapter 4. Discussion

The conducted integrated study made it possible to constrain the provenances of clastic material, the paleogeography of Baltica in the Middle-Late Riphean, and the stratigraphic position of the studied deposits. Given below is interpretation of the obtained data.

4.1. Estimation of maximum depositional age

4.1.1. U-Th-Pb detrital zircon dating

One of the objectives of this study was to determine the lower limit / maximum depositional ages (MDA) of the clastic rocks in Middle Timan. So far there is no generally accepted approach to determining MDA on the basis of detrital zircon dates (Dickinson and Gehrels, 2009; Coutts et al., 2019; Johnstone et al., 2019; Malone et al., 2016; Vermeesch, 2021). The most commonly used are the following algorithms of determining this age proposed by W. Dickinson and G. Gehrels (Dickinson, Gehrels, 2009):

1) the age of the youngest peak on the detrital zircon age distribution plots (youngest graphical peak, YPP), provided that this peak is based on the age estimates on at least three grains;

2) the age of the youngest detrital zircon grain cluster (YGC 1σ), determined by computing the weighted average of the youngest two or more dates that overlap within uncertainty at 1σ. These grains may not form a peak on the age distribution plot.

It is known that zircons with close to depositional age are found in the backarc, forearc, and marginal basin settings and at convergent plate boundaries. Zircons with the age older than depositional age are characteristic of the passive margin or rift settings (Cawood et al., 2012).

We have calculated the maximum depositional ages for the metasedimentary rocks in the study area using both the YPP and YGC methods (Table 1).

Table 1. Maximum depositional ages of the Middle Timan sedimentary rocks based on the results of detrital zircon dating.

Sample#	Formation	Youngest Graphical Peak, YPP (YPP 1 σ), Ma	Youngest Grain Cluster, (YGC 1 σ), Ma
9016/2	Svetlinskaya	1225	1198 ± 36
9017/4	Svetlinskaya	1153	1096 ± 23
9020/3	Novobobrovskaya	1209	1200±12
9048/*	Vizingskaya	1213	1223 ± 10
9045/1	Vizingskaya	1115	1125± 19
9034/2	Paunskaya	1228	1234 ± 11
9007/1	Lunvozhskaya	1140	1107 ± 29
9007/4	Lunvozhskaya	1122	1015 ± 10

The MDAs derived from the age of the youngest peak on the detrital zircon age distribution plot (YPP) vary from 1115 to 1228 Ma, which are by 30-80 m.y. older than those (1015-1234 Ma) inferred from the age of the youngest detrital zircon cluster (YGC 1σ).

4.1.2. U-Th-Pb detrital rutile dating

Detrital rutiles were dated from two metasandstone samples collected from the Lunvozhskaya (sample 9007/3) and Vizingskaya (sample 9045/1) Formations.

Up to now, there is no well-developed technique for calculating MDA on the basis of the U-Th-Pb detrital rutile ages, therefore we applied the same approach as was used for detrital zircons. The maximum depositional ages obtained from the detrital rutile dating are much younger than those derived from detrital zircon dates.

For the Lunvozhskaya Formation, the MDA estimated on the basis of the age of the youngest peak on the rutile age distribution plot (YPP) is 864 Ma and that for the Vizingskaya Formation is 867 Ma. The MDAs based on the weighted average ages of the youngest rutile grain clusters (YGC 1σ) are 885±21 and 867±11 Ma, respectively.

The MDAs for the Vizingskaya Formation (sample 9045/1) calculated by the two methods overlap within 1σ error. For the Lunvozhskaya Formation, the ages obtained using the YPP and YGC algorithms are comparable within 1σ error (Table 2).

Table 2. MDA of the Middle Timan metasedimentary rocks calculated from detrital rutile dating.

Sample#	Formation	Youngest Graphical Peak, YPP (YPP 1σ), Ma	Youngest Grain Cluster, (YGC 1σ), Ma
9007/3	Lunvozhskaya	864	885±21
9045/1	Vizingskaya	867	867±11

The MDA (864-885 Ma) obtained from the dating of detrital rutiles by YPP and YGC methods (Table 2) is 150-360 m.y. younger than that determined from detrital zircon dating by the same methods (Table 1).

At the current, largely reconnaissance stage of research, when using the rutile ages for determining the stratigraphic position of rock units, one should bear in mind that these are only approximate ages which are subject to further refinement. In our case, ages obtained for sample 9007/3 from the Lunvozhskaya Formation (885-904 Ma) and sample 9045/1 from the Vizingskaya Formation (878–926 Ma) need to be more exactly defined. Our data show that MDA determinations based solely on zircon dating are ambiguous, especially with regard to the rocks with not reliably established geodynamic settings. In the case of the rocks deposited, synchronously with magmatism, in active margin and island arc geodynamic settings, the MDA determinations based on zircon dating are fairly reliable, while for rocks formed in other geodynamic settings, it is better to use an integrated approach to establishing their depositional age.

4.1.3. Metamorphic events in the provenance area

The U-Th-Pb ages of detrital zircons and rutiles from samples of the Lunvozhskaya (9007/3) and Vizingskaya (9045/1) Formations can be conventionally divided into 2 groups: Middle-Late Riphean (younger than ca. 1300 Ma) and Early Riphean and older (Figure 4.1). In the first group, the age distributions of zircons and rutiles differ significantly. For the sample from Vizingskaya Formations (9045/1), the age of the youngest rutile cluster (YGC 1σ) is 867 ± 11 Ma, which is much younger (by ca. 250 Ma) than the age of the youngest zircon group (1127 ± 18 Ma) from the same sample.

The sample from the Lunvozhskaya Formation (9007/3) showed a somewhat different age distribution of detrital rutiles. On the KDE plots, rutiles form peaks at 925-1004 and 1054-1170 Ma, and the youngest grain has an age of 747 ± 12 Ma (Figure 3.20). Ages of the youngest zircons from

two samples of the Lunvozhskaya Formation are much older (by ~290 Ma) - 1012±11 and 1042±29 Ma. Overall, detrital zircons are only Middle Riphean in age, while a significant number of detrital rutiles have Late Riphean age (ca. 900–1050 Ma) (Figure 4.1).

The age distribution plots for the Early Riphean and older detrital rutiles and zircons from the same samples correlate well in the interval 1560–2000 Ma, and correspond to magmatic and metamorphic events known in the basement of Baltica and its framing (Petrov, 1999; Baltybaev et al., 2004; Baltybaev and Levchenkov, 2005; Baltybaev, 2005; Korja et al., 2006; Balagansky et al., 2016; Amelin et al., 1997; Bayanova et al., 2002; Bogdanova et al., 2008; Larin, 2009; Rämö et al., 2014 and others).

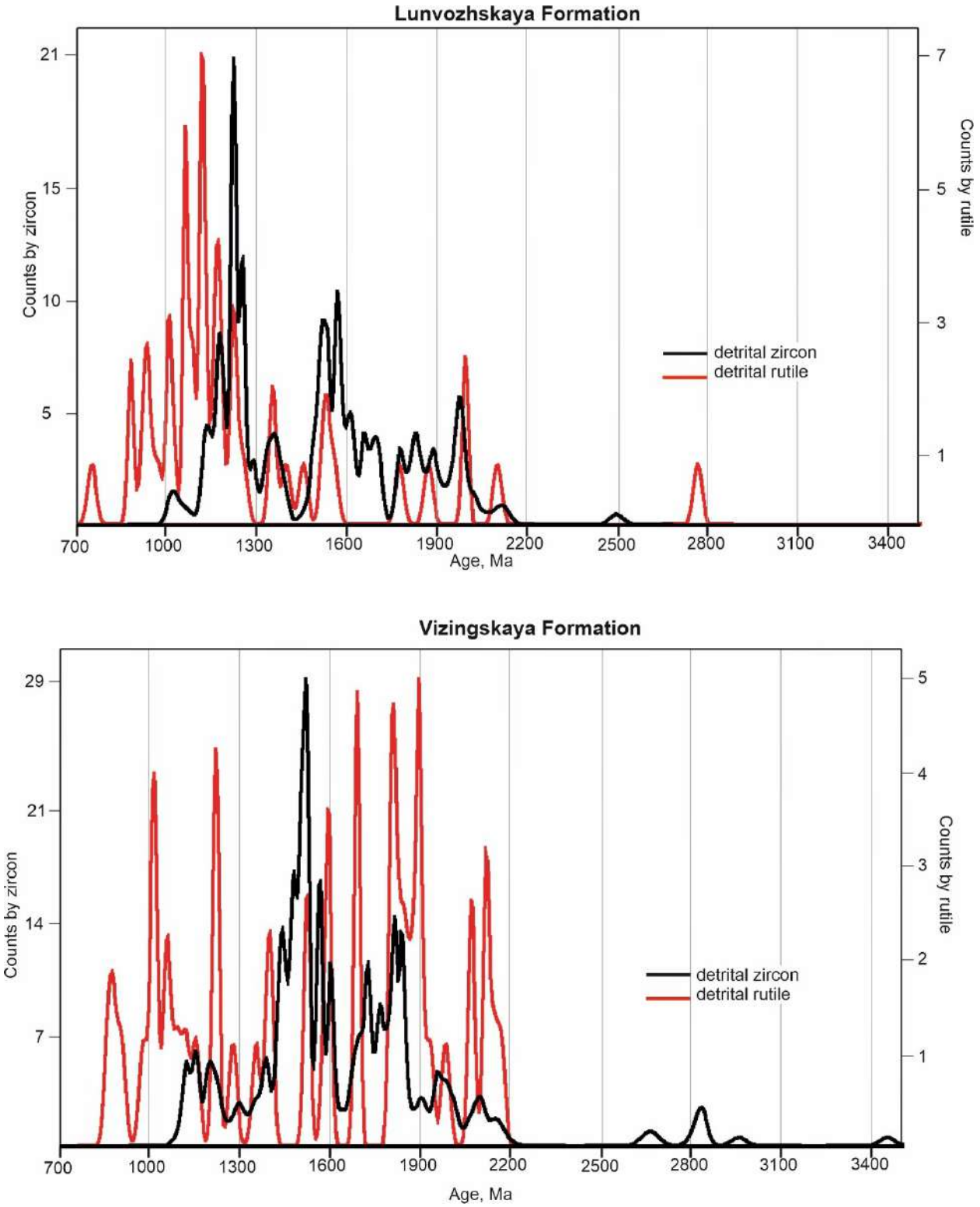

Figure 4.1. Combined kernel density estimate (KDE) plots for detrital zircons and detrital rutiles from clastic rocks of the Vizingskaya (a) and Lunvozhskaya (b) Formations.

The U-Th-Pb isotope system of zircons defines either the crystallization age of igneous rocks or the age of high-temperature metamorphic processes (e.g., Rubatto et al., 2001), while rutile is characterized by a much lower closing temperature of the U-Th-Pb isotope system estimated at ca. 500–600°C (Cherniak, 2000; Vry and Baker, 2006). Therefore, the U-Th-Pb age of rutiles defines the

age of cooling subsequent to the last medium-to-high temperature metamorphic event, while the U-Th-Pb age of zircons defines the age of crystallization or a high-temperature metamorphic event. Besides, it is rare for rutile to be subject to reworking by sedimentary processes, so it can provide fair constraints on the age of metamorphic events in the initial provenance area of clastic material.

Thus, zircon and rutile usually define different stages of magmatic and/or metamorphic processes. Moreover, rutiles from metamorphic terranes with low rates of cooling usually show younger U-Th-Pb ages than those determined from dating of zircons from the same terranes (Mezger et al., 1989; Möller et al., 2000; Vry and Baker, 2006) (Fig. 4.2). In our case, a significant difference in the ages of detrital rutiles and detrital zircons testifies against their origin in a single magmatic process. Therefore, the age of detrital rutiles defines the age of the youngest metamorphic events, but the temperature during these events was insufficient to reset the U-Th-Pb isotope system of zircons.

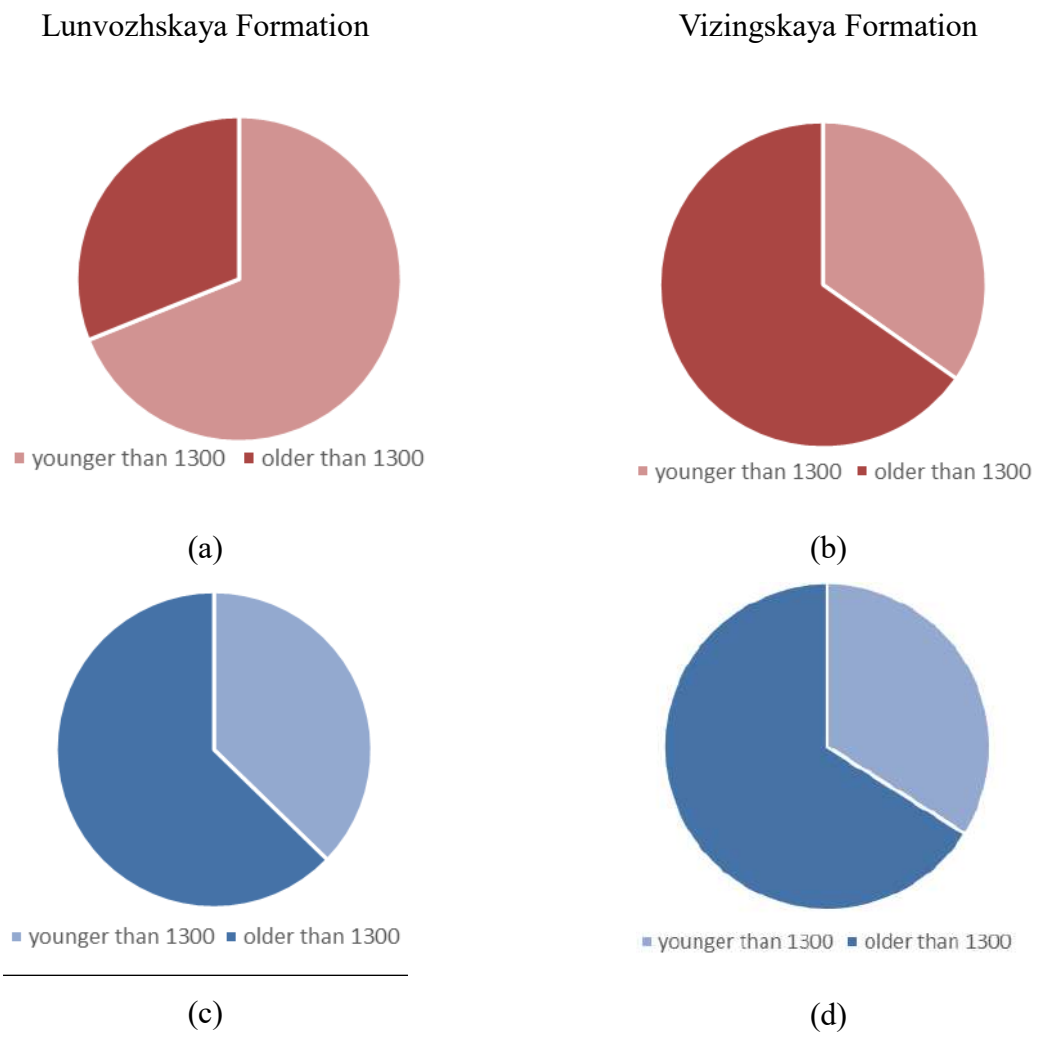

Figure 4.2. Circular age distribution diagrams for detrital rutiles (a, b) and detrital zircons (c, d)

Thus, a detailed isotope-geochronological study of the heavy fraction minerals rutile and zircon allows to present the **first provision to be defended - The age of the youngest detrital rutile populations formed by at least three to five grains (~ 900-1050 Ma) defines the age of the last phase of metamorphism in the provenance area for clastic rocks.**

4.2. Chemical composition of detrital tourmaline and reconstruction of provenances

As a result of the conducted work, it was found that tourmalines from different stratigraphic intervals have a similar chemical composition suggesting their common provenance.

Our data on the chemical composition of detrital tourmalines from the Precambrian deposits of Middle Timan indicate a metasedimentary origin of the rocks in the provenance area. The data points on an Al–$Fe_{50}Al_{50}$–$Mg_{50}Al_{50}$ diagram (Henry and Guidotti, 1985) fall mainly into two fields (4 and 5, Fig. 4.3) corresponding to metapelites and metapsammites with a low and high alumina content (31 and 24 grains, respectively). Two tourmaline grains from the Vizingskaya and Lunvozhskaya Formations are localized in the field of ultramafic rocks and low-Ca and Cr- and V-rich metasediments, and one grain from the Novobobrovskaya Formation plots into the field of Fe-rich quartz-tourmaline rocks, metapelites, and calc-silicate hornfels. The chemical compositions of the studied tourmalines indicate that the erosion products of granites (if any) were not the source of the tourmaline grains. Also, no tourmalines were found, for which metacarbonates or metapyroxenites could be the source.

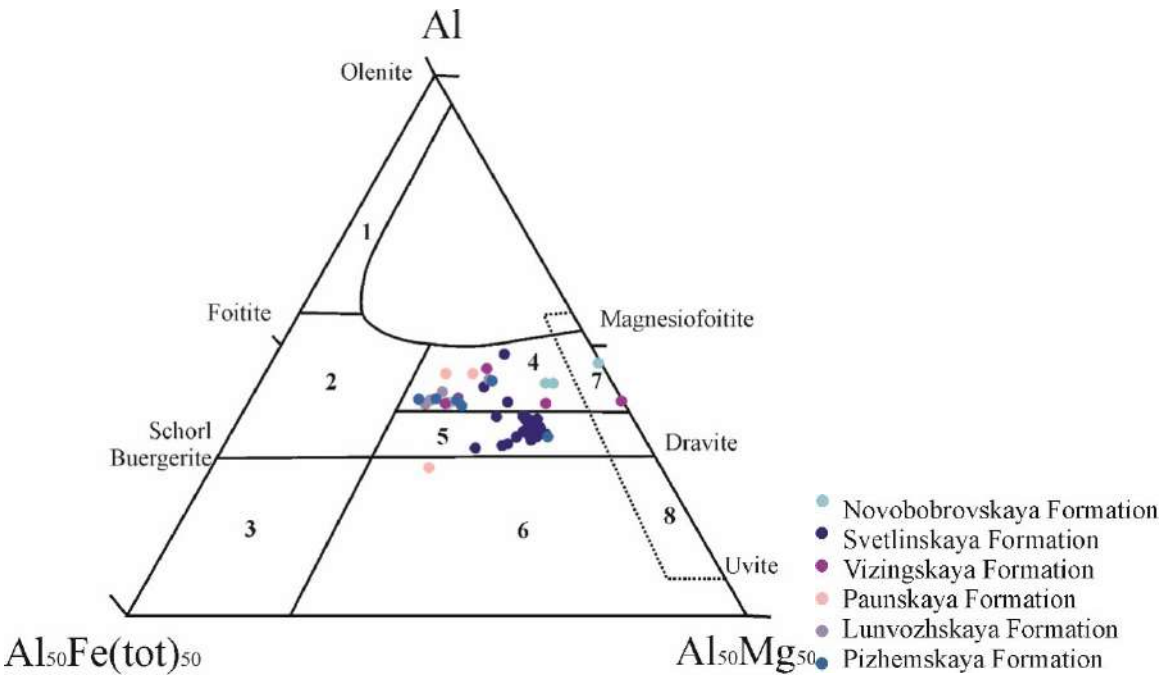

Figure 4.3. Chemical composition of detrital tourmalines on an Al–$Fe_{50}Al_{50}$–$Mg_{50}Al_{50}$ petrogenetic diagram (Henry and Guidotti, 1985*). (1) Li-rich granitoids in association with aplites and pegmatites; (2) Li-poor granitoids in association with aplites and pegmatites; 3 – Fe-rich quartz-tourmaline rocks and hydrothermally altered granites; (4) metapelites and metapsammites saturated with alumina; (5) metapelites and metapsammites poor in alumina; (6) Fe-rich quartz-tourmaline rocks, metapelites, and calc-silicate hornfels; 7 – ultramafics, low-Ca and Cr- and V-rich metasediments; 8 – metacarbonates, metapyroxenites.*

The dravite/schorl ratio (Figure 3.13c) suggests that most of the grains had a metamorphic origin (Kowal-Linka and Stawikowski, 2013). The studied tourmalines probably crystallized during the course of metamorphism of the B-rich sedimentary rocks. It may be assumed that paragneisses and mica schists metamorphosed to the amphibolite facies were the main source of tourmalines.

Tourmaline, as compared to zircon, is less stable during the detrital material transport (Morton and Hallsworth, 1999). The prevalence of angular and subangular shapes suggests that tourmalines were not reworked from older sedimentary complexes. Zircon grains are much better rounded, which indicates they were repeatedly reworked during transport of sediment. This conclusion is further confirmed by a wide scatter of the detrital zircon ages (Brusnitsyna et al., 2021).

A small number of the analyzed detrital tourmalines from the Riphean clastic rocks is most likely due to their lower contents, as compared to zircons, in the sampled rocks. Our data on the chemical composition of tourmalines indicate that metamorphic complexes were a significant source of clastic material in Timan in the Middle and Late Riphean. Moreover, the metamorphic rocks were likely dominated by paragneisses and schists, which originally had a sedimentary nature. This is in

good agreement with the widely ranging ages of detrital zircons from the studied strata and may indicate their reworking from older sedimentary and metasedimentary complexes (Brusnitsyna et al., 2022).

4.2.1. Morphology of grains in the heavy minerals fraction (zircon and tourmaline)

Investigations conducted over the last decades showed that the role of heavy fraction minerals from sandstones in reconstructing clastic rocks provenances has been overestimated to some extent. A comprehensive study of (Morton and Hallsworth, 1999) showed that weathering processes in the source area do not significantly affect the diversity of heavy mineral complexes prior to sediment transport. Those authors (Morton and Hallsworth, 1999) also noted that transport processes do not have a marked effect on the heavy minerals diversity either, even on moving for long distances. In the course of transport, the shape and degree of roundness of detrital minerals is controlled by a number of processes such as chemical weathering in the clastic material provenance area, hydraulic sorting, and diagenetic changes associated with the depth of occurrence, circulation of interstitial fluids, and/or multiple processing and recycling of clastic material (Morton and Hallsworth, 1999, Garzanti et al., 2009, Garzanti et al., 2008 and others). At the same time, studies of the zircon grains roundness (e.g., Zoleikhaei et al., 2016) showed that they retain their close-to-euhedral shape even after several cycles of transfer and precipitation. In our samples, the dated zircons are predominantly subangular and subrounded (Figure 3.9, 3.10, 3.11). The number of angular grains varies from 2% to 6%, ranging as high as 14% in the Novobobrovskaya Formation. Subangular zircons make up 21% to 47% of the population, and subrounded grains are within 35%-59%. Rounded zircon grains account for 13-27% of the total population. In the Novobobrovskaya Formation, only 3% of zircons are rounded.

Tourmaline is less stable to sediment transport than zircon (Morton and Hallsworth, 1999). Studies of the degree of roundness of detrital tourmalines showed the prevalence of angular (49%) and subangular (46%) grains. Subrounded crystals amount to 5% of the total population (Fig. 3.12). No rounded tourmalines have been found.

Thus, the rounded shape of zircon grains suggests they were repeatedly reworked, e.g., in the tidal zone of a sedimentary basin. However, the shape of zircons can say little about the sediment transport distance. The prevalence of angular and subangular tourmaline grains indicate they were not transported over a long distance and not reworked from older sedimentary complexes. Their provenance was likely located in close proximity to the sedimentary basin.

4.3. Petrography of clastic rocks and reconstruction of detrital material provenances

The petrographic characteristics and structural and textural features of all studied clastic rocks are similar for all stratigraphic units. Most samples have a psammitic or silty texture, massive or, less

often, layered structure, and interstitial or basal chlorite-sericite cement (probably originally clayey?). The clastic fraction mainly consists of quartz and feldspar; in some rocks the amount of rock fragments (siltstones, quartzites, etc.) reaches 40% of the total rock volume.

As seen from the classification diagram (Figure 3.1.), the studied clastic rocks compositionally correspond to arkoses, subarkoses, quartz arenites, litharenites and sublitharenites. On a Q–F–L diagram (Dickinson et al., 1983), most of the data points for the Svetlinskaya Formation metasandstones and the Novobobrovskaya Formation metamorphosed silty sandstones are concentrated in the field of the erosion products of orogenic complexes, with single samples falling into the field of the erosion products of the basement highs (Figure 4.4.). The composition points for the Vizingskaya Formation metasandstones are localized in the fields of the erosion products of both the basement highs and, to a lesser extent, orogenic complexes. Metasedimentary rocks of the Lunvozhskaya Formation lie, on the Dickinson diagram, within the field of reworked basement highs (Figure 4.4.). Thus, all data points are concentrated in two fields that are fields of the erosion products of orogenic complexes and basement highs. The location of the eroded orogenic complexes which were the source for the rocks from which more than a half our samples were collected is not obvious and requires clarification using other analytical methods. The origin of basement highs is seemingly beyond doubt: these are highs of the EEP crystalline basement of Archean-Early Proterozoic age. However, the basement complexes can also be exposed in terranes/microcontinents in neighboring fold-and-thrust belts. This interpretation suggesting the clastic material input from a single provenance is supported by the fact that samples from all formations, except for the Lunvozhskaya Formation, fall into the fields of the erosion products of both the orogens and basement highs.

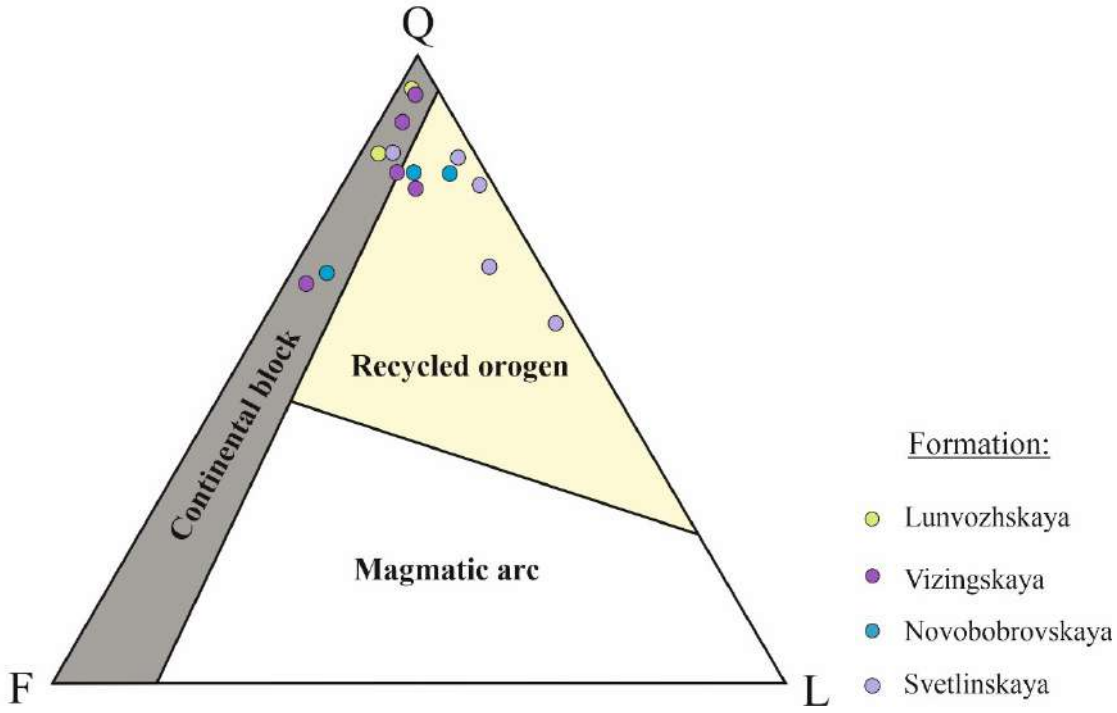

Figure 4.4. Diagram of sandstone compositions and tectonic settings in their provenance areas (Dickinson et al., 1983)

Summarizing the data obtained on the chemical composition of tourmalines, the morphology of detrital tourmaline and zircon grains, and the petrographic composition of sandstones allows to present **the second provision to be defended - A significant number of rounded detrital zircon grains, the composition of sandstones, and the chemical composition of detrital tourmalines indicate a widespread occurrence of sedimentary (metasedimentary) rocks in the source area.**

4.3.1. Location of clastic material provenances for the Riphean strata of Middle Timan: interpretation of U-Th-Pb ages of detrital zircons

The main results of the detrital zircon age distribution study are the following.

Samples from the Chetlasskaya Group are dominated by Early Proterozoic zircons, accounting for 45% of the total zircon population. Detrital zircons with Early Riphean ages make up ca. 36% (26% to 50%), and those with Middle Riphean ages constitute ca. 15% of the total number of dated grains. The proportion of Archean zircons is ca. 5%. In the sample from the Paunskaya Formation (Bystrinskaya Group), most zircons are of Early Proterozoic age (51%). Nine percent of zircons are Archean in age. Early Riphean detrital zircons contribute 27%, and Middle Riphean zircons make up 12% of the whole population.

Samples from the Vymskaya Group contain 40% of Middle Riphean and 29% of Early Riphean zircon grains. Zircons with Early Proterozoic age comprise 30% of the total population. Zircon grains of Archean age were not found.

Comparison of the ages of detrital zircons from the Riphean deposits of Timan obtained in our study and in earlier works (Udoratina et al., 2017; Soboleva et al. 2019; Kuznetsov et al. 2010; Andreichev et al. 2013) revealed their close similarity (Table 3). The conducted statistical analysis showed that all zircons belong to a single population, suggesting that the studied metasedimentary rocks of Middle Timan had a single source of clastic material. There is also a similarity in the age distribution of detrital zircons from the Precambrian rocks of Middle Timan (this study and Udoratina et al. 2017; Soboleva et al. 2019) and North Timan (Andreichev et al. 2013, 2014). However, our data do not correlate with the ages of detrital zircons from the Precambrian sedimentary rocks of South Timan (Dzhezhimskaya Formation) (Kuznetsov et al. 2010a), which were probably sourced from a different provenance.

Table 3. Degree of overlap of confidence intervals of cumulative curves for the U-Th-Pb detrital zircon age distributions in the Precambrian sedimentary rocks of the Timan region. Calculations based on the approach outlined by Andersen et al. (2016, 2018).

	Svetlinskaya Fm.	Novobobrovskaya Fm.	Vizingskaya Fm.	Paunskaya Fm.	Lunvozhskaya Fm.	Malochernoretskaya Fm.	Djejim Fm.	Yambozerskaya Fm.
Svetlinskaya Fm.		0	0	0	0.05	0	0.11	0.07
Novobobrovskaya Fm.	0		0	0	0.11	0.05	0.05	0.11
Vizingskaya Fm.	0	0		0	0.1	0.03	0.11	0.11
Paunskaya Fm.	0	0	0		0.01	0	0.01	0.05
Lunvozhskaya Fm.	0.05	0.11	0.1	0.01		0	0.17	0
Malochernoretskaya Fm.	0	0.05	0.03	0	0		0.14	0
Djejim Fm.	0.11	0.05	0.11	0.01	0.17	0.14		0.16
Yambozerskaya Fm.	0.07	0.11	0.11	0.05	0	0	0.16	

The table has been color-coded so that green color shows full overlap, yellow is for < 5% difference and red is for > 5% difference. Data from this study and (Andreichev et al., 2013, 2014; Kuznetsov et al., 2010a, Soboleva et al., 2019, Udoratina et al., 2017).

The distributions of the U–Th–Pb ages of detrital zircons from the metasedimentary rocks of the Chetlassky Kamen and the Volsko-Vymskaya Ridge are closely similar, which is further confirmed by a statistical test. This suggests a single source of clastic material for all studied Precambrian deposits of Middle Timan.

Archean zircon grains are subordinate in amount in the total zircon population. Their possible sources are magmatic and metamorphic rocks of the same age, exposed in the northwestern part of Baltica (Figure 4.5) (Balagansky et al., 2016; Baltybaev et al., 2004; Baltybaev, Levchenkov, 2005; Bibikova et al., 2009; Bogdanova et al., 2008, 2016; Egorova, 2014; Korja et al., 2006; Larin, 2009; Petrov, 1999; Sergeev et al., 2007; Zozulya et al., 2007). These rocks were formed in the course of the accretionary event that completed formation of the Fennokarelian protocontinent around 2500–2600 Ma (Bogdanova et al. 2008, 2016).

Detrital zircons with the ages of 1.9–1.7 Ga were found in all samples; they correspond to the age of several accretionary episodes in the southwestern part of Fennoscandia, called Svecofennian Orogeny (Bogdanova et al., 2008; Korja et al., 2006; Lahtinen et al., 2005; Nironen, 1997). Detrital zircons with Early Proterozoic (1.9–1.7 Ga) ages could have been supplied from the Early Proterozoic basement complexes of the East European Platform (Petrov, 1999; Baltybaev et al., 2004; Baltybaev and Levchenkov, 2005; Baltybaev, 2005; Korja et al., 2006; Balagansky et al., 2016 and others). At the same time, considering the presence of numerous rounded and subrounded grains of this age (Figure 3.9, 3.10), suggesting their repeated reworking (Pettijohn, 1975), they could have been sourced from older sedimentary rocks, particularly those exposed within the Grenvillian-Sveconorwegian Orogen in the northern and northwestern (in present-day coordinates) sectors of Baltica (Bingen et al., 2008; Mints, 2017; etc.).

The Early Riphean zircons make up 50% of all dated grains and form peaks at 1470–1550 and 1170–1370 Ma.

The likely sources of zircons with Early Riphean (1500–1570 Ma) crystallization ages are rapakivi granites, widespread in the Baltic Shield (Figure 4.5) (Amelin et al., 1997; Bayanova et al., 2002; Bogdanova et al., 2008; Larin, 2009; Rämö et al., 2014; etc.). The rapakivi granites were also the main sources of detrital material during the accumulation of the Lower Riphean sediments of the Pasha–Ladoga graben (Kuptsova et al., 2011; Ivleva et al., 2016; Ershova et al., 2019). At the same time, magmatic and metamorphic events coeval with the rapakivi granites are widely manifested within the southwestern part of the Sveconorwegian Orogen known there as the 1520-1660 Ma Gothian Orogeny (Bingen et al., 2008a, 2008b; Roberts et al., 2013; Slagstad et al., 2020).

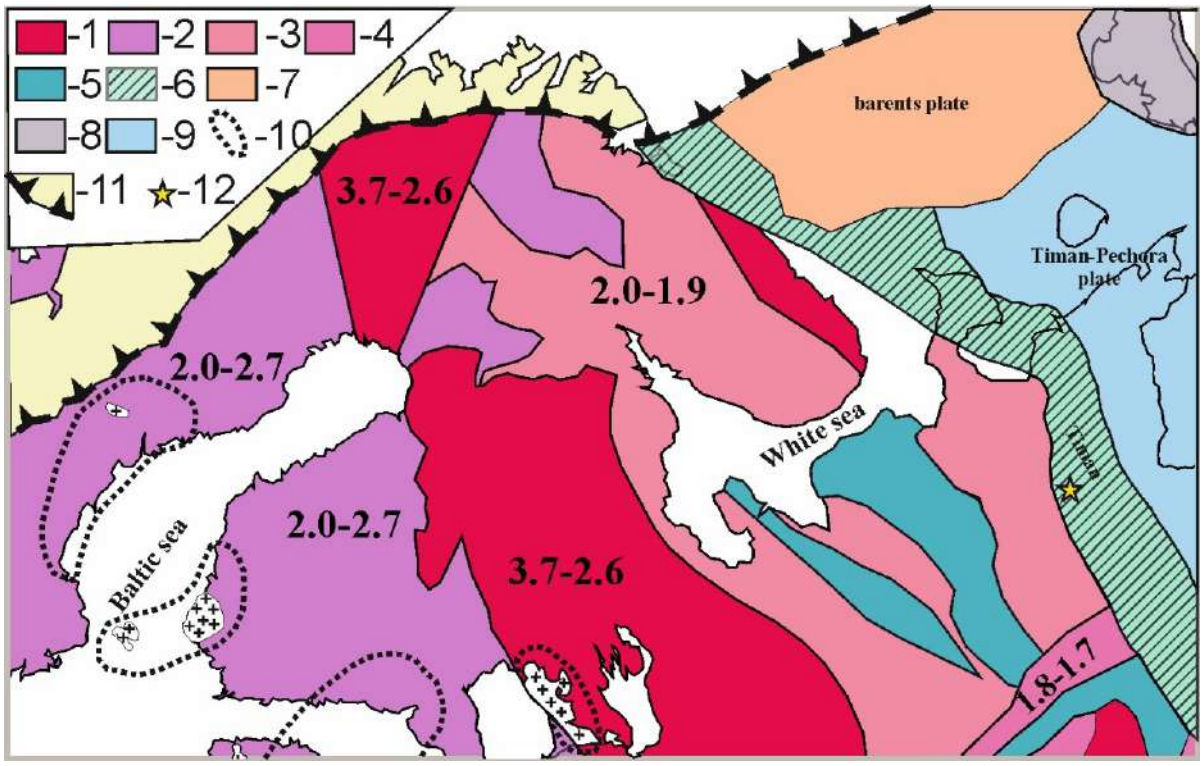

Figure 4.5. Tectonic sketch map of the northern part of the East European Platform (a), simplified after (Bogdanova et al., 2008; Larin, 2009).

1–4 – Archean-Proterozoic blocks of the Baltica basement; 5 – aulacogens and sedimentary basins of the inner part of the passive Baltica margin; 6 - Timan Range; 7 - Barents Sea plate; 8 – Pay Khoy-Novaya Zemlya fold belt; 9 - Timan-Pechora plate; 10 – distribution area of rapakivi granites with an age of 1500–1600 Ma; 11 - front of the Caledonian fold belt; (12) sampling sites of detrital zircons for U–Pb dating, this study.

Zircon is a very stable mineral that can be repeatedly reworked in different sedimentary basins of varying age. This fact sets some limits on the reconstruction of clastic material provenances based solely on detrital zircon ages. For example, the Archean and Early Proterozoic zircons could have been reworked from older sedimentary rocks. This assumption is confirmed by our data on detrital rutile dating showing that the number of Late-Middle Riphean and Early-Late Riphean rutiles far exceeds that of the Early Proterozoic and Archean grains.

The youngest zircons from the dated populations correlate well with magmatic and tectonic events in the interval 1135–1170 Ma, which are interpreted (Bingen and Solli, 2009) as evidence for the formation of the active margin and back-arc basin during the early evolution stages of the Grenvillian-Sveconorwegian Orogen. The disruption of the U-Th-Pb isotope system and the occurrence of a tectonic and/or metamorphic event (ca. 1150 Ma) in the provenance area is further supported by combined statistical processing of concordant and discordant grains from sample 9034/2

collected from the Paunskaya Formation (Figure 3.15) However, intense tectonic events accompanied by syncollisional granitic magmatism in the Grenvillian-Sveconorwegian Orogen at ca. 1020–1050 Ma (Bingen et al., 2008; Rivers et al., 2012; Spencer et al., 2015) are not reflected in detrital zircons from the Riphean deposits of Middle Timan.

4.3.2. Paleogeography of northeastern Baltica in the Early and Middle Riphean

The interpretation of the Grenvillian-Sveconorwegian Orogen as the main source of clastic rocks for the Riphean deposits of Middle Timan requires more detailed studying the paleogeography of the northern part of the EEP and neighboring regions. Magmatic and metamorphic events in the interval 1.0–1.4 Ga are widely manifested within the Grenvillian-Sveconorwegian Orogen (including the terranes amalgamated within it) located in the northwestern (in present-day coordinates) sector of Baltica (Bingen et al., 2008; Mints, 2017 and others). Magmatic activity in the time interval 1280–1480 Ma was relatively low, but bimodal magmatism has been established in the southwesternmost part of the Sveconorwegian terrane (Pedersen et al., 2009; Spencer et al., 2014; Roberts and Slagstad, 2015; Slagstad et al., 2020). Large-scale bimodal magmatism (1080-1280 Ma) has been identified in the Telemarkia terrane in southern Norway (Bingen et al. 2021). It is believed that bimodal magmatism took place throughout the Grenvillian-Sveconorwegian Orogen area on the northwestern margin of Baltica between 1130 and 1280 Ma (Slagstad et al., 2020).

Lorenz and co-authors (Lorenz et al., 2012) suggested that the Grenvillian-Sveconorwegian-Orogen extended all around the northern margin of Baltica and further northward (in the present-day coordinates), approaching the objects in Middle Timan discussed in this study. The view of (Lorenz et al., 2012) is supported by the widespread occurrence of Middle Riphean detrital zircons on the northern and northeastern margins of Baltica. The presence of Middle Riphean detrital zircons was reported from the sandstones of the Middle Riphean Isherimskaya Formation in the Northern Urals (Petrov et al., 2015; Maslov et al., 2018b), the rocks of the basal layers of the Karatavian in the Southern Urals (Maslov et al., 2018a), the Upper Riphean rocks in the Southern (Kuznetsov et al., 2010) and Northern Timan (Andreichev et al., 2013, 2014), the Rybachiy and Sredniy Peninsulas (Mikhailenko et al., 2016), and metasedimentary rocks in Northern Norway (Zhang et al., 2015, 2016). Comparison of the distribution of the U–Th–Pb ages of detrital zircons from the Middle and Upper Riphean sequences of Baltica and its periphery (Timan Range, pre-Caledonian complexes of Scandinavia, Southern and Middle Urals) (Figure 4.6; Table 3) suggests their close similarity, probably indicative of a single source area of detrital material. Consequently, it is most probable that the Grenvillian-Sveconorwegian Orogen was among the main sources of sediment supply for the Upper Precambrian clastic rocks of Timan, the Southern and Middle Urals, and the Pre-Caledonian

complexes of Scandinavia. This supports the assumption of its substantially wider development in northern Baltica (in present-day coordinates) (Lorenz et al., 2012).

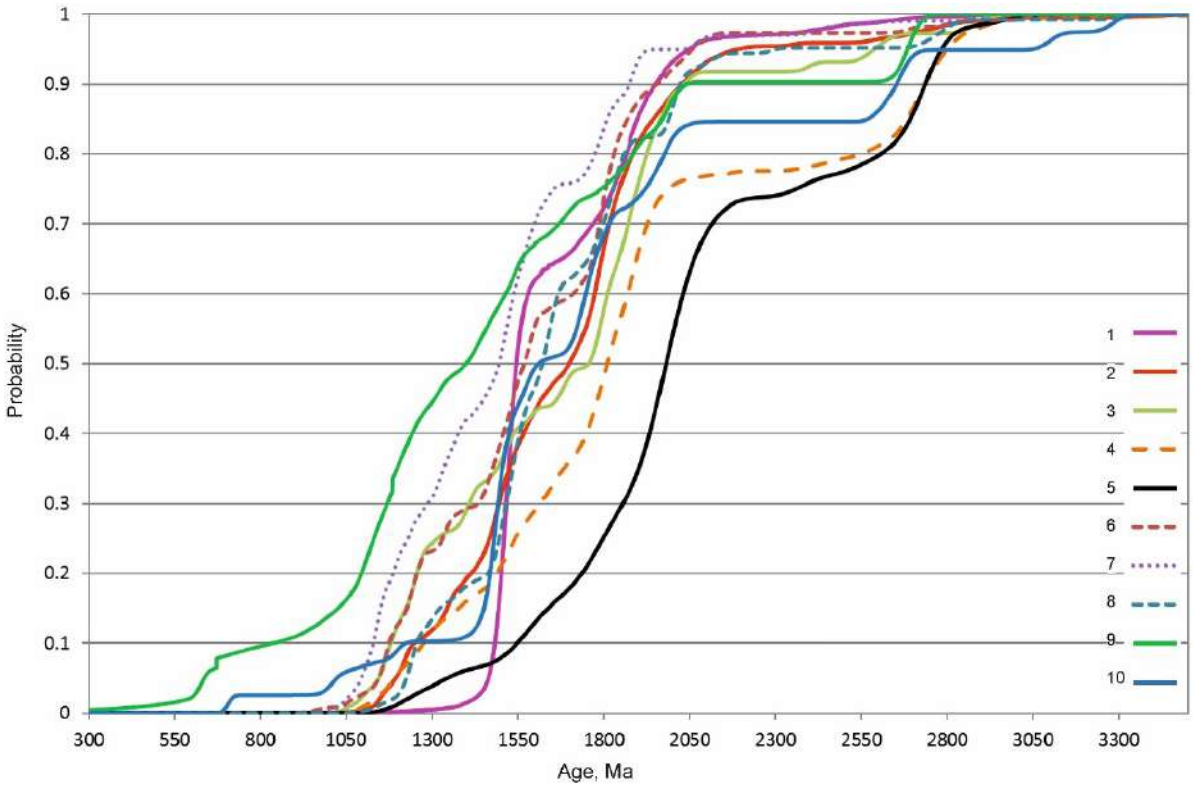

Figure 4.6. Cumulative curves of the isotopic ages of detrital zircons from the Chetlasskaya Group and the Riphean sequences of Baltica and its periphery.

1 – Riphean sedimentary rocks of the Pasha–Ladoga graben (Kuptsova et al., 2011; Ivleva et al., 2016); 2 – Chetlasskaya Group, Middle Timan (this study; Udoratina et al., 2017); 3 – Riphean sedimentary rocks of the Kola Peninsula (Mikhailenko et al., 2016); 4 – Upper Riphean (Neoproterozoic) sedimentary rocks of Northern Norway (Zhang et al., 2015); 5 – Riphean sedimentary rocks of Southern Timan (Kuznetsov et al., 2010); 6 - arkosic sandstones of the Upper Riphean Biryanskaya Subformation of the Zilmerdakskaya Formation in the Southern Urals (Maslov et al., 2018a); 7 – Riphean sequences of Northern Timan (Andreichev et al., 2013, 2014); 8 – Middle Riphean clastic rocks of the Middle Urals (Petrov et al., 2015; Maslov et al., 2018b); 9 - titanium ores from the Malorucheiskaya Formation (Pizhemskoe ore occurrence) (Krasotkina et al., 2016); 10 - conglomerate-breccia of the Middle Devonian Pizhemskaya Formation (Pizhemskoe ore occurrence) (Krasotkina et al., 2017)

The Lu-Hf isotopic data for detrital zircons from the studied Riphean deposits of Middle Timan are shown in Fig. 4.7a. It can be seen that zircons with the ages of 1.0–1.4 Ga fall between the evolutionary trends of the depleted mantle (DM) and the chondritic uniform reservoir (CHUR). Several data points are located close to the DM isotope signature, suggesting these zircons crystallized

from juvenile magma. Some of the data points lie below the CHUR isotopic evolutionary trend, suggesting crystallization of zircon grains from magmas originated from a depleted mantle source (juvenile magmas) mixed with varying amounts of assimilated older crustal material, which is consistent with the continental magmatic arc geodynamic setting (Griffin et. al., 2002).

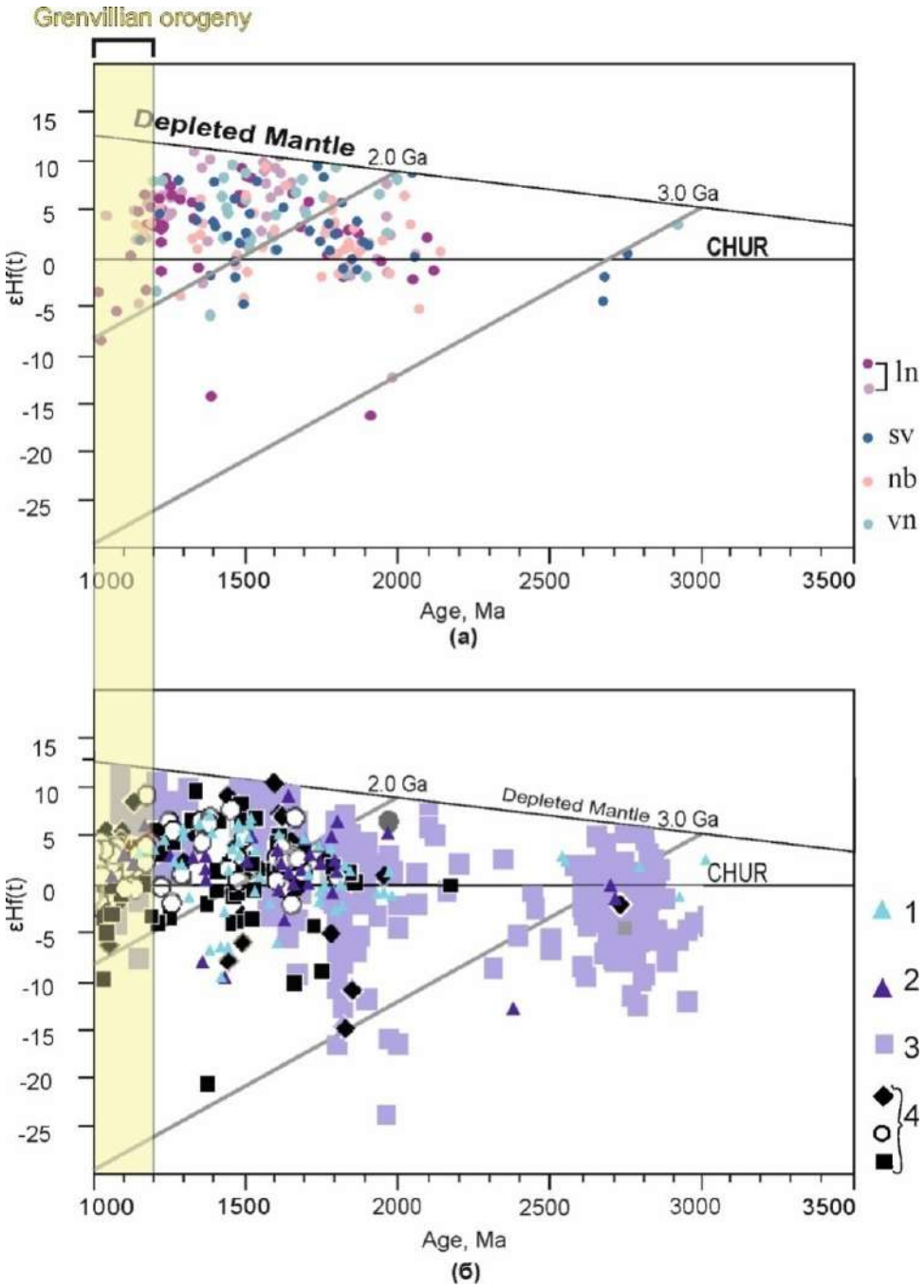

Figure 4.7. Diagrams of the isotopic (Lu-Hf) composition of detrital zircons from (a) clastic rocks of Middle Timan (b) other areas with synchronous zircon ages to the Grenvillian Orogeny.

(a) Riphean deposits of Middle Timan. Formations: lv - Lunvozhskaya; sv - Svetlinskaya; nb - Novobobrovskaya; vn - Vizingskaya

(b) 1 - Sedimentary rocks, pre- and syncollisional with the Grenvillian Orogeny (Scotland) (Spencer, 2015); 2 - Sedimentary rocks, pre- and syncollisional with the Grenvillian Orogeny (Labrador) (Spencer, 2015); 3 - Fennoscandian granitoids (Kristoffersen, 2014); 4 - Sedimentary rocks of northern Norway [Kristoffersen, 2014])

Comparison of our data with the data from Scandinavia (Kristoffersen et al., 2014), Scotland and Labrador (Spencer et al., 2015) shows similarities in Lu-Hf characteristics of younger than 2 Ga zircons from coeval rocks in these regions (Figure 4.5). Most of their composition points on the diagrams have positive εHf(t) values and are located between the depleted mantle and CHUR lines. Several zircons with ages of 1.9 and 1.6 Ga have negative εHf(t) values up to -20. The population of Archean zircons on the plot in Figure 4.5b is much greater than in Figure 4.5a, but their isotopic characteristics are similar, and zircons with an age of ca. 2.7–2.8 Ga show weakly negative to zero εHf(t) values. This suggests that source areas of detrital zircons from clastic deposits of Middle Timan and sedimentary rocks of Norway, Labrador and Scotland experienced a similar tectonic evolution, moreover the zircons likely have been supplied from the same provenance.

Our petrographic studies also showed that a possible detrital material source for the studied rocks could be orogenic zones (Figure 4.4). An earlier U–Th–Pb dating of detrital zircons from the Upper Riphean sandstones of the Dzhezhimskaya Formation in South Timan (Kuznetsov et al., 2010) demonstrated the prevalence of Early Proterozoic and Late Archean grains; at the same time, the studied population contained ~7% of grains with ages from 1350 to 1200 Ma. The authors of that study suggested that the rocks of the Dzhezhimskaya Formation were largely derived from erosion products of the crystalline complexes in the northern and central parts of Baltica. However, the studies based on estimation of the isotopic ages of detrital zircons from the Riphean rocks of Middle and Northern Timan, including the Chetlasskaya Group (Andreichev et al., 2013, 2014; Udoratina et al., 2017; Soboleva et al., 2019) suggest that the sources of detrital material for these rocks consisted of the crystalline basement complexes of Baltica together with the rocks of the Grenvillian-Sveconorwegian orogen at its northwestern periphery.

The stages and geological features of the Sveconorwegian-Grenvillian Orogeny are much better manifested and most comprehensively studied in the Laurentian part of the orogen than in Baltica. This is partly due to the fact that in Laurentia there are well preserved orogenic complexes and their erosion products. Spencer and co-authors (Spencer et al. 2015) identified pre-orogenic, synorogenic and post-orogenic deposits of the Grenvillian orogeny (Figure 4.8), notably differing in the detrital zircon age distribution. To apply this concept to the Precambrian rocks of central and northeast Baltica, it is necessary to have suitable pre-orogenic material. The best candidates are the Riphean rocks within the Pasha-Ladoga graben located on the southern margin of the Baltic Shield. The age of the rocks is well constrained by the MDA (1470–1480 Ma) inferred from detrital zircon dating and by the crystallization age of the intruding mafic sill (~1459 Ma) (Kuptsova et al., 2011). Most of the U-Th-Pb dated detrital zircons from these sedimentary sequences yielded ages in the ranges 1550-1600 Ma and 1900-2000 Ma, which, combined with their immature composition, suggest they were eroded from the

proximal basement rocks of Baltica (Ershova et al., 2019; Kuptsova et al., 2011; Ivleva et al., 2016). Therefore, these pre-orogenic deposits reflect the composition and age of the exposed continental crust before the orogeny. Spencer and co-authors (2015) showed that rocks deposited during the Sveconorwegian-Grenvillian Orogeny have the same detrital zircon age distributions as observed in the Laurentian basement, with peaks at 1100 and 1500 Ma on the KDE plot (Figure 4.8). The results of U-Th-Pb dating of detrital zircons from the Riphean sedimentary and metasedimentary rocks of the northeastern EEP (in present-day coordinates) show age distributions similar to those observed in coeval sediments in the Laurentian part of the orogen. Moreover, Spencer and co-authors (2015) showed that detrital zircons with an age of 0.95–1 Ga, not recorded in the Middle Timan samples, are only present in post-orogenic deposits, representing the main stage of the collisional process.

Thus, the data obtained for Middle Timan suggest that all studied rocks can be interpreted as synorogenic. Similar detrital zircon age distributions are established for Precambrian sedimentary rocks from northern and eastern parts of Baltica (in present-day coordinates), from Scandinavia to the Northern Urals. This suggests that a large orogenic system was the main source for Precambrian sedimentary rocks. From this it follows that the age of the studied clastic rocks may be younger (late Middle Riphean-early Late Riphean) than the MDA calculated from zircon dating and may correspond to the MDA estimated from rutile dating, reflecting the age of the main orogenic stage.

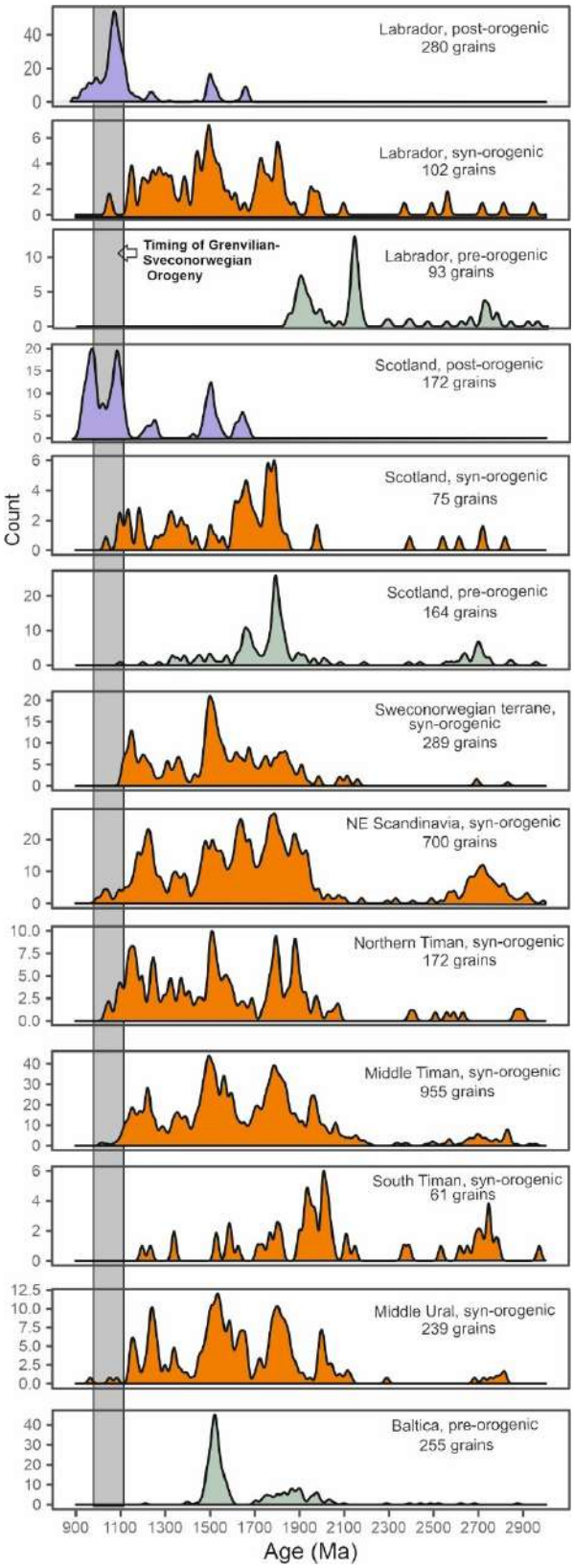

Figure 4.8. Comparison of the detrital zircon age distribution plots for Riphean clastic deposits of Northern Baltica and Laurentia *(data from our study and Andreichev et al., 2013, 2014; Ivleva et al., 2016, 2018; Kuptsova et al., 2011; Kuznetsov et al., 2010a; Lorenz et al., 2012; Maslov et al., 2018a, 2018b; Mikhailenko et al., 2016; Slagstad et al., 2020; Spencer et al., 2014, 2015; Udoratina et al., 2017; Zhang et al., 2015, 2016)*

At present, two tectonic models exist for the formation of the Grenvillian-Sveconorwegian Orogen. The first model assumes a non-collisional (accretional or Andean-type) orogeny (Granseth et al., 2020; Slagstad et al., 2013, 2017, 2018, 2020), while the second model claims a collisional nature of orogeny (Bingen et al., 2021; Gower et al., 2008; Rivers, 2008, 2012). Bingen and co-authors (Bingen et al., 2021) updated the second model suggesting that the orogenic plateau formed during the Grenvillian-Sveconorwegian Orogeny underwent a post-orogenic collapse ca. 930 Ma ago. Moreover, they (Bingen et al., 2021) concluded that the syn- to late-Sveconorwegian plutons (920-1066 Ma) formed at approximately the same depth of ca.16 km. Subsequently, the plutons are exposed as a result of erosion of the overlying rocks and tectonic extension. The extension episode occurred, according to $^{40}Ar/^{39}Ar$ muscovite and biotite dating, at ca. 860-930 Ma. Similar ages are recorded by the youngest detrital rutile grains from the Lunvozhskaya and Vizingskaya Formations. Thus, the absence of syn- and late-Sveconorwegian zircons from the studied Timan rocks can be explained by that the main source of clastic material was an orogenic plateau (Figure 4.9) composed of numerous terranes of various affinity, with a complex magmatic and metamorphic history of the Grenvillian-Sveconorwegian Orogen (Bingen et al., 2021). However, the syn- and post-Sveconorwegian plutons were eroded and exposed after completion of deposition of the Timan Precambrian rocks and, thus, could not be reflected in the sedimentary record. The absence or a low number of Archean zircons within the dated populations suggest they could be sourced from the Grenvillian-Sveconorwegian Orogen, since the Archean rocks are not exposed within this orogen (Cawood et al., 2007).

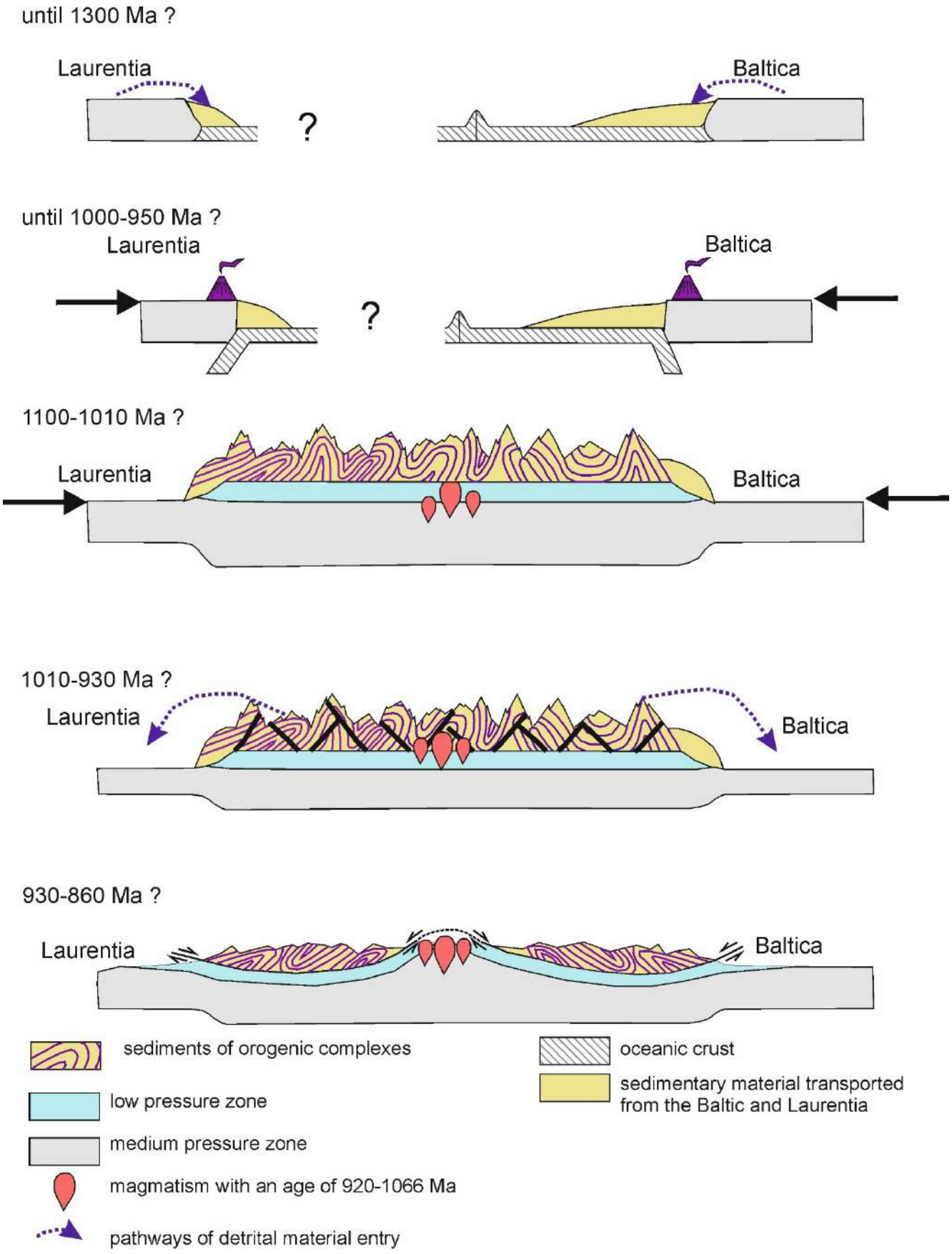

Figure 4.9. Schematic section for the formation and collapse of the orogenic plateau during the Grenvillian-Sveconorwegian Orogeny (simplified after Rivers, 2012, 2015).

Fragments of the Grenvillian-Sveconorwegian Orogen are currently located in the southwestern part of the Baltic Shield, several thousand kilometers west of the study area, and extend eastward under the Caledonian orogenic complexes (Kirkland et al., 2007; Roffeis and Corfu, 2014). However, the presence of coarse-grained clasts and unstable to sedimentary reworking and long-term transport minerals in the clastic rocks of the northeastern EEP indicates the proximity of the detrital material source area. Thus, our data confirm the tectonic model proposed by Lorentz (Lorentz et. al., 2012), which assumes that the Grenvillian-Sveconorwegian Orogen extended further northeast, across the Barents Sea, from its nearest outcrop in southern Sweden (Figure.10). At the same time, the available MDA data calculated from the U–Th–Pb detrital rutile dates indicate that sedimentation could continue until approximately 900 Ma. In this case, the absence of detrital zircons, which are the erosion products of syncollisional orogens, can only be explained by that the collapse of the orogen in the provenance area must have occurred somewhat later than suggested by the Rivers's model (Rivers, 2012, 2015) (Figure 4.9), probably also ca. 900 m.y. ago.

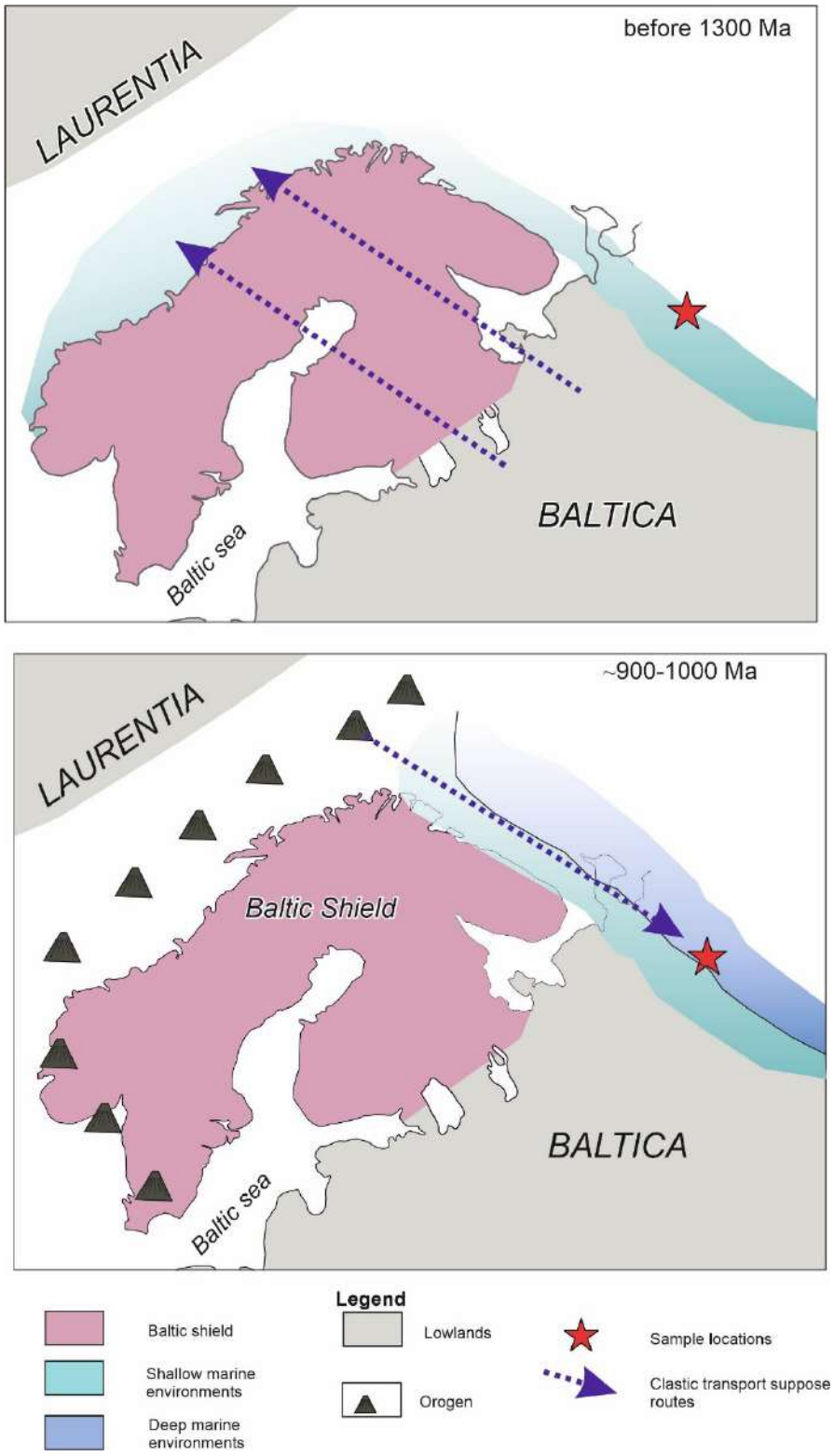

Figure 4.10. Simplified paleogeographic map of northeastern Baltica (in present-day coordinates), showing a possible direction of the clastic material transport.

The above data allow to present **the third provision to be defended - The integrated study of the Riphean clastic successions of Middle Timan indicates that the main provenance of clastic material was the Sveconorwegian-Grenvillian Orogen (including associated older terranes).**

Conclusions

Based on the results of our integrated study, the main conclusions are the following:

1. A detailed petrographic analysis of the Precambrian clastic rocks of Middle Timan was carried out, which revealed they are fairly “mature” sediments with compositions corresponding to arkoses, subarkoses, quartz arenites, sublitharenites and litharenites. Interpretation of petrographic data obtained with the use of tectonic setting diagrams points to the continental basement rocks and orogenic complexes as the main provenances for clastic rocks.

2. The degree of roundness of detrital zircons and tourmalines was determined. Among detrital zircons, subangular and subrounded grains predominate, while tourmalines are angular and subangular in shape. The rounded shape of zircons suggests they were involved in several recycling stages.

3. The study of the chemical composition of detrital tourmalines from the clastic rocks of Middle Timan showed they were sourced from metamorphosed sedimentary rocks.

4. An isotope-geochronological study of heavy minerals was carried out, including U-Th-Pb (LA-ICPMS) dating of zircons, U-Th-Pb (LA-ICPMS) dating of rutiles; and Lu-Hf isotopic-geochemical analysis of zircons.

5. Detrital zircon dating showed that possible source(s) of detrital material could be Archean, Proterozoic, and Early-to-Middle Riphean complexes.

6. The youngest detrital rutile ages obtained define the ages of metamorphic events in the source area of detrital material.

7. The obtained detrital zircon ages indicate a younger age of sedimentary rocks than was determined earlier (RF_{1-2}). The age of the Middle Timan clastic rocks is estimated as late Middle Riphean-early Late Riphean. The stratigraphy of the Timan Riphean rocks needs to be revised or, at least, refined based on the updated ages of formations.

Nevertheless, there are some issues that call for further, more detailed investigation. For example, more extensive studies of various minerals of the heavy fraction of sedimentary rocks such as rutile, tourmaline, monazite, etc., are required. Our study showed that in addition to U-Th-Pb dating of zircons, the U-Th-Pb dating of detrital rutiles proved effective not only in determining the age of the last metamorphic event in the source area of clastic material, but also in constraining the maximum depositional age for the Lunvozhskaya Formation (ca. 885-904 Ma) and the Vizingskaya Formation (ca. 878-926 Ma). The study of the chemical composition of the heavy minerals is also an important

tool for establishing the provenance areas for clastic rocks, which complements significantly the results of isotope dating of minerals.

References

1. Amelin Y.V., Larin A.M., Tucker R.D. Chronology of multiphase emplacement of the Salmi rapakivi granite-anorthosite complex, Baltic Shield: implications for magmatic evolution // Contributions to Mineralogy and Petrology.1997. № 4(127). P. 353–368.

2. Andersen T., Andersson U.B., Graham S., Åberg G., Simonsen S.L. Granitic magmatism by melting of juvenile continental crust: new constraints on the source of Palaeoproterozoic granitoids in Fennoscandia from Hf isotopes in zircon // Journal of the Geological Society. 2009. № 2(166). P. 233–247.

3. Andersen T., Elburg M.A., Magwaza B.N. Sources of bias in detrital zircon geochronology: Discordance, concealed lead loss and common lead correction // Earth-Science Reviews. 2019. № 197. P. 1-15.

4. Andersen T., Kristoffersen M., Elburg M.A. How far can we trust provenance and crustal evolution information from detrital zircons? A South African case study // Gondwana Research. 2016. № 34. P. 129–148.

5. Andersen T., Kristoffersen M., Elburg M.A. Visualizing, interpreting and comparing detrital zircon age and Hf isotope data in basin analysis - a graphical approach // Basin Res. 2018. № 1(30). P. 132–147.

6. Andreichev V.L. Isotopic geochronology of intrusive magmatism in the Northern Timan. Yekaterinburg: Institute of Geology; 1998.

7. Andreichev V.L. Evolution of the basement of the Pechora plate according to isotope-geochronological data. Syktyvkar; 2010.

8. Andreichev, V.L., Soboleva, A.A., Gehrels, G.E., 2013. U-Pb age of detrital zircons from the Upper Precambrian terrigenous section of North Timan // Dokl. Earth Sc. № 450. P. 592–596.

9. Andreichev, V.L., Soboleva, A.A., Gehrels, G., 2014. U-Pb dating and provenance of detrital zircons from the Upper Precambrian deposits of North Timan // Stratigr. Geol. Correl. № 22. P. 147–159.

10. Andreichev V.L., Soboleva A.A., Sergeev S.A., Presnyakov S.L. Zircon chronology of intrusive magmatism of the Kanin Peninsula // Izvestiya Vysshikh Uchebnykh Zavedenii. Geologiya i Razvedka. 2018. №. 4. P. 30–38.

11. Andreichev V.L., Soboleva A.A., Hourigan J.K. Results of U-Pb (LA-ICP-MS) dating of detrital zircons from terrigenous deposits of the upper part of the Precambrian section of the

Northern Timan // Bulletin of the Moscow Society of Naturalists, Department of Geology. 2017. №. 92. P. 10–20.

12. Andreichev V.L., Soboleva A.A., Khubanov V.B., Sobolev I.D. U-Pb (LA-ICP-MS) age of detrital zircons from metasedimentary rocks at the base of the Upper Precambrian section of the Middle Timan // Bulletin of the Moscow Society of Naturalists, Department of Geology. 2018. №. 2(93). P. 14–26.

13. Andreichev V.L., Soboleva A.A., Udoratina O.V., Ronkin Yu.L., Coble M.A., Miller E.L. Granites of the Northern Timan – probable indicators of Neoproterozoic stages of Rodinia breakup // Geodynamics & Tectonophysics. 2020. № 2(11). P. 201–218.

14. Andreichev V.L., Soboleva A.A., Dovzhikova E.G., Ronkin Yu.L., Miller E.L., Coble M.A. Granitoids in the Bolshezemel Zone of the Pechora Basin Basement: Composition and U–Pb Age // Russian Geology and Geophysics. 2022. №2 (64). P. 1-10.

15. Arif M., Henry D.J., Moon C.J. Cr-bearing tourmaline associated with emerald deposits from Swat, NW Pakistan: Genesis and its exploration significance // American Mineralogist. 2010. № 5-6 (95). P. 799–809.

16. Baksheev I.A., Kudryavtseva O.E. Nickeloan tourmaline from the Berezovskoe gold deposit, Middle Urals, Russia // The Canadian Mineralogist. 2004. № 4(42). P. 1065–1078.

17. Balagansky, V.V., Gorbunov, I.A., Mudruk, S.V., 2016. Paleoproterozoic Lapland-Kola and Svecofennian orogens (Baltic shield) // Bulletin of the Kola Science Center RAS. № 26. P. 5–11.

18. Baltybaev, Sh.K. Fennoscandian beetophennids: spatio-temporal correlation of endogenous processes (PhD Thesis). IGGD RAS. 2005

19. Baltybaev, Sh.K., Levchenkov, O.A. Volcanics in Svecofennides of the Ladoga region and results of U-Pb and Pb-Pb dating of rocks and minerals as a basis for correlation of Svecofennian events // Stratigraphy and Geological Correlation. 2005. № 13. P. 119–133.

20. Baltybaev, Sh.K., Levchenkov, O.A., Berezhnaya, N.G., Levskii, L.K., Makeev, A.F., Yakovleva, S.Z. Age and duration of Svecofennian plutono-metamorphic activity in the Ladoga area, southeastern Baltic shield // Petrology. 2004. № 12. P. 330–347.

21. Bayanova, T.B., Pozhilenko, V.I., Smolkin, V.F., Kudryashov, N.M., Kaulina, T.V., Vetrin, V.R. Catalog of geochronological data for the northeastern part of the Baltic Shield // Kola Science Center RAS. Apatity. 2002. 53 p.

22. Beckholmen M., Glodny J. Timanian blueschist-facies metamorphism in the Kvarkush metamorphic basement, Northern Urals, Russia // Memoirs. 2004. № 1(30). P. 125–134.

23. Berryman E.J., Zhang D., Wunder B., Duffy T.S. Compressibility of synthetic Mg-Al tourmalines to 60 GPa // American Mineralogist. 2019. № 7(104). P. 1005–1015.

24. Bibikova, E.V., Bogdanova, S.V., Postnikov, A.V., Popova, L.P., Kirnozova, T.I., Fugzan, M.M., Glushchenko, V.V. Sarmatia-Volgo-Uralia junction zone: Isotopic-geochronologic characteristic of supracrustal rocks and granitoids // Stratigr. Geol. Correl. 2009. № 17. P. 561–573.

25. Biernacka J. Insight into diagenetic processes from authigenic tourmaline: An example from Carboniferous and Permian siliciclastic rocks of western Poland // Sedimentary Geology. 2019. № 389. P. 73–90.

26. Biernacka J. Provenance of Upper Cretaceous quartz-rich sandstones from the North Sudetic Synclinorium, SW Poland: constraints from detrital tourmaline // Geological Quarterly. 2012. № 2(56). P. 315–332.

27. Bingen B., Andersson J., Söderlund U., Möller Ch. The Mesoproterozoic in the Nordic countries // Episodes. 2008a. № 1(31). P. 29–34.

28. Bingen B., Nordgulen Ø., Viola G. A four-phase model for the sveconorwegian orogeny, SW Scandinavia // Norwegian journal of geology. 2008b. № 88. P. 43–72.

29. Bingen B., Solli A. Geochronology of magmatism in the Caledonian and Sveconorwegian belts of Baltica: synopsis for detrital zircon provenance studies // Norwegian J Geol. 2009. № 89. P. 267–290.

30. Bingen B., Viola G., Möller C., Vander Auwera J., Laurent A., Yi K. The Sveconorwegian orogeny // Gondwana Research. 2021. № 90. P. 273–313.

31. Bogdanova S.V., Bingen B., Gorbatschev R., Kheraskova T.N., Kozlov V.I., Puchkov V.N., Volozh Yu.A. The East European Craton (Baltica) before and during the assembly of Rodinia // Precambrian Research. 2008. № 1(160). P. 23–45.

32. Bogdanova S.V., Gorbatschev R., Garetsky R.G. EUROPE\East European Craton☆. B: Reference Module in Earth Systems and Environmental Sciences. Elsevier; 2016. P. 1-18.

33. Brusnitsyna, E.A., Ershova, V.B., Khudoley, A.K., Andersen, T., Maslov, A.V. Results of U – Pb (LA-ICP-MS) dating of detrital zircons from rocks of the Chetlass Group of Middle Thiman: age and provenance // Stratigraphy and Geological Correlation. 2021. № 29. P. 1–23.

34. Brustnitsyna E., Ershova V., Khudoley A., Maslov A., Andersen T., Stockli D., Kristoffersen M. Age and provenance of the Precambrian Middle Timan clastic succession: Constraints from detrital zircon and rutile studies // Precambrian Research. 2022. № 371. P. 1-18.

35. Brusnitsyna, E.A., Vereshchagin, O.S., Ershova, V.B. Detrital Tourmaline from the Riphean Terrigenous Deposits of the Middle Timan: Chemical Composition and Genesis // Geol. Ore Deposits. 2022. № 64. P. 646–656.

36. Cawood P.A., Hawkesworth C.J., Dhuime B. Detrital zircon record and tectonic setting // Geology. 2012. №10(40). P. 875–878.

37. Cawood P.A., Nemchin A.A., Strachan R., Prave T., Krabbendam M. Sedimentary basin and detrital zircon record along East Laurentia and Baltica during assembly and breakup of Rodinia // JGS. 2007. №2 (164). P. 257–275.

38. Cherniak D.J. Pb diffusion in rutile // Contrib Mineral Petrol. 2000. № 139. P. 198–207.

39. Copeland P. On the use of geochronology of detrital grains in determining the time of deposition of clastic sedimentary strata // Basin Research. 2020. № 6(32). P. 1532–1546.

40. Coutts D.S., Matthews W.A., Hubbard S.M. Assessment of widely used methods to derive depositional ages from detrital zircon populations // Geoscience Frontiers. 2019. № 4(10). P. 1421–1435.

41. Dickinson W.R. Interpreting detrital modes of graywacke and arkose // Journal of sadimentary petrology. 1970. № 2(40). P. 695–707.

42. Dickinson W.R., Beard L.S., Brakenridge G.R., Erjavec J.L., Ferguson R.C., Inman K.F., Knepp R.A., Lindberg F.A., Ryberg P.T. Provenance of North American sandstones in relation to tectonic setting // Bull Geol Soc Am. 1983. № 94. P. 222–235.

43. Dickinson W.R., Gehrels G.E. Use of U–Pb ages of detrital zircons to infer maximum depositional ages of strata: A test against a Colorado Plateau Mesozoic database // Earth and Planetary Science Letters. 2009. № 1(288). P. 115–125.

44. Dolnik T.A. Stromatolites and microphytoliths in the Riphean and Vendian stratigraphy of the folded framing of the southern Siberian Platform. SB RAS, Novosibirsk: GEO. 2000.

45. Dobretsov N.L., Sobolev V.S., Khlestov V.V. Facies of regional metamorphism of moderate pressures. Moscow: Nedra. 1972. 287 p.

46. Egorova, Yu.S. Sanukitoids of the Fenno-Karelian province of the Baltic shield: geology, composition, sources (phdthesis). IGGD RAS, Saint-Petrsburg. 2014. 20 p.

47. Elburg M.A., Andersen T., Bons P.D., Simonsen S.L., Weisheit A. New constraints on Phanerozoic magmatic and hydrothermal events in the Mt Painter Province, South Australia // Gondwana Research. 2013. № 2(24). P. 700–712.

48. Ershova V.B., Ivleva A.S., Podkovyrov V.N., Khudoley A.K., Fedorov P.V., Stockli D., Anfinson O., Maslov A.V., Khubanov V. Detrital zircon record of the Mesoproterozoic to Lower Cambrian sequences of NW Russia: implications for the paleogeography of the Baltic interior // GFF. 2019. № 4(141). P. 279–288.

49. Ertl A., Marschall H.R., Giester G., Henry D.J., Schertl H.P., Ntaflos T., Luvizotto G.L., Nasdala L., Tillmanns E. Metamorphic ultrahigh-pressure tourmaline: Structure, chemistry, and correlations to P-T conditions // American Mineralogist. 2010. № 1(95). P. 1–10.

50. Faure G. Fundamentals of isotopic geology. Moscow: MIR. 1989. 590 p.

51. Garzanti E., Andò S., Vezzoli G. Settling equivalence of detrital minerals and grain-size dependence of sediment composition // Earth and Planetary Science Letters. 2008. № 1-2(273). P. 138–151.

52. Garzanti E, Andò S, Vezzoli G. Grain-size dependence of sediment composition and environmental bias in provenance studies. Earth and Planetary Science Letters. январь 2009 г.;277(3–4):422–32.

53. Gee D.G., Pease V. The Neoproterozoic Timanide Orogen of eastern Baltica: introduction // Geological Society, London, Memoirs. 2004. № 1(30). P. 1–3.

54. Gee D.G., Beliakova L., Pease V., Larionov A., Dovshikova L. New, Single Zircon (Pb-Evaporation) Ages from Vendian Intrusions in the Basement beneath the Pechora Basin, Northeastern Baltica // Polarforschung. 2000. № 1(68). P. 161–170.

55. Getzen, V.G. Tectonics of Timan. Science, Leningrad. 1987. 171 p.

56. Gower C., Kamo S., Krogh T. Indentor tectonism in the eastern Grenville Province // Precambrian Research. 2008. № 12(167). P. 201–212.

57. Granseth A., Slagstad T., Roberts N.M.W., Hagen-Peter G., Kirkland C.L., Møkkelgjerd S.H.H., Røhr T.S., Coint N., Sørensen B.E. Multi-isotope tracing of the 1.3–0.9 Ga evolution of Fennoscandia; crustal growth during the Sveconorwegian orogeny // Gondwana Research. 2020. № 91. P. 31–39.

58. Griffin W.L., Wang X., Jackson S.E., Pearson N.J., O'Reilly S.Y., Xu X., Zhou X. Zircon chemistry and magma mixing, SE China: In-situ analysis of Hf isotopes, Tonglu and Pingtan igneous complexes // Lithos. 2002. № 3-4(61). P. 237–269.

59. Henry D.J., Dutrow B.L. Metamorphic tourmaline and its petrologic applications // Reviews in Mineralogy. 1996. № 33. P. 503–558.

60. Henry D.J., Guidotti C.V. Tourmaline as a petrogenetic indicator mineral - An example from the staurolite-grade metapelites of NW Maine // American Mineralogist. 1985. № 70. P. 1-15.

61. Henry D.J., Novak M., Hawthorne F.C., Ertl A., Dutrow B.L., Uher P., Pezzotta F. Nomenclature of the tourmaline-supergroup minerals // American Mineralogist. 2011. № 96. P. 895-913

62. Huhma H., Mänttäri I., Peltonen P., Kontinen A., Halkoaho T., Hanski E., Hokkanen T., Hölttä P., Juopperi H., Konnunaho J., Layahe Y., Luukkonen E., Pietikäinen K., Pulkkinen A., Sorjonen-Ward P., Vaasjoki M., Whitehouse M. The age of the Archaean greenstone belts in Finland // Geological Survey of Finland, Special Paper. 2012. № 54. P. 74–175.

63. Ingersoll R.V., Bullard T.F., Ford R.L., Grimm J.P., Pickle J.D., Sares S.W. The effect of grain size on detrital modes: a test of the Gazzi-Dickinson pointcounting method // Journal of Sedimentary Research. 1984. № 1(54). P. 103–116.

64. Ivleva, A.S., Podkovyrov, V.N., Ershova, V.B., Anfinson, O., Khudoley, A.K., Fedorov, P.V., Maslov, A.V., Zdobin, D.Yu. Results of U-Pb (LA ICP MS) dating of zircons from the Upper Vendian - Lower Cambrian sediments of the eastern Baltic monoclise // Doklady Earth Sciences. 2016. № 468. P. 441–446.

65. Ivleva, A.S., Podkovyrov, V.N., Ershova, V.B., Khubanov, V.B., Khudoley, A.K., Sychev, S.N., Vdovina, N.I., Maslov, A.V. U–Pb LA–ICP–MS Age of Detrital Zircons from the Lower Riphean and Upper Vendian Deposits of the Luga–Ladoga Monocline // Dokl. Earth Sc. 2018. № 480. P. 695–699.

66. Jackson S.E., Pearson N.J., Griffin W.L., Belousova E.A. The application of laser ablation-inductively coupled plasma-mass spectrometry to in situ U–Pb zircon geochronology // Chemical Geology. 2004. № 1(211). P. 47–69.

67. Johnstone S.A., Schwartz T.M., Holm-Denoma C.S. A Stratigraphic Approach to Inferring Depositional Ages From Detrital Geochronology Data // Journal of Sedimentary Research. 2019. №7. P. 1-19.

68. Kaneva T.A., Udoratina O.V., Starikova E.V., Khubanov V.B. Estimation of the lower age limit of the Neoproterozoic Sokolninskaya Formation of the Northwestern Pai-Khoi based on U-Pb dating of detrital zircons // Bulletin of the Moscow Society of Naturalists, Department of Geology. 2015. №. 6(90). P. 3-10.

69. Kirkland C.L., Daly J.S., Whitehouse M.J. Granitic magmatism of Grenvillian and late Neoproterozoic age in Finnmark, Arctic Norway—Constraining pre-Scandian deformation in the Kalak Nappe Complex // Precambrian Research. 2006. №1-2(145). P. 24–52.

70. Kirillin S.I., Ivanov V.N., Kotelnikov V.G., et al. State geological map of the Russian Federation. Scale 1: 200,000 (new series), Timanskaya Series. Sheet Q-39-XXXIII, XXXIV (Timan). Explanatory Note. VSEGEI. St. Petersburg: Cartographic factory VSEGEI. 2020.

71. Korago E.A., Kovaleva G.N., Lopatin B.G., Orgo V.V. The Precambrian rocks of Novaya Zemlya // Geological Society, London, Memoirs. 2004. №1 (30). P. 135–143.

72. Korja A., Lahtinen R., Nironen M. The Svecofennian orogen: a collage of microcontinents and island arcs // Geological Society, London, Memoirs. 2006. № 1(32). P. 561–578.

73. Kostyuchenko S., Sapozhnikov R., Egorkin A., Gee D.G., Berzin R., Solodilov L. Crustal structure and tectonic model of northeastern Baltica, based on deep seismic and potential field data // Geological Society, London, Memoirs. 2006. № 1(32). P. 521–539.

74. Kowal-Linka M., Stawikowski W. Garnet and tourmaline as provenance indicators of terrigenous material in epicontinental carbonates (Middle Triassic, S Poland) // Sedimentary Geology.2013. № 291. P. 27–47.

75. Krasotkina A.O. Isotope-geochemical features and age of accessory minerals of the Ichet'yu ore occurrence and the Pizhma deposit (Middle Timan). 2018. 216 p.

76. Kristoffersen M., Andersen T., Andresen A. U–Pb age and Lu–Hf signatures of detrital zircon from Palaeozoic sandstones in the Oslo Rift, Norway // Geological Magazine. 2014. № 5(151). P. 816–829.

77. Kuptsova, A.V., Khudoley, A.K., Davis, V., Rainbirg, R.H., Kovach, V.P., Zagornaya, N.Yu. The age and provenance of sandstones of the Riphean Priozersk and Salmi formations in the eastern slope of the Pashsko-Ladoga Basin (southern edge of the Baltic Shield) // Stratigraphy and Geological Correlation. 2011. № 19. P. 3–19.

78. Kuznetsov, N.B., Soboleva, A.A., Udoratina, O.V., Hertseva, M.V., Andreichev, V.L., Dorokhov, N.S. Pre-Uralian tectonic evolution of the north-east and east framing of the East European Craton. Part 1. Pre-Uralides, Timanides and pre-Ordovician granitoid volcano-plutonic associations of the North Urals and Timan-Pechora region // Lithosphere. 2006. № 4. P. 3–22.

79. Kuznetsov, N.B., Soboleva, A.A., Udoratina, O.V., Hertseva, M.V., Andreichev, V.L., Dorokhov, N.S. Pre-Uralian tectonic evolution of the north-east and east framing of the East European Craton. Part 2. Neoproterozoic-Cambrian Baltica-Arctida collision // Lithosphere. 2007. № 1. P. 32–45.

80. Kuznetsov, N.B., Natapov, L.M., Belousova, E.A., Griffin, U.L., O'Relly, S.Y., Kulikova, K.V., Soboleva, A.A., Udoratina, O.V. The first results of U/Pb dating and isotope geochemical studies of detrital zircons from the Neoproterozoic sandstones of the Southern Timan (Djejim-Parma Hill) // Dokl. Earth Sc. 2010. № 435. P. 1676–1683.

81. Kuznetsov N.B., Natapov L.M., Belousova E.A., O`Reilly S.Y., Griffin W.L. Geochronological, geochemical and isotopic study of detrital zircon suites from late Neoproterozoic clastic strata along the NE margin of the East European Craton: Implications for plate tectonic models // Gondwana Research. 2010. № 2(17). P. 583–601.

82. Lahtinen R. Main geological features of Fennoscandia // Geological Survey of Finland, Special Paper. 2012. № 53. P. 13–18.

83. Lahtinen R., Korja A., Nironen M. Chapter 11 Paleoproterozoic tectonic evolution. Developments in Precambrian Geology. Elsevier. 2005. P. 481–531.

84. Larin, A.M. Rapakivi granites in the geological history of the earth. Part. Magmatic associations with rapakivi granites: Age, geochemistry, and tectonic setting // Stratigr. Geol. Correl. 2009. № 17. P. 235–258.

85. Larionov A. N., Andreichev V. L., Gee D. G. The Vendian alkaline igneous suite of northern Timan: ion microprobe U-Pb zircon ages of gabbros and syenite // The Neoproterozoic Timanide Orogen of Eastern Baltica, 2004. № 30. P. 69–74.

86. Lorenz H., Gee D.G., Larionov A.N., Majka J. The Grenville–Sveconorwegian orogen in the high Arctic // Geological Magazine. 2012. № 5(149). P. 875–891.

87. Ludwig T. Isoplot 3.00: A geochronological toolkit for Microsoft Excel // Berkeley Geochronology Center. 2003. P. 70.

88. Luvizotto G.L., Zack T., Meyer H.P., Ludwig T., Triebold S., Kronz A., Münker C., Stockli D.F., Prowatke S., Klemme S., Jacob D.E., von Eynatten H. Rutile crystals as potential trace element and isotope mineral standards for microanalysis // Chemical Geology. 2009. № 3(261). P. 346–369.

89. Makeev A.B., Andreichev V.L., Bryanchaninova N.I. Age of lamprophyres in the Middle Timan: first Rb-Sr data // Reports of the Academy of Sciences. 2009. №. 1 (426). P. 94–97.

90. Makeev A.B., Krasotkina A.O., Skublov S.G. Geochemistry and U-Pb age of zircon from the Pizhma titanium deposit (Middle Timan) // Bulletin of the Institute of Geology of the Komi Scientific Center of the Ural Branch of the Russian Academy of Sciences. 2016. №. 5. P. 38–52.

91. Malone D.H., Stein C.A., Craddock J.P., Kley J., Stein S., Malone J.E. Maximum depositional age of the Neoproterozoic Jacobsville Sandstone, Michigan: Implications for the evolution of the Midcontinent Rift // Geosphere. 2016. № 4(12). P. 1271–1282.

92. Malyshev N.A. Tectonics, evolution and oil and gas content of sedimentary basins in the European North of Russia. Ural Branch of the Russian Academy of Sciences. Ekaterinburg. 2002. 268 p.

93. Maslov, A.V., Erokhin, Yu.V., Gerdes, A., Ronkin, Yu.L., Ivanov, K.S. First Results of U–Pb LA–ICP–MS Isotope Dating of Detrital Zircons from Arkose Sandstone of the Biryan Subformation of Zilmerdak Formation (Upper Riphean, South Urals) // Dokl. Earth Sc. 2018. № 482. P. 1275–1277.

94. Maslov, A.V., Petrov, G.A., Ronkin, Yu.L. Reconstruction of Source-Rock Composition of the Middle and Upper Riphean Rocks of the Isherim and Bashkir Anticlinoria, Urals // Geochem. Int. 2018. № 56. P. 403–418.

95. Mezger K., Hanson G.N., Bohlen S.R. High-precision U-Pb ages of metamorphic rutile: application to the cooling history of high-grade terranes // Earth and Planetary Science Letters. 1989. № 1(96). P. 106–118.

96. Mikhailenko, Yu.V., Soboleva, A.A., Hourigan, J.K. U–Pb age of detrital zircons from Upper Precambrian deposits of the Sredni and Rybachi peninsulas (northern margin of the Kola Peninsula) // Stratigr. Geol. Correl. 2016. № 24. P. 439–463.

97. Mikhailenko Yu.V. Specific features of the structure and composition of the Karuyarvin Formation of the Kilda Series of Ripheids in the Sredny Peninsula: the northern framing of the Kola Peninsula. Ukhta. 2016. 204 p.

98. Mints M.V. Meso-Neoproterozoic Grenville-Sveconorwegian intracontinental orogen: history, tectonics, geodynamics // Geodynamics & Tectonophysics. 2017. № 3(8). P. 619–642.

99. Möller A., Mezger K., Schenk V. U–Pb dating of metamorphic minerals: Pan-African metamorphism and prolonged slow cooling of high pressure granulites in Tanzania, East Africa // Precambrian Research. 2000. № 3(104). P. 123–146.

100. Morton A., Hallsworth C.R. Processes controlling the composition of heavy mineral assemblages in sandstones // Sedimentary Geology. 1999. № 124. P. 3–29.

101. Nironen M. The Svecofennian Orogen: a tectonic model // Precambrian Research. 1997. № 1(86). P. 21–44.

102. Olovyanishnikov, V.G. Upper Precambrian Timan and Kanin Peninsula. Russian Academy of Sciences, Ural branch. Komi Science Center, Ekaterinburg. 1998. 163 p.

103. Olovyanishnikov V.G. Geological development of the Kanin Peninsula and Northern Timan. Geoprint Publishers. Syktyvkar. 2004. 79 p.

104. Oparenkova L.I., Ivanov N.F., Kolokoltsev V.G. Legend of the Timan series of sheets of the State Geological Map of the Russian Federation, scale 1:200000 (second edition). Ukhta; 1999. 103 p.

105. Orlov, S.Yu., Kuznetsov, N.B., Miller, E.L., Soboleva, A.A., Udoratina, O.V. Age constraints for the Pre-Uralide-Timanide orogenic event inferred from the study of detrital zircons // Dokl. Earth Sc. 2011. № 440. P. 1216–1221.

106. Paton C., Hellstrom J., Paul B., Woodhead J., Hergt J. Iolite: Freeware for the visualisation and processing of mass spectrometric data // Journal of Analytical Atomic Spectrometry. 2011. № 12(26). P. 2508-2518.

107. Parmuzin N.M., Mazurkevich K.N., Semenova L.R., Kossovaya O.L., Alekseev M.A., Vuks V.Ya., Gavrilov V.A., Gorbatsevich N.R., Evdokimova I. .O., Kotlyar G.V., Petrov B.V., Stepunin A.V., Tolmacheva T.Yu., Shametko V.G., Sharpenok L.N., Yakobson K.E. State geological map of the Russian Federation. Scale 1: 1,000,000 (3d edition). Mezenskaya series. Sheet Q-39 - Naryan-Mar. Explanatory note. St. Petersburg: Cartographic factory VSEGEI. 2015. 393 p.

108. Pease V., Dovshikova E., Beliakova L., Gee D.G. Late Neoproterozoic granitoid magmatism in the basement to the Pechora Basin, NW Russia: geochemical constraints indicate westward subduction beneath NE Baltica // Geological Society, London, Memoirs. 2004. № 30. P. 75–85.

109. Pedersen S., Andersen T., Konnerup-Madsen J., Griffin W.L. Recurrent mesoproterozoic continental magmatism in South-Central Norway // International Journal of Earth Sciences (Geol Rundsch). 2009. № 5(98). P. 1151–1171.

110. Petrus J.A., Kamber B.S. VizualAge: A Novel Approach to Laser Ablation ICP-MS U-Pb Geochronology Data Reduction // Geostandards and Geoanalytical Research. 2012. № 3(36). P. 247–270.

111. Petrov, V.P. Early Proterozoic metamorphism of the Baltic Shield, Kola Scientific Center of the Russian Academy of Sciences. Apatity Publishers. 1999. 325 p.

112. Petrov, G.A., Ronkin, Y.L., Gerdes, A., Maslov, A.V. First results of U – Pb (LA-ICP-MS) dating of detrital zircons from metasandstones of the Ischem anticlinorium (Northern Urals) // Doklady Earth Sciences. 2015. № 464. P. 589–593.

113. Pettijohn F.J. Sedimentary Rocks. 3rd Edition. Harper and Row, New York; 1975. 628 p.

114. Puchkov V.N. Geology of the Urals and Cis-Urals (topical issues of stratigraphy, tectonics, geodynamics and metallogeny). Ufa: DesignPolygraphService; 2010. 280 p.

115. Pystin A.M., Andreichev V.L., Konanova N.V., Pystina Yu.I., Soboleva A.A., Udoratin V.V., Udoratin O.V. Timan-Severouralsk region: deep structure, material-structural evolution, age limits // News of the Komi Science Center of the Ural Branch of the Russian Academy of Sciences. 2018. №. 4. P. 59–67.

116. Rämö O.T., Turkki V., Mänttäri I., Heinonen A., Larjamo K., Lahaye Y. Age and isotopic fingerprints of some plutonic rocks in the Wiborg rapakivi granite batholith with special reference to the dark wiborgite of the Ristisaari Island. Bulletin of the Geological Society of Finland. 2014. № 86. P. 77–91.

117. Reimink J.R., Davies J.H.F.L., Waldron J.W.F., Rojas X. Dealing with discordance: a novel approach for analysing U–Pb detrital zircon datasets // Journal of the Geological Society. 2016. № 4(173). P. 577–585.

118. Rivers T. Assembly and preservation of lower, mid, and upper orogenic crust in the Grenville Province—Implications for the evolution of large hot long-duration orogens // Precambrian Research. 2008. № 3-4(167). P. 237–259.

119. Rivers T. Upper-crustal orogenic lid and mid-crustal core complexes: Signature of a collapsed orogenic plateau in the hinterland of the Grenville Province // Canadian Journal of Earth Sciences. 2012. № 1(49). P. 1–42.

120. Rivers T. Tectonic Setting and Evolution of the Grenville Orogen: An Assessment of Progress Over the Last 40 Years // Geoscience Canada. 2015. № 1(42). P. 77–124.

121. Roberts D., Siedlecka A., Olovyanishnikov V.G. Neoproterozoic, passive-margin, sedimentary systems of the Kanin Peninsula, and northern and central Timan, NW Russia // Geological Society, London, Memoirs. 2004. № 1(30). P. 5–17.

122. Roberts N.M.W. The boring billion? – Lid tectonics, continental growth and environmental change associated with the Columbia supercontinent // Geoscience Frontiers. 2013. № 6(4). P. 681–691.

123. Roberts N.M.W, Slagstad T. Continental growth and reworking on the edge of the Columbia and Rodinia supercontinents; 1.86–0.9 Ga accretionary orogeny in southwest Fennoscandia // International Geology Review. 2015. № 11-12(57). P. 1582–1606.

124. Roffeis C., Corfu F. Caledonian nappes of southern Norway and their correlation with Sveconorwegian basement domains // Geological Society, London, Special Publications. 2014. № 1(390). P. 193–221.

125. Rosa D.R.N, Finch A.A., Andersen T., Inverno C.M.C. U–Pb geochronology and Hf isotope ratios of magmatic zircons from the Iberian Pyrite Belt // Mineralogy and Petrology. 2009. № 1(95). P. 47–69.

126. Rubatto D. Zircon: The Metamorphic mineral // Reviews in mineralogy and Geochemistry. 2017. № 83. P. 261–295.

127. Satkoski A.M., Wilkinson B.H., Hietpas J., Samson S.D. Likeness among detrital zircon populations--An approach to the comparison of age frequency data in time and space // Geological Society of America Bulletin. 2013. № 11-12(125). P. 1783–1799.

128. Sergeev, S.A., Bibikova, E.V., Matukov, D.I., Lobach-Zhuchenko, S.B. Age of the magmatic and metamorphic processes in the Vodlozero complex, Baltic shield: An ion microprobe (SHRIMP II) U-Th-Pb isotopic study of zircons // Geochem. Int. 2007. № 45. P. 198–205.

129. Slagstad T., Kulakov E., Kirkland C.L., Roberts N.M.W., Ganerød M. Breaking the Grenville–Sveconorwegian link in Rodinia reconstructions // Terra Nova. 2019. № 5(31). P. 430–437.

130. Slagstad T., Marker M., Roberts N.M.W., Saalmann K., Kirkland C.L., Kulakov E., Ganerød M., Røhr T.S., Møkkelgjerd S.H.H., Granseth A., Sørensen B.E. The Sveconorwegian orogeny – Reamalgamation of the fragmented southwestern margin of Fennoscandia // Precambrian Research. 2020. № 350. P. 1-25.

131. Slagstad T., Roberts N.M.W., Marker M., Røhr T.S., Schiellerup H. A non-collisional, accretionary Sveconorwegian orogen: A non-collisional, accretionary Sveconorwegian orogen // Terra Nova. 2013. № 1(25). P. 30–37.

132. Slagstad T., Roberts N.M.W., Coint N., Høy I., Sauer S., Kirkland C.L., Marker M., Røhr T.S., Henderson I.H.S., Stormoen M.A., Skår Ø., Sørensen B.E., Bybee G. Magma-driven, high-grade metamorphism in the Sveconorwegian Province, southwest Norway, during the terminal stages of Fennoscandian Shield evolution // Geosphere. 2018. № 2(14). P. 861–882.

133. Slagstad T., Roberts N.M.W., Kulakov E. Linking orogenesis across a supercontinent; the Grenvillian and Sveconorwegian margins on Rodinia // Gondwana Research. 2017. № 44. P. 109–115.

134. Sláma J., Košler J., Condon D.J., Crowley J.L., Gerdes A., Hanchar J.M., Horstwood M.S.A., Morris G., Nasdala L., Norberg N., Schaltegger U., Schoene B., Tubrett M.N., Whitehouse M.J. Plešovice zircon — A new natural reference material for U–Pb and Hf isotopic microanalysis // Chemical Geology. 2008. № 1(249). P. 1–35.

135. Soboleva, A.A., Andreichev, V.L., Burtsev, I.N., Nikulova, N.Yu., Khubanov, V.B., Sobolev, I.D. Detrital zircons from Upper Precambrian rocks of the Vymskaya Group of Middle Timan (U-Pb age and provenance) // Bulletin of the Moscow Society of Naturalists. Department of Geology. 2019. № 94. P. 3–16.

136. Spencer C.J., Cawood P.A., Hawkesworth C.J., Prave A.R., Roberts N.M.W., Horstwood M.S.A., Whitehouse M.J. Generation and preservation of continental crust in the Grenville Orogeny // Geoscience Frontiers. 2015. № 3(6). P. 357–372.

137. Spencer C.J., Roberts N.M.W., Cawood P.A., Hawkesworth C.J., Prave A.R., Antonini A.S.M., Horstwood M. S.A. Intermontane basins and bimodal volcanism at the onset of the Sveconorwegian Orogeny, southern Norway // Precambrian Research. 2014. №252. P. 107–118.

138. Stacey J.S., Kramers J.D. Approximation of terrestrial lead isotope evolution by a two-stage model // Earth and Planetary Science Letters. 1975. №2(26). P. 207–221.

139. Triebold S., von Eynatten H., Zack T. A recipe for the use of rutile in sedimentary provenance analysis // Sedimentary Geology. 2012. №282. P. 268–275.

140. Trumbull R.B., Krienitz M.S., Gottesmann B., Wiedenbeck M. Chemical and boron-isotope variations in tourmalines from an S-type granite and its source rocks: the Erongo granite and tourmalinites in the Damara Belt, Namibia // Contributions to Mineralogy and Petrology. 2007. № 1(155). P. 1–18.

141. Udoratina, O.V., Burtsev, I.N., Nikulova, N.Yu., Khubanov, V.B. Age of metasandstones of the Upper Precambrian Chetlas Group of Middle Timan from U-Pb dating of detrital zircons // Bulletin of the Moscow Society of Naturalists. Department of Geology. 2017. № 92. P. 15–32.

142. Van Hinsberg V.J., Henry D.J., Dutrow B.L. Tourmaline as a Petrologic Forensic Mineral: A Unique Recorder of Its Geologic Past // Elements. 2011. № 5(7). P. 327–332.

143. Vereshchagin O.S., Khudoley A.K., Ershova V.B., Prokopiev A.V., Schneider G.V. Provenance of Jurassic-Cretaceous siliciclastic rocks from the northern Siberian Craton: an integrated heavy mineral study // Journal of Geosciences. 2018. № 2(63). P. 199–213.

144. Vermeesch P. On the visualisation of detrital age distributions // Chemical Geology. 2012. № 312–313. P. 190–194.

145. Vry J.K., Baker J.A. LA-MC-ICPMS Pb–Pb dating of rutile from slowly cooled granulites: Confirmation of the high closure temperature for Pb diffusion in rutile // Geochimica et Cosmochimica Acta. 2006. № 7(70). P. 1807–1820.

146. Wang C.C., Wiest J.D., Jacobs J., Bingen B., Whitehouse M.J., Elburg M.A., Sørstrand T.S., Mikkelsen L., Hestnes Å. Tracing the Sveconorwegian orogen into the Caledonides of West Norway: Geochronological and isotopic studies on magmatism and migmatization // Precambrian Research. 2021. №362. P. 1-23.

147. Wiedenbeck M., Allé P., Corfu F., Griffin W.L., Meier M., Oberli F., Von Quadt A., Roddick J.C., Spiegel W. Three natural zircon standards for U-Th-Pb, Lu-Hf, trace element and REE analysis // Geostandards Newsletter. 1995. № 19. P. 1–23.

148. Yakobson K.E., Vovshina A.Yu., Seregina N.D. Mezen serial legend. Saint Petersburg; 2002.

149. Zack T., Stockli D.F., Luvizotto G.L., Barth M.G., Belousova E., Wolfe M.R., Hinton R.W. In situ U–Pb rutile dating by LA-ICP-MS: 208Pb correction and prospects for geological applications // Contributions to Mineralogy and Petrology. 2011. № 3(162). P. 515–530.

150. Zhang W., Roberts D., Pease V. Provenance characteristics and regional implications of Neoproterozoic, Timanian-margin successions and a basal Caledonian nappe in northern Norway // Precambrian Research. 2015. № 268. P. 153–167.

151. Zhang W., Roberts D., Pease V. Provenance of sandstones from Caledonian nappes in Finnmark, Norway: Implications for Neoproterozoic–Cambrian palaeogeography // Tectonophysics. 2016. № 691. P. 198–205.

152. Zoleikhaei Y., Frei D., Morton A., Zamanzadeh S.M. Roundness of heavy minerals (zircon and apatite) as a provenance tool for unraveling recycling: A case study from the Sefidrud and Sarbaz rivers in N and SE Iran // Sedimentary Geology. 2016. № 342. P. 106–117.

153. Zonenshain L.P., Kuzmin M.I., Natapov L.M. Tectonics of lithospheric plates. T. 1. Moscow: Nedra. 1990. 328 p.

154. Zozulya, D.R., Bayanova, T.B., Serov, P.N. Age and isotopic geochemical characteristics of Archean carbonatites and alkaline rocks of the Baltic shield // Dokl. Earth Sc. 2007. № 415. P. 874–879.

Appendix 1

Results of U-Pb dating of detrital zircon (Oslo University)

Sample #	***ppm***		***Isotope Ratios***					**207/206**		**207/235**		**206/238**		**Best Age**		
Grain #	**U**	**^{206}Pb**	**^{207}Pb/ ^{235}U**	**1 σ error**	**^{206}Pb/^{238} U***	**1 σ error**	**RHO**	**Age Ma**	**1 σ error**	**Age Ma**	**1 σ error**	**Age Ma**	**1 σ error**	**Ma**	**±1 σ**	**D, %**
Sample 9034/2																
64°34'31,3" 50°36'39.3"																
9034_2-80	133	29,8	2,26190	0,05188	0,19984	0,00443	0,97	1248	11	1200	16	1174	24	1248	11	-6
9034_2_14	183	40,9	2,71878	0,03879	0,23211	0,00226	0,68	1314	20	1334	11	1346	12	1314	20	2
9034_2-73	386	104,9	2,95547	0,04214	0,24311	0,00323	0,93	1386	9	1396	11	1403	17	1386	9	1
9034_2_07	178	47,6	2,95156	0,05291	0,23282	0,00386	0,93	1466	12	1395	14	1349	20	1466	12	-9
9034_2-76	196	57,3	3,29559	0,05391	0,25933	0,00402	0,95	1471	10	1480	13	1486	21	1471	10	1
9034_2_20	305	76,9	3,30662	0,04524	0,25811	0,00209	0,59	1486	21	1483	11	1480	11	1486	21	0
9034_2_26	155	33,5	3,02377	0,06279	0,23543	0,00273	0,56	1491	32	1414	16	1363	14	1491	32	-9
9034_2_12	222	60,1	3,60828	0,05005	0,28048	0,00266	0,68	1494	18	1551	11	1594	13	1494	18	6
9034_2-95	416	119,1	3,31686	0,05616	0,25368	0,00406	0,95	1525	10	1485	13	1457	21	1525	10	-5
9034_2_04	60	19,7	3,89666	0,07641	0,28634	0,00546	0,97	1600	8	1613	16	1623	27	1600	8	1
9034_2-97	184	56,7	3,86559	0,06112	0,27579	0,00409	0,94	1655	10	1607	13	1570	21	1655	10	-5
9034_2-94	216	73,1	4,46912	0,07575	0,30041	0,00469	0,92	1764	12	1725	14	1693	23	1764	12	-4
9034_2-109	301	98,8	4,38117	0,07710	0,29235	0,00486	0,94	1778	11	1709	15	1653	24	1778	11	-8
9034_2-75	359	118,4	4,45350	0,07323	0,29272	0,00453	0,94	1805	10	1722	14	1655	23	1805	10	-9
9034_2_29	188	57,5	4,76280	0,07779	0,31018	0,00257	0,51	1822	25	1778	14	1742	13	1822	25	-5
9034_2_31	160	47,1	4,58187	0,08165	0,29843	0,00269	0,51	1822	27	1746	15	1683	13	1822	27	-8
9034_2_15	210	54,9	4,69754	0,07957	0,30510	0,00402	0,78	1827	19	1767	14	1717	20	1827	19	-6
9034_2-69	260	96,9	5,01657	0,08378	0,32429	0,00508	0,94	1835	10	1822	14	1811	25	1835	10	-1
9034_2-74	232	78,7	4,74131	0,07511	0,30099	0,00445	0,93	1868	10	1775	13	1696	22	1868	10	-10
9034_2-62	117	44,6	5,30730	0,08926	0,33545	0,00530	0,94	1876	10	1870	14	1865	26	1876	10	-1
9034_2_01	139	49,2	4,88008	0,07551	0,30719	0,00468	0,99	1883	4	1799	13	1727	23	1883	4	-9

Sample #	*ppm*		*Isotope Ratios*					207/206		207/235		206/238		Best Age		
Grain #	**U**	**^{206}Pb**	**^{207}Pb/ ^{235}U**	**1 σ error**	**^{206}Pb/^{238} U***	**1 σ error**	**RHO**	**Age Ma**	**1 σ error**	**Age Ma**	**1 σ error**	**Age Ma**	**1 σ error**	**Ma**	**±1 σ**	**D, %**
9034_2-105	64	25,2	5,81086	0,12245	0,34801	0,00699	0,95	1973	11	1948	18	1925	33	1973	11	-2
9034_2_10	151	61,4	6,42523	0,12666	0,37773	0,00735	0,99	2005	5	2036	17	2066	34	2005	5	3
9034_2-77	221	116	9,57690	0,18891	0,45361	0,00839	0,94	2381	11	2395	18	2411	37	2381	11	1
9034_2-59	207	111,2	11,58041	0,24141	0,46338	0,00895	0,93	2664	12	2571	19	2454	39	2664	12	-9
9034_2-82	177	114,7	13,86481	0,33443	0,54556	0,01249	0,95	2692	12	2741	23	2807	52	2692	12	4
9034_2-98	95	54,2	12,97476	0,28184	0,49763	0,01009	0,93	2734	12	2678	20	2604	43	2734	12	-5
9034_2-113	155	85,7	12,24425	0,29234	0,46444	0,01003	0,91	2753	16	2623	22	2459	44	2753	16	-12
9034-2-121	417	202,8	10,72220	0,35447	0,42866	0,01363	0,96	2666	15	2499	31	2300	61	2666	15	-16
9034-2-115	462	117,1	2,82396	0,06162	0,21946	0,00461	0,96	1495	11	1362	16	1279	24	1495	11	-17
9034-2-116	162	46,8	3,43854	0,08284	0,25178	0,00587	0,97	1606	11	1513	19	1448	30	1606	11	-11
9034-2-117	322	73,8	2,23043	0,04566	0,19937	0,00392	0,96	1225	11	1191	14	1172	21	1225	11	-5
9034-2-119	420	99	2,60169	0,05802	0,20576	0,00442	0,96	1461	11	1301	16	1206	24	1461	11	-21
9034_2-123	39	18,3	8,51707	0,19610	0,41296	0,00884	0,93	2341	14	2288	21	2228	40	2341	14	-5
9034-2-125	144	73	12,17170	0,28979	0,44557	0,00965	0,91	2811	16	2618	22	2376	43	2811	16	-18
9034_2-128	281	99,2	5,01665	0,10020	0,31172	0,00585	0,94	1907	12	1822	17	1749	29	1907	12	-9
9034_2-129	389	86,5	2,19911	0,03772	0,19604	0,00316	0,94	1230	11	1181	12	1154	17	1230	11	-7
9034_2-130	354	98,4	3,60000	0,07637	0,24532	0,00494	0,95	1742	11	1551	17	1414	26	1742	11	-23
9034_2-131	157	42,2	3,05325	0,05180	0,23798	0,00373	0,92	1489	12	1421	13	1376	19	1489	12	-8
9034_2-132	408	106,1	2,93308	0,04975	0,22966	0,00364	0,93	1480	11	1390	13	1333	19	1480	11	-11
9034_2-133	244	57,4	2,69203	0,05346	0,20938	0,00394	0,95	1493	11	1326	15	1226	21	1493	11	-22
9034_2-134	193	66,9	4,95069	0,11069	0,30854	0,00626	0,91	1901	16	1811	19	1734	31	1901	16	-10
Sample 9007/1																
64°37'35,4'' 51°43'43.2''																

Sample #	*ppm*		*Isotope Ratios*					207/206		207/235		206/238		Best Age		
Grain #	**U**	**^{206}Pb**	**^{207}Pb/ ^{235}U**	**1 σ error**	**^{206}Pb/^{238} U***	**1 σ error**	**RHO**	**Age Ma**	**1 σ error**	**Age Ma**	**1 σ error**	**Age Ma**	**1 σ error**	**Ma**	**±1 σ**	**D, %**
9007-1-1	238	40,2	2,55190	0,10973	0,21593	0,00913	0,98	1332	15	1287	31	1260	48	1332	15	-6
9007-1-2	46	6,5	1,93036	0,08303	0,17942	0,00755	0,98	1148	18	1092	29	1064	41	1148	18	-8
9007-1-8	159	34,4	4,26085	0,19359	0,28408	0,01267	0,98	1779	15	1686	37	1612	64	1779	15	-10
9007-1-12	110	20,4	3,36272	0,14446	0,25106	0,01057	0,98	1570	17	1496	34	1444	54	1570	17	-9
9007-1-13	160	35,2	4,70998	0,21112	0,30044	0,01320	0,98	1859	17	1769	38	1693	65	1859	17	-10
9007-1-16	304	50,3	2,71396	0,11152	0,22652	0,00914	0,98	1358	15	1332	30	1316	48	1358	15	-3
9007-1-17	263	35,2	2,01552	0,07906	0,18390	0,00707	0,98	1184	15	1121	27	1088	38	1184	15	-9
9007-1-18	266	49	3,33866	0,13958	0,25529	0,01047	0,98	1525	15	1490	33	1466	54	1525	15	-4
9007-1-19	166	40,1	5,64208	0,25792	0,33766	0,01512	0,98	1974	16	1923	39	1875	73	1974	16	-5
9007-1-22	1228	177	2,26482	0,09444	0,19977	0,00820	0,98	1251	14	1201	29	1174	44	1251	14	-7
9007-1-29	1087	143,3	2,03054	0,08090	0,18668	0,00730	0,98	1169	15	1126	27	1103	40	1169	15	-6
9007-1-30	367	94,8	6,25239	0,28827	0,37477	0,01693	0,98	1971	16	2012	40	2052	79	1971	16	4
9007-1-31	194	35,4	3,53703	0,14245	0,27117	0,01068	0,98	1520	16	1536	32	1547	54	1520	16	2
9007-1-32	209	38,5	3,87491	0,15941	0,27635	0,01110	0,98	1655	16	1608	33	1573	56	1655	16	-5
9007-1-34	147	26,4	3,58142	0,14436	0,26855	0,01057	0,98	1562	16	1545	32	1533	54	1562	16	-2
9007-1-35	193	44,9	5,31452	0,22979	0,35093	0,01485	0,98	1797	16	1871	37	1939	71	1797	16	7
9007-1-36	129	26,5	4,22650	0,18976	0,30928	0,01362	0,98	1608	16	1679	37	1737	67	1608	16	7
9007-1-37	130	18	2,41744	0,10235	0,21081	0,00871	0,98	1273	18	1248	30	1233	46	1273	18	-3
9007-1-38	387	75,9	3,88518	0,17096	0,29565	0,01280	0,98	1534	15	1611	36	1670	64	1534	15	8
9007-1-39	240	43,1	3,56833	0,14169	0,27332	0,01064	0,98	1522	15	1543	31	1558	54	1522	15	2
9007-1-40	348	61,3	3,51086	0,14301	0,26723	0,01068	0,98	1534	15	1530	32	1527	54	1534	15	0
9007-1-41	271	63,1	3,53000	0,11833	0,26754	0,00791	0,88	1542	28	1534	27	1528	40	1542	28	-1
9007-1-42	549	148,5	3,87704	0,13487	0,31341	0,00950	0,87	1420	31	1609	28	1757	47	1420	31	19
9007-1-43	131	30,4	3,60475	0,12080	0,27003	0,00767	0,85	1564	32	1551	27	1541	39	1564	32	-1
9007-1-44	158	27	2,53830	0,07103	0,19669	0,00530	0,96	1500	13	1283	20	1157	29	1500	13	-30
9007-1-45	316	69,2	3,26986	0,10639	0,24882	0,00790	0,98	1534	13	1474	25	1432	41	1534	13	-7
9007-1-46	350	116,5	6,59492	0,22428	0,38494	0,01281	0,98	2018	12	2059	30	2099	60	2018	12	4

Sample #	*ppm*		*Isotope Ratios*					207/206		207/235		206/238		Best Age		
Grain #	U	^{206}Pb	^{207}Pb/ ^{235}U	1 σ error	^{206}Pb/^{238} U*	1 σ error	RHO	Age Ma	1 σ error	Age Ma	1 σ error	Age Ma	1 σ error	Ma	±1 σ	D, %
9007-1-47	318	72,5	3,49395	0,09821	0,26171	0,00719	0,98	1564	11	1526	22	1499	37	1564	11	-4
9007-1-48	290	53,2	2,35900	0,06207	0,21059	0,00541	0,98	1227	11	1230	19	1232	29	1227	11	0
9007-1-49	208	35,7	2,15235	0,05557	0,19722	0,00497	0,98	1176	11	1166	18	1160	27	1176	11	-1
9007-1-50	421	106,6	3,87628	0,11691	0,29024	0,00858	0,98	1565	11	1609	24	1643	43	1565	11	5
9007-1-51	319	59,7	2,44408	0,06555	0,21510	0,00531	0,92	1255	20	1256	19	1256	28	1255	20	0
9007-1-52	211	48,5	4,18966	0,13476	0,26766	0,00764	0,89	1857	27	1672	26	1529	39	1857	27	-21
9007-1-53	564	101,5	2,26942	0,06295	0,20299	0,00539	0,96	1224	16	1203	20	1191	29	1224	16	-3
9007-1-54	235	75,7	6,24487	0,20632	0,37168	0,01191	0,97	1984	14	2011	29	2037	56	1984	14	3
9007-1-55	101	16,5	2,06642	0,06598	0,18756	0,00514	0,86	1195	32	1138	22	1108	28	1195	32	-8
9007-1-56	95	26,6	5,26871	0,17727	0,32152	0,01030	0,95	1939	18	1864	29	1797	50	1939	18	-8
9007-1-57	250	57	3,29275	0,09453	0,26091	0,00728	0,97	1458	12	1479	22	1494	37	1458	12	2
9007-1-58	87	19,3	3,32084	0,10183	0,25829	0,00704	0,89	1493	26	1486	24	1481	36	1493	26	-1
9007-1-59	65	13,1	3,30878	0,16481	0,24177	0,00755	0,63	1610	71	1483	39	1396	39	1610	71	-15
9007-1-60	249	41,9	2,11504	0,07701	0,19730	0,00522	0,73	1140	47	1154	25	1161	28	1140	47	2
9007-1-61	200	30,6	2,07057	0,06475	0,18081	0,00441	0,78	1271	37	1139	21	1071	24	1271	37	-19
9007-1-63	169	48	4,31937	0,13576	0,32622	0,00996	0,97	1548	13	1697	26	1820	48	1548	13	15
9007-1-64	389	106,1	4,48826	0,14154	0,31114	0,00955	0,97	1708	13	1729	26	1746	47	1708	13	2
9007-1-66	100	14,7	1,72646	0,04929	0,16919	0,00410	0,85	1042	29	1018	18	1008	23	1042	29	-3
9007-1-67	91	23,3	4,12061	0,12559	0,29455	0,00854	0,95	1651	17	1658	25	1664	43	1651	17	1
9007-1-68	211	41,8	2,71019	0,07729	0,22582	0,00620	0,96	1361	15	1331	21	1313	33	1361	15	-4
9007-1-69	853	220,3	4,27893	0,13315	0,29827	0,00903	0,97	1698	13	1689	26	1683	45	1698	13	-1
9007-1-70	133	26,2	2,63187	0,07177	0,22751	0,00599	0,97	1290	14	1310	20	1321	31	1290	14	2
9007-1-71	63	11,5	2,71667	0,07945	0,20465	0,00568	0,95	1553	17	1333	22	1200	30	1553	17	-29
9007-1-72	168	34,7	2,90336	0,09241	0,23995	0,00643	0,84	1377	32	1383	24	1386	33	1377	32	1
9007-1-73	135	22,2	2,17451	0,07263	0,19047	0,00528	0,83	1265	35	1173	23	1124	29	1265	35	-13
9007-1-74	280	66,4	3,72524	0,12501	0,27571	0,00784	0,85	1586	32	1577	27	1570	40	1586	32	-1
9007-1-75	269	46,8	2,27660	0,07050	0,20164	0,00524	0,84	1243	32	1205	22	1184	28	1243	32	-5
9007-1-76	191	53,4	5,01846	0,18121	0,32651	0,01001	0,85	1824	35	1822	31	1821	49	1824	35	0
9007-1-77	118	20,2	2,15875	0,06589	0,19797	0,00510	0,84	1174	33	1168	21	1164	27	1174	33	-1
9007-1-78	130	31	3,79883	0,12946	0,27714	0,00792	0,84	1613	34	1592	27	1577	40	1613	34	-2

Sample #	*ppm*		*Isotope Ratios*					207/206		207/235		206/238		Best Age		
Grain #	**U**	**^{206}Pb**	**^{207}Pb/ ^{235}U**	**1 σ error**	**^{206}Pb/^{238} U***	**1 σ error**	**RHO**	**Age Ma**	**1 σ error**	**Age Ma**	**1 σ error**	**Age Ma**	**1 σ error**	**Ma**	**±1 σ**	**D, %**
9007-1-79	197	23,6	1,54870	0,06437	0,13913	0,00355	0,61	1215	63	950	26	840	20	1215	63	-45
9007-1-80	451	104,5	3,63618	0,13013	0,26868	0,00801	0,83	1589	35	1557	28	1534	41	1589	35	-4
9007-1-81	178	41,6	3,79197	0,13432	0,27403	0,00801	0,83	1631	35	1591	28	1561	41	1631	35	-4
9007-1-82	235	42,3	2,34526	0,07697	0,21084	0,00575	0,83	1214	35	1226	23	1233	31	1214	35	2
9007-1-83	62	18,2	5,82488	0,23055	0,34548	0,01129	0,83	1990	39	1950	34	1913	54	1990	39	-4
9007-1-84	188	45,2	3,83526	0,14083	0,27941	0,00818	0,80	1616	42	1600	30	1588	41	1616	42	-2
9007-1-85	145	24,6	2,17684	0,07362	0,19823	0,00529	0,79	1188	39	1174	24	1166	28	1188	39	-2
9007-1-86	93	22	3,80300	0,13357	0,27661	0,00807	0,83	1619	35	1593	28	1574	41	1619	35	-3
9007-1-87	76	17,4	3,55619	0,12235	0,26955	0,00789	0,85	1542	33	1540	27	1538	40	1542	33	0
9007-1-88	389	93,8	3,70655	0,13125	0,27642	0,00841	0,86	1572	32	1573	28	1573	42	1572	32	0
9007-1-89	88	26,4	5,66503	0,22142	0,35078	0,01150	0,84	1913	38	1926	34	1938	55	1913	38	1
9007-1-90	241	42,8	2,57778	0,11065	0,20870	0,00577	0,65	1417	62	1294	31	1222	31	1417	62	-16
9007-1-91	123	24,1	2,71789	0,09253	0,22825	0,00641	0,83	1346	35	1333	25	1325	34	1346	35	-2
9007-1-92	70	11	2,26294	0,18144	0,19219	0,00732	0,48	1325	129	1201	56	1133	40	1325	129	-17
9007-1-93	187	45,3	3,82070	0,12035	0,28450	0,00855	0,95	1575	17	1597	25	1614	43	1575	17	2
9007-1-94	164	38,9	3,69876	0,11419	0,27847	0,00835	0,97	1554	13	1571	25	1584	42	1554	13	2
9007-1-95	72	19,6	5,01136	0,17411	0,32137	0,01034	0,93	1850	23	1821	29	1796	50	1850	23	-3
9007-1-96	58	19,1	6,49451	0,23471	0,38922	0,01365	0,97	1971	15	2045	32	2119	63	1971	15	7
9007-1-97	155	26,7	2,15860	0,06267	0,20225	0,00571	0,97	1132	13	1168	20	1187	31	1132	13	5
9007-1-98	39	7,1	2,38400	0,07825	0,21419	0,00607	0,86	1215	33	1238	23	1251	32	1215	33	3
9007-1-99	191	35,9	2,48962	0,07378	0,21889	0,00623	0,96	1257	16	1269	21	1276	33	1257	16	1
9007-1-100	133	40,1	5,64471	0,19532	0,35493	0,01190	0,97	1885	16	1923	30	1958	57	1885	16	4
9007-1-101	209	51,3	3,91654	0,12441	0,28858	0,00897	0,98	1595	11	1617	26	1634	45	1595	11	2
9007-1-102	153	46,6	5,76416	0,20077	0,36115	0,01232	0,98	1892	12	1941	30	1988	58	1892	12	5
9007-1-103	184	43,4	3,65049	0,11406	0,27788	0,00849	0,98	1534	12	1561	25	1581	43	1534	12	3
9007-1-104	245	44,6	2,39242	0,06989	0,21354	0,00609	0,98	1228	12	1240	21	1248	32	1228	12	2
9007-1-105	393	74,4	2,69241	0,08241	0,22063	0,00660	0,98	1393	12	1326	23	1285	35	1393	12	-8
9007-1-106	363	86,9	3,73199	0,11954	0,28017	0,00875	0,98	1560	13	1578	26	1592	44	1560	13	2
9007-1-107	314	122,3	10,3920 5	0,41129	0,46089	0,01778	0,98	2493	14	2470	37	2443	78	2493	14	-2

Sample #	*ppm*		*Isotope Ratios*					207/206		207/235		206/238		Best Age		
Grain #	**U**	**^{206}Pb**	**^{207}Pb/ ^{235}U**	**1 σ error**	**^{206}Pb/^{238} U***	**1 σ error**	**RHO**	**Age Ma**	**1 σ error**	**Age Ma**	**1 σ error**	**Age Ma**	**1 σ error**	**Ma**	**±1 σ**	**D, %**
9007-1-108	199	32,8	2,32451	0,07380	0,19062	0,00560	0,93	1392	22	1220	23	1125	30	1392	22	-24
9007-1-109	78	11,9	2,12292	0,07854	0,17684	0,00551	0,84	1362	37	1156	26	1050	30	1362	37	-30
9007-1-110	398	73,3	2,40346	0,07315	0,21533	0,00620	0,95	1220	18	1244	22	1257	33	1220	18	3
Sample 9007/4																
64°37'35,4'' 51°43'43.2''																
9007-4-27	272	62,6	0,09739	0,00036	0,26728	0,00489	0,98	1575	7	1547	15	1527	25	1575	7	-3
9007-4-45	432	104,9	0,10308	0,00040	0,28727	0,00509	0,98	1680	7	1651	15	1628	25	1680	7	-3
9007-4-1	218	44,3	0,08716	0,00030	0,23676	0,00376	0,98	1364	7	1368	12	1370	20	1364	7	0
9007-4-3	342	57,6	0,07791	0,00026	0,19717	0,00291	0,98	1145	6	1155	10	1160	16	1145	6	1
9007-4-5	232	51,4	0,09398	0,00033	0,25782	0,00412	0,98	1508	7	1491	13	1479	21	1508	7	-2
9007-4-6	336	59,8	0,08532	0,00035	0,20688	0,00324	0,97	1323	8	1253	12	1212	17	1323	8	-9
9007-4-7	251	65,4	0,10856	0,00039	0,30237	0,00518	0,98	1775	6	1736	15	1703	26	1775	6	-4
9007-4-9	203	55	0,11099	0,00042	0,31460	0,00536	0,98	1816	7	1787	15	1763	26	1816	7	-3
9007-4-10	172	43,4	0,10296	0,00038	0,29306	0,00491	0,98	1678	7	1666	14	1657	24	1678	7	-1
9007-4-12	142	24,6	0,08110	0,00034	0,20446	0,00313	0,96	1224	8	1208	11	1199	17	1224	8	-2
9007-4-14	430	96,9	0,09403	0,00030	0,26334	0,00424	0,98	1509	6	1508	13	1507	22	1509	6	0
9007-4-15	184	49,7	0,11030	0,00040	0,31604	0,00568	0,98	1804	7	1786	15	1770	28	1804	7	-2
9007-4-17	255	46,7	0,08359	0,00028	0,21498	0,00334	0,98	1283	7	1266	12	1255	18	1283	7	-2
9007-4-19	78	14,7	0,08554	0,00035	0,22134	0,00345	0,97	1328	8	1304	12	1289	18	1328	8	-3
9007-4-20	323	58,3	0,08176	0,00027	0,21125	0,00340	0,98	1240	6	1237	12	1235	18	1240	6	0
9007-4-22	181	30,1	0,07872	0,00028	0,19657	0,00308	0,98	1165	7	1160	11	1157	17	1165	7	-1
9007-4-24	182	35,5	0,08622	0,00031	0,22960	0,00356	0,98	1343	7	1337	12	1332	19	1343	7	-1
9007-4-28	738	169,5	0,10404	0,00046	0,26992	0,00479	0,97	1697	8	1608	15	1540	24	1697	8	-10
9007-4-29	223	48,2	0,09296	0,00033	0,25550	0,00427	0,98	1487	6	1475	13	1467	22	1487	6	-1
9007-4-30	400	75,2	0,08235	0,00026	0,22242	0,00346	0,98	1254	6	1279	12	1295	18	1254	6	3
9007-4-31	128	35	0,11251	0,00045	0,32265	0,00586	0,98	1840	7	1820	16	1803	29	1840	7	-2
9007-4-33	157	27,1	0,08066	0,00032	0,20423	0,00314	0,97	1213	8	1203	11	1198	17	1213	8	-1

Sample #	*ppm*		*Isotope Ratios*					207/206		207/235		206/238		Best Age		
Grain #	**U**	**^{206}Pb**	**^{207}Pb/ ^{235}U**	**1 σ error**	**^{206}Pb/^{238} U***	**1 σ error**	**RHO**	**Age Ma**	**1 σ error**	**Age Ma**	**1 σ error**	**Age Ma**	**1 σ error**	**Ma**	**±1 σ**	**D, %**
9007-4-34	260	61,2	0,09881	0,00034	0,27829	0,00469	0,98	1602	6	1591	14	1583	24	1602	6	-1
9007-4-35	270	49,9	0,08391	0,00028	0,21967	0,00356	0,98	1290	7	1284	12	1280	19	1290	7	-1
9007-4-36	201	31,4	0,07690	0,00030	0,18666	0,00283	0,97	1119	8	1108	11	1103	15	1119	8	-1
9007-4-37	235	38	0,07892	0,00030	0,19306	0,00300	0,97	1170	8	1149	11	1138	16	1170	8	-3
9007-4-39	463	114,1	0,10473	0,00038	0,29106	0,00493	0,98	1710	7	1675	14	1647	25	1710	7	-4
9007-4-40	357	104,9	0,11719	0,00045	0,34610	0,00631	0,98	1914	7	1915	16	1916	30	1914	7	0
9007-4-41	262	77,2	0,12391	0,00047	0,34767	0,00661	0,98	2013	7	1967	17	1923	32	2013	7	-5
9007-4-43	244	74,9	0,13031	0,00055	0,36164	0,00678	0,98	2102	7	2046	17	1990	32	2102	7	-6
9007-4-46	191	55,1	0,10786	0,00048	0,30401	0,00596	0,98	1764	8	1735	17	1711	29	1764	8	-3
9007-4-47	132	40,6	0,11519	0,00055	0,32569	0,00659	0,97	1883	8	1848	18	1817	32	1883	8	-4
9007-4-48	235	37,4	0,07321	0,00030	0,16754	0,00270	0,97	1020	8	1005	11	999	15	1020	8	-2
9007-4-49	176	33,3	0,08383	0,00045	0,20012	0,00354	0,96	1289	10	1216	13	1176	19	1289	10	-10
9007-4-51	132	28,4	0,08220	0,00037	0,22775	0,00399	0,97	1250	9	1295	13	1323	21	1250	9	6
9007-4-52	250	48,6	0,08158	0,00037	0,20615	0,00351	0,97	1236	9	1218	12	1208	19	1236	9	-2
9007-4-53	130	24,4	0,08093	0,00042	0,19979	0,00343	0,96	1220	10	1190	13	1174	18	1220	10	-4
9007-4-55	104	31,4	0,11462	0,00066	0,32467	0,00672	0,96	1874	10	1841	18	1813	33	1874	10	-3
9007-4-56	238	58,1	0,10169	0,00052	0,26672	0,00519	0,97	1655	9	1580	16	1524	26	1655	9	-9
9007-4-58	332	84,2	0,10178	0,00057	0,27147	0,00500	0,96	1657	10	1595	15	1548	25	1657	10	-7
9007-4-60	67	10,1	0,07294	0,00043	0,16076	0,00255	0,94	1012	11	977	11	961	14	1012	11	-5
9007-4-61	255	46,2	0,08225	0,00048	0,19421	0,00328	0,95	1251	11	1182	12	1144	18	1251	11	-9
9007-4-62	78	21,3	0,10836	0,00080	0,29433	0,00560	0,93	1772	13	1712	17	1663	28	1772	13	-7
9007-4-63	127	24,5	0,08121	0,00046	0,20847	0,00365	0,95	1227	10	1223	13	1221	19	1227	10	0
9007-4-64	123	39,2	0,11971	0,00074	0,34612	0,00706	0,96	1952	10	1933	18	1916	34	1952	10	-2
9007-4-65	160	28,7	0,07903	0,00042	0,19454	0,00323	0,95	1173	10	1155	12	1146	17	1173	10	-2
9007-4-66	523	172,4	0,12175	0,00076	0,35922	0,00762	0,96	1982	11	1980	19	1978	36	1982	11	0
9007-4-67	132	24,5	0,08241	0,00045	0,20210	0,00338	0,95	1255	10	1211	12	1187	18	1255	10	-6
9007-4-68	176	40,6	0,09253	0,00042	0,25442	0,00466	0,97	1478	9	1468	15	1461	24	1478	9	-1
9007-4-69	200	37,6	0,08043	0,00044	0,20534	0,00346	0,95	1207	11	1205	12	1204	18	1207	11	0
9007-4-70	399	90,6	0,09441	0,00067	0,24683	0,00442	0,93	1516	13	1460	15	1422	23	1516	13	-7

Sample #	*ppm*		*Isotope Ratios*					207/206		207/235		206/238		Best Age		
Grain #	**U**	**^{206}Pb**	**^{207}Pb/ ^{235}U**	**1 σ error**	**^{206}Pb/^{238} U***	**1 σ error**	**RHO**	**Age Ma**	**1 σ error**	**Age Ma**	**1 σ error**	**Age Ma**	**1 σ error**	**Ma**	**±1 σ**	**D, %**
9007-4-71	398	118,7	0,11149	0,00057	0,32611	0,00627	0,97	1824	9	1822	17	1820	30	1824	9	0
9007-4-72	112	25,4	0,09311	0,00048	0,24806	0,00426	0,96	1490	10	1453	14	1428	22	1490	10	-4
9007-4-74	118	33,9	0,11203	0,00064	0,31656	0,00609	0,96	1833	10	1800	17	1773	30	1833	10	-3
9007-4-75	250	44,4	0,07956	0,00038	0,19475	0,00315	0,96	1186	9	1161	12	1147	17	1186	9	-3
9007-4-77	74	12,9	0,07981	0,00043	0,19457	0,00325	0,95	1192	10	1162	12	1146	18	1192	10	-4
9007-4-78	194	32,5	0,07720	0,00042	0,18582	0,00304	0,95	1126	10	1108	12	1099	16	1126	10	-2
9007-4-80	633	109,4	0,07701	0,00034	0,19074	0,00316	0,97	1121	9	1124	12	1125	17	1121	9	0
9007-4-82	488	104,4	0,08815	0,00047	0,24032	0,00418	0,96	1386	10	1387	14	1388	22	1386	10	0
9007-4-83	166	28,3	0,07848	0,00043	0,19247	0,00316	0,95	1159	11	1143	12	1135	17	1159	11	-2
9007-4-84	427	79,7	0,08095	0,00042	0,21052	0,00353	0,95	1220	10	1227	13	1232	19	1220	10	1
9007-4-88	356	111,8	0,12045	0,00075	0,35669	0,00720	0,96	1963	11	1965	18	1966	34	1963	11	0
9007-4-89	242	44	0,08220	0,00049	0,20630	0,00349	0,94	1250	12	1224	13	1209	19	1250	12	-3
9007-4-90	252	39,9	0,07511	0,00041	0,17883	0,00296	0,95	1072	11	1064	11	1061	16	1072	11	-1
9007-4-91	175	57,1	0,13198	0,00085	0,37277	0,00761	0,95	2124	11	2084	19	2042	36	2124	11	-4
9007-4-95	190	38,7	0,08096	0,00026	0,20289	0,00209	0,96	1220	6	1201	8	1191	11	1220	6	-2
9007-4-96	107	39,8	0,12688	0,00048	0,36581	0,00493	0,96	2055	6	2032	12	2010	23	2055	6	-2
9007-4-98	86	17,3	0,08125	0,00034	0,19885	0,00199	0,92	1228	8	1190	8	1169	11	1228	8	-5
9007-4-99	284	83,8	0,10322	0,00032	0,29052	0,00335	0,97	1683	6	1661	10	1644	17	1683	6	-2
9007-4-101	76	19,4	0,09404	0,00035	0,25226	0,00292	0,95	1509	7	1474	9	1450	15	1509	7	-4
9007-4-105	526	130,3	0,09449	0,00034	0,24621	0,00276	0,95	1518	7	1459	9	1419	14	1518	7	-7
9007-4-106	113	29,3	0,09381	0,00029	0,25871	0,00317	0,97	1504	6	1492	10	1483	16	1504	6	-1
9007-4-108	127	26	0,08083	0,00025	0,20249	0,00205	0,96	1217	6	1199	7	1189	11	1217	6	-2
9007-4-109	178	62,7	0,11954	0,00040	0,34492	0,00433	0,97	1949	6	1929	11	1910	21	1949	6	-2
9007-4-110	350	73,5	0,08072	0,00023	0,20830	0,00218	0,97	1215	5	1218	8	1220	12	1215	5	0
9007-4-111	207	42	0,08068	0,00025	0,20188	0,00206	0,96	1214	6	1195	8	1185	11	1214	6	-2
9007-4-113	613	130,5	0,08156	0,00038	0,21087	0,00233	0,92	1235	8	1234	9	1233	12	1235	8	0

Appendix 2

Results of U-Pb dating of detrital zircon (University of Austin)

Sample #	***ppm***		***Isotope Ratios***					**207/235**		**206/238**		**207/206**		**Best age**		
Grain #	**U**	**U/ Th**	**207/ 235**	**2σ error**	**206/ 238**	**2σ error**	**RHO**	**Age, Ma**	**2σ error**	**Age, Ma**	**2σ error**	**Age, Ma**	**2σ error**	**Ma**	**2σ error**	**D, %**
Sample 9017/4																
64°37'35, 4'' 51°43'43. 2''																
9017_4_3	412	1,24	3,87000	0,06100	0,29020	0,00400	0,54	1605	13	1645	20	1554	27	1554	27	6
9017_4_5	152	0,94	4,56400	0,09100	0,30400	0,00400	0,47	1739	17	1711	20	1771	33	1771	33	3
9017_4_6	117	0,39	3,56600	0,08200	0,27860	0,00480	0,50	1540	19	1586	23	1491	38	1491	38	6
9017_4_7	390	1,20	3,54700	0,08000	0,26830	0,00580	0,52	1534	18	1530	30	1533	35	1533	35	0
9017_4_8	326	1,37	4,50000	0,13000	0,31420	0,00860	0,93	1724	23	1758	42	1698	20	1698	20	4
9017_4_9	266	1,23	2,22200	0,05200	0,20180	0,00370	0,54	1187	17	1184	20	1193	42	1193	42	1
9017_4_10	153	0,55	3,40000	0,05400	0,26100	0,00360	0,57	1502	12	1494	19	1514	27	1514	27	1
9017_4_12	31	1,09	11,97000	0,42000	0,47900	0,01200	0,75	2594	33	2520	54	2635	39	2635	39	4
9017_4_13	206	0,33	5,74000	0,34000	0,35300	0,01900	0,98	1891	62	1928	93	1899	29	1899	29	2
9017_4_1	148	0,30	4,4680	0,0820	0,3323	0,0055	0,42	1723	15	1853	28	1576	36	1576	36	18

Sample #	*ppm*		*Isotope Ratios*					207/235		206/238		207/206		Best age		
Grain #	**U**	**U/ Th**	**207/ 235**	**2σ error**	**206/ 238**	**2σ error**	**RHO**	**Age, Ma**	**2σ error**	**Age, Ma**	**2σ error**	**Age, Ma**	**2σ error**	**Ma**	**2σ error**	**D, %**
4			0	0	0	0										
9017_4_15	162	0,23	4,27000	0,11000	0,29780	0,00950	0,30	1680	21	1675	48	1656	55	1656	55	1
9017_4_16	115	0,75	3,68600	0,06500	0,28640	0,00400	0,58	1565	14	1623	20	1490	28	1490	28	9
9017_4_17	99	0,37	3,45700	0,08300	0,26320	0,00430	0,39	1518	20	1506	22	1520	47	1520	47	1
9017_4_18	180	0,63	5,14100	0,08500	0,34170	0,00490	0,58	1843	14	1894	23	1789	26	1789	26	6
9017_4_19	290	0,74	3,76900	0,09300	0,27360	0,00600	0,71	1583	20	1564	29	1624	33	1624	33	4
9017_4_20	116	0,49	4,94900	0,08900	0,32510	0,00410	0,48	1806	15	1814	20	1799	29	1799	29	1
9017_4_21	401	1,02	4,24400	0,09100	0,31920	0,00770	0,89	1678	18	1782	38	1556	22	1556	22	15
9017_4_22	130	0,11	3,51000	0,15000	0,24340	0,00750	0,59	1518	32	1402	39	1661	56	1661	56	16
9017_4_25	144	0,52	3,28100	0,08000	0,24430	0,00460	0,60	1474	19	1408	24	1568	38	1568	38	10
9017_4_26	149	0,27	2,85300	0,09100	0,22230	0,00610	0,64	1364	24	1292	32	1488	47	1488	47	13
9017_4_27	115	0,96	3,22000	0,11000	0,25320	0,00540	0,67	1455	26	1454	28	1459	49	1459	49	0
9017_4_29	41	0,52	2,15200	0,08900	0,19560	0,00520	0,49	1155	29	1150	28	1162	76	1162	76	1
9017_4_30	449	0,51	2,62400	0,05000	0,21790	0,00450	0,69	1305	14	1270	24	1371	31	1371	31	7
9017_4_31	231	0,78	3,35400	0,05000	0,25910	0,00300	0,66	1493	12	1486	16	1503	24	1503	24	1
9017_4_33	255	1,50	5,44000	0,11000	0,34830	0,00610	0,91	1888	18	1928	29	1842	19	1842	19	5

Sample #	*ppm*		*Isotope Ratios*					207/235		206/238		207/206		Best age		
Grain #	**U**	**U/ Th**	**207/ 235**	**2σ error**	**206/ 238**	**2σ error**	**RHO**	**Age, Ma**	**2σ error**	**Age, Ma**	**2σ error**	**Age, Ma**	**2σ error**	**Ma**	**2σ error**	**D, %**
9017_4_35	67	1,92	4,18000	0,13000	0,27970	0,00660	0,56	1663	26	1588	33	1754	51	1754	51	9
9017_4_36	245	1,29	2,72600	0,05900	0,22940	0,00330	0,60	1333	16	1331	17	1342	32	1342	32	1
9017_4_38	170	0,85	3,69800	0,06400	0,28470	0,00370	0,47	1568	14	1614	18	1508	31	1508	31	7
9017_4_39	274	2,14	4,42000	0,13000	0,30330	0,00840	0,89	1705	25	1703	41	1721	25	1721	25	1
9017_4_40	109	1,14	4,88000	0,11000	0,31410	0,00550	0,58	1794	18	1759	27	1830	31	1830	31	4
9017_4_41	303	2,12	2,00100	0,07400	0,19040	0,00510	0,68	1110	25	1122	28	1084	54	1084	54	4
9017_4_42	615	1,97	2,75900	0,06100	0,23450	0,00580	0,70	1341	17	1356	30	1326	35	1326	35	2
9017_4_45	255	1,26	3,67200	0,06800	0,27290	0,00390	0,64	1562	15	1554	20	1583	28	1583	28	2
9017_4_47	133	0,61	4,63500	0,09800	0,31250	0,00490	0,68	1752	18	1751	24	1749	29	1749	29	0
9017_4_48	404	0,30	3,26000	0,13000	0,25190	0,00950	0,93	1465	30	1455	51	1441	30	1441	30	1
9017_4_49	85	0,35	6,37000	0,50000	0,36000	0,02500	0,87	2004	71	1970	120	2036	54	2036	54	3
9017_4_50	526	0,79	2,37100	0,08700	0,20220	0,00660	0,87	1225	26	1184	35	1252	31	1252	31	5
9017_4_52	241	0,68	2,33900	0,06000	0,20750	0,00480	0,64	1220	19	1214	26	1223	39	1223	39	1
9017_4_53	978	3,08	3,78700	0,06500	0,28090	0,00500	0,85	1586	14	1594	25	1583	17	1583	17	1
9017_4_54	94	0,65	2,74000	0,14000	0,22700	0,00840	0,85	1327	36	1316	44	1369	46	1369	46	4
9017_4_5	204	1,23	9,8400	0,2900	0,4360	0,0110	0,86	2415	27	2335	49	2493	26	2493	26	6

Sample #	*ppm*		*Isotope Ratios*					207/235		206/238		207/206		Best age		
Grain #	**U**	**U/ Th**	**207/ 235**	**2σ error**	**206/ 238**	**2σ error**	**RHO**	**Age, Ma**	**2σ error**	**Age, Ma**	**2σ error**	**Age, Ma**	**2σ error**	**Ma**	**2σ error**	**D, %**
5			0	0	0	0										
9017_4_57	191	2,64	4,50000	0,14000	0,28830	0,00780	0,81	1723	27	1630	39	1839	30	1839	30	11
9017_4_58	253	1,04	3,93000	0,19000	0,26870	0,00970	0,94	1598	43	1529	50	1702	42	1702	42	10
9017_4_60	141	0,59	4,73000	0,11000	0,31710	0,00700	0,77	1768	20	1772	35	1795	37	1795	37	1
9017_4_63	10	0,01	5,48000	0,64000	0,33000	0,05500	0,57	1833	91	1810	270	2160	290	2160	290	16
9017_4_64	415	0,61	3,67000	0,13000	0,25600	0,00980	0,64	1556	28	1464	50	1701	60	1701	60	14
9017_4_66	487	0,97	3,56400	0,09600	0,26850	0,00590	0,75	1536	21	1534	30	1542	31	1542	31	1
9017_4_68	26	0,02	6,30000	0,38000	0,34300	0,02100	0,58	1999	52	1890	100	2134	99	2134	99	11
9017_4_69	536	1,31	3,57700	0,05300	0,27810	0,00380	0,82	1544	12	1581	19	1494	17	1494	17	6
9017_4_70	102	0,24	3,46000	0,11000	0,25680	0,00590	0,70	1510	24	1471	30	1564	44	1564	44	6
9017_4_71	389	18,60	6,45000	0,10000	0,37810	0,00490	0,84	2036	14	2070	24	2007	18	2007	18	3
9017_4_72	232	0,95	3,37800	0,06200	0,25470	0,00420	0,56	1496	14	1462	21	1551	31	1551	31	6
9017_4_74	122	1,03	4,64000	0,13000	0,31230	0,00830	0,82	1750	24	1749	40	1754	31	1754	31	0
9017_4_75	165	2,05	2,51600	0,08000	0,21830	0,00570	0,79	1269	23	1271	30	1275	38	1275	38	0
9017_4_76	142	0,96	4,17000	0,13000	0,28410	0,00800	0,80	1662	25	1609	40	1740	35	1740	35	8
9017_4_77	184	0,84	4,61800	0,07200	0,31190	0,00410	0,54	1751	13	1749	20	1756	27	1756	27	0

Sample #	*ppm*		*Isotope Ratios*					207/235		206/238		207/206		Best age		
Grain #	**U**	**U/ Th**	**207/ 235**	**2σ error**	**206/ 238**	**2σ error**	**RHO**	**Age, Ma**	**2σ error**	**Age, Ma**	**2σ error**	**Age, Ma**	**2σ error**	**Ma**	**2σ error**	**D, %**
9017_4_78	221	1,76	5,30000	0,13000	0,33610	0,00900	0,82	1862	22	1864	44	1856	30	1856	30	0
9017_4_79	158	0,60	4,41700	0,09200	0,29790	0,00630	0,65	1712	17	1679	31	1760	31	1760	31	5
9017_4_83	307	0,52	3,63700	0,09200	0,25380	0,00490	0,70	1552	20	1457	25	1697	32	1697	32	14
9017_4_84	290	0,71	2,90000	0,06300	0,23090	0,00440	0,55	1381	17	1338	23	1453	38	1453	38	8
9017_4_85	229	2,10	1,98900	0,04000	0,18820	0,00280	0,48	1110	14	1111	15	1114	36	1114	36	0
9017_4_86	89	0,10	3,20000	0,11000	0,24000	0,00690	0,64	1449	26	1385	36	1541	51	1541	51	10
9017_4_87	190	0,59	2,70000	0,06000	0,21630	0,00390	0,58	1330	16	1262	21	1387	37	1387	37	9
9017_4_88	326	0,54	4,42000	0,13000	0,28540	0,00740	0,84	1711	24	1616	37	1781	29	1781	29	9
9017_4_89	157	1,03	3,23330	0,08100	0,25840	0,00480	0,72	1461	19	1481	24	1430	34	1430	34	4
9017_4_90	334	2,38	4,64600	0,08300	0,31060	0,00460	0,64	1756	14	1742	23	1774	26	1774	26	2
9017_4_91	293	2,17	6,74000	0,13000	0,37540	0,00690	0,77	2076	17	2058	31	2058	25	2058	25	0
9017_4_94	282	1,17	5,13500	0,06700	0,33090	0,00470	0,62	1841	11	1841	23	1845	22	1845	22	0
9017_4_95	220	3,76	4,50000	0,10000	0,29650	0,00650	0,74	1726	19	1672	32	1797	28	1797	28	7
9017_4_96	432	1,36	3,70200	0,06600	0,27950	0,00440	0,76	1571	14	1588	22	1547	22	1547	22	3
9017_4_97	204	0,77	4,00200	0,09800	0,28850	0,00600	0,52	1632	20	1633	30	1617	42	1617	42	1
9017_4_9	211	1,30	3,6710	0,0820	0,2624	0,0043	0,71	1561	18	1501	22	1638	27	1638	27	8

Sample #	*ppm*		*Isotope Ratios*					207/235		206/238		207/206		Best age		
Grain #	**U**	**U/ Th**	**207/ 235**	**2σ error**	**206/ 238**	**2σ error**	**RHO**	**Age, Ma**	**2σ error**	**Age, Ma**	**2σ error**	**Age, Ma**	**2σ error**	**Ma**	**2σ error**	**D, %**
8			0	0	0	0										
9017_4_99	73	0,55	2,18800	0,08000	0,19960	0,00530	0,87	1168	25	1171	28	1160	61	1160	61	1
9017_4_100	461	0,82	2,86900	0,05700	0,23720	0,00470	0,80	1372	15	1374	25	1365	23	1365	23	1
9017_4_101	335	0,53	2,40000	0,07000	0,19930	0,00540	0,77	1237	21	1170	29	1361	36	1361	36	14
9017_4_102	98	0,23	4,82000	0,15000	0,31700	0,01300	0,84	1778	26	1762	68	1825	50	1825	50	3
9017_4_103	107	0,10	3,90000	0,18000	0,26700	0,01000	0,81	1602	38	1520	51	1717	49	1717	49	11
9017_4_104	181	0,99	2,79600	0,05900	0,23120	0,00390	0,28	1350	16	1340	21	1358	35	1358	35	1
9017_4_105	95	0,10	3,68000	0,18000	0,27400	0,01600	0,54	1558	40	1553	82	1590	110	1590	110	2
9017_4_107	102	1,23	5,19000	0,12000	0,33130	0,00650	0,59	1848	20	1842	32	1847	36	1847	36	0
9017_4_108	398	1,13	2,38600	0,06500	0,19230	0,00400	0,74	1234	20	1133	22	1359	37	1359	37	17
9017_4_109	42	0,04	3,72000	0,19000	0,25300	0,01300	0,42	1565	41	1448	69	1740	110	1740	110	17
9017_4_110	1923	1,85	2,20700	0,09800	0,19920	0,00800	0,85	1171	31	1168	43	1197	50	1197	50	2
9017_4_111	128	0,59	3,30000	0,06800	0,24610	0,00460	0,62	1477	16	1417	24	1562	32	1562	32	9
9017_4_114	484	1,38	5,52000	0,17000	0,34760	0,00810	0,88	1905	25	1919	39	1904	29	1904	29	1
9017_4_115	802	2,19	2,31600	0,08900	0,18820	0,00690	0,89	1205	27	1108	37	1387	36	1387	36	20
9017_4_116	103	0,12	2,52000	0,11000	0,20250	0,00720	0,75	1269	31	1186	39	1424	54	1424	54	17

Sample #	*ppm*		*Isotope Ratios*					207/235		206/238		207/206		Best age		
Grain #	**U**	**U/ Th**	**207/ 235**	**2σ error**	**206/ 238**	**2σ error**	**RHO**	**Age, Ma**	**2σ error**	**Age, Ma**	**2σ error**	**Age, Ma**	**2σ error**	**Ma**	**2σ error**	**D, %**
9017_4_118	112	0,80	4,19000	0,20000	0,29700	0,01400	0,74	1651	39	1651	62	1683	40	1683	40	2
9017_4_119	770	1,55	2,81300	0,04400	0,23510	0,00430	0,55	1356	12	1360	23	1375	36	1375	36	1
9017_4_121	159	0,86	4,96200	0,09700	0,32210	0,00560	0,59	1808	17	1798	28	1823	31	1823	31	1
9017_4_125	8	0,01	8,93000	0,94000	0,39000	0,03500	0,84	2274	89	2100	160	2440	120	2440	120	14
9017_4_126	333	1,66	2,07200	0,04000	0,19340	0,00320	0,49	1137	13	1139	17	1135	36	1135	36	0
9017_4_127	221	0,33	4,41000	0,14000	0,28330	0,00710	0,76	1708	26	1606	36	1835	37	1835	37	12
9017_4_128	213	0,85	4,49000	0,12000	0,29760	0,00690	0,80	1720	23	1676	34	1781	31	1781	31	6
9017_4_129	275	0,78	3,57700	0,09900	0,26830	0,00780	0,67	1545	23	1530	40	1587	49	1587	49	4
9017_4_130	110	0,45	2,73900	0,08900	0,20930	0,00600	0,64	1336	25	1229	33	1463	52	1463	52	16
Sample 9045/1																
64°17'23, 5'' 50°34'52, 9''																
9045-1_1	89	0,84	12,19000	0,17000	0,48500	0,00570	0,56	2620	13	2554	26	2647	20	2647	20	4
9045-1_2	255	2,27	4,21900	0,06700	0,29040	0,00520	0,62	1675	13	1642	26	1700	28	1700	28	3
9045-1_4	439	1,69	2,78400	0,04200	0,22200	0,00280	0,16	1349	11	1292	15	1420	29	1420	29	9
9045-1_5	413	4,42	3,48600	0,05700	0,26320	0,00330	0,62	1522	13	1509	17	1527	24	1527	24	1

Sample #	*ppm*		*Isotope Ratios*					207/235		206/238		207/206		Best age		
Grain #	U	U/ Th	207/ 235	2σ error	206/ 238	2σ error	RHO	Age, Ma	2σ error	Age, Ma	2σ error	Age, Ma	2σ error	Ma	2σ error	D, %
9045-1_6	109	1,06	3,35900	0,09800	0,25760	0,00470	0,28	1488	23	1480	23	1478	59	1478	59	0
9045-1_7	220	1,97	4,61900	0,07600	0,31110	0,00390	0,40	1750	14	1746	19	1748	27	1748	27	0
9045-1_8	225	1,20	6,73600	0,07800	0,37950	0,00390	0,38	2076	10	2073	18	2063	22	2063	22	0
9045-1_9	92	1,55	3,45100	0,09100	0,25200	0,00480	0,54	1512	21	1448	25	1591	53	1591	53	9
9045-1_10	169	3,16	5,11000	0,08100	0,32700	0,00470	0,44	1835	13	1822	23	1838	24	1838	24	1
9045-1_11	446	3,25	3,52700	0,05800	0,26750	0,00400	0,74	1531	13	1527	20	1527	20	1527	20	0
9045-1_12	239	2,24	3,81200	0,05500	0,28300	0,00300	0,44	1593	12	1606	15	1562	26	1562	26	3
9045-1_13	156	2,02	2,25300	0,05300	0,20360	0,00360	0,51	1193	17	1193	19	1184	42	1184	42	1
9045-1_14	218	2,26	2,05600	0,03200	0,19310	0,00200	0,26	1135	11	1138	11	1120	32	1120	32	2
9045-1_15	170	0,97	3,15100	0,09300	0,24890	0,00510	0,47	1448	21	1432	26	1469	55	1469	55	3
9045-1_16	664	11,90	3,81400	0,06200	0,28100	0,00350	0,72	1593	13	1596	17	1594	22	1594	22	0
9045-1_18	296	2,61	2,12500	0,03200	0,19790	0,00200	0,08	1155	10	1164	11	1128	28	1128	28	3
9045-1_19	130	1,40	3,24500	0,06300	0,25440	0,00380	0,54	1464	16	1460	19	1476	33	1476	33	1
9045-1_20	110	1,69	12,13000	0,21000	0,48250	0,00800	0,73	2612	16	2536	35	2676	21	2676	21	5
9045-1_21	119	1,57	5,00300	0,08100	0,33550	0,00480	0,51	1817	14	1867	24	1765	28	1765	28	6
9045-1_22	267	1,98	4,4860	0,0530	0,3053	0,0025	0,26	1727,1	9,9	1717	12	1745	23	1745	23	2

Sample #	*ppm*		*Isotope Ratios*					207/235		206/238		207/206		Best age		
Grain #	**U**	**U/ Th**	**207/ 235**	**2σ error**	**206/ 238**	**2σ error**	**RHO**	**Age, Ma**	**2σ error**	**Age, Ma**	**2σ error**	**Age, Ma**	**2σ error**	**Ma**	**2σ error**	**D, %**
			0	0	0	0										
9045-1_23	65	0,65	14,10000	0,24000	0,50850	0,00800	0,64	2753	16	2648	34	2841	22	2841	22	7
9045-1_24	41	0,47	3,30000	0,13000	0,26370	0,00670	0,45	1466	31	1506	34	1418	68	1418	68	6
9045-1_25	457	6,19	3,51700	0,07600	0,25580	0,00530	0,83	1530	18	1467	27	1624	22	1624	22	10
9045-1_28	68	0,79	14,97000	0,20000	0,54330	0,00690	0,50	2811	13	2795	29	2824	20	2824	20	1
9045-1_29	617	3,26	3,62900	0,04600	0,27430	0,00340	0,68	1554	10	1562	17	1551	19	1551	19	1
9045-1_30	452	2,03	3,39200	0,04500	0,26400	0,00350	0,74	1501	10	1510	18	1495	18	1495	18	1
9045-1_31	373	4,83	3,45700	0,03800	0,27220	0,00290	0,53	1516,4	8,6	1551	15	1473	21	1473	21	5
9045-1_32	146	2,22	3,13900	0,05000	0,24990	0,00310	0,34	1441	12	1437	16	1450	32	1450	32	1
9045-1_33	34	1,00	4,72000	0,13000	0,31480	0,00610	0,52	1762	22	1765	31	1763	42	1763	42	0
9045-1_34	104	2,35	2,87500	0,07800	0,23390	0,00320	0,31	1370	20	1354	17	1393	50	1393	50	3
9045-1_35	294	6,88	4,28000	0,14000	0,28360	0,00530	0,42	1685	26	1608	26	1781	40	1781	40	10
9045-1_36	293	2,52	3,51500	0,05100	0,27490	0,00330	0,63	1528	11	1565	17	1486	20	1486	20	5
9045-1_37	384	2,88	3,37500	0,04500	0,26050	0,00240	0,56	1497	10	1494	13	1501	21	1501	21	0
9045-1_38	142	2,09	6,86000	0,12000	0,38020	0,00650	0,58	2093	15	2075	30	2113	27	2113	27	2
9045-1_39	149	1,61	4,37000	0,07100	0,30140	0,00410	0,56	1706	13	1697	20	1716	26	1716	26	1

Sample #	*ppm*		*Isotope Ratios*					207/235		206/238		207/206		Best age		
Grain #	**U**	**U/ Th**	**207/ 235**	**2σ error**	**206/ 238**	**2σ error**	**RHO**	**Age, Ma**	**2σ error**	**Age, Ma**	**2σ error**	**Age, Ma**	**2σ error**	**Ma**	**2σ error**	**D, %**
9045-1_40	134	0,84	3,26900	0,06900	0,25980	0,00320	0,37	1471	17	1488	16	1439	40	1439	40	3
9045-1_41	81	1,10	3,18000	0,13000	0,25390	0,00730	0,83	1460	31	1460	37	1417	50	1417	50	3
9045-1_42	326	2,33	3,56300	0,06300	0,26140	0,00400	0,72	1542	14	1496	21	1602	24	1602	24	7
9045-1_44	226	2,84	2,42200	0,05200	0,21250	0,00340	0,45	1246	15	1242	18	1252	40	1252	40	1
9045-1_45	110	0,86	3,21000	0,06000	0,24930	0,00280	0,38	1458	14	1434	15	1490	36	1490	36	4
9045-1_46	63	1,05	2,03100	0,05900	0,18980	0,00310	0,27	1119	20	1120	17	1111	61	1111	61	1
9045-1_47	113	3,46	5,65000	0,09800	0,34510	0,00420	0,52	1921	15	1910	20	1940	28	1940	28	2
9045-1_49	166	2,69	2,24100	0,04500	0,20290	0,00240	0,21	1195	14	1190	13	1192	44	1192	44	0
9045-1_50	707	2,32	4,20300	0,06200	0,28920	0,00370	0,75	1672	12	1637	19	1720	18	1720	18	5
9045-1_51	520	4,55	4,83900	0,04800	0,31720	0,00280	0,48	1790,7	8,4	1775	14	1815	18	1815	18	2
9045-1_52	1654	5,04	2,23300	0,03500	0,20660	0,00310	0,87	1190	11	1210	16	1155	15	1155	15	5
9045-1_53	440	3,23	3,33200	0,05900	0,25840	0,00430	0,79	1487	14	1480	22	1500	20	1500	20	1
9045-1_55	99	2,27	4,39000	0,13000	0,29990	0,00600	0,42	1705	25	1690	29	1722	52	1722	52	2
9045-1_56	384	2,49	1,94400	0,05000	0,17810	0,00380	0,49	1095	17	1056	21	1171	47	1171	47	10
9045-1_57	53	0,77	3,45100	0,08800	0,26660	0,00520	0,34	1512	20	1522	27	1490	50	1490	50	2
9045-1_58	167	2,05	4,5730	0,0600	0,3079	0,0031	0,45	1742	11	1730	15	1759	22	1759	22	2

Sample #	*ppm*		*Isotope Ratios*					207/235		206/238		207/206		Best age		
Grain #	**U**	**U/ Th**	**207/ 235**	**2σ error**	**206/ 238**	**2σ error**	**RHO**	**Age, Ma**	**2σ error**	**Age, Ma**	**2σ error**	**Age, Ma**	**2σ error**	**Ma**	**2σ error**	**D, %**
			0	0	0	0										
9045-1_59	268	3,20	3,20000	0,06000	0,24820	0,00350	0,46	1455	15	1429	18	1501	34	1501	34	5
9045-1_61	361	2,51	4,82000	0,07100	0,32080	0,00440	0,73	1787	12	1792	22	1785	21	1785	21	0
9045-1_62	202	4,47	2,10600	0,03500	0,19710	0,00220	0,38	1148	11	1161	12	1123	33	1123	33	3
9045-1_63	385	3,13	3,75900	0,04800	0,27750	0,00280	0,60	1582	10	1578	14	1581	21	1581	21	0
9045-1_64	86	2,58	3,09700	0,07700	0,24720	0,00500	0,51	1427	19	1423	26	1418	44	1418	44	0
9045-1_65	204	6,06	7,65000	0,11000	0,40480	0,00510	0,75	2188	13	2190	23	2178	18	2178	18	1
9045-1_66	362	2,23	4,79300	0,05400	0,31990	0,00320	0,50	1781,9	9,6	1789	16	1763	20	1763	20	1
9045-1_67	55	3,47	2,24800	0,08600	0,20160	0,00500	0,13	1190	27	1183	27	1190	92	1190	92	1
9045-1_68	67	1,00	3,38600	0,08000	0,26350	0,00480	0,58	1500	19	1506	24	1472	40	1472	40	2
9045-1_69	207	3,54	3,68300	0,06000	0,26880	0,00330	0,40	1568	13	1534	17	1593	31	1593	31	4
9045-1_70	206	3,45	3,20500	0,05100	0,25110	0,00280	0,44	1456	12	1444	14	1456	28	1456	28	1
9045-1_71	479	4,29	3,17300	0,04900	0,24560	0,00270	0,43	1449	12	1415	14	1482	27	1482	27	5
9045-1_72	127	4,54	3,48400	0,08400	0,25580	0,00300	0,35	1519	19	1468	15	1570	42	1570	42	6
9045-1_73	205	5,18	5,27800	0,06500	0,33810	0,00360	0,48	1863	11	1877	17	1834	21	1834	21	2
9045-1_74	123	2,90	3,44100	0,06800	0,26330	0,00380	0,69	1510	16	1506	20	1508	30	1508	30	0

Sample #	*ppm*		*Isotope Ratios*					207/235		206/238		207/206		Best age		
Grain #	**U**	**U/ Th**	**207/ 235**	**2σ error**	**206/ 238**	**2σ error**	**RH O**	**Age, Ma**	**2σ erro r**	**Age, Ma**	**2σ error**	**Age, Ma**	**2σ error**	**Ma**	**2σ erro r**	**D, %**
9045-1_75	288	5,02	2,0190 0	0,0370 0	0,1815 0	0,0027 0	0,40	1120	12	1075	14	1188	37	1188	37	10
9045-1_77	156	4,54	4,3630 0	0,0800 0	0,3015 0	0,0045 0	0,65	1701	15	1698	22	1694	27	1694	27	0
9045-1_78	92	2,64	6,5600 0	0,1100 0	0,3821 0	0,0048 0	0,43	2053	14	2085	22	2003	28	2003	28	4
9045-1_79	204	2,84	3,2320 0	0,0470 0	0,2517 0	0,0032 0	0,55	1463	11	1447	16	1477	24	1477	24	2
9045-1_82	163	3,17	2,9670 0	0,0510 0	0,2435 0	0,0030 0	0,32	1399	14	1404	15	1379	34	1379	34	2
9045-1_84	166	2,40	3,2980 0	0,0580 0	0,2587 0	0,0040 0	0,56	1479	14	1482	20	1469	31	1469	31	1
9045-1_85	392	7,17	3,4140 0	0,0430 0	0,2628 0	0,0026 0	0,51	1505,7	9,9	1503	13	1512	22	1512	22	1
9045-1_86	203	3,00	2,0770 0	0,0310 0	0,1959 0	0,0020 0	0,26	1141	10	1153	11	1118	32	1118	32	3
9045-1_87	112	2,02	3,3300 0	0,0860 0	0,2534 0	0,0055 0	0,53	1485	20	1455	28	1531	43	1531	43	5
9045-1_88	119	0,90	3,3510 0	0,0600 0	0,2593 0	0,0026 0	0,33	1491	14	1488	13	1496	34	1496	34	1
9045-1_89	95	1,66	4,8610 0	0,0820 0	0,3211 0	0,0036 0	0,37	1792	14	1794	17	1793	29	1793	29	0
9045-1_90	134	4,64	4,9400 0	0,0760 0	0,3230 0	0,0034 0	0,37	1808	13	1804	17	1816	27	1816	27	1
9045-1_91	358	5,35	3,4790 0	0,0450 0	0,2660 0	0,0022 0	0,45	1521	10	1520	11	1526	22	1526	22	0
9045-1_92	75	1,11	3,3690 0	0,0740 0	0,2593 0	0,0037 0	0,28	1492	17	1486	19	1511	41	1511	41	2
9045-1_93	156 0	4,93	2,3040 0	0,0440 0	0,2000 0	0,0043 0	0,91	1210	14	1174	23	1291	18	1291	18	9
9045-1_94	27	1,46	4,4300	0,1800	0,3014	0,0078	0,48	1702	34	1695	39	1703	69	1703	69	0

Sample #	*ppm*		*Isotope Ratios*					207/235		206/238		207/206		Best age		
Grain #	U	U/ Th	207/ 235	2σ error	206/ 238	2σ error	RHO	Age, Ma	2σ error	Age, Ma	2σ error	Age, Ma	2σ error	Ma	2σ error	D, %
			0	0	0	0										
9045-1_95	398	3,86	2,91400	0,04700	0,24480	0,00310	0,51	1383	12	1411	16	1346	27	1346	27	5
9045-1_96	99	2,72	4,17500	0,08400	0,29560	0,00400	0,37	1664	16	1668	20	1663	36	1663	36	0
9045-1_97	95	3,69	2,08100	0,04600	0,19300	0,00280	0,31	1141	15	1137	15	1151	44	1151	44	1
9045-1_98	100	1,73	4,88100	0,09600	0,32190	0,00450	0,46	1794	17	1798	22	1808	33	1808	33	1
9045-1_99	262	2,60	4,96300	0,05900	0,32730	0,00360	0,56	1811	10	1824	18	1800	20	1800	20	1
9045-1_100	281	4,32	3,43500	0,05900	0,26240	0,00340	0,54	1509	13	1501	17	1522	28	1522	28	1
9045-1_101	67	2,04	13,67000	0,22000	0,49340	0,00840	0,59	2725	15	2582	36	2834	25	2834	25	9
9045-1_104	239	2,13	3,82800	0,06500	0,27970	0,00350	0,58	1595	14	1589	17	1602	26	1602	26	1
9045-1_105	119	2,37	3,44400	0,06900	0,25910	0,00290	0,25	1510	16	1484	15	1549	39	1549	39	4
9045-1_106	928	11,29	2,98000	0,11000	0,23730	0,00680	0,95	1393	27	1370	36	1435	23	1435	23	5
9045-1_107	180	3,27	6,11700	0,06800	0,36290	0,00340	0,44	1990,9	9,7	1995	16	1985	20	1985	20	1
9045-1_108	91	1,57	3,63200	0,07200	0,27090	0,00300	0,35	1555	16	1545	15	1568	36	1568	36	1
9045-1_109	128	2,53	3,31700	0,06800	0,25400	0,00400	0,41	1483	16	1458	21	1506	36	1506	36	3
9045-1_110	53	4,81	2,14900	0,07000	0,19540	0,00370	0,19	1156	22	1152	19	1155	64	1155	64	0
9045-1_112	217	2,21	5,05400	0,06800	0,32420	0,00390	0,44	1826	11	1809	19	1850	24	1850	24	2

Sample #	*ppm*		*Isotope Ratios*					207/235		206/238		207/206		Best age		
Grain #	U	U/ Th	207/ 235	2σ error	206/ 238	2σ error	RHO	Age, Ma	2σ error	Age, Ma	2σ error	Age, Ma	2σ error	Ma	2σ error	D, %
9045-1_113	62	4,05	4,67000	0,16000	0,30020	0,00850	0,26	1758	28	1691	42	1835	71	1835	71	8
9045-1_114	351	3,32	3,47800	0,05000	0,26350	0,00270	0,55	1522	11	1507	14	1529	24	1529	24	1
9045-1_115	280	1,18	3,36300	0,05800	0,25470	0,00360	0,69	1495	14	1462	18	1546	23	1546	23	5
9045-1_117	302	3,43	3,67800	0,03800	0,27530	0,00260	0,58	1565,2	8,3	1567	13	1563	18	1563	18	0
9045-1_118	67	2,79	5,50000	0,16000	0,33010	0,00770	0,36	1896	26	1837	37	1951	45	1951	45	6
9045-1_120	48	1,74	4,87000	0,18000	0,31470	0,00730	0,54	1790	31	1762	36	1813	57	1813	57	3
9045-1_122	287	3,60	2,42700	0,04100	0,20640	0,00250	0,40	1248	12	1209	14	1309	33	1309	33	8
9045-1_123	169	6,16	2,12700	0,04700	0,18870	0,00270	0,37	1157	16	1114	15	1217	46	1217	46	8
9045-1_124	664	13,84	4,01300	0,06900	0,27370	0,00440	0,68	1634	14	1558	22	1724	24	1724	24	10
9045-1_125	209	2,89	3,45500	0,05000	0,25650	0,00300	0,53	1515	11	1471	15	1566	24	1566	24	6
9045-1_126	140	2,97	3,50400	0,05400	0,26690	0,00310	0,54	1526	12	1524	16	1518	30	1518	30	0
9045-1_128	630	9,85	2,83200	0,04800	0,22480	0,00330	0,52	1363	13	1307	17	1442	29	1442	29	9
9045-1_129	454	2,21	4,85800	0,07100	0,32090	0,00390	0,78	1792	12	1793	19	1780	16	1780	16	1
9045-1_131	57	1,49	4,02000	0,11000	0,28690	0,00450	0,47	1633	21	1625	22	1624	45	1624	45	0
9045-1_132	86	4,30	2,17600	0,05300	0,19170	0,00310	0,39	1171	17	1130	17	1235	44	1235	44	9
9045-	640	13,6	2,6490	0,0380	0,2228	0,0025	0,71	1312	11	1296	13	1332	20	1332	20	3

Sample #	***ppm***		***Isotope Ratios***					**207/235**		**206/238**		**207/206**		**Best age**		
Grain #	**U**	**U/ Th**	**207/ 235**	**2σ error**	**206/ 238**	**2σ error**	**RHO**	**Age, Ma**	**2σ error**	**Age, Ma**	**2σ error**	**Age, Ma**	**2σ error**	**Ma**	**2σ error**	**D, %**
1_133		0	0	0	0	0										
9045-1_134	221	3,91	4,64400	0,06500	0,31230	0,00380	0,62	1755	12	1751	19	1750	23	1750	23	0
9045-1_135	403	3,09	3,41400	0,03900	0,26150	0,00240	0,31	1507,2	8,7	1497	12	1514	23	1514	23	1
9045-1_136	217	3,02	3,32800	0,05700	0,25480	0,00350	0,46	1487	14	1462	18	1516	31	1516	31	4
9045-1_137	79	3,69	3,91200	0,07900	0,28370	0,00390	0,41	1611	16	1609	20	1604	37	1604	37	0
9045-1_139	218	2,87	3,43100	0,05000	0,26290	0,00290	0,52	1509	12	1504	15	1515	24	1515	24	1
9045-1_140	306	3,90	3,39100	0,05600	0,25290	0,00320	0,45	1501	13	1453	16	1564	30	1564	30	7

Appendix 3

Results of U-Pb dating of detrital rutile

Sample	U/Th	206 cps	207 cps	208 cps	208c/206c	206/238 mes	age 206-238	2σ error
Sample 9007/3								
64°37'35,4" 51°43'43.2"								
9007-3_14	0,863000	22880	14900	38200	2,10	0,50	747	24
9007-3_34	1,147000	10580	4860	13900	2,10	0,34	875	65
9007-3_35	1,290000	20710	14210	35300	2,10	0,69	878	33
9007-3_26	-42120,000000	7160	510	7	2,10	0,15	917	29
9007-3_6	790,000000	174200	12900	1000	2,10	0,16	928	14
9007-3_14	1,490000	5360	1700	4510	2,10	0,23	939	60
9007-3_27	4,180000	14820	5920	13900	2,10	0,28	966	38
9007-3_41	3,900000	54700	8250	17100	2,10	0,19	1001	39
9007-3_29	2,170000	57800	25800	60100	2,10	0,31	1004	23
9007-3_21	1,234000	29000	11350	31200	2,10	0,31	1018	36
9007-3_17	-332700,00000	68300	5260	68	2,10	0,18	1054	12
9007-3_36	2,449000	570000	52910	88400	2,10	0,18	1055	11
9007-3_15	-99590,000000	22490	2007	1070	2,10	0,18	1059	30
9007-3_34	0,555000	23550	17550	43900	2,10	1,21	1064	87
9007-3_33	14,720000	24590	1930	910	2,10	0,18	1080	26
9007-3_10	5,660000	47600	15480	33800	2,10	0,27	1084	27
9007-3_33	2,650000	28600	11170	27100	2,10	0,32	1107	32
9007-3_42	55,300000	77100	5890	1550	2,10	0,19	1107	19
9007-3_16	1,167000	412900	47800	121300	2,10	0,19	1114	8
9007-3_18	1,720000	11640	1450	4230	2,10	0,21	1115	46
9007-3_12	6,280000	2210000	300000	324000	2,10	0,20	1124	11
9007-3_29	13,200000	71300	8800	9900	2,10	0,20	1126	53
9007-3_15	1,820000	54400	35400	87500	2,10	0,77	1148	50

Sample	U/Th	206 cps	207 cps	208 cps	208c/206c	206/238 mes	age 206-238	2σ error
9007-3_24	270,000000	91300	9340	6800	2,10	0,20	1160	24
9007-3_8	4,600000	59500	16700	36100	2,10	0,27	1163	34
9007-3_13	5,710000	2090000	289000	378000	2,10	0,21	1174	13
9007-3_21	1,625000	32800	15150	38700	2,10	0,42	1181	31
9007-3_20	74,000000	32000	6410	10400	2,10	0,24	1213	49
9007-3_23	3,350000	17460	5460	11900	2,10	0,29	1216	62
9007-3_28	62,500000	89900	13470	17100	2,10	0,23	1229	29
9007-3_19	15,290000	2076000	170000	60700	2,10	0,22	1251	21
9007-3_22	0,752000	23500	13900	34500	2,10	0,62	1343	67
9007-3_25	1,810000	24100	13500	31400	2,10	0,57	1353	105
9007-3_22	2,420000	42800	6780	12200	2,10	0,26	1393	41
9007-3_38	24,900000	36500	3790	2170	2,10	0,26	1450	73
9007-3_7	3,322000	1348000	133000	139900	2,10	0,27	1516	23
9007-3_9	2,190000	1092000	121000	168200	2,10	0,27	1529	24
9007-3_5	0,712000	642000	178200	418000	2,10	0,31	1552	240
9007-3_38	1,580000	30900	18100	42000	2,10	0,82	1770	154
9007-3_40	-95200,000000	35460	4150	33	2,10	0,34	1866	37
9007-3_2	25,600000	292000	39100	13100	2,10	0,37	1988	52
9007-3_37	0,351000	41300	31700	76400	2,10	2,04	1989	283
9007-3_37	0,762000	9840	4340	9200	2,10	0,56	2095	201
9007-3_11	7,390000	2548000	608000	98400	2,10	0,53	2761	103
9007-3_3	1,870000	886000	78700	61000	2,10	0,72	3612	502
Sample 9045/1								
64°17'23,5" 50°34'52,9"								
9045-1_1	3,600000	34400	7500	16020	2,10	0,17	858	24
9045-1_2	3,950000	28190	6160	13190	2,10	0,18	876	22
9045-1_3	1,033000	19880	7510	20200	2,10	0,27	975	28
9045-1_4	5,180000	15240	1930	1540	2,10	0,33	1819	47
9045-1_5	1,146000	16500	2640	5040	2,10	0,33	1796	44
9045-1_6	1,118000	93300	30600	80500	2,10	0,25	1002	25
9045-1_7	26,100000	31420	3250	2290	2,10	0,20	1150	28

Sample	U/Th	206 cps	207 cps	208 cps	208c/206c	206/238 mes	age 206-238	2σ error
9045-1_8	-132800,000000	28410	2480	138	2,10	0,18	1087	27
9045-1_9	1,226000	27670	11080	29020	2,10	0,26	902	21
9045-1_10	0,710000	36600	16650	46600	2,10	0,35	1047	45
9045-1_10	0,567000	35480	19560	51600	2,10	0,53	1273	36
9045-1_11	1,713000	26500	7840	17700	2,10	0,31	1350	56
9045-1_14	-66900,000000	23730	1960	355	2,10	0,21	1210	34
9045-1_15	1,819000	42200	11710	29800	2,10	0,24	1017	36
9045-1_16	1,667000	46100	13930	36300	2,10	0,26	1060	31
9045-1_17	-109000,000000	358000	34000	1660	2,10	0,27	1523	22
9045-1_18	236,000000	338000	33650	4790	2,10	0,28	1595	20
9045-1_19	1,099000	53500	22760	55500	2,10	0,32	1116	27
9045-1_20	109,000000	107000	12450	710	2,10	0,34	1889	55
9045-1_21	-252000,000000	78300	8690	59	2,10	0,30	1681	37
9045-1_22	-246000,000000	87600	9880	26	2,10	0,33	1846	35
9045-1_23	-29000,000000	242100	23800	439	2,10	0,28	1590	32
9045-1_24	-841000,000000	236200	23580	26	2,10	0,28	1577	34
9045-1_25	-12000,000000	70700	6870	2110	2,10	0,24	1388	34
9045-1_26	-16300,000000	64400	5920	452	2,10	0,24	1400	24
9045-1_27	2,610000	12270	1764	2100	2,10	0,39	2062	59
9045-1_28	5,880000	129000	15910	17490	2,10	0,28	1516	37
9045-1_29	-175000,000000	88800	10090	107	2,10	0,34	1892	39
9045-1_30	-70000,000000	72400	10070	4430	2,10	0,41	2138	53
9045-1_31	-18800,000000	8180	706	94	2,10	0,21	1216	36
9045-1_32	-152000,000000	59800	6830	128	2,10	0,32	1809	32
9045-1_33	-104000,000000	56100	6610	630	2,10	0,30	1690	32
9045-1_34	-337000,000000	183000	21040	1070	2,10	0,38	2070	47
9045-1_35	-308000,000000	146200	16370	284	2,10	0,34	1877	52
9045-1_36	123,400000	735000	82600	6150	2,10	0,33	1833	27
9045-1_37	-83400,000000	36070	3870	58	2,10	0,30	1686	37
9045-1_38	-89300,000000	33700	3690	18	2,10	0,36	1980	55
9045-1_39	-105400,000000	36200	4160	9	2,10	0,34	1901	61
9045-1_40	-22400,000000	29100	3150	87	2,10	0,35	1927	61

Sample	U/Th	206 cps	207 cps	208 cps	208c/206c	206/238 mes	age 206-238	2σ error
9045-1_41	20,800000	19520	2370	730	2,10	0,33	1802	72
9045-1_42	-26500,000000	18800	2140	134	2,10	0,34	1862	61
9045-1_43	6,330000	54800	10170	13200	2,10	0,44	2164	54
9045-1_44	15,000000	72700	9440	4250	2,10	0,39	2112	41
9045-1_45	-158000,000000	71900	8240	449	2,10	0,39	2117	44
9045-1_47	1,643000	59400	27040	65000	2,10	0,40	1223	31
9045-1_49	0,944000	51900	19400	53900	2,10	0,28	1011	40

Appendix 4

Lu-Hf isotope characteristics of detrital zircons

Grain spot	$^{176}Hf/^{177}Hf$	± 1 s.e.	$^{178}Hf/^{177}Hf$	± 1 s.e.	$^{176}Yb/^{177}Hf$	± 1 s.e.	$^{176}Lu/^{177}Hf$	± 1 s.e.	Total Hf (V)	Age (Ma)	$^{176}Hf/^{177}Hf$ (t)1	$\varepsilon_{Hf\,(t)2}$	± 2 s.e.
Sample 9007/4													
9007-4-3	0,282214	0,000025	1,467250	0,000044	0,062518	0,001100	0,001070	0,000028	3,7	1145	0,282191	4,7	1,8
9007-4-5	0,281928	0,000038	1,467280	0,000074	0,077319	0,001300	0,001415	0,000031	3,8	1508	0,281888	2,2	2,7
9007-4-6	0,282166	0,000025	1,467280	0,000063	0,120975	0,002500	0,002513	0,000048	2,5	1323	0,282103	5,6	1,8
9007-4-15	0,281767	0,000031	1,467290	0,000050	0,096723	0,005500	0,001868	0,000100	2,4	1804	0,281703	2,4	2,2
9007-4-17	0,282174	0,000027	1,467360	0,000033	0,075912	0,003400	0,001514	0,000097	3,7	1283	0,282137	5,9	1,9
9007-4-19	0,282079	0,000013	1,467360	0,000035	0,056185	0,000400	0,001009	0,000002	2,9	1328	0,282054	4,0	0,9
9007-4-22	0,282249	0,000014	1,467280	0,000037	0,057327	0,000300	0,001014	0,000002	3,3	1165	0,282227	6,4	1,0
9007-4-24	0,281923	0,000018	1,467250	0,000038	0,046601	0,000410	0,000844	0,000012	3,0	1343	0,281902	-1,1	1,3
9007-4-29	0,282152	0,000018	1,467280	0,000037	0,109585	0,005400	0,001962	0,000110	3,8	1487	0,282097	9,1	1,3
9007-4-31	0,281778	0,000020	1,467230	0,000037	0,144353	0,003300	0,002550	0,000046	2,9	1840	0,281689	2,8	1,4
9007-4-33	0,282123	0,000022	1,467330	0,000057	0,057425	0,000370	0,000992	0,000010	3,6	1213	0,282100	3,0	1,6
9007-4-36	0,282102	0,000015	1,467350	0,000037	0,057333	0,002300	0,001038	0,000019	3,2	1119	0,282080	0,2	1,1
9007-4-37	0,281969	0,000015	1,467240	0,000042	0,050308	0,004700	0,000916	0,000094	3,4	1170	0,281949	-3,3	1,1
9007-4-39	0,281895	0,000016	1,467290	0,000041	0,066743	0,000410	0,001225	0,000006	3,7	1710	0,281855	5,7	1,1
9007-4-40	0,281143	0,000020	1,467240	0,000055	0,058158	0,003700	0,001006	0,000073	3,7	1914	0,281106	-16,2	1,4
9007-4-43	0,281542	0,000024	1,467300	0,000036	0,064872	0,001500	0,001131	0,000027	4,1	2102	0,281497	2,0	1,7
9007-4-48	0,281934	0,000024	1,467190	0,000041	0,090789	0,009000	0,001820	0,000180	3,0	1020	0,281899	-8,5	1,7
9007-4-53	0,281984	0,000018	1,467360	0,000032	0,032568	0,000860	0,000587	0,000016	3,4	1220	0,281970	-1,4	1,3
9007-4-55	0,281707	0,000020	1,467350	0,000034	0,066203	0,001500	0,001387	0,000032	3,6	1874	0,281658	2,5	1,4
9007-4-58	0,281948	0,000022	1,467290	0,000048	0,061890	0,001300	0,001119	0,000017	4,0	1657	0,281913	6,5	1,6
9007-4-60	0,282058	0,000016	1,467200	0,000035	0,039045	0,000200	0,000732	0,000008	2,8	1012	0,282044	-3,5	1,1
9007-4-65	0,282177	0,000034	1,467280	0,000051	0,106223	0,001300	0,001848	0,000049	3,2	1173	0,282136	3,4	2,4
9007-4-67	0,282194	0,000023	1,467330	0,000044	0,069105	0,002100	0,001123	0,000044	3,6	1255	0,282167	6,3	1,6
9007-4-68	0,282061	0,000020	1,467330	0,000039	0,072598	0,001400	0,001348	0,000033	3,7	1478	0,282023	6,3	1,4

Grain spot	$^{176}Hf/^{177}Hf$	± 1 s.e.	$^{178}Hf/^{177}Hf$	± 1 s.e.	$^{176}Yb/^{177}Hf$	± 1 s.e.	$^{176}Lu/^{177}Hf$	± 1 s.e.	Total Hf (V)	Age (Ma)	$^{176}Hf/^{177}Hf$ (t)1	$e_{Hf\ (t)2}$	± 2 s.e.
9007-4-69	0,282138	0,000022	1,467340	0,000044	0,052957	0,001900	0,000889	0,000035	3,8	1207	0,282118	3,5	1,6
9007-4-71	0,281631	0,000021	1,467310	0,000043	0,106827	0,000550	0,001912	0,000008	4,3	1824	0,281565	-2,0	1,5
9007-4-72	0,282024	0,000016	1,467340	0,000029	0,060986	0,001500	0,001093	0,000027	3,1	1490	0,281993	5,5	1,1
9007-4-75	0,282212	0,000048	1,467250	0,000110	0,099305	0,018000	0,001547	0,000290	3,3	1186	0,282177	5,1	3,4
9007-4-77	0,282162	0,000029	1,467310	0,000075	0,106801	0,012000	0,001916	0,000220	3,0	1192	0,282119	3,2	2,1
9007-4-82	0,281534	0,000035	1,467320	0,000098	0,069768	0,000720	0,001165	0,000009	3,9	1386	0,281503	-14,2	2,5
9007-4-84	0,282143	0,000030	1,467360	0,000055	0,119530	0,001200	0,002254	0,000023	1,9	1220	0,282091	2,8	2,1
9007-4-89	0,282216	0,000016	1,467370	0,000051	0,046065	0,000520	0,000804	0,000006	3,7	1250	0,282197	7,3	1,1
9007-4-91	0,281413	0,000016	1,467320	0,000039	0,033686	0,002000	0,000635	0,000041	4,4	2124	0,281387	-1,4	1,1
9007-4-95	0,282076	0,000020	1,467370	0,000041	0,053307	0,000620	0,000932	0,000003	4,3	1220	0,282055	1,5	1,4
9007-4-96	0,281438	0,000021	1,467320	0,000038	0,043153	0,000560	0,000790	0,000009	3,4	2055	0,281407	-2,3	1,5
9007-4-98	0,282157	0,000042	1,467150	0,000097	0,135439	0,006600	0,002641	0,000086	2,0	1228	0,282096	3,2	3,0
9007-4-99	0,281831	0,000027	1,467310	0,000053	0,054496	0,000620	0,000990	0,000011	4,0	1683	0,281799	3,1	1,9
9007-4-101	0,281889	0,000022	1,467240	0,000038	0,065675	0,001900	0,001155	0,000050	2,8	1509	0,281856	1,1	1,6
9007-4-105	0,282211	0,000036	1,467150	0,000054	0,342969	0,012000	0,005698	0,000180	3,7	1518	0,282047	8,1	2,6
9007-4-108	0,282189	0,000029	1,467320	0,000078	0,089089	0,002500	0,001593	0,000068	3,9	1217	0,282152	4,9	2,1
9007-4-110	0,282127	0,000016	1,467370	0,000041	0,038238	0,000880	0,000659	0,000011	4,5	1215	0,282112	3,5	1,1
9007-4-111	0,282211	0,000047	1,467320	0,000100	0,060859	0,000950	0,001183	0,000013	3,7	1214	0,282184	6,0	3,3
9007-4-90	0,281983	0,000023	1,467210	0,000059	0,094705	0,003400	0,001622	0,000072	4,5	1072	0,281950	-5,5	1,6
Sample 9020/3													
9020-3-2	0,282010	0,000056	1,467290	0,000068	0,108249	0,014000	0,001653	0,000210	2,9	1631	0,281959	7,6	4,0
9020-3-5	0,281709	0,000023	1,467220	0,000050	0,074407	0,005200	0,001471	0,000110	3,8	1839	0,281658	1,6	1,6
9020-3-6	0,282135	0,000016	1,467260	0,000037	0,084222	0,001700	0,001426	0,000021	3,8	1352	0,282099	6,1	1,1
9020-3-7	0,281742	0,000022	1,467260	0,000056	0,041340	0,002600	0,000795	0,000063	4,1	1493	0,281720	-4,1	1,6
9020-3-8	0,282053	0,000040	1,467270	0,000080	0,072419	0,007200	0,001369	0,000140	3,2	1500	0,282014	6,5	2,8
9020-3-9	0,281919	0,000033	1,467220	0,000028	0,118616	0,008600	0,002120	0,000160	3,0	1471	0,281860	0,4	2,3

Grain spot	$^{176}Hf/^{177}Hf$	± 1 s.e.	$^{178}Hf/^{177}Hf$	± 1 s.e.	$^{176}Yb/^{177}Hf$	± 1 s.e.	$^{176}Lu/^{177}Hf$	± 1 s.e.	Total Hf (V)	Age (Ma)	$^{176}Hf/^{177}Hf$ (t)1	$e_{Hf\ (t)2}$	± 2 s.e.
9020-3-13	0,281737	0,000170	1,467340	0,000500	0,125215	0,011000	0,002670	0,000240	1,6	1843	0,281644	1,2	12,1
9020-3-15	0,281774	0,000037	1,467410	0,000030	0,066303	0,001200	0,001185	0,000017	4,1	1761	0,281734	2,6	2,6
9020-3-19	0,281357	0,000024	1,467360	0,000049	0,066591	0,001000	0,001079	0,000012	3,3	2070	0,281314	-5,2	1,7
9020-3-21	0,282414	0,000044	1,467360	0,000048	0,154332	0,005900	0,002422	0,000094	4,4	1368	0,282351	15,5	3,1
9020-3-24	0,281718	0,000025	1,467390	0,000034	0,046655	0,000600	0,000864	0,000010	3,8	1856	0,281688	3,1	1,8
9020-3-27	0,281615	0,000021	1,467370	0,000060	0,041344	0,000085	0,000749	0,000002	3,7	1805	0,281589	-1,6	1,5
9020-3-31	0,282165	0,000028	1,467360	0,000060	0,084454	0,001500	0,001423	0,000015	3,5	1190	0,282133	3,6	2,0
9020-3-32	0,282057	0,000017	1,467270	0,000038	0,073286	0,001600	0,001273	0,000023	3,7	1359	0,282024	3,6	1,2
9020-3-36	0,282177	0,000014	1,467310	0,000041	0,041201	0,000160	0,000746	0,000002	3,5	1140	0,282161	3,5	1,0
9020-3-42	0,281696	0,000020	1,467300	0,000028	0,069774	0,000540	0,001364	0,000011	3,6	1803	0,281649	0,5	1,4
9020-3-43	0,281669	0,000017	1,467200	0,000050	0,066156	0,008400	0,001043	0,000110	3,5	1879	0,281632	1,6	1,2
9020-3-73	0,281823	0,000022	1,467300	0,000046	0,066738	0,007800	0,001250	0,000150	3,3	1505	0,281787	-1,4	1,6
9020-3-74	0,282019	0,000018	1,467340	0,000036	0,042583	0,000400	0,000696	0,000003	3,7	1324	0,282002	2,0	1,3
9020-3-76	0,282728	0,000070	1,467250	0,000040	0,378006	0,019000	0,006206	0,000370	4,3	1613	0,282538	27,7	5,0
9020-3-78	0,281536	0,000023	1,467300	0,000036	0,070520	0,001800	0,001474	0,000031	3,1	1973	0,281481	-1,5	1,6
9020-3-79	0,281654	0,000023	1,467330	0,000035	0,060357	0,000670	0,001138	0,000010	3,2	1749	0,281616	-1,9	1,6
9020-3-82	0,281673	0,000025	1,467400	0,000051	0,024253	0,000320	0,000402	0,000007	3,5	1784	0,281659	0,4	1,8
9020-3-84	0,281532	0,000043	1,467310	0,000057	0,082388	0,003300	0,001257	0,000044	4,2	2058	0,281483	0,5	3,1
9020-3-86	0,281743	0,000023	1,467280	0,000028	0,091105	0,006800	0,001774	0,000140	3,0	2022	0,281675	6,5	1,6
9020-3-88	0,281837	0,000025	1,467260	0,000050	0,110648	0,007000	0,001882	0,000140	3,8	1706	0,281776	2,8	1,8
9020-3-90	0,282146	0,000074	1,467290	0,000073	0,160247	0,024000	0,002992	0,000430	2,4	1564	0,282057	9,5	5,3
9020-3-91	0,282023	0,000062	1,467270	0,000089	0,141417	0,013000	0,002428	0,000220	3,0	1341	0,281961	1,0	4,4
9020-3-93	0,281682	0,000017	1,467310	0,000050	0,054662	0,000470	0,001008	0,000005	3,4	1827	0,281647	1,0	1,2
9020-3-95	0,281844	0,000023	1,467270	0,000043	0,154179	0,004100	0,002951	0,000079	2,9	1766	0,281745	3,1	1,6
9020-3-96	0,282090	0,000085	1,467190	0,000050	0,143228	0,021000	0,002657	0,000330	2,1	1747	0,282002	11,7	6,0
9020-3-100	0,282286	0,000170	1,467180	0,000056	0,277228	0,040000	0,004367	0,000550	2,7	1778	0,282139	17,3	12,1
9020-3-101	0,281481	0,000024	1,467330	0,000059	0,056006	0,001000	0,001131	0,000031	4,7	2140	0,281435	0,7	1,7
9020-3-104	0,281789	0,000033	1,467290	0,000042	0,073819	0,000990	0,001244	0,000017	3,5	1793	0,281747	3,7	2,3

Grain spot	$^{176}Hf/^{177}Hf$	± 1 s.e.	$^{178}Hf/^{177}Hf$	± 1 s.e.	$^{176}Yb/^{177}Hf$	± 1 s.e.	$^{176}Lu/^{177}Hf$	± 1 s.e.	Total Hf (V)	Age (Ma)	$^{176}Hf/^{177}Hf$ (t)1	$e_{Hf\ (t)2}$	± 2 s.e.
9020-3-105	0,281876	0,000022	1,467240	0,000044	0,038228	0,000870	0,000665	0,000012	3,2	1285	0,281860	-3,9	1,6
9020-3-111	0,282138	0,000015	1,467310	0,000035	0,035059	0,000530	0,000637	0,000003	3,1	1164	0,282124	2,7	1,1
9020-3-115	0,281854	0,000028	1,467370	0,000047	0,049796	0,000240	0,000906	0,000006	4,1	1556	0,281827	1,2	2,0
9020-3-119	0,282029	0,000029	1,467320	0,000053	0,162313	0,001200	0,002885	0,000021	4,2	1527	0,281946	4,7	2,1
9020-3-123	0,281694	0,000018	1,467200	0,000046	0,152518	0,007100	0,002888	0,000130	3,3	1834	0,281593	-0,8	1,3
9020-3-124	0,281638	0,000024	1,467320	0,000059	0,083148	0,003000	0,001528	0,000064	3,7	2042	0,281579	3,5	1,7
9020-3-125	0,281673	0,000033	1,467270	0,000053	0,096245	0,009700	0,001742	0,000200	4,4	1881	0,281611	0,9	2,3
9020-3-130	0,281868	0,000035	1,467240	0,000065	0,076956	0,006100	0,001324	0,000130	3,1	1468	0,281831	-0,7	2,5
9020-3-132	0,282239	0,000047	1,467240	0,000051	0,187828	0,006300	0,003497	0,000067	2,7	1218	0,282159	5,2	3,3
9020-3-133	0,281903	0,000064	1,467240	0,000049	0,146238	0,015000	0,002508	0,000260	2,9	1783	0,281818	6,1	4,5
9020-3-134	0,281706	0,000025	1,467340	0,000038	0,161758	0,004800	0,003072	0,000130	2,5	1950	0,281592	1,9	1,8
9020-3-135	0,281830	0,000040	1,467280	0,000039	0,080009	0,003400	0,001209	0,000027	4,0	1783	0,281789	5,0	2,8
9020-3-136	0,282022	0,000023	1,467280	0,000040	0,032094	0,000610	0,001013	0,000200	3,5	1351	0,281996	2,5	1,6
9020-3-139	0,282174	0,000026	1,467280	0,000061	0,084508	0,000650	0,001562	0,000021	3,7	1222	0,282138	4,6	1,8
9020-3-140	0,281890	0,000014	1,467310	0,000045	0,082139	0,003900	0,001249	0,000050	4,4	1595	0,281852	2,9	1,0
Sample 9016/2													
9016-2-6	0,282139	0,000016	1,467290	0,000032	0,040512	0,001300	0,000739	0,000027	3,5	1722	0,282115	15,2	1,1

Grain spot	$^{176}Hf/^{177}Hf$	± 1 s.e.	$^{178}Hf/^{177}Hf$	± 1 s.e.	$^{176}Yb/^{177}Hf$	± 1 s.e.	$^{176}Lu/^{177}Hf$	± 1 s.e.	Total Hf (V)	Age (Ma)	$^{176}Hf/^{177}Hf$ (t)1	$e_{Hf\ (t)2}$	± 2 s.e.
9016-2-7	0,281725	0,000013	1,467240	0,000028	0,050008	0,001000	0,000947	0,000015	3,4	1874	0,281691	3,6	0,9
9016-2-8	0,281992	0,000042	1,467240	0,000042	0,208731	0,011000	0,002966	0,000130	3,5	1967	0,281881	12,5	3,0
9016-2-9	0,281924	0,000019	1,467350	0,000047	0,056919	0,001300	0,001041	0,000020	3,6	1628	0,281892	5,1	1,3
9016-2-11	0,281941	0,000033	1,467220	0,000038	0,169466	0,004000	0,002725	0,000057	2,9	1962	0,281839	10,9	2,3
9016-2-14	0,282130	0,000019	1,467310	0,000035	0,030094	0,000190	0,000532	0,000001	2,7	1396	0,282116	7,7	1,3
9016-2-16	0,282158	0,000019	1,467230	0,000045	0,046734	0,000270	0,000841	0,000003	2,7	1216	0,282139	4,4	1,3
9016-2-17	0,282230	0,000030	1,467280	0,000046	0,081370	0,000850	0,001365	0,000011	2,9	1278	0,282197	7,9	2,1
9016-2-20	0,281804	0,000021	1,467340	0,000043	0,034515	0,003200	0,000679	0,000070	2,7	1606	0,281783	0,7	1,5
9016-2-26	0,282063	0,000020	1,467320	0,000031	0,047692	0,001300	0,000865	0,000025	2,4	1337	0,282041	3,7	1,4
9016-2-28	0,281711	0,000016	1,467300	0,000032	0,024531	0,000580	0,000512	0,000005	2,5	1494	0,281697	-4,9	1,1
9016-2-30	0,282013	0,000036	1,467290	0,000060	0,128984	0,001500	0,002279	0,000017	2,0	1742	0,281938	9,4	2,6
9016-2-32	0,281613	0,000029	1,467290	0,000042	0,093390	0,011000	0,001732	0,000220	1,9	1874	0,281551	-1,3	2,1
9016-2-33	0,281789	0,000055	1,467230	0,000057	0,071783	0,013000	0,001253	0,000200	2,2	1779	0,281747	3,4	3,9
9016-2-34	0,282120	0,000016	1,467310	0,000049	0,038415	0,001100	0,000689	0,000016	2,3	1150	0,282105	1,7	1,1
9016-2-39	0,281967	0,000022	1,467350	0,000033	0,078074	0,000400	0,001400	0,000010	2,8	1441	0,281929	2,1	1,6
9016-2-42	0,281864	0,000024	1,467400	0,000054	0,045114	0,000680	0,000852	0,000010	2,1	1464	0,281840	-0,5	1,7
9016-2-43	0,282328	0,000240	1,467270	0,000053	0,154612	0,025000	0,002378	0,000320	1,9	1712	0,282251	19,8	17,0
9016-2-44	0,281512	0,000026	1,467200	0,000055	0,062325	0,001400	0,001243	0,000025	2,1	2066	0,281463	0,0	1,8
9016-2-47	0,282379	0,000092	1,467210	0,000056	0,196141	0,014000	0,003266	0,000160	1,9	1474	0,282288	15,6	6,5
9016-2-49	0,281658	0,000031	1,467380	0,000056	0,051025	0,000940	0,001060	0,000013	2,3	1893	0,281620	1,5	2,2
9016-2-50	0,281034	0,000031	1,467330	0,000039	0,050289	0,000760	0,000867	0,000010	2,2	2700	0,280989	-2,1	2,2
9016-2-52	0,281745	0,000032	1,467270	0,000063	0,050510	0,000740	0,000944	0,000009	2,2	1750	0,281714	1,6	2,3
9016-2-53	0,281802	0,000026	1,467330	0,000072	0,020355	0,000140	0,000366	0,000002	2,2	1467	0,281792	-2,1	1,8
9016-2-54	0,282101	0,000036	1,467220	0,000054	0,200347	0,008500	0,003778	0,000170	2,1	1393	0,282001	3,6	2,6
9016-2-56	0,281909	0,000020	1,467320	0,000048	0,052162	0,004300	0,000934	0,000033	2,3	1481	0,281883	1,4	1,4
9016-2-61	0,282244	0,000091	1,467250	0,000043	0,145481	0,015000	0,002218	0,000180	1,7	1486	0,282182	12,1	6,5
9016-2-62	0,283005	0,000230	1,467180	0,000069	0,339643	0,059000	0,005047	0,000830	1,8	1593	0,282853	38,4	16,3
9016-2-64	0,281710	0,000031	1,467360	0,000060	0,068381	0,007900	0,001281	0,000160	2,5	1782	0,281667	0,7	2,2
9016-2-67	0,281797	0,000026	1,467320	0,000039	0,049333	0,000540	0,000937	0,000007	2,6	1716	0,281766	2,7	1,8
9016-2-68	0,281647	0,000024	1,467320	0,000050	0,076166	0,000830	0,001402	0,000011	1,8	1912	0,281596	1,1	1,7
9016-2-70	0,281739	0,000028	1,467310	0,000047	0,039293	0,002300	0,000669	0,000031	2,3	2058	0,281713	8,7	2,0

Grain spot	$^{176}Hf/^{177}Hf$	± 1 s.e.	$^{178}Hf/^{177}Hf$	± 1 s.e.	$^{176}Yb/^{177}Hf$	± 1 s.e.	$^{176}Lu/^{177}Hf$	± 1 s.e.	Total Hf (V)	Age (Ma)	$^{176}Hf/^{177}Hf$ (t)1	$\varepsilon_{Hf\,(t)2}$	± 2 s.e.
9016-2-72	0,281647	0,000026	1,467230	0,000039	0,095203	0,001000	0,001809	0,000012	2,3	1828	0,281584	-1,2	1,8
9016-2-73	0,280961	0,000020	1,467230	0,000049	0,042450	0,000240	0,000761	0,000003	2,1	2695	0,280922	-4,6	1,4
9016-2-74	0,282024	0,000031	1,467240	0,000042	0,160406	0,008500	0,002733	0,000130	2,4	1516	0,281946	4,4	2,2
9016-2-76	0,281926	0,000039	1,467310	0,000054	0,056816	0,003200	0,000951	0,000040	2,3	1503	0,281899	2,5	2,8
9016-2-78	0,281980	0,000061	1,467330	0,000064	0,137636	0,009400	0,002599	0,000180	1,2	1762	0,281893	8,2	4,3
9016-2-79	0,281751	0,000025	1,467250	0,000034	0,082911	0,001500	0,001439	0,000019	2,2	1800	0,281702	2,3	1,8
9016-2-80	0,281025	0,000023	1,467340	0,000044	0,019133	0,000450	0,000347	0,000007	1,7	2776	0,281007	0,3	1,6
9016-2-84	0,282054	0,000025	1,467250	0,000048	0,060055	0,002400	0,000948	0,000035	2,5	1539	0,282026	7,8	1,8
9016-2-86	0,282075	0,000036	1,467250	0,000074	0,092970	0,004100	0,001887	0,000130	2,1	1465	0,282023	6,0	2,6
9016-2-88	0,281886	0,000032	1,467360	0,000065	0,079260	0,001700	0,001381	0,000021	1,9	1385	0,281850	-2,0	2,3
9016-2-89	0,282098	0,000025	1,467320	0,000058	0,052136	0,000280	0,000954	0,000008	2,2	1349	0,282074	5,2	1,8
9016-2-91	0,281984	0,000039	1,467280	0,000070	0,113584	0,006600	0,001733	0,000099	2,5	1816	0,281924	10,6	2,8
9016-2-92	0,283031	0,000078	1,467400	0,000052	0,422165	0,007000	0,006355	0,000049	1,3	1819	0,282811	42,2	5,5
9016-2-94	0,281998	0,000038	1,467260	0,000060	0,029956	0,000860	0,000564	0,000013	2,1	1401	0,281983	3,1	2,7
9016-2-97	0,281839	0,000037	1,467410	0,000054	0,093764	0,006600	0,001735	0,000100	2,5	1823	0,281779	5,6	2,6
9016-2-99	0,281620	0,000031	1,467260	0,000044	0,039004	0,000210	0,000780	0,000008	2,2	1857	0,281592	-0,3	2,2
9016-2-103	0,282113	0,000130	1,467250	0,000072	0,248120	0,042000	0,003772	0,000550	1,7	1923	0,281975	14,9	9,2
Sample 9048/5													
9048-5-1	0,282050	0,000057	1,467410	0,000086	0,144802	0,004900	0,002611	0,000085	1,9	1817	0,281960	11,9	4,0
9048-5-3	0,282194	0,000023	1,467200	0,000068	0,102473	0,002800	0,001945	0,000035	2,1	1215	0,282149	4,8	1,6
9048-5-4	0,282717	0,000069	1,467220	0,000071	0,296531	0,015000	0,004336	0,000220	2,5	1845	0,282565	34,0	4,9
9048-5-5	0,282144	0,000033	1,467230	0,000047	0,080047	0,006600	0,001268	0,000091	2,0	1562	0,282106	11,2	2,3
9048-5-7	0,281042	0,000036	1,467240	0,000036	0,065591	0,010000	0,001219	0,000190	2,1	2956	0,280973	3,4	2,6
9048-5-8	0,282048	0,000038	1,467300	0,000071	0,096955	0,002000	0,001933	0,000082	2,0	1506	0,281993	5,9	2,7
9048-5-9	0,281999	0,000038	1,467360	0,000066	0,189848	0,006600	0,003748	0,000200	2,2	1606	0,281885	4,4	2,7
9048-5-10	0,281796	0,000035	1,467180	0,000057	0,112836	0,002700	0,002096	0,000043	1,9	1954	0,281718	6,4	2,5
9048-5-12	0,281780	0,000033	1,467340	0,000050	0,051875	0,002600	0,000808	0,000010	2,2	2096	0,281748	10,8	2,3
9048-5-16	0,282121	0,000046	1,467220	0,000051	0,117533	0,006100	0,001737	0,000075	1,9	1505	0,282072	8,7	3,3
9048-5-20	0,282471	0,000100	1,467210	0,000058	0,301946	0,028000	0,005019	0,000370	1,8	1805	0,282299	23,6	7,1
9048-5-21	0,281897	0,000049	1,467330	0,000059	0,064157	0,002400	0,001124	0,000033	2,1	1522	0,281865	1,7	3,5

Grain spot	$^{176}Hf/^{177}Hf$	± 1 s.e.	$^{178}Hf/^{177}Hf$	± 1 s.e.	$^{176}Yb/^{177}Hf$	± 1 s.e.	$^{176}Lu/^{177}Hf$	± 1 s.e.	Total Hf (V)	Age (Ma)	$^{176}Hf/^{177}Hf$ (t)1	$e_{Hf\ (t)2}$	± 2 s.e.
9048-5-25	0,281653	0,000043	1,467250	0,000065	0,095487	0,001100	0,001706	0,000018	2,2	1980	0,281589	2,5	3,1
9048-5-26	0,282290	0,000021	1,467320	0,000030	0,117073	0,003800	0,001912	0,000054	3,8	1196	0,282247	7,8	1,5
9048-5-27	0,281955	0,000036	1,467340	0,000032	0,111730	0,005200	0,001828	0,000078	3,2	1809	0,281892	9,3	2,6
9048-5-28	0,281959	0,000018	1,467330	0,000030	0,089398	0,006900	0,001671	0,000120	3,6	1674	0,281906	6,7	1,3
9048-5-29	0,282017	0,000049	1,467270	0,000027	0,131322	0,008900	0,002066	0,000130	4,1	1892	0,281943	13,0	3,5
9048-5-30	0,281901	0,000034	1,467360	0,000050	0,063447	0,008000	0,001012	0,000110	4,3	1522	0,281872	2,0	2,4
9048-5-34	0,281916	0,000071	1,467180	0,000056	0,192193	0,036000	0,002880	0,000460	3,0	1708	0,281823	4,5	5,0
9048-5-35	0,282075	0,000068	1,467350	0,000042	0,106884	0,033000	0,000767	0,000003	3,1	1426	0,282054	6,2	4,8
9048-5-42	0,282069	0,000093	1,467270	0,000048	0,162421	0,017000	0,002807	0,000330	2,2	1447	0,281992	4,5	6,6
9048-5-47	0,281628	0,000034	1,467170	0,000079	0,103707	0,003800	0,001864	0,000078	3,4	1839	0,281563	-1,7	2,4
9048-5-48	0,282618	0,000100	1,467170	0,000066	0,257739	0,023000	0,003647	0,000310	3,5	1460	0,282517	23,4	7,1
9048-5-51	0,281995	0,000022	1,467200	0,000038	0,121052	0,015000	0,002408	0,000290	3,4	1431	0,281930	1,9	1,6
9048-5-56	0,282076	0,000034	1,467300	0,000030	0,141896	0,006800	0,002397	0,000120	4,3	1442	0,282011	5,1	2,4
9048-5-57	0,282395	0,000120	1,467320	0,000048	0,138506	0,025000	0,002052	0,000340	3,5	1276	0,282346	13,1	8,5
9048-5-59	0,281760	0,000013	1,467270	0,000034	0,052948	0,002600	0,000986	0,000072	3,3	1387	0,281734	-6,0	0,9
9048-5-63	0,282013	0,000035	1,467290	0,000035	0,171690	0,006100	0,002589	0,000084	3,2	1695	0,281930	8,0	2,5
9048-5-64	0,282132	0,000019	1,467410	0,000035	0,051552	0,000460	0,000864	0,000005	4,4	1151	0,282113	2,1	1,3
9048-5-66	0,281878	0,000020	1,467220	0,000038	0,102140	0,006400	0,001729	0,000110	3,4	1598	0,281826	2,1	1,4
9048-5-67	0,282530	0,000054	1,467270	0,000041	0,323954	0,014000	0,005041	0,000220	2,9	1473	0,282389	19,2	3,8
9048-5-68	0,282184	0,000037	1,467290	0,000050	0,188502	0,001500	0,002922	0,000021	4,4	1432	0,282105	8,2	2,6
9048-5-69	0,282428	0,000160	1,467290	0,000045	0,284781	0,032000	0,004238	0,000500	3,4	1815	0,282282	23,3	11,4
9048-5-70	0,282028	0,000100	1,467170	0,000062	0,350592	0,053000	0,004699	0,000750	4,1	1205	0,281921	-3,5	7,1
9048-5-72	0,281840	0,000036	1,467260	0,000051	0,113181	0,004000	0,001902	0,000060	3,0	1606	0,281782	0,7	2,6
9048-5-74	0,282280	0,000110	1,467270	0,000140	0,255265	0,022000	0,004729	0,000380	1,3	1686	0,282129	14,8	7,8
9048-5-75	0,281240	0,000120	1,467340	0,000069	0,223565	0,028000	0,003522	0,000370	2,8	3449	0,281006	16,2	8,6
9048-5-76	0,282274	0,000076	1,467200	0,000090	0,125023	0,022000	0,001937	0,000300	4,3	1226	0,282229	7,9	5,4
9048-5-79	0,281592	0,000018	1,467220	0,000054	0,065665	0,002000	0,002271	0,000630	3,9	1910	0,281510	-2,0	1,3
9048-5-82	0,282135	0,000089	1,467290	0,000036	0,137959	0,022000	0,002103	0,000330	3,8	1726	0,282066	13,5	6,3
9048-5-83	0,282169	0,000140	1,467210	0,000074	0,302011	0,040000	0,005219	0,000640	3,5	1953	0,281975	15,6	9,9
9048-5-84	0,281229	0,000022	1,467300	0,000032	0,059597	0,002700	0,001135	0,000120	3,7	2806	0,281168	6,8	1,6
9048-5-90	0,281772	0,000037	1,467240	0,000041	0,081117	0,010000	0,001279	0,000170	3,6	2014	0,281723	8,0	2,6

Grain spot	$^{176}Hf/^{177}Hf$	± 1 s.e.	$^{178}Hf/^{177}Hf$	± 1 s.e.	$^{176}Yb/^{177}Hf$	± 1 s.e.	$^{176}Lu/^{177}Hf$	± 1 s.e.	Total Hf (V)	Age (Ma)	$^{176}Hf/^{177}Hf$ (t)1	$\varepsilon_{Hf\,(t)2}$	± 2 s.e.
9048-5-98	0,282236	0,000120	1,467230	0,000060	0,122904	0,024000	0,001967	0,000380	3,1	1520	0,282179	12,8	8,5
9048-5-100	0,281939	0,000036	1,467220	0,000049	0,181682	0,008800	0,003184	0,000160	3,1	1768	0,281832	6,2	2,6
9048-5-103	0,282048	0,000056	1,467180	0,000078	0,146089	0,013000	0,002537	0,000230	3,1	1966	0,281953	15,1	4,0
9048-5-104	0,281883	0,000026	1,467330	0,000048	0,084282	0,003800	0,001305	0,000047	5,5	1518	0,281845	0,9	1,8
9048-5-105	0,282190	0,000044	1,467260	0,000058	0,150595	0,009600	0,002422	0,000160	3,8	1462	0,282123	9,5	3,1
Sample 9007-1													
9007-1-1	0,282337	0,000040	1,467250	0,000043	0,184222	0,018000	0,003521	0,000340	3,2	1332	0,282248	11,0	2,8
9007-1-2	0,281940	0,000042	1,467310	0,000052	0,039914	0,001100	0,000713	0,000024	3,6	1148	0,281925	-4,7	3,0
9007-1-12	0,282038	0,000017	1,467330	0,000041	0,059430	0,002400	0,001213	0,000067	3,4	1570	0,282002	7,7	1,2
9007-1-16	0,282240	0,000024	1,467260	0,000041	0,114629	0,002900	0,002172	0,000093	2,9	1358	0,282184	9,3	1,7
9007-1-19	0,281521	0,000017	1,467320	0,000037	0,058399	0,003200	0,001042	0,000058	3,8	1974	0,281482	-1,5	1,2
9007-1-22	0,282236	0,000021	1,467230	0,000062	0,126737	0,009600	0,002257	0,000160	3,8	1251	0,282183	6,8	1,5
9007-1-25	0,282257	0,000031	1,467370	0,000073	0,139004	0,006200	0,002510	0,000110	3,3	1385	0,282191	10,2	2,2
9007-1-27	0,282091	0,000037	1,467200	0,000059	0,104700	0,004900	0,002126	0,000085	2,8	1602	0,282026	9,3	2,6
9007-1-30	0,281902	0,000087	1,467140	0,000084	0,407691	0,010000	0,006815	0,000150	1,9	1971	0,281647	4,3	6,2
9007-1-32	0,281993	0,000033	1,467280	0,000066	0,075499	0,002600	0,001397	0,000051	3,6	1655	0,281949	7,8	2,3
9007-1-35	0,281793	0,000041	1,467220	0,000086	0,081056	0,003900	0,001663	0,000072	1,9	1797	0,281736	3,5	2,9
9007-1-40	0,282200	0,000027	1,467330	0,000054	0,121069	0,006800	0,002270	0,000120	3,0	1534	0,282134	11,5	1,9
9007-1-43	0,282076	0,000026	1,467270	0,000076	0,063512	0,005400	0,001137	0,000096	3,2	1564	0,282042	9,0	1,8
9007-1-46	0,281926	0,000021	1,467210	0,000042	0,238263	0,004800	0,004329	0,000075	2,7	2018	0,281760	9,4	1,5
9007-1-49	0,282227	0,000019	1,467370	0,000046	0,084596	0,003000	0,001328	0,000051	4,1	1176	0,282198	5,6	1,3
9007-1-50	0,282285	0,000110	1,467190	0,000072	0,248540	0,036000	0,004337	0,000540	3,8	1565	0,282156	13,0	7,8
9007-1-51	0,282193	0,000042	1,467240	0,000053	0,073364	0,011000	0,001223	0,000140	3,3	1255	0,282164	6,2	3,0
9007-1-53	0,282211	0,000019	1,467310	0,000047	0,059876	0,000320	0,000983	0,000011	4,0	1224	0,282188	6,4	1,3
9007-1-54	0,281635	0,000024	1,467370	0,000032	0,067514	0,000610	0,001348	0,000008	3,5	1984	0,281584	2,4	1,7
9007-1-55	0,282276	0,000057	1,467220	0,000094	0,160631	0,004300	0,003022	0,000082	1,5	1195	0,282208	6,4	4,0
9007-1-56	0,281652	0,000045	1,467330	0,000120	0,140298	0,005000	0,002945	0,000120	1,5	1939	0,281543	-0,1	3,2

Grain spot	$^{176}Hf/^{177}Hf$	± 1 s.e.	$^{178}Hf/^{177}Hf$	± 1 s.e.	$^{176}Yb/^{177}Hf$	± 1 s.e.	$^{176}Lu/^{177}Hf$	± 1 s.e.	Total Hf (V)	Age (Ma)	$^{176}Hf/^{177}Hf$ (t)1	$\varepsilon_{Hf\,(t)2}$	± 2 s.e.
9007-1-58	0,282079	0,000025	1,467230	0,000074	0,114449	0,006300	0,002194	0,000120	2,5	1493	0,282017	6,4	1,8
9007-1-60	0,282146	0,000017	1,467330	0,000036	0,072464	0,004300	0,001365	0,000100	3,4	1140	0,282117	1,9	1,2
9007-1-64	0,282235	0,000087	1,467240	0,000061	0,343633	0,032000	0,005514	0,000460	3,0	1708	0,282056	12,8	6,2
9007-1-66	0,282278	0,000029	1,467180	0,000064	0,086252	0,008800	0,001544	0,000170	2,4	1042	0,282248	4,3	2,1
9007-1-68	0,281890	0,000018	1,467360	0,000034	0,095653	0,002900	0,001660	0,000036	4,2	1361	0,281847	-2,6	1,3
9007-1-69	0,281927	0,000020	1,467260	0,000054	0,123857	0,007100	0,002583	0,000160	3,4	1698	0,281844	5,0	1,4
9007-1-70	0,282216	0,000023	1,467280	0,000041	0,128226	0,008200	0,002399	0,000180	3,4	1290	0,282158	6,8	1,6
9007-1-72	0,282010	0,000037	1,467240	0,000058	0,105283	0,003500	0,001968	0,000089	2,9	1377	0,281959	1,7	2,6
9007-1-74	0,282045	0,000020	1,467320	0,000061	0,142999	0,011000	0,003124	0,000240	3,9	1586	0,281951	6,2	1,4
9007-1-75	0,282137	0,000017	1,467300	0,000026	0,049430	0,003100	0,000848	0,000044	3,8	1243	0,282117	4,3	1,2
9007-1-77	0,282156	0,000031	1,467280	0,000061	0,136532	0,003500	0,002536	0,000086	2,6	1174	0,282100	2,1	2,2
9007-1-78	0,281988	0,000023	1,467300	0,000027	0,069117	0,003800	0,001159	0,000046	3,6	1613	0,281953	6,9	1,6
9007-1-80	0,281857	0,000022	1,467300	0,000046	0,038435	0,002000	0,000628	0,000036	5,2	1589	0,281838	2,3	1,6
9007-1-81	0,282246	0,000090	1,467190	0,000082	0,188129	0,022000	0,003272	0,000360	3,2	1631	0,282145	14,2	6,4
9007-1-82	0,282177	0,000015	1,467260	0,000046	0,103091	0,006600	0,001849	0,000150	3,6	1214	0,282135	4,3	1,1
9007-1-83	0,281196	0,000012	1,467250	0,000033	0,043672	0,000610	0,000784	0,000009	3,1	1990	0,281166	-12,3	0,9
9007-1-84	0,282129	0,000041	1,467370	0,000045	0,140284	0,012000	0,002560	0,000190	2,7	1616	0,282051	10,5	2,9
9007-1-85	0,282147	0,000026	1,467250	0,000032	0,044817	0,001700	0,000795	0,000050	4,0	1188	0,282129	3,5	1,8
9007-1-86	0,282048	0,000051	1,467280	0,000067	0,069283	0,002800	0,001554	0,000070	1,7	1619	0,282000	8,7	3,6
9007-1-88	0,281954	0,000026	1,467220	0,000034	0,101455	0,003000	0,001651	0,000050	4,0	1572	0,281905	4,3	1,8
9007-1-89	0,281673	0,000028	1,467250	0,000030	0,097954	0,009900	0,001850	0,000190	3,0	1913	0,281606	1,5	2,0
9007-1-93	0,282131	0,000026	1,467370	0,000031	0,151563	0,017000	0,002766	0,000340	3,5	1575	0,282048	9,4	1,8
9007-1-94	0,281906	0,000016	1,467290	0,000036	0,055888	0,001700	0,001081	0,000072	3,5	1554	0,281874	2,8	1,1
9007-1-95	0,281650	0,000028	1,467160	0,000075	0,138491	0,011000	0,002756	0,000220	2,7	1850	0,281553	-1,8	2,0
9007-1-96	0,281864	0,000042	1,467330	0,000048	0,206001	0,008400	0,003285	0,000150	2,2	1971	0,281741	7,6	3,0
9007-1-100	0,282186	0,000100	1,467180	0,000078	0,274515	0,022000	0,004730	0,000350	2,0	1885	0,282017	15,5	7,1
9007-1-97	0,282238	0,000025	1,467270	0,000086	0,096225	0,012000	0,001526	0,000190	3,2	1132	0,282205	4,9	1,8
9007-1-98	0,282573	0,000082	1,467200	0,000060	0,262508	0,031000	0,004487	0,000480	1,8	1215	0,282470	16,2	5,8
9007-1-99	0,282155	0,000024	1,467240	0,000038	0,089643	0,008500	0,001587	0,000160	3,2	1257	0,282117	4,6	1,7

Appendix 5

Likeness test of cumulative curves for detrital zircons

	Svetlin-skaya Fm.	**Novobo-brovskaya Fm.**	**Vizing-skaya Fm.**	**Paun-skaya Fm.**	**Lunvozh-skaya Fm.**	**Maloche-rnoretskaya Fm.**	**Djejim Fm.**	**Yambozer-skaya Fm.**
Svetlinskaya Fm.		0,76	0,89	0,67	0,73	0,76	0,43	0,66
Novobobrov-skaya Fm.	0,76		0,76	0,69	0,64	0,64	0,48	0,54
Vizingskaya Fm.	0,89	0,76		0,7	0,69	0,72	0,47	0,59
Paunskaya Fm.	0,67	0,69	0,7		0,55	0,57	0,5	0,52
Lunvozh-skaya Fm.	0,73	0,64	0,69	0,55		0,77	0,4	0,76
Malocherno-retskaya Fm.	0,76	0,64	0,72	0,57	0,77		0,37	0,73
Djejim Fm.	0,43	0,48	0,47	0,5	0,4	0,37		0,33
Yambozer-skaya Fm.	0,66	0,54	0,59	0,52	0,76	0,73	0,33	

Satkoski, A.M., Wilkinson, B.H., Hietpas, J., Samson, S.D. Likeness among detrital zircon populations-An approach to the comparison of age frequency data in time and space (2013). Bulletin of the Geological Society of America, 125 (11-12), pp. 1783-1799

Appendix 6

Chemical composition of detrital tourmalines

		Paunskaya Formation								
Oxide/No.		1	2	3	4	5	6	7	8	9
Na_2O		2,45	2,48	2,59	2,45	2,39	2,52	2,82	2,48	2,46
CaO		0,32	0,34	0,40	0,42	0,47	0,57	0,48	0,35	0,49
K_2O		0,00	0,00	0,00	0,00	0,00	0,00	0,00	0,00	0,00
SiO_2		37,25	37,70	37,85	37,03	37,22	37,65	39,10	35,66	37,90
Al_2O_3		31,90	31,61	31,44	31,10	30,45	31,30	32,18	28,35	31,60
MgO		7,56	8,28	8,55	8,28	8,82	8,48	9,30	7,72	8,80
TiO_2		0,74	0,81	0,81	0,56	1,18	1,14	1,18	1,87	0,84
MnO		0,00	0,00	0,00	0,00	0,00	0,00	0,00	0,00	0,00
FeO		6,13	5,90	5,97	5,73	5,52	5,68	5,53	6,91	5,46
ZnO		0,00	0,00	0,00	0,00	0,00	0,00	0,00	0,00	0,00
F		0,00	0,00	0,00	0,00	0,00	0,00	0,00	0,00	0,00
H_2O		3,67	3,71	3,72	3,64	3,67	3,71	3,85	3,51	3,73
B_2O_3		10,64	10,76	10,80	10,57	10,63	10,75	11,17	10,17	10,83
Sum		100,65	101,58	102,14	99,78	100,35	101,80	105,61	97,01	102,11
The coefficients in the formula are calculated for 15 cations (*Y*+*Z*+*T*)										
X	Ca	0,06	0,06	0,07	0,07	0,08	0,10	0,08	0,06	0,08
	Na	0,78	0,78	0,81	0,78	0,76	0,79	0,85	0,82	0,77
	K	0,00	0,00	0,00	0,00	0,00	0,00	0,00	0,00	0,00
	вак	0,17	0,16	0,12	0,15	0,16	0,11	0,07	0,11	0,15
Y+*Z*	Al	6,23	6,11	6,05	6,11	5,95	6,05	5,99	5,81	6,06
	Ti	0,09	0,10	0,10	0,07	0,15	0,14	0,14	0,24	0,10
	Mg	1,84	1,99	2,05	2,03	2,15	2,04	2,16	1,97	2,11
	Mn	0,00	0,00	0,00	0,00	0,00	0,00	0,00	0,00	0,00
	Fe	0,84	0,80	0,80	0,79	0,75	0,77	0,72	0,99	0,73
	Zn	0,00	0,00	0,00	0,00	0,00	0,00	0,00	0,00	0,00
T	Si	6,09	6,09	6,09	6,09	6,08	6,09	6,08	6,09	6,08
	Al	-0,09	-0,09	-0,09	-0,09	-0,08	-0,09	-0,08	-0,09	-0,08
V+*W*	F	0,00	0,00	0,00	0,00	0,00	0,00	0,00	0,00	0,00
	OH	3,60	3,69	3,71	3,73	3,75	3,60	3,64	3,67	3,72
	O	0,40	0,31	0,29	0,27	0,25	0,40	0,36	0,33	0,28
B	B	3,00	3,00	3,00	3,00	3,00	3,00	3,00	3,00	3,00
Mg/(Mg+Fe)		0,69	0,71	0,72	0,72	0,74	0,73	0,75	0,67	0,74
$X_{□/(X□+Na+K)}$		0,18	0,17	0,13	0,16	0,17	0,12	0,08	0,12	0,16

		Paunskaya Formation								
Oxide/No.		10	11	12	13	14	15	16	17	18
Na_2O		2,38	2,34	2,65	2,65	2,62	2,30	2,37	2,29	2,99
CaO		0,61	0,62	0,33	0,33	0,51	0,27	0,31	0,53	0,62
K_2O		0,00	0,00	0,00	0,00	0,00	0,00	0,00	0,00	0,00
SiO_2		37,70	36,60	37,90	38,01	38,45	36,07	36,34	36,46	36,44
Al_2O_3		31,20	30,01	31,55	31,52	31,52	30,02	30,46	30,42	30,07
MgO		8,57	8,51	8,60	8,60	8,94	7,93	8,33	8,47	8,18
TiO_2		1,02	1,37	0,92	0,92	1,23	1,00	0,64	0,99	1,06
MnO		0,00	0,00	0,00	0,00	0,00	0,00	0,00	0,00	0,00
FeO		5,74	5,82	6,00	6,00	5,97	6,31	5,38	5,33	6,18
ZnO		0,00	0,00	0,00	0,00	0,00	0,00	0,00	0,00	0,00
F		0,00	0,00	0,00	0,00	0,00	0,00	0,00	0,00	0,00
H_2O		3,71	3,62	3,74	3,74	3,79	3,57	3,58	3,60	3,60
B_2O_3		10,75	10,49	10,85	10,85	10,99	10,35	10,38	10,44	10,43
Sum		101,68	99,38	102,53	102,63	104,02	97,81	97,80	98,53	99,57
The coefficients in the formula are calculated for 15 cations (*Y*+*Z*+*T*)										
X	Ca	0,11	0,11	0,06	0,06	0,09	0,05	0,06	0,09	0,11
	Na	0,75	0,75	0,82	0,82	0,80	0,75	0,77	0,74	0,97
	K	0,00	0,00	0,00	0,00	0,00	0,00	0,00	0,00	0,00
	вак	0,15	0,14	0,12	0,12	0,11	0,20	0,18	0,17	-0,08
Y+*Z*	Al	6,04	5,92	6,03	6,03	5,96	6,00	6,09	6,03	5,97
	Ti	0,12	0,17	0,11	0,11	0,15	0,13	0,08	0,12	0,13
	Mg	2,06	2,10	2,05	2,05	2,11	1,99	2,08	2,10	2,03
	Mn	0,00	0,00	0,00	0,00	0,00	0,00	0,00	0,00	0,00
	Fe	0,78	0,81	0,80	0,80	0,79	0,89	0,75	0,74	0,86
	Zn	0,00	0,00	0,00	0,00	0,00	0,00	0,00	0,00	0,00
T	Si	6,09	6,06	6,07	6,09	6,08	6,06	6,08	6,07	6,07
	Al	-0,09	-0,06	-0,07	-0,09	-0,08	-0,06	-0,08	-0,07	-0,07
V+*W*	F	0,00	0,00	0,00	0,00	0,00	0,00	0,00	0,00	0,00
	OH	3,67	3,70	3,74	3,72	3,69	3,84	3,79	3,72	3,50
	O	0,33	0,30	0,26	0,28	0,31	0,16	0,21	0,28	0,50
B	B	3,00	3,00	3,00	3,00	3,00	3,00	3,00	3,00	3,00
Mg/(Mg+Fe)		0,73	0,72	0,72	0,72	0,73	0,69	0,73	0,74	0,70
$X_{□/(X□+Na+K)}$		0,17	0,16	0,13	0,13	0,12	0,21	0,19	0,18	-0,09

		Paunskaya Formation								
Oxide/No.		19	20	21	22	23	24	25	26	27
Na_2O		2,41	2,45	2,56	2,53	2,46	2,49	2,43	2,31	2,86
CaO		0,34	0,67	0,32	0,44	0,30	0,49	0,65	0,56	0,51
K_2O		0,00	0,00	0,00	0,00	0,00	0,00	0,00	0,00	0,00
SiO_2		37,61	37,85	38,09	38,03	37,22	37,11	37,06	37,15	39,16
Al_2O_3		31,65	30,63	31,91	31,10	30,68	30,68	30,75	30,42	32,99
MgO		8,29	8,84	8,83	9,01	8,60	8,66	8,66	8,70	9,13
TiO_2		0,82	1,50	0,94	1,07	0,90	0,96	0,95	1,08	1,04
MnO		0,00	0,00	0,00	0,00	0,00	0,00	0,00	0,00	0,00
FeO		5,85	6,13	5,42	5,74	5,91	5,51	5,32	5,63	5,44
ZnO		0,00	0,00	0,00	0,00	0,00	0,00	0,00	0,00	0,00
F		0,00	0,00	0,00	0,00	0,00	0,00	0,00	0,00	0,00
H_2O		3,71	3,73	3,76	3,74	3,67	3,66	3,65	3,65	3,87
B_2O_3		10,75	10,82	10,90	10,86	10,64	10,60	10,59	10,60	11,24
Sum		101,42	102,62	102,73	102,52	100,38	100,16	100,06	100,10	106,24
The coefficients in the formula are calculated for 15 cations (*Y*+*Z*+*T*)										
X	Ca	0,06	0,12	0,05	0,08	0,05	0,09	0,11	0,10	0,08
	Na	0,76	0,76	0,79	0,79	0,78	0,79	0,77	0,73	0,86
	K	0,00	0,00	0,00	0,00	0,00	0,00	0,00	0,00	0,00
	вак	0,19	0,12	0,15	0,14	0,17	0,12	0,11	0,17	0,06
Y+*Z*	Al	6,11	5,88	6,07	5,95	5,99	6,01	6,03	5,97	6,07
	Ti	0,10	0,18	0,11	0,13	0,11	0,12	0,12	0,13	0,12
	Mg	2,00	2,12	2,10	2,15	2,09	2,12	2,12	2,13	2,11
	Mn	0,00	0,00	0,00	0,00	0,00	0,00	0,00	0,00	0,00
	Fe	0,79	0,82	0,72	0,77	0,81	0,76	0,73	0,77	0,70
	Zn	0,00	0,00	0,00	0,00	0,00	0,00	0,00	0,00	0,00
T	Si	6,08	6,08	6,07	6,09	6,08	6,08	6,08	6,09	6,06
	Al	-0,08	-0,08	-0,07	-0,09	-0,08	-0,08	-0,08	-0,09	-0,06
V+*W*	F	0,00	0,00	0,00	0,00	0,00	0,00	0,00	0,00	0,00
	OH	3,74	3,69	3,74	3,77	3,83	3,71	3,65	3,74	3,60
	O	0,26	0,31	0,26	0,23	0,17	0,29	0,35	0,26	0,40
B	B	3,00	3,00	3,00	3,00	3,00	3,00	3,00	3,00	3,00
Mg/(Mg+Fe)		0,72	0,72	0,74	0,74	0,72	0,74	0,74	0,73	0,75
$X_{□/(X□+Na+K)}$		0,20	0,14	0,16	0,15	0,18	0,13	0,13	0,19	0,06

		Paunskaya Formation							Novobobrovskaya Formation	
Oxide/No.		28	29	30	31	32	33	34	35	36
Na_2O		2,14	2,52	2,01	2,32	2,54	2,29	2,34	1,99	2,05
CaO		0,57	0,22	0,21	0,42	0,49	0,73	0,54	0,52	0,17
K_2O		0,00	0,00	0,00	0,00	0,00	0,00	0,00	0,00	0,00
SiO_2		36,04	37,24	27,33	37,12	37,22	37,33	37,54	39,76	35,68
Al_2O_3		30,66	31,58	24,07	30,88	31,34	30,73	30,70	35,83	31,16
MgO		7,21	8,18	6,68	8,61	8,35	8,75	9,19	5,49	4,99
TiO_2		0,81	0,62	21,83	0,76	0,88	1,37	0,96	0,33	0,82
MnO		0,00	0,00	0,00	0,00	0,00	0,00	0,00	0,00	0,00
FeO		7,16	5,84	4,59	5,44	5,61	6,16	5,14	8,97	9,67
ZnO		0,00	0,00	0,00	0,00	0,00	0,00	0,00	0,00	0,00
F		0,00	0,00	0,00	0,00	0,00	0,00	0,00	0,00	0,00
H_2O		3,58	3,67	2,73	3,65	3,67	3,73	3,75	3,91	3,56
B_2O_3		10,37	10,66	7,92	10,60	10,65	10,81	10,87	11,34	10,33
Sum		98,54	100,53	97,36	99,80	100,76	101,90	101,03	108,15	98,44
The coefficients in the formula are calculated for 15 cations (*Y*+*Z*+*T*)										
X	Ca	0,10	0,04	0,04	0,07	0,09	0,13	0,09	0,09	0,03
	Na	0,70	0,80	0,68	0,74	0,80	0,72	0,74	0,59	0,67
	K	0,00	0,00	0,00	0,00	0,00	0,00	0,00	0,00	0,00
	вак	0,20	0,16	0,28	0,19	0,11	0,16	0,17	0,32	0,30
Y+*Z*	Al	6,09	6,14	3,72	6,06	6,10	5,89	5,96	6,56	6,27
	Ti	0,10	0,08	2,87	0,09	0,11	0,17	0,12	0,04	0,10
	Mg	1,80	1,99	1,74	2,10	2,03	2,11	2,22	1,25	1,26
	Mn	0,00	0,00	0,00	0,00	0,00	0,00	0,00	0,00	0,00
	Fe	1,00	0,80	0,67	0,75	0,77	0,83	0,70	1,15	1,37
	Zn	0,00	0,00	0,00	0,00	0,00	0,00	0,00	0,00	0,00
T	Si	6,04	6,07	4,77	6,09	6,07	6,04	6,09	6,09	6,04
	Al	-0,04	-0,07	1,23	-0,09	-0,07	-0,04	-0,09	-0,09	-0,04
V+*W*	F	0,00	0,00	0,00	0,00	0,00	0,00	0,00	0,00	0,00
	OH	3,76	3,76	5,99	3,78	3,64	3,77	3,79	3,51	3,75
	O	0,24	0,24	-1,99	0,22	0,36	0,23	0,21	0,49	0,25
B	B	3,00	3,00	3,00	3,00	3,00	3,00	3,00	3,00	3,00
Mg/(Mg+Fe)		0,64	0,71	0,72	0,74	0,73	0,72	0,76	0,52	0,48
$X_{□/(X□+Na+K)}$		0,23	0,17	0,29	0,20	0,12	0,18	0,19	0,35	0,31

		Novobobrovskaya Formation			Vizingskaya Formation				Svetlinskaya Formation	
Oxide/No.		37	38	39	40	41	42	43	44	45
Na_2O		1,86	2,20	2,03	2,00	2,35	2,33	1,63	2,02	1,80
CaO		0,52	0,39	0,54	0,24	0,46	0,52	1,27	0,00	0,81
K_2O		0,00	0,00	0,00	0,00	0,11	0,12	0,10	0,00	0,00
SiO_2		36,48	36,55	37,51	33,97	36,20	36,54	35,66	36,78	34,85
Al_2O_3		31,15	29,00	33,79	29,37	31,72	32,12	32,76	31,64	30,69
MgO		5,85	6,20	6,01	5,28	8,23	8,16	9,38	5,29	6,21
TiO_2		1,16	0,96	1,00	0,84	0,73	0,74	0,58	1,08	0,95
MnO		0,00	0,00	0,00	0,00	0,00	0,00	0,00	0,00	0,00
FeO		8,38	11,99	7,05	8,55	3,28	3,70	0,00	9,49	5,72
ZnO		0,00	0,00	0,00	0,00	0,00	0,00	0,00	0,00	0,00
F		0,00	0,00	0,00	0,00	0,00	0,00	0,00	0,00	0,00
H_2O		3,64	3,65	3,75	3,39	3,56	3,65	3,56	3,62	3,43
B_2O_3		10,57	10,59	10,86	9,84	10,33	10,58	10,33	10,51	9,94
Sum		99,61	101,53	102,54	93,48	96,97	98,46	95,27	100,43	94,39
The coefficients in the formula are calculated for 15 cations (*Y*+*Z*+*T*)										
X	Ca	0,09	0,07	0,09	0,05	0,08	0,09	0,23	0,00	0,15
	Na	0,60	0,71	0,64	0,69	0,77	0,75	0,53	0,65	0,61
	K	0,00	0,00	0,00	0,00	0,02	0,03	0,02	0,00	0,00
	вак	0,30	0,23	0,27	0,26	0,13	0,13	0,21	0,35	0,24
Y+*Z*	Al	6,23	5,69	6,48	6,21	6,38	6,37	6,56	6,25	6,42
	Ti	0,15	0,12	0,12	0,11	0,09	0,09	0,07	0,13	0,12
	Mg	1,46	1,53	1,45	1,40	2,06	2,02	2,37	1,30	1,62
	Mn	0,00	0,00	0,00	0,00	0,00	0,00	0,00	0,00	0,00
	Fe	1,17	1,66	0,95	1,27	0,46	0,51	0,00	1,31	0,84
	Zn	0,00	0,00	0,00	0,00	0,00	0,00	0,00	0,00	0,00
T	Si	6,09	6,04	6,05	6,05	6,09	6,08	6,03	6,08	6,09
	Al	-0,09	-0,04	-0,05	-0,05	-0,09	-0,08	-0,03	-0,08	-0,09
V+*W*	F	0,00	0,00	0,00	0,00	0,00	0,00	0,00	0,00	0,00
	OH	3,60	4,00	3,40	3,73	3,39	3,41	3,24	3,75	3,32
	O	0,40		0,60	0,27	0,61	0,59	0,76	0,25	0,68
B	B	3,00	3,00	3,00	3,00	3,00	3,00	3,00	3,00	3,00
Mg/(Mg+Fe)		0,55	0,48	0,60	0,52	0,82	0,80	1,00	0,50	0,66
$X_{□/(X□+Na+K)}$		0,34	0,24	0,30	0,28	0,14	0,14	0,28	0,35	0,28

		Svetlinskaya Formation				Lunvoghskaya Formation				
Oxide/No.		46	47	48	49	50	51	52	53	54
Na_2O		2,54	2,06	2,04	1,71	1,49	1,68	1,83	2,14	2,00
CaO		0,00	0,16	0,54	0,62	1,89	0,47	0,57	0,29	0,88
K_2O		0,00	0,00	0,00	0,00	0,00	0,00	0,00	0,00	0,00
SiO_2		35,94	34,98	37,13	35,42	36,30	34,23	35,18	38,14	37,04
Al_2O_3		29,79	30,48	32,05	30,90	31,55	31,73	30,62	32,52	31,57
MgO		9,04	4,62	6,19	5,83	10,74	6,09	5,72	5,85	8,58
TiO_2		0,00	1,05	1,07	1,08	0,39	0,73	0,99	1,18	0,89
MnO		0,00	0,00	0,00	0,00	0,00	0,00	0,00	0,00	0,00
FeO		4,89	10,03	8,61	8,46	0,18	5,97	8,41	9,49	4,23
ZnO		0,00	0,00	0,00	0,00	0,00	0,00	0,00	0,00	0,00
F		0,00	0,00	0,00	0,00	0,00	0,00	0,00	0,00	0,00
H_2O		3,59	3,49	3,71	3,54	3,62	3,42	3,51	3,76	3,64
B_2O_3		10,41	10,13	10,75	10,26	10,51	9,91	10,19	10,89	10,57
Sum		96,20	97,00	102,09	97,82	96,68	94,23	97,02	104,26	99,41
The coefficients in the formula are calculated for 15 cations (*Y*+*Z*+*T*)										
X	Ca	0,00	0,03	0,09	0,11	0,34	0,09	0,10	0,05	0,15
	Na	0,83	0,69	0,64	0,56	0,48	0,57	0,61	0,66	0,64
	K	0,00	0,00	0,00	0,00	0,00	0,00	0,00	0,00	0,00
	вак	0,17	0,28	0,26	0,32	0,18	0,35	0,29	0,29	0,21
Y+*Z*	Al	6,03	6,23	6,19	6,19	6,26	6,46	6,21	6,20	6,21
	Ti	0,00	0,14	0,13	0,14	0,05	0,10	0,13	0,14	0,11
	Mg	2,28	1,19	1,50	1,47	2,67	1,58	1,46	1,39	2,10
	Mn	0,00	0,00	0,00	0,00	0,00	0,00	0,00	0,00	0,00
	Fe	0,69	1,45	1,17	1,20	0,03	0,87	1,20	1,27	0,58
	Zn	0,00	0,00	0,00	0,00	0,00	0,00	0,00	0,00	0,00
T	Si	6,08	6,03	6,04	6,01	6,05	5,95	6,03	6,09	6,09
	Al	-0,08	-0,03	-0,04	-0,01	-0,05	0,05	-0,03	-0,09	-0,09
V+*W*	F	0,00	0,00	0,00	0,00	0,00	0,00	0,00	0,00	0,00
	OH	4,00	3,72	3,67	3,74	3,44	3,66	3,69	3,67	3,54
	O		0,28	0,33	0,26	0,56	0,34	0,31	0,33	0,46
B	B	3,00	3,00	3,00	3,00	3,00	3,00	3,00	3,00	3,00
Mg/(Mg+Fe)		0,77	0,45	0,56	0,55	0,99	0,65	0,55	0,52	0,78
$X_{□/(X□+Na+K)}$		0,17	0,29	0,29	0,37	0,27	0,38	0,32	0,30	0,25

		Paunskaya Formation					Pizhemskaya Formation			
Oxide/No.		55	56	57	58	59	60	61	62	63
Na_2O		1,59	1,86	1,88	1,78	1,69	1,66	1,91	1,53	2,06
CaO		0,77	0,43	0,60	1,42	1,25	0,45	0,66	0,33	0,11
K_2O		0,00	0,00	0,00	0,00	0,20	0,00	0,09	0,00	0,00
SiO_2		35,86	35,01	35,39	35,20	30,51	32,95	36,34	34,40	37,09
Al_2O_3		33,55	31,03	32,05	28,70	25,30	28,83	32,72	30,49	31,66
MgO		6,52	6,26	6,53	7,77	6,17	4,69	6,60	5,10	5,10
TiO_2		0,47	0,72	0,86	0,88	0,65	1,00	0,93	0,54	1,49
MnO		0,00	0,00	0,00	0,00	0,00	0,00	0,00	0,00	0,00
FeO		4,91	6,62	6,41	7,50	7,87	9,32	6,35	8,59	10,00
ZnO		0,00	0,00	0,00	0,00	0,00	0,00	0,00	0,00	0,00
F		0,00	0,00	0,00	0,00	0,00	0,00	0,00	0,00	0,00
H_2O		3,58	3,50	3,53	3,52	3,05	3,29	3,63	3,44	3,70
B_2O_3		10,39	10,14	10,25	10,20	8,84	9,54	10,53	9,96	10,74
Sum		97,64	95,57	97,50	96,96	85,52	91,73	99,75	94,38	101,96
The coefficients in the formula are calculated for 15 cations (*Y*+*Z*+*T*)										
X	Ca	0,14	0,08	0,11	0,26	0,26	0,09	0,12	0,06	0,02
	Na	0,52	0,62	0,61	0,59	0,64	0,59	0,61	0,52	0,65
	K	0,00	0,00	0,00	0,00	0,05	0,00	0,02	0,00	0,00
	вак	0,35	0,30	0,28	0,15	0,05	0,33	0,25	0,42	0,33
Y+*Z*	Al	6,63	6,34	6,34	5,83	5,81	6,17	6,38	6,34	6,20
	Ti	0,06	0,09	0,11	0,11	0,10	0,14	0,12	0,07	0,18
	Mg	1,63	1,61	1,64	1,98	1,80	1,27	1,63	1,33	1,25
	Mn	0,00	0,00	0,00	0,00	0,00	0,00	0,00	0,00	0,00
	Fe	0,69	0,95	0,90	1,07	1,29	1,42	0,88	1,26	1,37
	Zn	0,00	0,00	0,00	0,00	0,00	0,00	0,00	0,00	0,00
T	Si	6,00	6,04	5,97	6,03	5,97	5,99	6,01	6,03	6,08
	Al	0,00	-0,04	0,03	-0,03	0,03	0,01	-0,01	-0,03	-0,08
V+*W*	F	0,00	0,00	0,00	0,00	0,00	0,00	0,00	0,00	0,00
	OH	3,46	3,65	3,63	3,80	3,80	3,80	3,52	3,84	3,66
	O	0,54	0,35	0,37	0,20	0,20	0,20	0,48	0,16	0,34
B	B	3,00	3,00	3,00	3,00	3,00	3,00	3,00	3,00	3,00
Mg/(Mg+Fe)		0,70	0,63	0,64	0,65	0,58	0,47	0,65	0,51	0,48
$X_{□/(X□+Na+K)}$		0,40	0,32	0,31	0,20	0,06	0,36	0,29	0,45	0,33

Appendix 7

Concordia diagrams based on the results of detrital zircon dating

Sample 9016/2

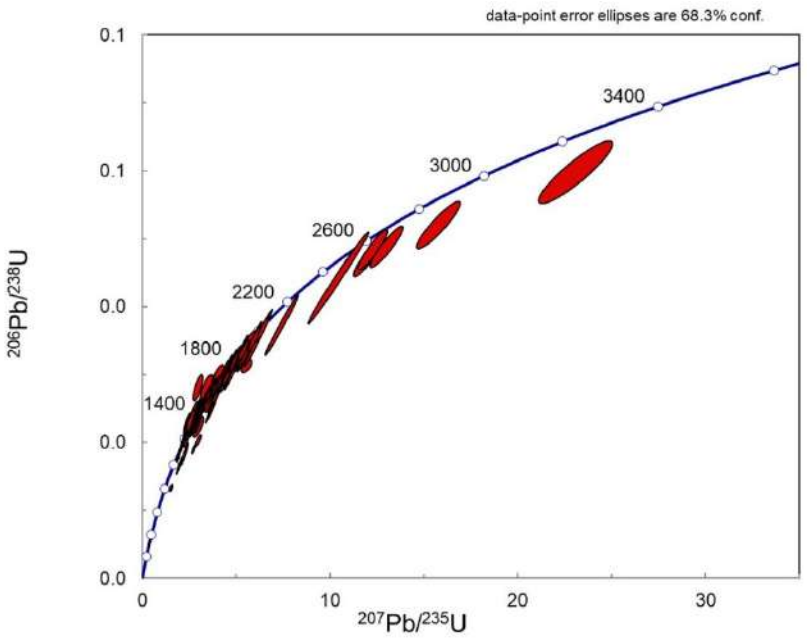

a – all 110 dated detrital zircon grains

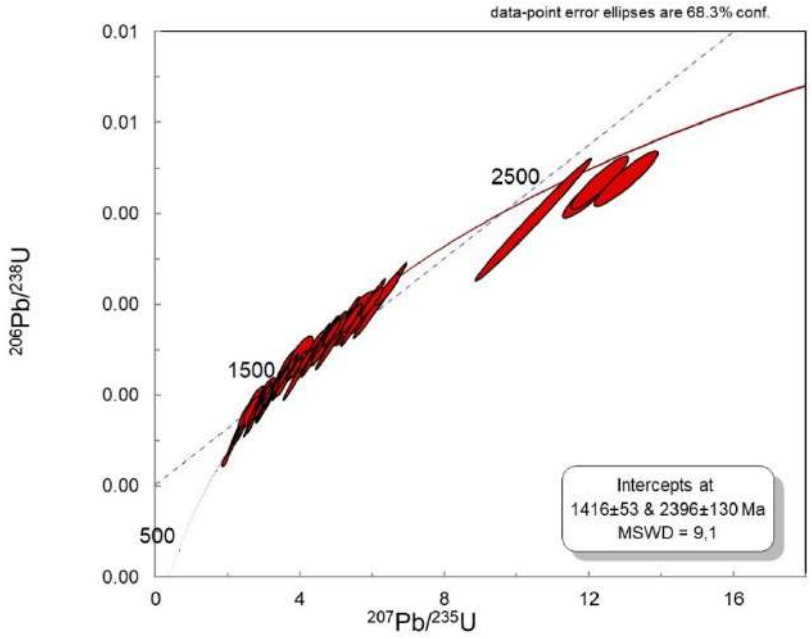

b – 88 grains with ±10% discordance

Sample 9017/4

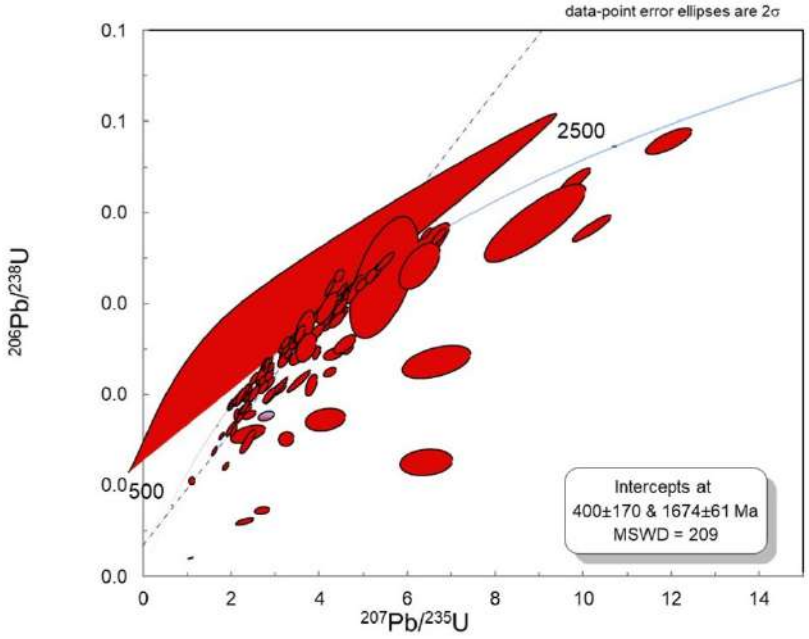

a – all 130 dated detrital zircon grains

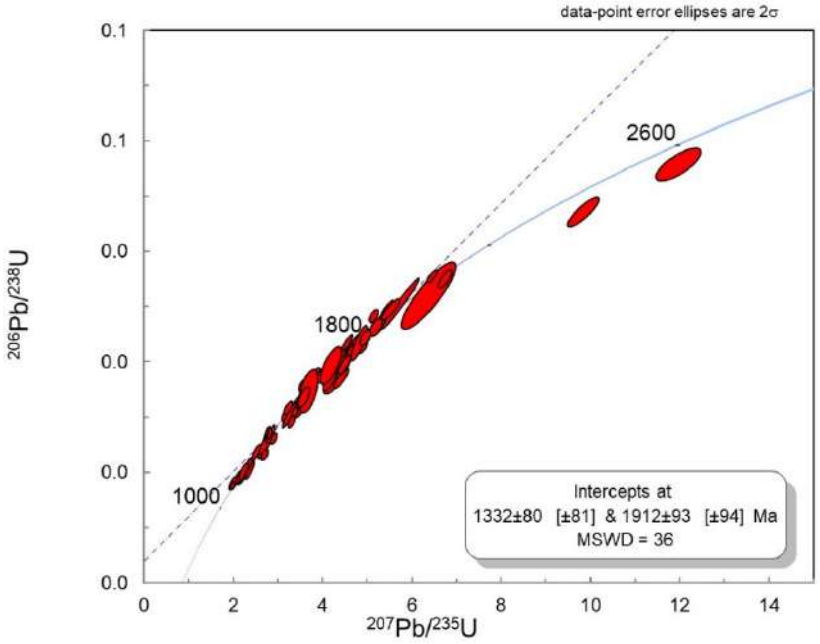

b – 75 grains with ±10% discordance

Sample 9020-3

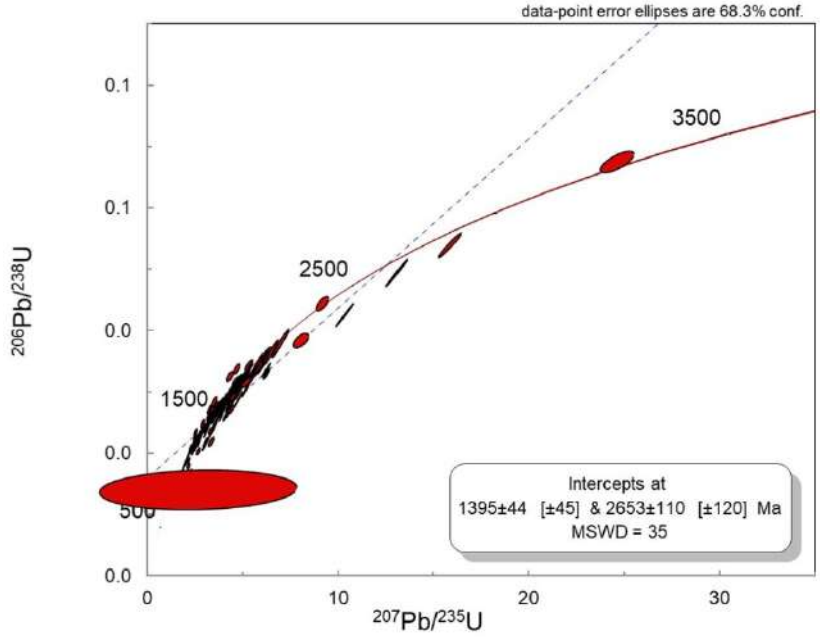

a – all 147 dated detrital zircon grains

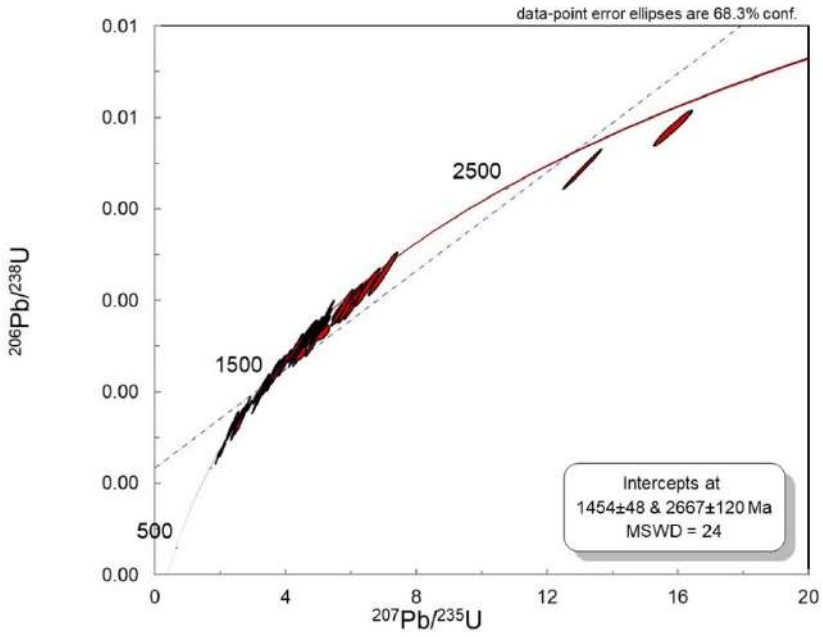

b – 91 grains with ±10% discordance

Sample 9048/5

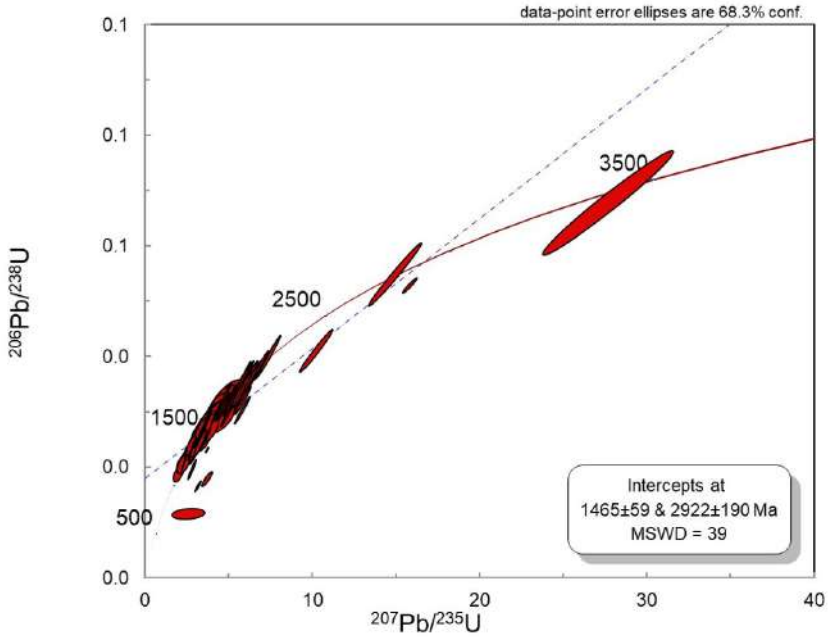

a – all 111 dated detrital zircon grains

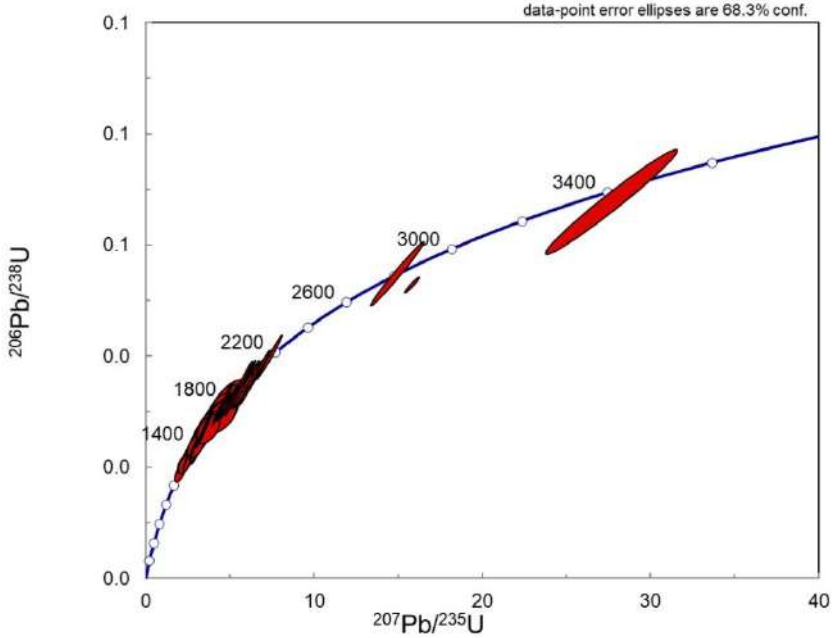

b – 94 grains with ±10% discordance

Sample 9045/1

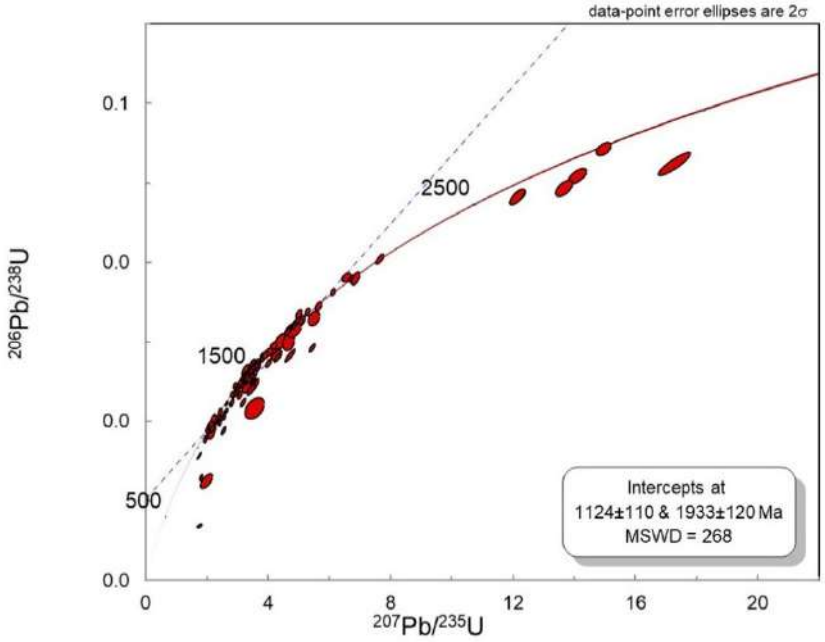

a – all 141 dated detrital zircon grains

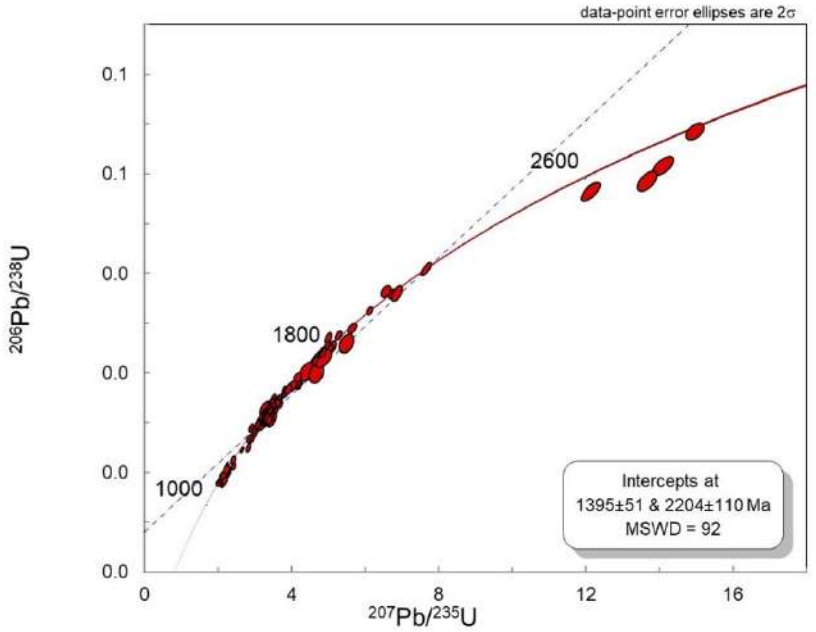

b – 113 grains with ±10% discordance

Sample 9034/2

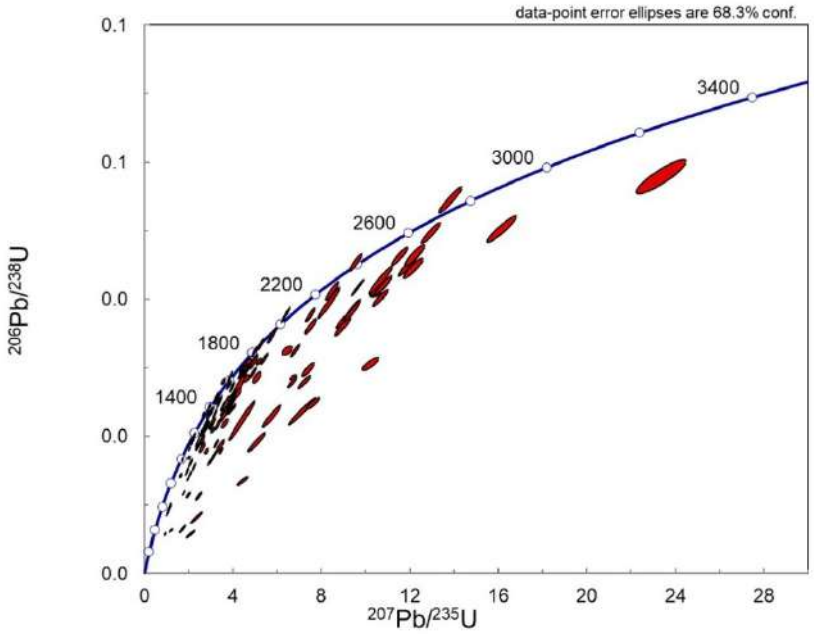

a – all 132 dated detrital zircon grains

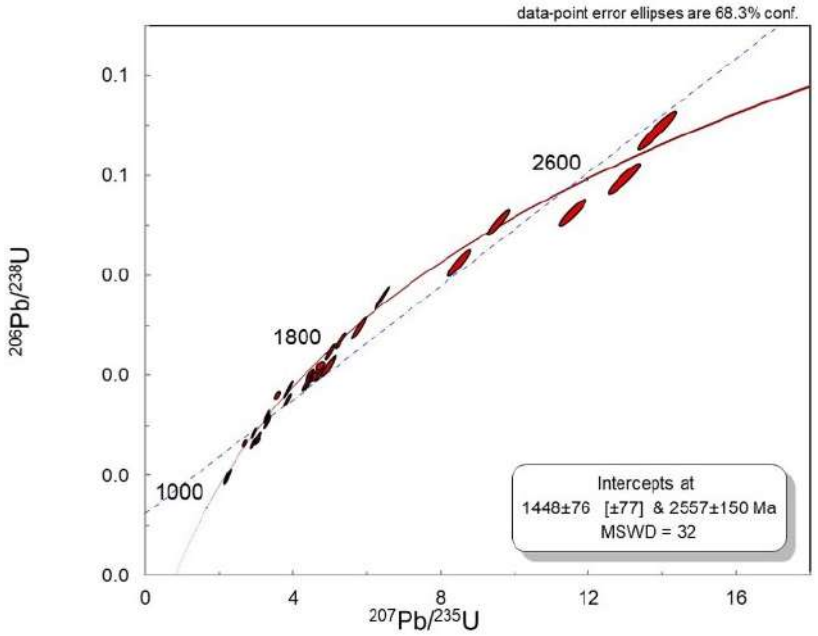

b – 33 grains with ±10% discordance

Sample 9007/1

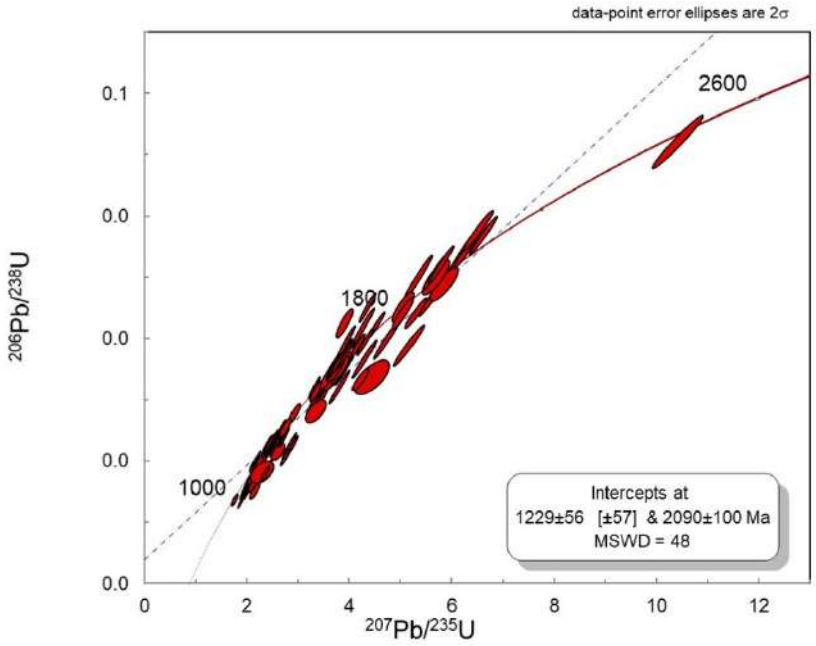

a – all 110 dated detrital zircon grains

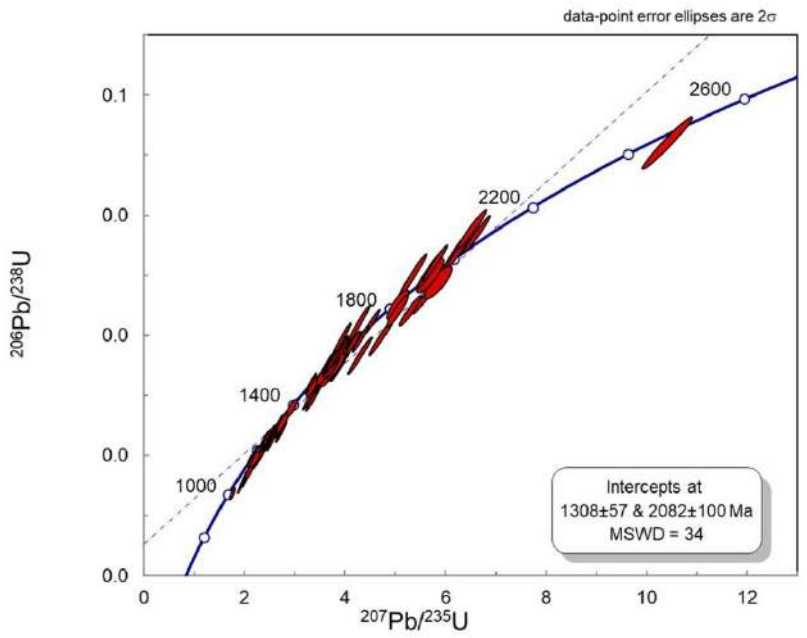

b – 76 grains with ±10% discordance

Sample 9007/4

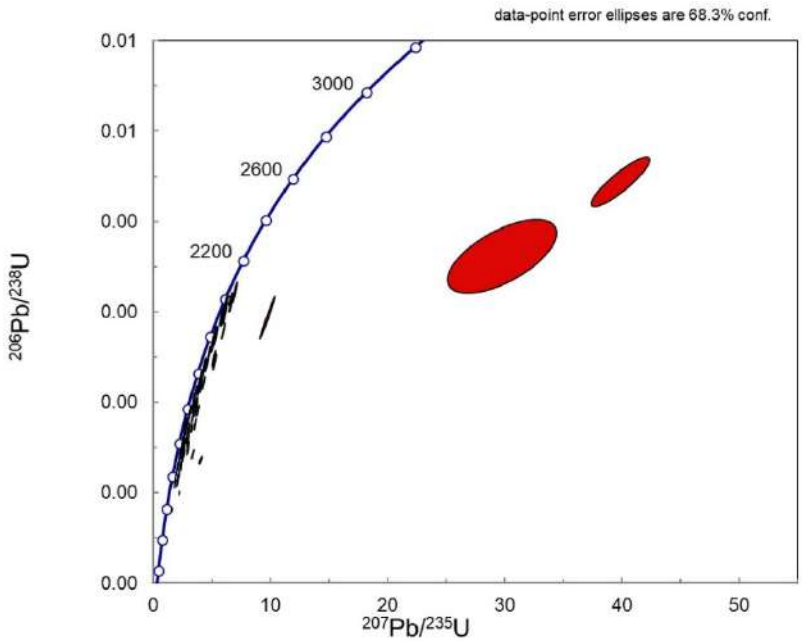

a – all 114 dated detrital zircon grains

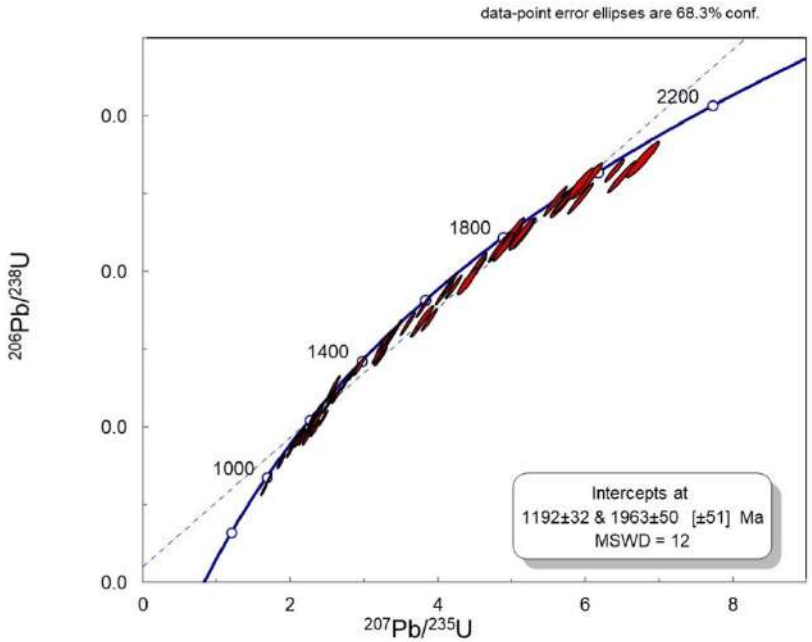

b – 77 grains with ±10% discordance